SUPRAMOLECULAR POLYMERS WITH REVERSED VISCOSITY/TEMPERATURE PROFILE

Dissertation

Zur Erlangung des akademischen Grades eines Doktors der Naturwissenschaft

-Dr. rer. Nat.-

vorgelegt von

Jan-Erik Ostwaldt

geboren in Steinheim

Fakultät für Chemie

der

Universität Duisburg-Essen

2020

DOI: 10.17185/duepublico/73161
URN: urn:nbn:de:hbz:464-20211108-093529-1

Declaration of authorship

I declare that I completed this work on my own and did not use any other source than stated.

Jan-Erik Ostwaldt, July 2020

The work presented in this thesis was accomplished in a period between January 2017 and July 2020 under the supervision of PD Dr. Jochen Niemeyer and Prof. Dr. Carsten Schmuck at the Faculty of Chemistry (Organic Chemistry) at the University of Duisburg-Essen.

First Reviewer: PD Dr. Jochen Niemeyer

Second Reviewer: Prof. Dr. Mathias Ulbricht

Chair: Prof. Dr. Eckhard Spohr

Date of examination: 21.10.20

In Memory of Carsten Schmuck

Acknowledgement

Bei den folgenden Personen möchte ich mich besonders bedanken, da ohne Sie meine Arbeit in dieser Form nicht möglich gewesen wäre:

Der Erste Dank geht an Herrn PROF. DR. CARSTEN SCHMUCK für die Möglichkeit in seiner Arbeitsgruppe zu promovieren und für die Unterstützung im Wechsel meines Forschungsschwerpunktes. Leider kannst Du nicht mehr miterleben, wie ich diese Arbeit abschließe und ich kann immer noch nicht fassen, dass du von uns gegangen bist. Ich hoffe Du bist zufrieden mit dieser Arbeit und meiner Leistung.

Ein ganz besonderer Dank geht an PD DR. JOCHEN NIEMEYER für die Übernahme der Betreuung meiner Doktorarbeit. Vielen Dank, für die Hilfestellung bei sämtlichen chemischen oder anderweitigen Problemen und auch für die wirklich angenehme Arbeitsatmosphäre. Ich bin froh, dass ich Teil Deines Forschungsteams sein durfte.

Sehr herzlich bedanken möchte ich mich bei Herrn PROF. DR. MATHIAS ULBRICHT für die freundliche Übernahme des Korreferats.

Ein weiterer, besonderer Dank geht an PROF. DR. MICHAEL GIESE für die Übernahme der Leitung des Arbeitskreises in der schweren Zeit. Danke, dass Du die Arbeit auf dich genommen hast, um den Arbeitskreis am Laufen zu halten und für einen „normalen“ Ablauf für alle Doktoranden gesorgt hast.

Ein großer Dank geht zudem an Evonik Oil Additives Darmstadt für die Möglichkeit in Kooperation diese Arbeit zu erstellen. Hier möchte ich mich besonders bei DR. STEFAN HILF, DR. STEFAN MAIER und DR. CHRISTIAN MBAYA MANI bedanken.

Des Weiteren möchte ich mich bei DR. CHRISTOPH HIRSCHHÄUSER für die Unterstützung bei jeglichen chemischen Problemen bedanken.

Mein Dank gilt auch den gemeinsamen analytischen Einrichtungen für die Instandhaltung von Geräten und Messung unzähliger Proben. Hier möchte ich mich vor allem bei DR. FELIX NIEMEYER und DR. TORSTEN SCHALLER in der NMR-Abteilung und GUDRUN HEINRICH und WERNER KAROW in der Massen-Abteilung bedanken.

Außerdem möchte ich mich bei PIA MEREU, URSULA NÜCHTER und ELISABETH VERHEGGEN für die Instandhaltung des Arbeitskreises und die Wartung der Geräte bedanken.

Vielen Dank an THIES DIRKSMEYER, TONI HÄTTASCH, HUIBIN HE, DANIEL SEBENA und ALEXANDER ZIMMERMANN, dass Ihr Euch meine Arbeit durchgelesen und korrigiert habt.

NAZLI BAGLI, MARCEL KLEIN-HITPAß, MATTHIAS KILLA und DENNIS ASCHMANN möchte ich ganz herzlich für die gemeinsamen Kaffeerunden und Mittagessen danken, die immer wieder von fehlgeschlagenen Experimenten oder Messungen abgelenkt haben und die ich sehr vermissen werde.

Danke auch an MARLEN EXTERNBRINK, MARIUS HEIMANN und PASCAL NASCHENWENG für die schöne Arbeitsatmosphäre und Unterstützung im täglichen Laboralltag.

Ich möchte all denen danken, die mich auf dem Weg durch die Studienzeit begleitet haben, MICHAEL TERHOST, DR. LUKAS ZIBULA, KATHARINA TERHORST, HANNAH TUMBRINK, LENA RICHTER, ANNA ENGELKE, JAN WOLFGRAMM, ULF BEDNARZIK, LENA QUAMBUSCH, FABIAN WESSELER und PHILIP PUNT. Die wochenlangen Lernsessions die sowohl lustig als auch nervig waren werde ich nie vergessen.

Ich möchte mich bei meinen Geschwistern DR. ANN-CHRISTIN OSTWALDT, MEIKE OSTWALDT und FELIX OSTWALDT bedanken, dass ihr immer für mich da seid, auch wenn wir in der ganzen Welt verteilt sind.

Ganz besonders möchte ich mich bei meinen Eltern, ULRIKE OSTWALDT und STEFAN OSTWALDT bedanken, dafür das ihr mich großgezogen habt und mich in allen Lebenslagen unterstützt habt. Danke für alles was Ihr für mich getan habt, dass ihr immer an mich geglaubt habt und mich zu dem Menschen gemacht habt, der ich heute bin.

Zu guter Letzt danke ich meiner Freundin MADELEINE DORSCH für Deine Unterstützung auch in schwierigen Zeiten, für deine Geduld und Deine ruhige und liebenswerte Art, die mich immer wieder auf den Boden bringt. Ich danke Dir für einfach alles.

Table of Content

1. Introduction

Lubricants influence our daily life by giving us many advantages in devices we use every day. Most devices, where parts are moving or get in contact depend on lubricants. Riding a bicycle, driving a car, going by bus, or any industrial production of anything we buy and consume was manufactured with machines that would not work in the long term without any lubricants.[1] For this reason it is important to optimize the properties of each lubricant and adjust it individually for each task. As for lubricants that are used in motor oils, fuel consumption and efficiency become more and more important for car owners and manufacturers. The car industry has to react to this development by optimization of motors but also of new oil formulations that reduce fuel consumption.[2] One of the most important properties of an oil is the viscosity which influences fuel consumption to a high degree. On the one hand, oils have to be as thin, due to low viscosity, as possible to reduce the friction of the moving parts and minimize the force the motor has to overcome. On the other hand, the oil needs a specific thickness or viscosity, because insufficient lubrication would lead to damage of the motor. The viscosity of motor oil is a parameter which is mostly influenced by temperature. Increasing the temperature of a liquid like a motor oil below its boiling point results in decreasing viscosity.[3]

This is a big disadvantage in all uses of motor oils because machines and motors are getting hot during operation. For this effect, the viscosity index (VI) was introduced that describes the dependency of oil viscosity on temperature. This parameter can be optimized by adding VI improvers. These are compounds that increase their viscosity with the temperature. The higher viscosity at elevated temperatures counteracts the loss of viscosity of the motor oil.[4] VI improvers of Evonik Oil Additives (EOA) are based on poly(alkyl methacrylates) which have been used in lubricants for more than 70 years.[5] Here, the hydrodynamic radius is increased by long polymers that are switching from small coiled structures at low temperatures, that are uncoiling within higher temperatures. This uncoiling mechanism is based on an increased solubility in higher temperatures. Unfortunately, the use of methacrylate-based VI improvers in fuel efficient formulations is limited due to the disintegration of the additive. Therefore, new systems are searched to replace the poly(alkyl methacrylates) with a new mechanism of developing increased viscosities at elevated temperatures. For this reason, this thesis is dealing with the development of a new VI improver system based on supramolecular interactions.

[1] W. Dresel and T. Mang, *Lubricants and Lubrication, Vol. Volume 2*, Wiley-VCH Verlag GmbH & Co. KGaA, Weinheim, Germany, **2017**.
[2] W. van Dam, P. Kleijwegt, M. Torreman and G. Parsons, *SAE Int.* **2009**, *01*, 2856.
[3] J. Williamson, *Nature* **1951**, *167*, 316-317.
[4] M. J. Covitch and K. J. Trickett, *Adv. Chem. Eng. Sc.* **2015**, *5*, 134-151.
[5] M. J. Covitch, *Olefin Copolymer Viscosity Modifiers. In: Lubricant Additives*, Boca Raton, **2009**.

2. Background Information

2.1 Supramolecular Chemistry

Supramolecular chemistry is a field of chemistry concerning interactions between molecules that gained an increased importance in the last decades.[6] Since aggregation in supramolecular systems is behaving equally to many biological systems like the structure of DNA or viruses, natures supramolecular chemistry can be investigated and better understood by researching supramolecular systems.[7] Studying smaller and not as complex systems as found in nature is the first step in understanding nature's chemistry.

While traditional chemistry is dealing with covalent bonds, supramolecular chemistry is all about weaker non-covalent interactions.[8] Large and synthetical challenging structures are often difficult to realise in covalent synthesis due to irreversibility or the usage of protecting groups to enable orthogonal synthesis. In contrast, supramolecular chemistry allows the self-assembly of molecular building blocks in a defined and programmed fashion, thus generating complex structures without the need for lengthy synthesis. In addition, the use of reversible, non-covalent interactions can give rise to dynamic systems that can adapt and change their properties in response to external influences.[9,10]

Supramolecular chemistry makes use of non-covalent forces between molecules, including forces like hydrogen bonds, metal coordination, van der Waals-, electrostatic- or hydrophobic forces.[11] The binding energy of supramolecular bonds compared to covalent is far lower.[12] The formation and breaking of supramolecular bonds are therefore highly dependent on external conditions like temperature, pH or solvent.[13] Therefore, these conditions are decisive in the successful formation of supramolecular systems. With each type of interaction or combination thereof, a broad spectrum of new supramolecular systems can be realised. The combination of different forces results in different binding units that can be used in molecular recognition, host-guest chemistry or molecular self-assembly.[14]

[6] J. L. Atwood, G. W. Gokel and Y. Murakami, *Supramol. Chem.* **1995**, *6*, 1762-1763.

[7] a) N. C. Seeman, *Angew. Chem., Int. Ed.* **1998**, *110*, 3408-3428; b) B. A. Yankner, *Neuron* **1996**, *16*, 921-932; c) F. Crick and J. Watson, *Angew. Chem., Int. Ed.* **1983**, *95*, 579-596.

[8] H. J. Schneider, *Angew. Chem., Int. Ed.* **2009**, *48*, 3924-3977.

[9] M. J. Serpe and S. L. Craig, *Langmuir* **2007**, *23*, 1626-1634.

[10] P. Cordier, F. Tournilhac, C. Soulié-Ziakovic and L. Leibler, *Nature* **2008**, *451*, 977-980.

[11] F. Biedermann and H. J. Schneider, *Chem. Rev.* **2016**, *116*, 5216-5300.

[12] L. Brunsveld, B. J. B. Folmer, E. W. Meijer and R. P. Sijbesma, *Chem. Rev.* **2001**, *101*, 4071-4097.

[13] T. Rehm and C. Schmuck, *Chem. Commun.* **2008**, 801-813.

[14] G. V. Oshovsky, D. N. Reinhoudt and W. Verboom, *Angew. Chem., Int. Ed.* **2007**, *46*, 2366-2393.

Especially molecular self-assembly is used to create large supramolecular systems. Attaching two or more binding units to one building block results in the formation of networks and polymers.[15] In addition, the binding units can contain different interaction forces, to obtain highly controllable assemblies. On the one hand, these binding units can be used to realise self-assembly, where self-complimentary binding units are used to generate homodimers or homomers (Figure 1).[16]

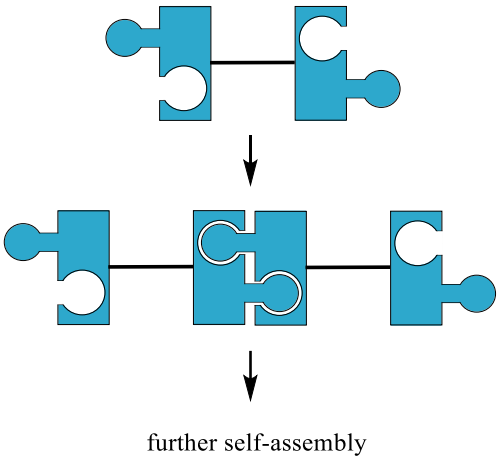

Figure 1: Self-assembly of self-complimentary binding units to form homodimers and homomers.

The blue binding unit is representing a self-complimentary group. Only the same kind of binding unit is able to interact with itself. In this example, a ditopic molecule is used, which enables the system to generate homomers with further self-assembly. The self-assembly of self-complimentary binding units can be used for the formation of large supramolecular polymers.

On the other hand, there are different binding units that can be complimentary to each other. Here, a specific counterpart to each binding unit is necessary to realise an interaction and to generate heterodimers and heteromers (Figure 2).

[15] T. F. A. De Greef, M. M. J. Smulders, M. Wolffs, A. P. H. J. Schenning, R. P. Sijbesma and E. W. Meijer, *Chem. Rev.* **2009**, *109*, 5687-5754.

[16] C. Wang, Z. Wang and X. Zhang, *Acc. Chem. Res.* **2012**, *45*, 608-618.

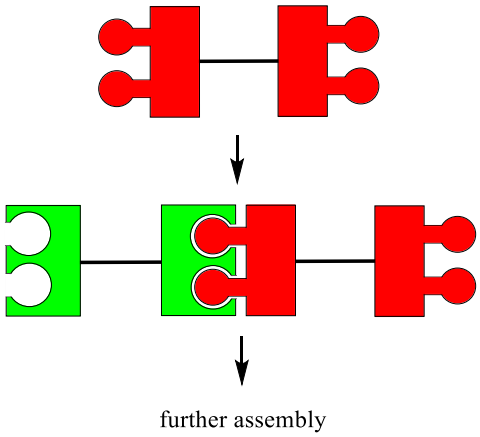

Figure 2: Assembly of hetero-complimentary binding units to form heterodimers and heteromers.

The red binding unit is hetero-complimentary and is not able to interact with itself. Only a specific counterpart (green) is able to interact and generate heterodimers or heteromers. This method can be used to initiate a polymerization by adding one kind of monomers to another. Using these self-complimentary and hetero-complimentary binding units, broad supramolecular structures can be realised, by combining these two methods (Figure 3).

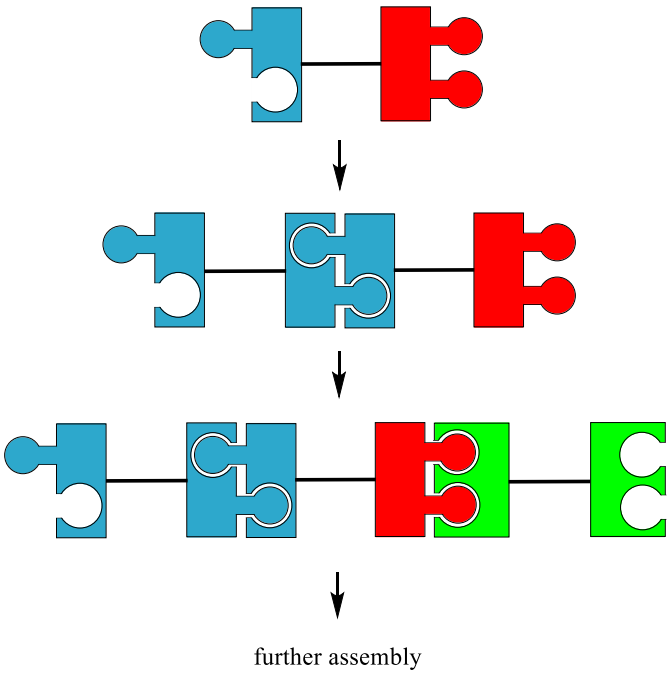

Figure 3: Formation of supramolecular aggregates, with functionalized monomers and different binding motifs.

Here, these different binding units are used to obtain a highly controllable formation of supramolecular systems. Besides the interaction forces, the shape complimentary properties of each binding unit is important, so that only a precise sequence of building blocks is possible.

2.2 Self-complementary Systems

Self-complementary systems are used in a broad field of supramolecular chemistry, especially in the formation of self-assembled supramolecular structures.[17] The advantages of self-assembled structures are, that every step of its synthesis is highly controllable and reversable. Each reaction can be precisely controlled. In addition to that, the synthesis is much easier, while the synthesis is concentrating on small building blocks that are able to carry out a self-assembly to achieve the desired structure.

2.2.1 Ureidopyrimidone Motif

The self-assembly of supramolecular molecules is of great interest in this thesis. Many self-assembling structures are based on hydrogen bonds. Since a single hydrogen-bond is mostly too weak to allow for an efficient self-assembly process at room temperature, in many cases double or triple hydrogen bonds are used.[18] Different binding units that contain multiple hydrogen bonds were developed and offer a variety of different functions. Patterns of multiple hydrogen bonds have been investigated for numerous receptors such as urea, guanines, barbiturates, self-assembled receptors or cyclic peptides.[19] Due to the structural complexity of these structures, the availability is limited and therefore, still more simple systems are searched.

Self-complementary binding motifs based on multiple hydrogen bonds were largely developed by *E. W. Meijer* and co-workers. The investigations also demonstrate how important the sequence of the hydrogen bond pattern is. Figure 4 shows heterodimeric complexes that bind via three hydrogen bonds, but differ in the sequence of hydrogen bond donors (D) and acceptors (A).[12]

[17] a) J. W. Steed and J. L. Atwood, *Supramolecular Chemistry*, Wiley, Chichester-Wiley, Chichester, **2000**; b) D. Philp and J. Fraser Stoddart, *Angew. Chem., Int. Ed.* **1996**, *35*, 1154-1196; c) F. Vögtle, *Supramolekulare Chemie*, Teubner, Stuttgart-Teubner, Stuttgart, **1992**; d) G. M. Whitesides, J. P. Mathias and C. T. Seto, *Science* **1991**, *254*, 1312-1319; e) F. Vögtle, *Cyclophan-Chemie*, Teubner, Stuttgart-Teubner, Stuttgart, **1990**.

[18] D. S. Lawrence, T. Jiang and M. Levett, *Chem. Rev.* **1995**, *95*, 2229-2260.

[19] a) T. W. Bell, Z. Hou, S. C. Zimmerman and P. A. Thiessen, *Angew. Chem., Int. Ed.* **1995**, *34*, 2163-2165; b) M. R. Ghadiri, J. R. Granja, R. A. Milligan, D. E. McRee and N. Khazanovich, *Nature* **1994**, *372*, 709-709; c) R. Wyler, J. de Mendoza and J. Rebek, *Angew. Chem., Int. Ed.* **1993**, *32*, 1699-1701; d) S. J. Geib, S. C. Hirst, C. Vicent and A. D. Hamilton, *J. Am. Chem. Soc.* **1991**, 1283-1285; e) T. W. Bell and J. Liu, *J. Am. Chem. Soc.* **1988**, *110*, 3673-3674.

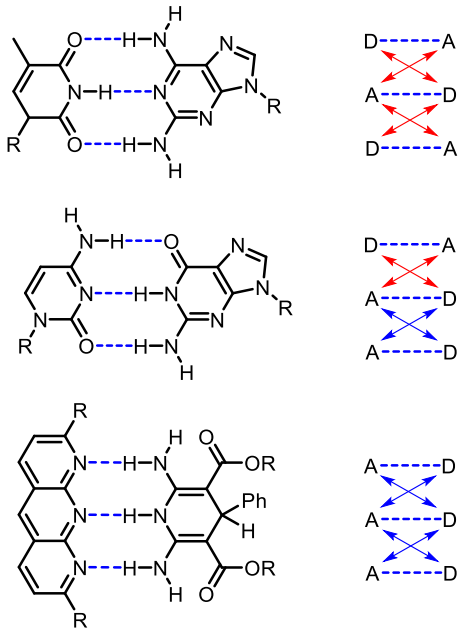

Figure 4: Complexes with different hydrogen-bonding motifs. Blue arrow: attractive secondary interaction, red arrow: repulsive secondary interaction; A: hydrogen bond acceptor, D: hydrogen bond donator.

While the DAD pattern seems to fit perfectly to the complimentary ADA motif, there are repulsive secondary interactions between the donor and the acceptor groups on opposite sides of the hydrogen-bond network. This leads to a somewhat lower association constant of $K_a = 10^2 - 10^3\ M^{-1}$. Using the DAA/ADD hydrogen bond pattern increases the association constant to $K_a = 10^4 - 10^5\ M^{-1}$ due to the occurrence of only one repulsive interaction. The AAA/DDD pattern, in contrast to that, results in an association constant of $K_a > 10^5\ M^{-1}$ due to the lack of any repulsive interaction.[12] *E. W. Meijer* and co-workers also investigated the use of self-complimentary subunits which feature four hydrogen bonds in a self-complimentary fashion. Therefore, the pattern of hydrogen donors (D) and acceptors (A) were changed until an optimal system with the minimum number of repulsive secondary interactions was found (Figure 5).[20]

[20] F. H. Beijer, R. P. Sijbesma, H. Kooijman, A. L. Spek and E. W. Meijer, *J. Am. Chem. Soc.* **1998**, *120*, 6761-6769.

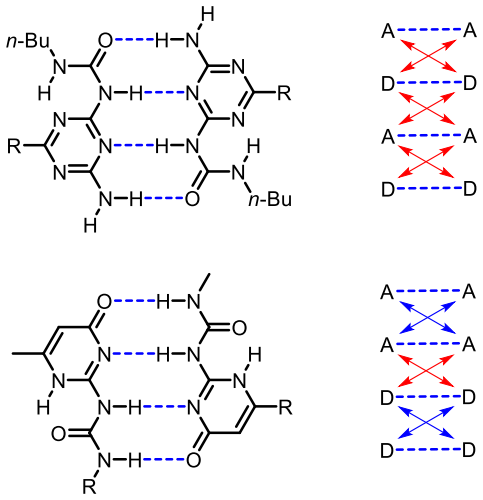

Figure 5: Tautomeric forms between monomer and dimer of the binding motif ADAD and AADD; Blue arrow: attractive secondary interaction, red arrow: repulsive secondary interaction; A: hydrogen acceptor, D: donator.

Increasing the number of hydrogen bonds in a binding unit does not automatically increase association constant.[21] The ADAD/DADA pair has an association constant of $K_a = 10^4$ - 10^5 M^{-1} due to the high number of repulsive secondary interactions. In comparison to that, the AADD/DDAA pair shows an association constant of $K_a > 10^6$ M^{-1}.[20] This motif contains an ureidopyrimidone function and has subsequently been used in many supramolecular systems. Besides the high association constant, the binding unit can be synthesized easily while using isocytosines and isocyanates in a simple coupling reaction.[22] One major application of the ureidopyrimidone unit was the development supramolecular polymers.

[21] a) F. H. Beijer, H. Kooijman, A. L. Spek, R. P. Sijbesma and E. W. Meijer, *Angew. Chem., Int. Ed.* **1998**, *37*, 75-78; b) D. L. Severance and W. L. Jorgensen, *J. Am. Chem. Soc.* **1990**, *112*, 4768-4774.

[22] F. H. Beijer, R. P. Sijbesma, J. A. J. M. Vekemans, E. W. Meijer, H. Kooijman and A. L. Spek, *J. Org. Chem.* **1996**, *61*, 6371-6380.

2.2.2 GCP-Motif

Another system which is able to perform supramolecular self-assembly based on hydrogen-bonding is the guanidinium carbonyl pyrrole (GCP) binding unit.[23] This binding motif was developed by Carsten Schmuck with the aim to bind anionic guest molecules, such as carboxylates, with high binding constants even in highly polar solvents (e.g. water).[24] This led to a system based on hydrogen bonds and electrostatic interactions.[25]

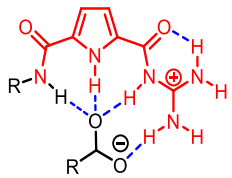

Figure 6: GCP binding motif, binding to a carboxylate.[23]

The basic structure of the GCP motif is containing a pyrrole building block, which is substituted with a guanidinium function.[26] During synthesis, an intermediate can be isolated with a free carboxylic acid and a guanidinium carbonyl pyrrole function.[27] This intermediate has an extremely low solubility, due to the zwitterionic character and self-complementary conditions. Therefore, a new binding unit was developed that was able to carry out homodimerization based in its self-complementarity (Figure 7).[28]

[23] C. Schmuck, *Eur. J. Chem.* **1999**, *9*, 2397-2403.

[24] a) M. A. Hossain and H. J. Schneider, *J. Am. Chem. Soc.* **1998**, *120*, 11208-11209; b) M. Davies, M. Bonnat, F. Guillier, J. D. Kilburn and M. Bradley, *J. Org. Chem.* **1998**, *63*, 8696-8703; c) R. Breslow, Z. Yang, R. Ching, G. Trojandt and F. Odobel, *J. Am. Chem. Soc.* **1998**, *120*, 3536-3537.

[25] C. Schmuck, *Chem. - Eur. J.* **2000**, *6*, 709-718.

[26] a) P. Barker, P. Gendler and H. Rapoport, *J. Org. Chem.* **1978**, *43*, 4849-4853; b) J. W. Harbuck and H. Rapoport, *J. Org. Chem.* **1972**, *37*, 3618-3622; c) J. B. Bicking, C. M. Robb, S. F. Kwong and E. J. Cragoe, *J. Med. Chem.* **1967**, *10*, 598-602.

[27] a) Y. J. Zhengt and R. L. Ornstein, *J. Am. Chem. Soc.* **1996**, *118*, 11237-11243; b) B. Dietrich, D. L. Fyles, T. M. Fyles and J.-M. Lehn, *Helv. Chim. Acta* **1979**, *62*, 2763-2787.

[28] C. Schmuck, *Chem. Commun.* **1999**, *9*, 843-844.

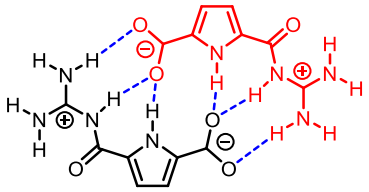

7

Figure 7: Self-complementary GCP zwitterion 1 forming a dimer.[29]

This system of a zwitterionic GCP-carboxylate can be used, in the formation of self-complementary dimers in various systems.[23] Even in polar solvents a high association constant occurred. With an association constant in DMSO of $K > 10^{10}$ M^{-1} and even in water of $K = 170$ M^{-1} the dimerization is even stronger than the hydrogen bond pattern of the ureidopyrimidone dimer with an association constant of 10^6 M^{-1} in chloroform.[29] Therefore, this binding motif can be used in the formation of supramolecular polymers. The dimerization only occurs in a specific pH range of 5 to 8, where the zwitterionic character occurs and the self-complementary properties can be obtained. If the pH value is changed beyond this range, the zwitterionic GCP-carboxylate is either protonated (to give a cation) or deprotonated (to give an anion). This destroys the self-complimentary of the binding motif and thus leads to disassembly of the supramolecular aggregates. This effect can be used to influence supramolecular systems with external conditions (pH) and was already used in various supramolecular polymers[30], gels[31] and nanostructures.[32]

2.2.3 ACP-Motif

Due to the high polarity of the GCP zwitterion, the solubility in unpolar solvents is limited. Therefore, a neutral analogue (ACP) was developed with similar properties. This also allowed for an investigation about the importance of electrostatic interactions for the dimerization process.[25]

[29] C. Schmuck, *Coord. Chem. Rev.* **2006**, *250*, 3053-3067.

[30] a) M. D. Segarra-Maset, V. J. Nebot, J. F. Miravet and B. Escuder, *Chem. Soc. Rev* **2013**, *42*, 7086-7098; b) P. Terech and R. G. Weiss, *Chem. Rev.* **1997**, *97*, 3133-3159.

[31] a) P. Sahoo, R. Sankolli, H. Y. Lee, S. R. Raghavan and P. Dastidar, *Chem. - Eur. J.* **2012**, *18*, 8057-8063; b) E. A. Appel, J. Del Barrio, X. J. Loh and O. A. Scherman, *Chem. Soc. Rev* **2012**, *41*, 6195-6214; c) J. W. Steed, *Chem. Commun.* **2011**, *47*, 1379-1383.

[32] a) Y. Hisamatsu, S. Banerjee, M. B. Avinash, T. Govindaraju and C. Schmuck, *Angew. Chem., Int. Ed.* **2013**, *52*, 12550-12554; b) M. T. Fenske, W. Meyer-Zaika, H. G. Korth, H. Vieker, A. Turchanin and C. Schmuck, *J. Am. Chem. Soc.* **2013**, *135*, 8342-8349; c) G. Gröger, W. Meyer-Zaika, C. Böttcher, F. Gröhn, C. Ruthard and C. Schmuck, *J. Am. Chem. Soc.* **2011**, *133*, 8961-8971.

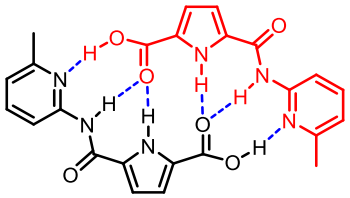

8

Figure 8: Neutral analogue of the GCP zwitterion, Amidopyridin carbonyl pyrrole (ACP) motif 2.[29]

In Figure 8 the self-assembly of this new ACP motif **8** is pictured, where a similar interaction occurs as seen in the GCP motif. By replacing the guanidinium function with an amino-methyl-pyridine a dimerization of the system occurs only mediated by hydrogen bonds. Investigations are proving a decrease of the association constant ($K > 10^6\ M^{-1}$ in chloroformic solution) which was expected due to the lack of ionic interactions. Addition of small amounts of competitive solvents like DMSO leads to further decrease of the association constants. This is the reason, why the application of the ACP motif **8** for supramolecular self-assembly is more likely carried out in unpolar solvents.[33]

The ACP binding unit was investigated in comparison to the GCP motif **7** also by X-ray crystal structure analysis as shown in Figure 9.[33]

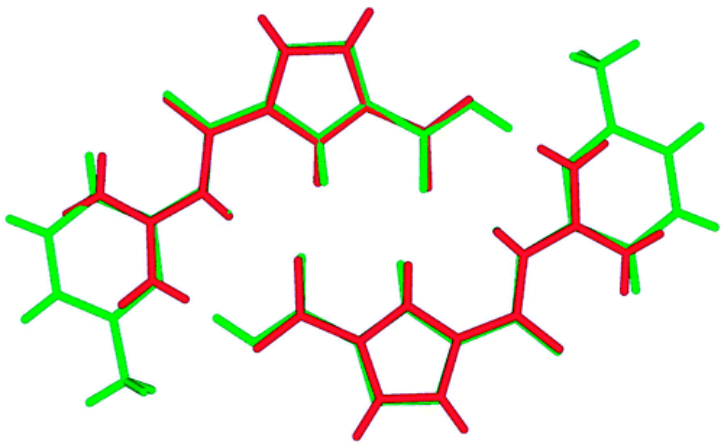

Figure 9: X-ray measurements: GCP zwitterion 7 (red) and ACP motif 8 (green) of *Schmuck et al.*[33] Reprinted with permission from ([33] C. Schmuck and W. Wienand, *J. Am. Chem. Soc.* 2003, *125*, 452-459.). Copyright (2020) American Chemical Society.

These X-ray measurements demonstrate the structures overlay in the main binding area. All binding lengths and angles are almost the same for both motifs **7** and **8**. Therefore the overall binding geometry is identical, but the strength of the dimerization is different.[33] Due to the high sensibility of the ACP

[33] C. Schmuck and W. Wienand, *J. Am. Chem. Soc.* **2003**, *125*, 452-459.

motif **2** to polar solvents and the fact, that there are self-complementary binding motifs which obtain a higher association constant (ureidopyrimidone), the motif **8** has only found limited application in supramolecular self-assembly so far.[20]

2.2.4 BINOL in supramolecular Chemistry

Another molecular building block used in this thesis is the 1,1′-binaphthyl-2,2′-diol (BINOL) unit. BINOL was first successfully synthesized in 1926 since the interest in this compound, due to its versatile synthetic chemistry and its inherent chirality increased over the years.[34] Due to its axial chirality, BINOL can occur as an *(R)*- or *(S)*-enantiomer.[35]

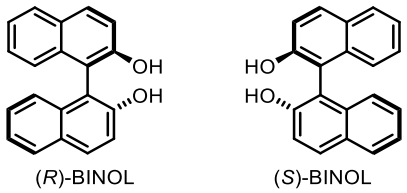

Figure 10: Conformations of BINOL.

The two naphthol units are orthogonally arranged, and the free rotation is hindered due to a high rotation barrier of 155 – 159 kJ/mol.[36] Additionally, the easy synthesis and substitution enables the use of this system as a building block in numerous scientific investigations.[37] In the following Figure 11 the possible substitution positions of BINOL are displayed.[38] In most cases, both naphthyl-rings are substituted at the same time to give C_2-symmetric derivatives.

[34] R. Pummerer, E. Prell and A. Rieche, *Chem. Ber.* **1926**, *95*, 2159-2161.
[35] L. Meca, D. Reha and Z. Havlas, *J. Org. Chem.* **2003**, *68*, 5677-5680.
[36] A. Sakakura, K. Suzuki and K. Ishihara, *Adv. Synth. Catal.* **2006**, *348*, 2457-2465.
[37] a) J. M. Brunel, *Chem. Rev.* **2005**, *105*, 857-897; b) Y. Chen, S. Yekta and A. K. Yudin, *Chem. Rev.* **2003**, *103*, 3155-3211.
[38] H. L. Liu, Q. L. Zhao, X. L. Hou and L. Pu, *Chem. Commun.* **2011**, *47*, 3646-3648.

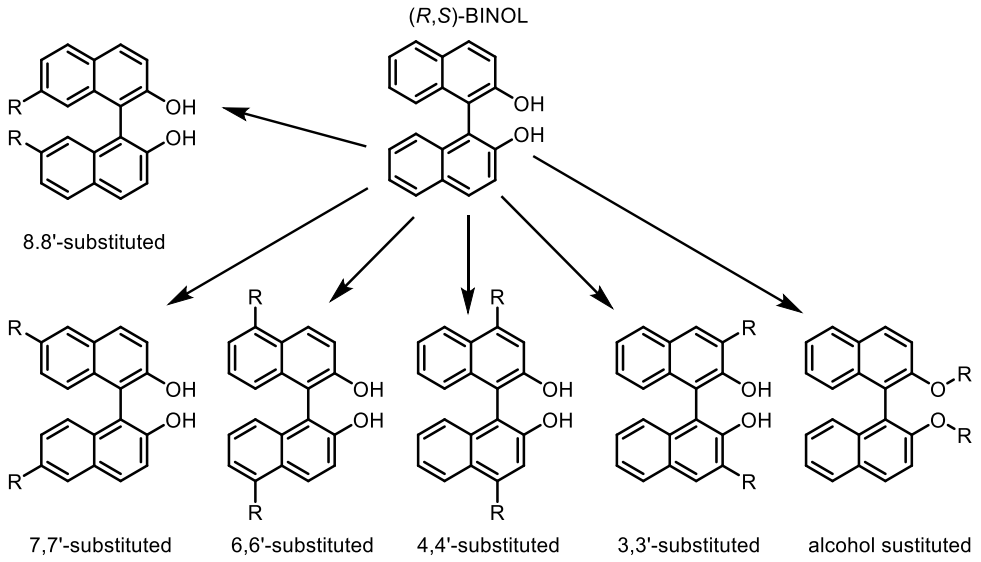

Figure 11: Possible structure motifs of BINOL due to substitution.

Besides the alcohol substitution of BINOL, almost every position can be modified. Therefore, it is possible for example, to carry out an etherification to obtain a crown ether with included BINOL function (Figure 12).

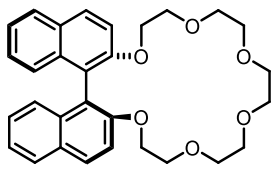

9

Figure 12: BINOL implemented crown ether 3 of *Cram et al.*[39]

Additionally, the position of the substitution can be controlled by different conditions, bromination methods, metalations or oxidative couplings.[40] With these methods, imidazole substituted BINOL can be generated in different positions (Figure 13).[41]

[39] E. B. Kyba, K. Koga, L. R. Sousa, M. G. Siegel and D. J. Cram, *J. Am. Chem. Soc.* **1973**, *95*, 2692-2693.

[40] a) C. Valente, E. Choi, M. E. Belowich, C. J. Doonan, Q. Li, T. B. Gasa, Y. Y. Botros, O. M. Yaghi and J. F. Stoddart, *Chem. Commun.* **2010**, *46*, 4911-4913; b) Y. Liu, Q. Miao, S. Zhang, X. Huang, L. Zheng and Y. Cheng, *Macromol. Chem. Phys.* **2008**, *209*, 685-694; c) P. J. Cox, W. Wang and V. Snieckus, *Tetrahedron Lett.* **1992**, *33*, 2253-2256; d) G. Sogah, Y. Dotsevi and D. J. Cram, *J. Am. Chem. Soc.* **1979**, *101*, 3035-3042.

[41] R. C. Helgeson, J. M. Timko, P. Moreau, S. C. Peacock, J. M. Mayer and D. J. Cram, *J. Am. Chem. Soc.* **1974**, *96*, 6762-6763.

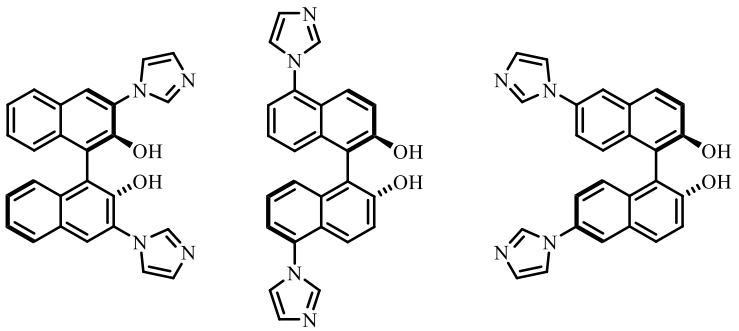

(*R*)-**10** (*R*)-**11** (*R*)-**12**

Figure 13: Substituted BINOL in the 3,3'- [*(R)*-10], 6,6'- [*(R)*-11] and 7,7'- [*(R)*-12] position of *Su* and *et al*.[42]

Using different bromination conditions or borates, lead to the formation of different imidazole-BINOL derivatives. In addition, the 1,1'-binaphthyl-backbone can be modified with alternative heteroatoms in the 2,2'-positions, such as phosphorous (e.g. in 2,2'-Bis(diphenylphosphino)-1,1'-binaphthyl [BINAP]) or nitrogen (e.g. in 1,1′-Binaphthyl-2,2′-diamine [BINAM]) (Figure 14).[43]

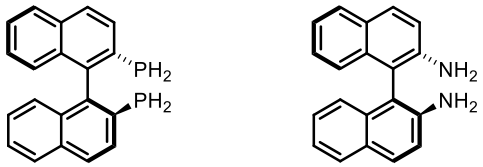

Figure 14: Derivates of BINOL: BINAP (left) and BINAM (right).[43]

BINAM is a highly versatile synthetic building block since the nucleophilic amino-groups can easily be modified (e.g. to give amide bonds, urea or carbamate functionalities).[44] For example, the attachment of amino acids or other carboxylates to give highly stable diamides with an orthogonally arrangement of the residues is easily possible.[45]

[42] L. Yang, F. Yang, J. Lan, G. Gao, J. You and X. Su, *Org. Biomol. Chem.* **2011**, *9*, 2618-2621.

[43] R. Noyori and H. Takaya, *Acc. Chem. Res.* **1990**, *23*, 345-350.

[44] R. Holakovský, M. Pojarová, M. Dušek, J. Čejka and I. Císařová, *Acta Crystallogr., Sect. E: Crystallogr. Commun.* **2011**, *67*.

[45] J. Otevrel, D. Svestka and P. Bobal, *Org. Biomol. Chem.* **2019**, *17*, 5244-5248.

2.2.5 Supramolecular Polymerization

Supramolecular polymerization is a large field in supramolecular chemistry. The classic definition of polymeric substances is the occurrence of long chains, of short repeating units linked by covalent bonds.[46] At the beginning of the history of supramolecular polymers, many examples are given, of a combination of covalent and supramolecular interactions.[47, 48]

The introduction of supramolecular polymers was a great addition to the self-assembly of molecules, to build large structures, used in chemistry[49], physics[50] or biology.[51] Therefore, supramolecular polymers were classified as the self-assembly of monomers, with reversible, noncovalent and directional interactions, to form linear, high molecular weight polymers.[15] Especially the generation of supramolecular polymers that carry out similar mechanical properties as covalent polymers, resulted in great attention.[52]

Polymerization reactions of covalent polymers are often carried out under kinetic control. Therefore, the size of the final polymer is determined during the polymerization process, but not influenced by the external conditions afterwards (e.g. elevated temperatures or dilution). In contrast to this, the formation of supramolecular polymers is related directly to concentration, temperature and pressure.[15]

The simplest supramolecular polymer can be generated from a ditopic monomer that contains two self-complimentary binding units, as shown in Figure 15. Mechanistically, there are three major growth mechanisms of supramolecular polymers, isodesmic, ring chain mediated and cooperative supramolecular polymerization.[15] The isodesmic supramolecular polymerization describes the formation of polymers, in which every reaction with a new monomer is identical (Figure 15).

[46] H. Staudinger, *Ber. d. D. Chem. Gesellschaft* **1920**, *53*, 1073-1073.

[47] a) C. Tang, E. M. Lennon, G. H. Fredrickson, E. J. Kramer and C. J. Hawker, *Science* **2008**, *322*, 429-432; b) M. Schappacher, *Science* **2008**, *319*, 1512-1516; c) X. Wang, I. Manners and M. Winnik, *Science* **2007**, *644*, 644-648.

[48] J. J. L. M. Cornelissen, M. Fischer, N. A. J. M. Sommerdijk and R. J. M. Nolte, *Science* **1998**, *280*, 1427-1430.

[49] D. J. Worsfold and S. Bywater, *Polym. Sci.* **1957**, *26*, 299-304.

[50] M. W. Zwierlein, C. A. Stan, C. H. Schunck, S. M. F. Raupach, S. Gupta, Z. Hadzibabic and W. Ketterle, *Phys. Rev. Lett.* **2003**, *91*, 2101-2104.

[51] F. M. Brodsky, C.-Y. Chen, C. Knuehl, M. C. Towler and D. E. Wakeham, *Annu. Rev. Cell Dev. Biol.* **2001**, *17*, 517-568.

[52] R. P. Sijbesma, F. H. Beijer, L. Brunsveld, B. J. B. Folmer, J. H. K. K. Hirschberg, R. F. M. Lange, J. K. L. Lowe and E. W. Meijer, *Science* **1997**, *278*, 1601-1604.

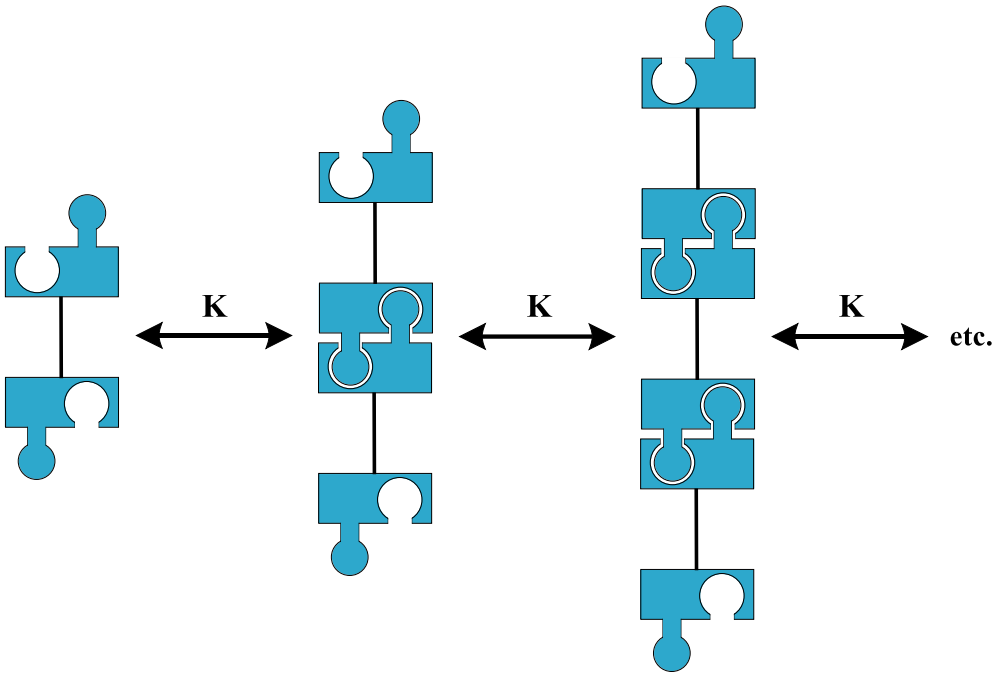

Figure 15: Example of an isodesmic supramolecular polymerization, with a ditopic monomer featuring two self-complimentary binding motifs (blue).[15]

Starting with the interaction of two monomers, the growth of the polymer results in equally step by step reactions, of a new monomer. Therefore, the associations constant K of every step of the polymerization is equal and the free Gibbs energy decreases with every step of the polymerization. There are many examples for isodesmic supramolecular polymerizations for example via π-π interactions, like the investigations of *Moore* and co-workers in Figure 16.[53]

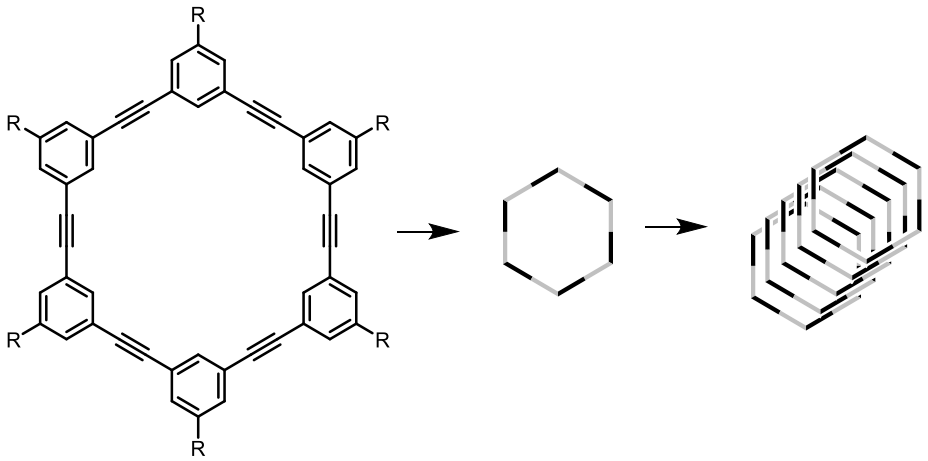

Figure 16: Example of a monomeric unit, which polymerises using isodesmic mechanism by *Moore* and co-workers.[53]

[53] D. Zhao and J. S. Moore, *Chem. Commun.* **2003**, *7*, 807-818.

Supramolecular polymers built in isodesmic polymerization are existing in an equilibrium between the monomeric unit and the polymer. This equilibrium can especially be influenced by temperature and concentration. Elevating the temperature of a supramolecular polymer leads to a cleavage of supramolecular interactions and pushes the equilibrium in the direction of the monomeric units. In contrast to that, increasing the concentration leads to a higher formation of the polymers.[15] Besides the isodesmic polymerization, there is the ring-chain polymerization (Figure 17).

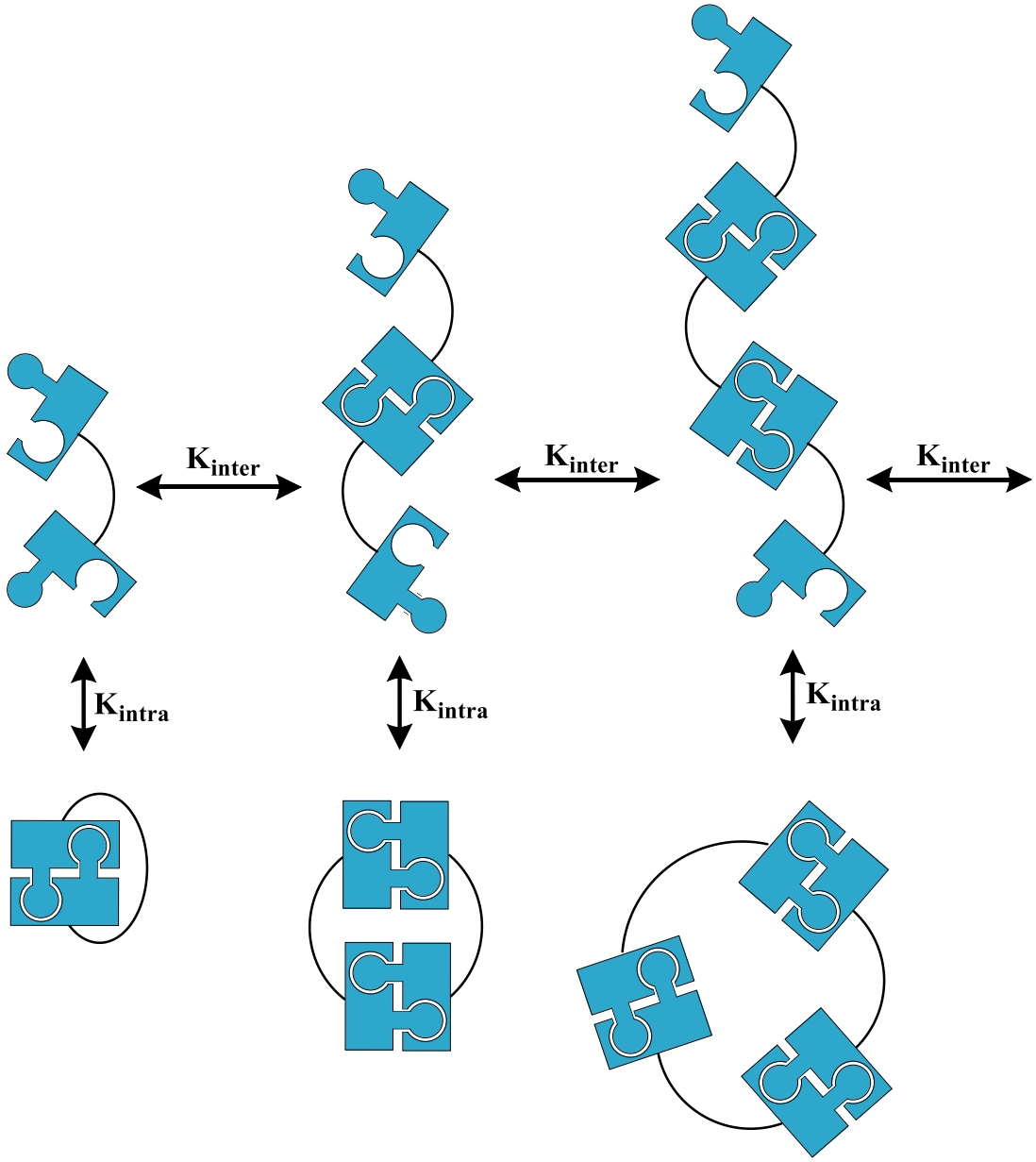

Figure 17: Schematic representation of a ring chain supramolecular polymerization.

This class of supramolecular polymerization occurs as a polymerization in which every monomeric unit is in equilibrium between an intermolecular polymerization/dimerization with another monomer and an

intramolecular formation of a cyclic structure (or ring).[54] The ring chain polymerization is especially dependent on the concentration of the system. In high concentrations, the formation of polymeric structures is favoured, due to the chance of two monomers interacting with each other. Therefore, at low concentrations, mostly cyclic ring structures are occurring. In the ring chain polymerization two different association constants occur. K_{inter} describes association constant of the polymerization and the growth of the polymer, similar to the isodesmic polymerization. But the formation of the cyclic structures occurs in a different association constant K_{intra}. K_{inter} and K_{intra} differ, due to the ring tension of the cyclic structures. Therefore, the progress of the polymerization can be observed by dividing K_{intra} with K_{inter}. Elevating the temperature results, equally to the lowering of the concentration, to the reformation of the monomeric units.[15] An example of a ring chain polymerization is another investigation by *E.W. Meijer* and co-workers with the ureidopyrimidone binding unit **13** (Figure 18).[55]

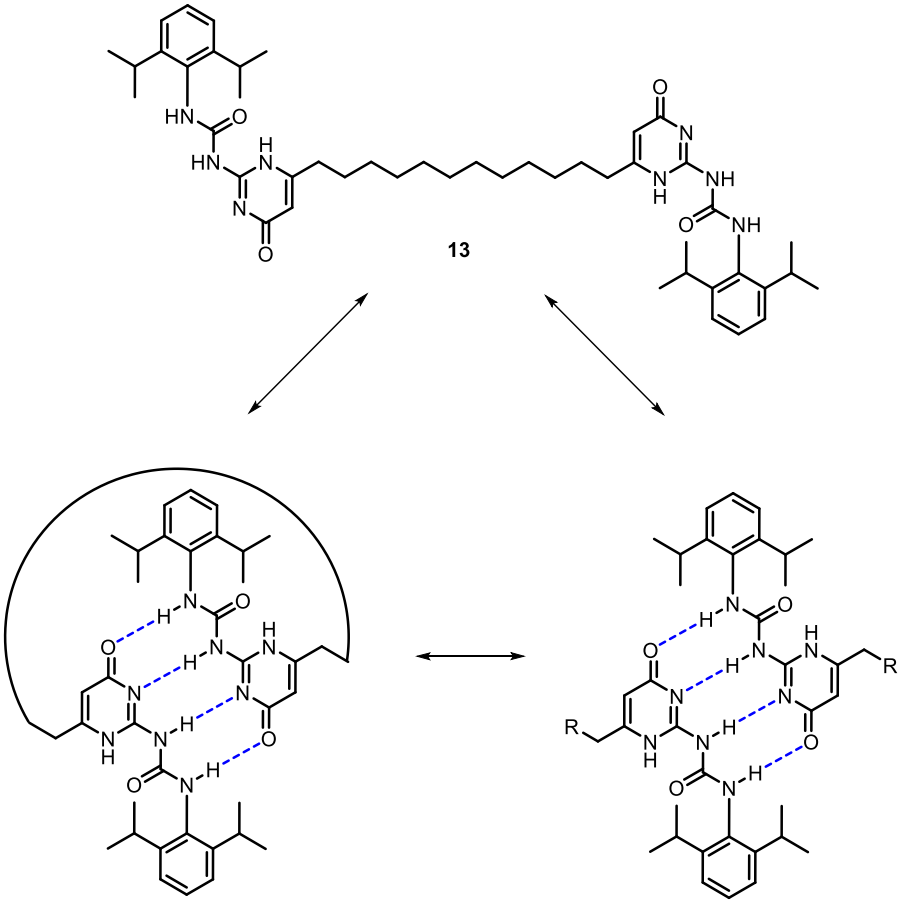

Figure 18: Ureidopyrimidone-undecane derivative 13 as ring chain polymer.[55]

[54] a) E. W. Spanagel and Wallace H. Carothers, *J. Am. Chem. Soc.* **1935**, *57*, 935-936; b) J. W. Hill and W. H. Carothers, *J. Am. Chem. Soc.* **1933**, *55*, 5031-5039.

[55] S. H. M. Söntjens, R. P. Sijbesma, M. H. P. Van Genderen and E. W. Meijer, *Macromolecules* **2001**, *34*, 3815-3818.

The third growth mechanism is the cooperative supramolecular polymerization. In this mechanism two different stages are occurring. The first stage is similar to the linear isodesmic supramolecular polymerization, where the polymerization occurs with a specific association constant K_n. After the formation of a specific degree of polymerization, the interaction of another monomer occurs with a different association constant K_e.[15]

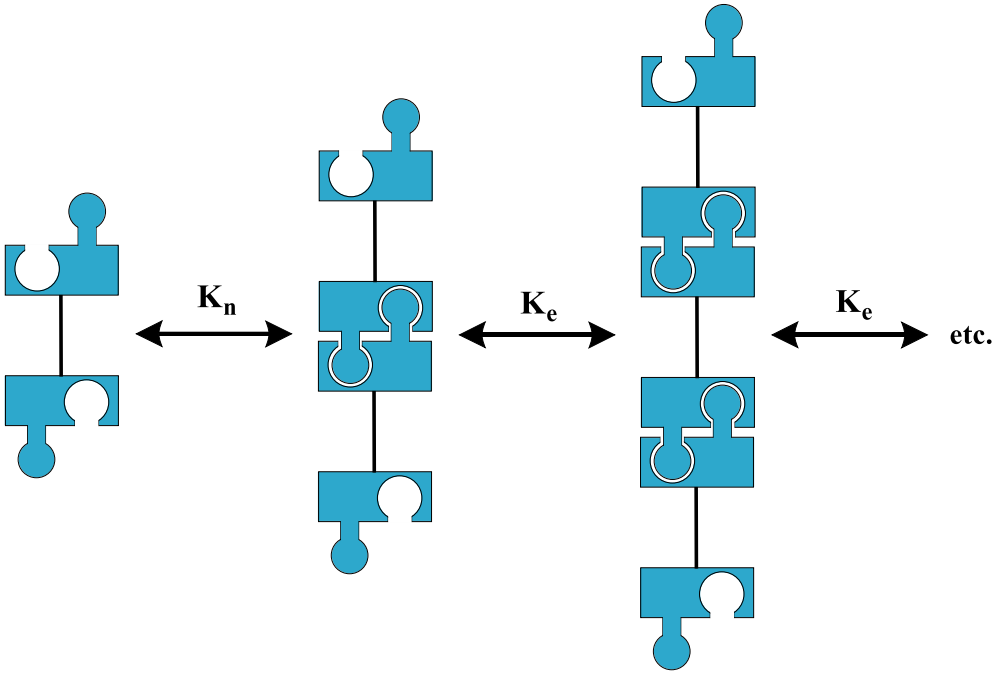

Figure 19: Schematic representation of the cooperative supramolecular polymerization.

Like in every supramolecular polymerization, an increase of the temperature and lowering of the concentration leads to a decrease of the polymeric structures. Special about this polymerization is, that there are two different association constants. In the first stage while the first monomers are interacting with each other, the association constant K_n occurs. This association constant is increasing in the second stage to K_e. This change of the association constant can occur in supramolecular systems that are changing the binding structure while interacting to favour another interaction.[15]

2.2.6 Examples of supramolecular Structures

Supramolecular monomers that feature two or more binding motifs as described before, are often used in supramolecular structures like supramolecular polymers. One binding motif mentioned before is the ureidopyrimidone binding motif of *E. W. Meijer* and co-workers.[15] Depending on the exact structure of

the multitopic monomer different structures can be observed, for example networks or linear structures.[56] Attaching two ureidopyrimidone motifs to a linker, results in an intermolecular interaction and the formation of supramolecular polymers (Figure 20).[52]

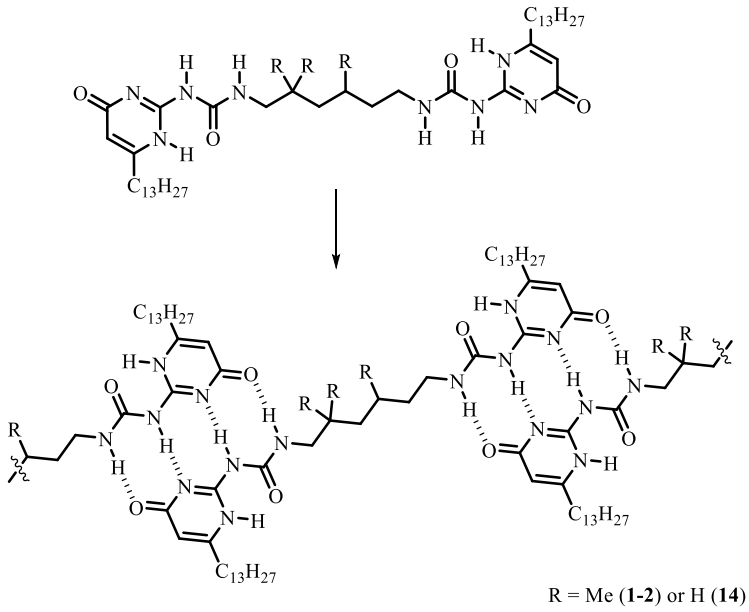

Figure 20: Polymerization of the ureidopyrimidone motif attached to a linear linker.[52]

The ureidopyrimidone was substituted with a C_{13} chain to enhance the solubility in unpolar solvents. In this case, chloroform was used since this enables a sufficiently strong pairing of the binding units (Figure 20). The linker unit is employed to enable an intramolecular cyclization or the intermolecular polymerization, so that the supramolecular polymerization follows a ring chain mechanism. Additionally to these ditopic monomers, which result in linear polymers, a tritopic system with three different binding units was described. This enabled the formation of a branched and crosslinked supramolecular polymer.[52] This material obtains mechanical properties that are comparable to these of normal covalent polymers, despite the fact that it is based on weak supramolecular interactions. Here, mechanical properties like viscosity were investigated in dependence of the concentration. The system showed in Figure 20 is able to form cyclic structures and exists in an equilibrium between linear polymeric and oligomeric cyclic structures. This equilibrium is controlled by increasing or decreasing the concentration. Elevating the concentration, results in a higher probability for intermolecular interactions and to a generation of polymeric structures. Decreasing the concentration leads to the

[56] a) A. Jangizehi, S. R. Ghaffarian, W. Schmolke and S. Seiffert, *Macromolecules* **2020**, *53*, 491-493; b) M. Golkaram, C. Fodor, E. Van R. and K. Loos, *Macromolecules* **2018**, *51*, 4910-4916.

formation of cyclic structures. This behaviour can be observed in measurements of the viscosity (Figure 21).

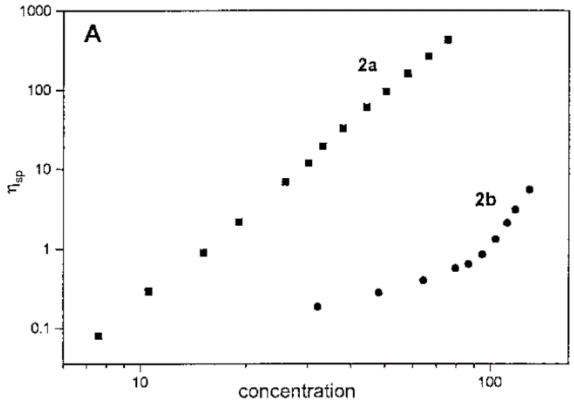

Figure 21: Specific viscosity in dependence of the concentration of compound 14 (2a) and 1-2 (2b) in chloroformic solutions.[52] From [R. P. Sijbesma, F. H. Beijer, L. Brunsveld, B. J. B. Folmer, J. H. K. K. Hirschberg, R. F. M. Lange, J. K. L. Lowe and E. W. Meijer, *Science* 1997, *278*, 1601-1604.]. Reprinted with permission from AAAS.

The specific viscosity (chapter 2.3 Viscosity) is indicating the size of the solved structures. Therefore, the viscosity is elevating in higher concentration due to the formation of polymeric structures. Similar to Meijer's system, most other supramolecular polymers are only stable in unpolar solvents like chloroform since hydrogen bonds are very sensitive to competing solvents.

Another example of supramolecular structures is based on the investigations of *C. Schmuck* and co-workers. The self-assembly system containing GCP is used to enable pH switchable structures (Figure 22).[32]

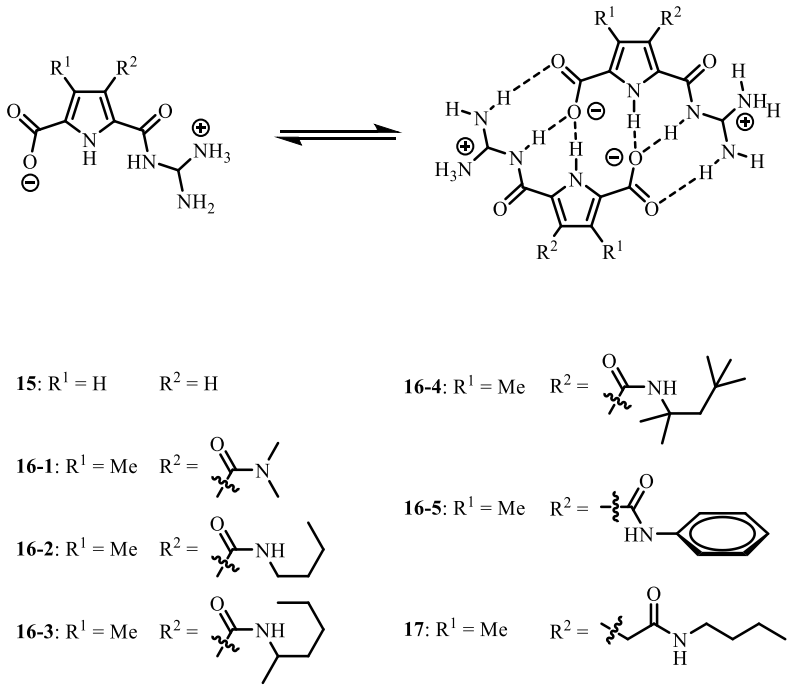

Figure 22: Investigations of Schmuck *et al.* of supramolecular structures based on the GCP motif.[32]

Because of the self-assembly in a pH range of 5 to 8, an assembly can be initiated by adjusting the pH range. However, since this binding motive does not form any aggregates larger that dimers, a second interaction type has to be developed to generate large supramolecular structures. Aromatic systems are able to perform intermolecular π-π-stacking.[57] This is the reason why the monomeric units in Figure 22 are attached with aryl- and alkyl-groups, to support the π-π-stacking.

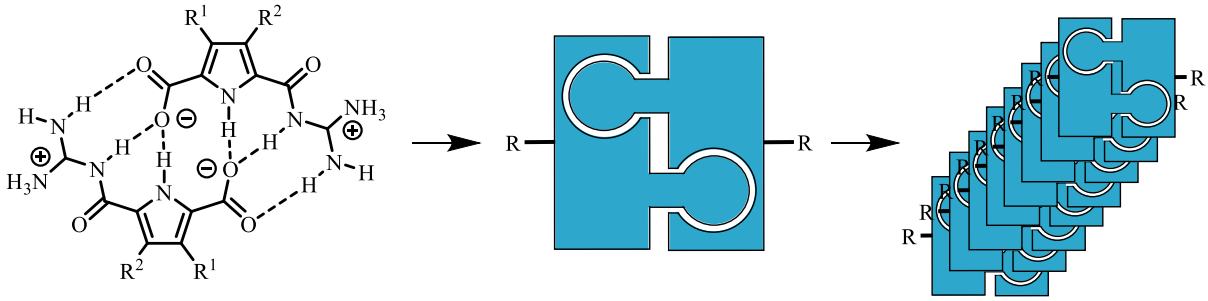

Figure 23: One-dimensional rod by π-stacking of GCP-dimer.

[57] R. Martel T.-Q. Nguyen, P. Avouris, M. L. Bushey, L. Brus, C. Nuckolls, *J. Am. Chem. Soc.* **2003**, *126*, 5234-5242.

This is a perfect example for polymerizations via cooperative self-assembly. Due to the interaction of these dimers, large supramolecular structures are formed. These large systems can be observed by AFM and TEM measurements (Figure 24).[32]

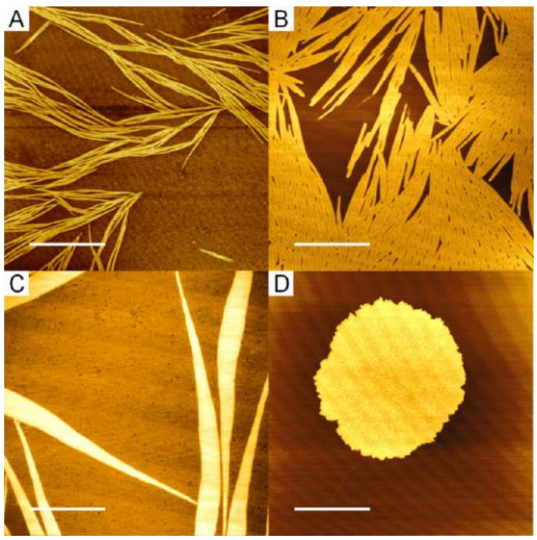

Figure 24: AFM images of the investigations of *Schmuck* and co-workers. A: 16-3, B: 16-4, C: 16-5 and D: 17.[32] Reprinted with permission from ([32] M. T. Fenske, W. Meyer-Zaika, H. G. Korth, H. Vieker, A. Turchanin and C. Schmuck, *J. Am. Chem. Soc.* 2013, *135*, 8342-8349). Copyright (2020) American Chemical Society

Here, large needle-like structures are observed for the structures of **16-3**, **16-4** and **16-5**. Structure **17** is showing a different behaviour, by generating circular layer-like structures in contrast to all other monomers. Therefore, these investigations are showing the importance of the influence of side chains. By adjusting the pH to higher values than 8 or lower than 5, these structures can be destroyed, which is a great result in developing new smart materials that can be tuned by changing the external conditions.

2.3 Viscosity

This thesis especially deals with the optimization of viscosity properties of different solvents. The viscosity is a way to measure the fluidity of a liquid or gaseous material. It is a parameter that describes the resistance to any deformation at a specific speed.[58] Looking at liquids, a flowing of the substance can be initiated by a specific force. The force which is counteracting to this deformation results in inner friction of the liquid. Therefore, the force that needs to be used, is proportional to the flow rate.[59] To explain this behaviour, Figure 25 is demonstrating a simplified liquid between to plates.

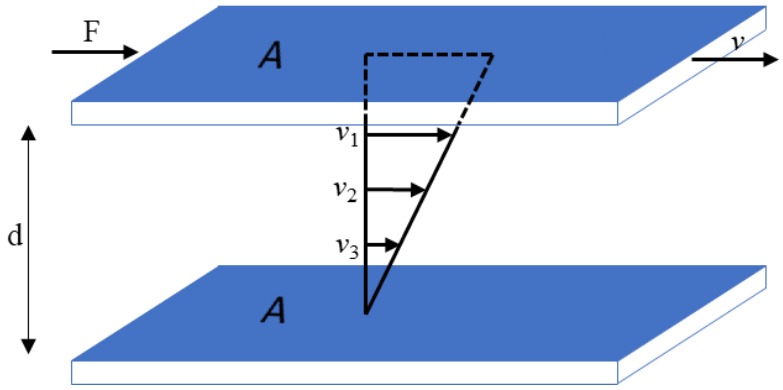

Figure 25: Explanation of the viscosity, liquid between two plates.

A liquid between two infinitely large parallel plates adheres to both of them equally and experiences a force, if one of these is moved. When one of these plates is moving with a speed *v* and the other one is not moving at all, the formation of layers inside the liquid occurs which all have different speeds (v_1, v_2, v_3, *etc.*).[59] The change in the speed of each layer in relation to the thickness of the layer is called shear speed. Newton defines the viscosity as the friction heat which is generated by the force F that accelerates one plate to a definitive speed. Experiments prove, that the force F is proportional to the speed of the moving plate *v* and the area A of both plates, but indirectly proportional to the distance d of the two plates. All these relations lead into a formula which contains the dynamic viscosity μ as the proportional factor.[60]

$$F = \mu \cdot \frac{v \cdot A}{d} \qquad \text{(equation 1)}$$

[58] D. I. N., *Viskosität - Teil 1: Rheologische Begriffe*, **2003**.
[59] W. Kulicke, *Fließverhalten von Stoffen und Stoffgemischen*, Hüthig & Wepf Verlag, Basel, **1986**.
[60] W. J. Bartz, *Viskosität und Fließverhalten*, Expert-Verlag, Malmsheim, **1994**.

Therefore, a liquid with high viscosity needs a higher force to be deformed and is thicker than one with a lower viscosity. If the dynamic viscosity is used in relation to the density ρ of the liquid, the kinematic viscosity v is obtained.[61]

$$\nu = \frac{\mu}{\rho} \qquad \text{(equation 2)}$$

These described properties are only applicable to Newtonian fluids, where the shear speed is behaving linear to the force.[62]

A special case of the viscosity is the calculation of the specific or intrinsic viscosity. The specific viscosity is the theoretical influence of an additive to the viscosity of a solution. The viscosity of a solution is influenced by two factors, the viscosity of the solvent and the additive. Knowing the viscosity of the solvent and the solution, enables the calculation of the specific viscosity, the viscosity of the additive.[63] Therefore, the formula can be described to calculate the specific viscosity η_{sp} with the viscosity of the solution η_c and the viscosity of the solvent η_0.[64]

$$\eta sp = \frac{\eta_c - \eta_0}{\eta_0} \qquad \text{(equation 3)}$$

Calculating the specific viscosity, only gives the relation of the viscosity of the additive to the solvent. Therefore, it can be seen as a percentual change of the viscosity of the additive.[64]

The viscosity of a fluid can only be measured if the substance is constantly deforming or moving. For this measurement, there are several devices useful, for example rotational-, capillary- or falling-sphere-viscometer. Rotational viscometers are build up with a sample holder that contains the substance and a device that is able to spin in contact to the substance. There are different geometrical possibilities for rotational viscometers (Figure 26).[62]

[61] H. A. Barnes, *J. Non-Newtonian Fluid Mech.* **2000**, *H. 94*, 213-217.
[62] T. G. Mezger, *Das Rheologie Handbuch*, 4. Auflage, Vincent Network, Hannover, **2012**.
[63] a) G. B. Jeffery, *The Royal Society* **1922**, *102*, 161-179; b) R. Simha, *J. Org. Chem.* **1940**, *44*, 25-34.
[64] J. W. Mehl, J. L. Oncley and R. Simha, *Science* **1940**, *92*, 132-133.

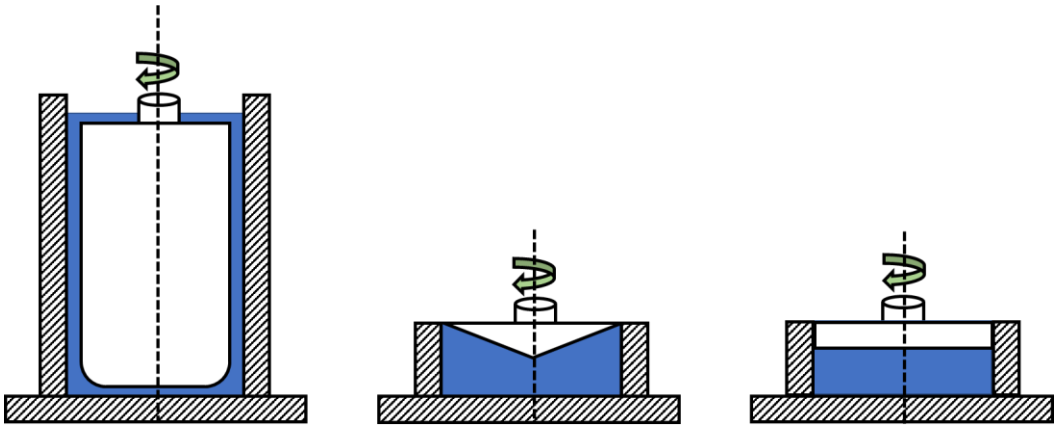

Figure 26: Rotational viscometers: Cylinder-, cone-plate- and plate-plate-measuring system.

Rotational viscometers are measuring the resistance and the torque via spinning the cylinder, cone or plate or by spinning the sample holder. Here the viscosity can be calculated even for substances with very high or very low viscosities. But the open structure of these devices can lead to a loss of the sample which is why at high shear rates capillary viscometers are used.[65]

Capillary viscometers are for example the *Ostwald*- or *Ubbelohde*-viscometer. Here, a U-shaped tube is filled on one side with a liquid (Figure 27).[66]

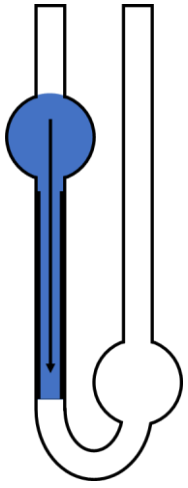

Figure 27: Ostwald-viscometer.

The liquid flows from the upper reservoir down through the capillary and into another reservoir. The time that is needed for the liquid to pass a specific volume is proportional to the kinematic viscosity.[59]

[65] G. Schramm, *Einführung in Rheologie und Rheometrie*, 2. Auflage, Thermo Electron GmbH, Karlsruhe, **2004**.

[66] J. Wilke, H. Kryk, J. Hartmann and D. Wagner, *Theorie und Praxis der Kapillarviskosimetrie – Eine Einführung*, Schott Geräte GmbH, Hofheim, **1995**.

Placing the device in heated baths enables the measurements in different temperatures. But here, volumes of at least 15 mL are necessary to carry out a measurement. To reduce the volume of the measurement, a falling-sphere viscometer can be used.[67]

Falling sphere viscometers are capillaries that are filled with the fluid substance and a small sphere which is able to move through the substance (Figure 28).[68]

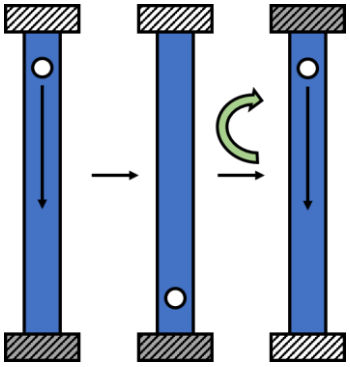

Figure 28: Falling-sphere-viscometer.

Rotating the capillary, leads to the falling of the sphere through the substance, which can be repeated by rotating the capillary again. The time needed for the ball to move through the capillary is proportional to the viscosity. Here, only small amounts of sample (0.1 mL) are necessary for a successful measurement. Therefore, all results in this thesis are based on measurements via falling-sphere viscometer.

2.3.1 Viscosity Index

The viscosity is extremely dependent on the temperature. Therefore, the value of the viscosity of a certain motor oil does not give much information unless the temperature is additionally stated. That is the reason, why *Dean* and *Davis* introduced the viscosity index (VI) in 1929 for all kinds of oils. Figure 29 is demonstrating the behaviour of the viscosity to the temperature of two oils, that have different VI.[69]

[67] H. A. Barnes, J. F. Hutton and K. Walters, *An introduction to rheology*, Elsevier Science Publisher, Amsterdam, **1989**.

[68] L. Gehm, *Rheologie. Praxisorientierte Grundlagen und Glossar*, Vincentz Network, **1998**.

[69] E. W. Dean and G. H. B. Davis, *"Viscosity Variation of Oils and Temperature," Chemical and Metallurgical Engineering*, Vol. 36, **1929**.

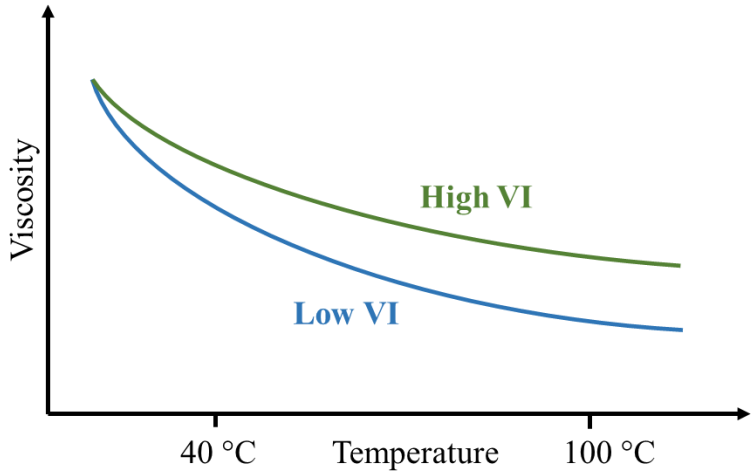

Figure 29: Development of the viscosity with the temperature of an oil with high (green) and low (blue) VI.[69]

Comparing the starting and end viscosity of these two oils, the green one with a high VI has a smaller dependency on the temperature. Standard oils without any additives are more likely to have a major dependency on the temperature. This means, elevating the temperature results in a decreased viscosity. In a temperature range of 100 °C a complete collapse of the viscosity might occur that means only 10% to 20% of the viscosity remains at around 100 °C in comparison to room temperature.[70] Therefore, especially lubricant manufactures are interested in oils with a higher VI or in additives that induce higher VI's.[71] The calculation of the VI is possible by using only the kinematic viscosity of 40 °C and 100 °C (Figure 30).

[70] E. W. Dean, A. D. Bauer and J. H. Bergland, *"Viscosity Index of Lubricating Oils," Industrial and Engineering Chemistry*, **1940**.

[71] I. C. Geniesse, *"A Comparison of Viscosity Index Proposals,"* No. 215, **1956**.

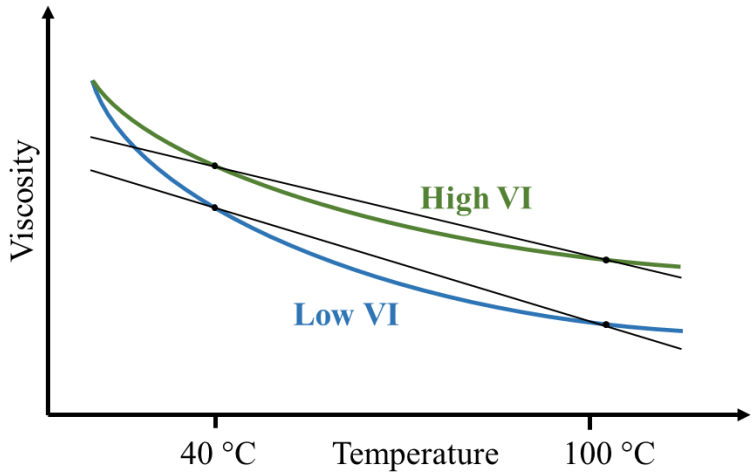

Figure 30: Calculation of the VI with the kinematic viscosity at 40 °C and 100 °C.

Therefore, for the formal definition of the VI, only the straight line between viscosity at 40 °C and 100 °C is important, while all other temperatures are not involved. That is the reason why the VI is proportional to the slope of this theoretical line.[72] To calculate the VI following equation can be used.

$$VI = 100\frac{x - \nu_{40}}{x - y} \qquad \text{(equation 4)}$$

While ν_{40} is the kinematic viscosity of the measured oil at 40 °C, *x* and *y* are values that are defined in specific databases. Value *x* describes the viscosity of an oil at 40 °C, that obtains a VI of 0 and owns the same viscosity at 100 °C like the measured oil. In contrast to that, *y* describes the viscosity of an oil at 40 °C with an VI of 100 and develops the same viscosity at 100 °C like the measured oil.[73] A lubricant with a low VI can therefore be described with VI values of 20 to 50, high VI values might have values above 100.[74] To increase the VI of a specific oil, additives can shift the VI to higher values.

2.3.2 Viscosity Index Improver

Motor oil manufactures are highly interested in oil formulations that result in a lower viscosity dependency on the temperature. Therefore, additives are mixed into these oils that might increase the VI. These additives are called viscosity index improver. These VI improvers need to have good properties in increasing the VI and need to be soluble in a broad temperature range. Examples for those VI improvers are olefin copolymers (OCP), polyalkyl methacrylates (PMA) or hydrogenated poly

[72] W. A. Wright, *"A Proposed Modification of the ASTM Viscosity Index," Proceedings*, Vol. 44, S, **1964**.
[73] G. W. Stachowiak and A. W. Batchelor, *Engineering Tribology*, 2nd ed., Butterworth-Heinemann, Boston, **2001**.
[74] J. C. Cragg and E. A. Evans, *J. Inst. Pet.* **1943**, *29*, 99-148, 315 - 337.

styrenes.[5] All these polymeric additives are improving the VI the same way. Increasing the temperature results in an expansion of the polymer in comparison to lower temperatures (Figure 31).

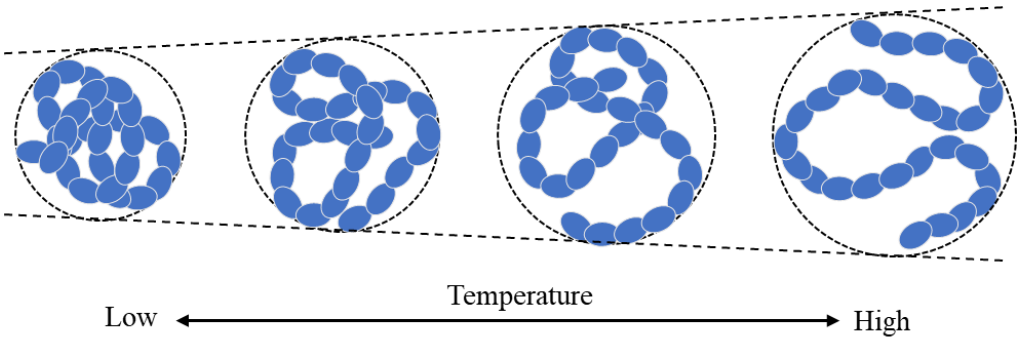

Figure 31: Expansion of additive polymers at elevated temperatures.[75]

These additives are reacting to the elevated temperature with intermolecular repulsion, resulting in an enlarged structure by increased solubility in higher temperatures. Therefore, the hydrodynamic radius of the additives increases and with it the viscosity too.[76] This effect can be measured in two different ways. One way is to observe the viscosity at elevated temperatures and the other way is to observe the hydrodynamic radius. Studies of the hydrodynamic radius via light scattering were able to investigate the expansion of poly(styrene) in cyclohexane.[77] But here increased hydrodynamic radii were only observed in a small range of temperatures from 34 °C to 55 °C.[78] Therefore, the usage of PMA is favoured in motor oils. An increase of the VI of an oil can be achieved even with small additions of the VI improver.[4] But there is a disadvantage of the PMA in motor oils. Besides the temperature, shear stress is a major influence on the oil. This can lead to cleavage of covalent bonds inside the PMA. This cleavage is demonstrated in Figure 32 where the red line represents a shear stress induced split.

[75] T. W. Selby, *The Non-Newtonian Characteristics of Lubricating Oils*, 1, **1958**.
[76] P. J. Flory, *Principle of Polymer Chemistry*, Ithaca, NY, **1952**.
[77] V. J. Novotny, *J. Chem. Phys.* **1983**, *78*, 183-189.
[78] a) B. Chu, Q. Ying and A. Y. Grosberg, *Macromolecules* **1995**, *28*, 180-189; b) Y. B. Melnichenko, G. D. Wignall, W. A. V. Hook, J. Szydlowski, H. Wilczura and L. P. Rebelo, *Macromolecules* **1998**, *31*, 8436-8438.

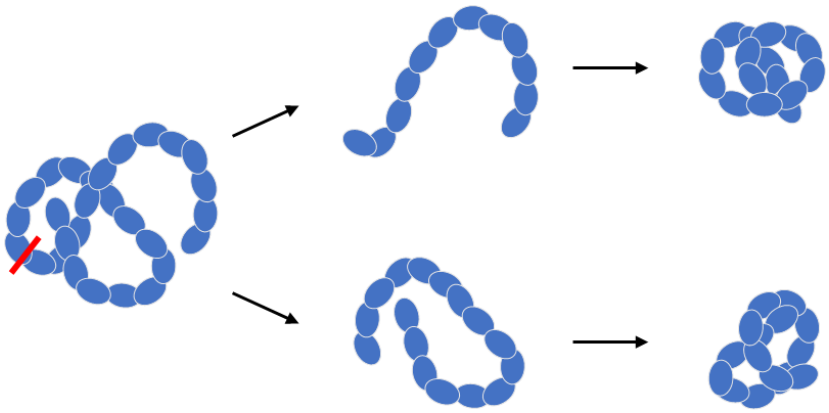

Figure 32: Loss of VI improvement, due to bond cleavage.

The cleavage results in two smaller structures, that are still able to improve the viscosity of the solvent, but in a reduced way. This bond cleavage results in a permanent reduction of VI improvement ability. Therefore, lubricants must be exchanged regularly to avoid this effect in long term.[4] Therefore, VI improver based on supramolecular interactions might be favourable, due to the possibility of reformation of cleaved bonds, due to non-covalent interactions.

2.3.3 Motor Oils

This thesis aims to find a suitable additive for motor oils, that improve the VI. Therefore, three different motor oils (Nynas NS8, Nexbase 3020, Nexbase 3043) were chosen to investigate a possible effect. Each motor oil has different properties in polarity and viscosity.

2.3.3.1 Nynas NS8

Nynas NS8 is a thin motor oil based on naphthenic structures. That means, it mostly contains different alkylated cyclopentane or cyclohexane functions (Figure 33).

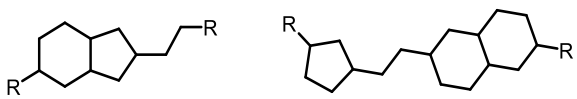

Figure 33: Examples for structures of naphthenic oils.

Nynas NS8 is therefore well suited for dissolving organic compounds.[79] Measurements of the viscosity exhibit a major decrease of the kinematic viscosity at elevated temperatures (Figure 34).

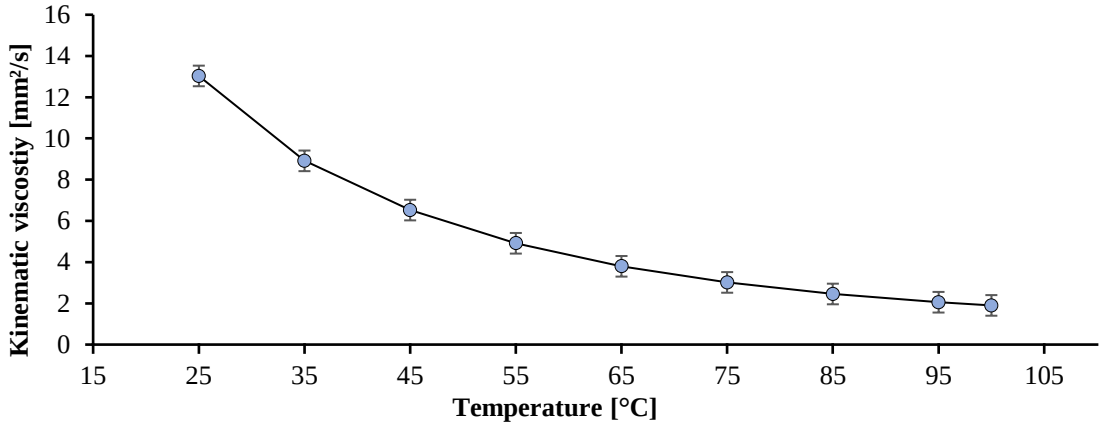

Figure 34: Kinematic viscosity in dependency on the temperature of Nynas NS8.

The kinematic viscosity occurs at 7.72 mm²/s at 40 °C and ends at 100 °C at 2.00 mm²/s. Therefore, Nynas NS8 obtains a VI of 47.

2.3.3.2 Nexbase 3020

Nexbase 3020 is similar to Nynas NS8 a thin lubrication/petroleum oil. Due to the saturated alkyl chains of C_{15} to C_{30} it is highly unpolar. An example structure is pictured in Figure 35.

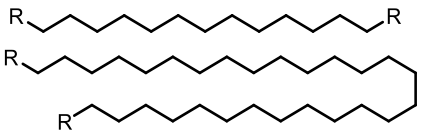

Figure 35: Examples of structures for C_{15} to C_{30} alkyl chains.

The solubility of organic molecules is limited due to the unpolar properties of this oil. Therefore, additives need to be adjusted to be dissolved.[80] Measurements of the viscosity in dependence on the temperature exhibit the decrease of the viscosity (Figure 36).

[79] *12.06.2020* **https://www.nynas.com/de/product-areas/base-oils/oils/NS-8**, *Nynas*.
[80] *12.06.2020* **https://www.neste.com/companies/solutions/base-oils/products/nexbase-3020**, *Nexbase*.

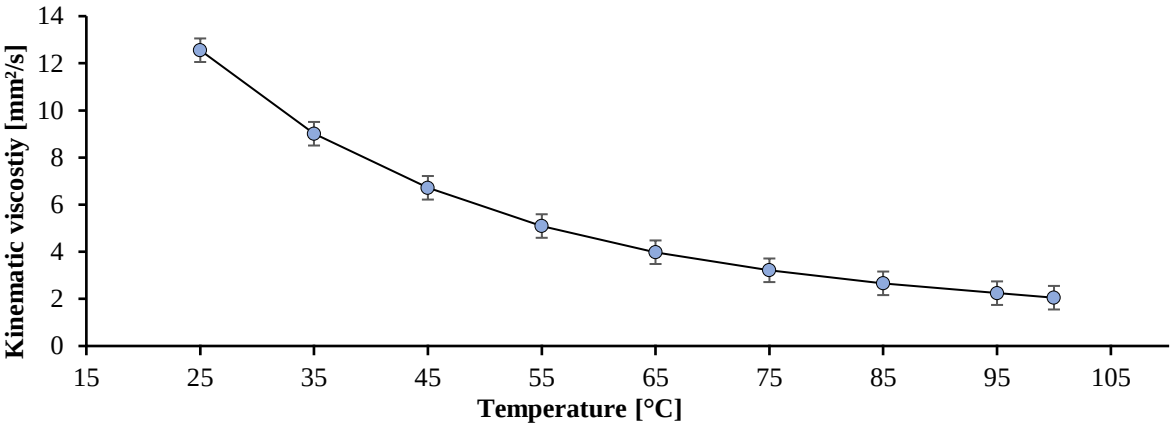

Figure 36: Kinematic viscosity in dependency on the temperature of Nexbase 3020.

The kinematic viscosity is behaving similar to the viscosity of Nynas NS8, in dependence on the temperature. The kinematic viscosity occurs at 7.86 mm²/s at 40 °C and ends at 100 °C with 2.1 mm²/s. These minor changes of a lower starting point and an elevated endpoint result in a higher VI of 88.

2.3.3.3 Nexbase 3043

At last Nexbase 3043 was chosen. It is a similar lubricating oil/petroleum oil of saturated alkyl chains. But here longer alkyl chains occur of C_{20} to C_{50}. Therefore, it is extremely unpolar and is the most challenging oil regarding solubility in this thesis. An example structure is demonstrated in Figure 37.

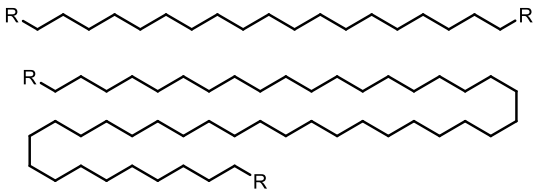

Figure 37: Examples of structures for C_{20} to C_{50} alkyl chains.

Nexbase 3043 is a very thick oil. Here, especially the solubility of any additive needs intensive adjustment for each compound.[81] For the Nexbase 3043 another viscosity measurement was prepared (Figure 38).

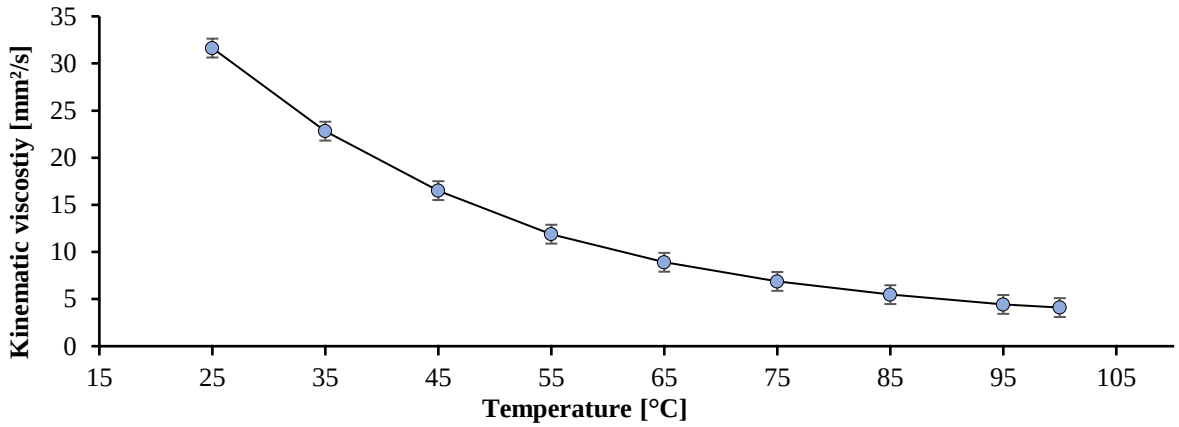

Figure 38: Kinematic viscosity in dependency on the temperature of Nexbase 3043.

With a kinematic viscosity of 19.66 mm²/s at 40 °C and an end viscosity of 4.1 mm^2/s at 100 °C Nexbase 3043 obtains a VI of 107.

[81] *12.06.2020* **https://www.neste.com/companies/solutions/base-oils/products/nexbase-3043**, *Nexbase*.

3. Project and Objective

Aim of this project is to develop a system based on supramolecular interactions to improve the viscosity index (VI) of a given solvent. Therefore, the introduction of a system is needed which is able to increase the viscosity at elevated temperatures. Dissolving this VI improver in a solvent, the system should result in a reversed viscosity/temperature profile which counteracts the viscosity loss of the solvent at higher temperatures. In our concept the desired effect is based on the equilibrium between a cyclic and a polymeric form of the monomer, consisting of a flexible linker unit (green) and two self-complementary binding units (blue, Figure 39).

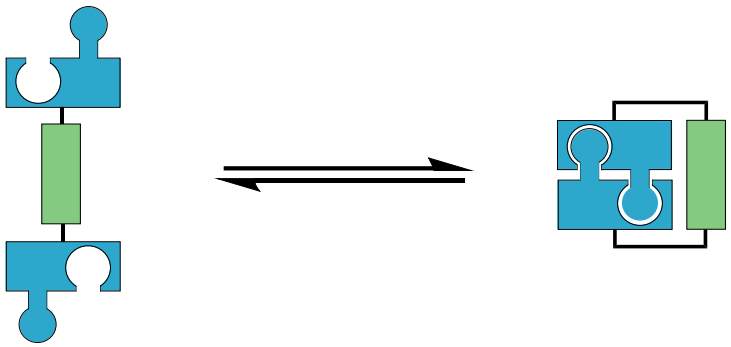

Figure 39: Monomeric structure with two self-complimentary binding units (blue) and a flexible linker unit (green) which is able to form cyclic structures.

This interaction favours the cyclic structure at room temperature. The dimerization of the binding units is based on supramolecular interactions e.g. hydrogen bonds, electrostatic interactions or dipole-dipole interactions, which allows the opening of the cyclic structure at elevated temperatures. For the same reason, the linker unit should have a flexible but pre-coordinating structure because the system needs to be able to adopt the cyclic conformation. An optimal linker unit would be able to change the conformation within different temperatures, to enable a ring-opening at elevated temperatures. Within this ring-opening reaction, a change of the intramolecular interaction of the binding units to an intermolecular interaction occurs. This change of the connectivity can be used to generate polymeric structures at elevated temperatures (Figure 40).

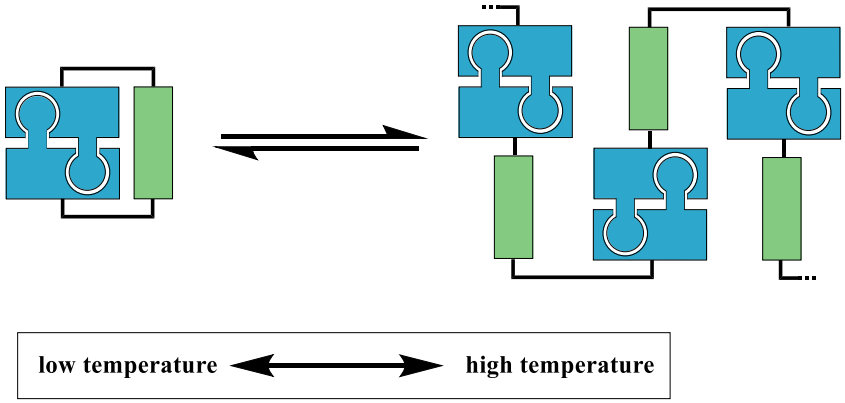

Figure 40: Formation of the polymeric structure at elevated temperatures, due to a ring opening reaction.

While the hydrodynamic radius of the cyclic structure occupies a defined space, the polymeric structures have indefined hydrodynamic radii, but are increased in size in comparison to the cyclic structure, which results in a higher viscosity. In this system we are using an enthalpic reaction to compensate for the entropic effect. Therefore, the ring tension of the cyclic system needs to be high enough to open the cyclic structure at elevated temperatures. For the generation of a system like this, different linker units like alkyl chains or aromatic groups are tested. For the binding units different motifs are used, to study their different behaviours.

The investigations start with the literature known system of *E. W. Meijer* and co-workers.[82] This system is tested to see how the effect can be measured, evaluated and used in different solvents. *E. W. Meijer* and co-workers introduced a system based on ureidopyrimidone binding units which is able to act as a VI improver by switching between the cyclic and polymeric structure.[82]

After evaluating this system, a substitution of the binding and linker units follows to observe the difference in the behaviour of each change. Different solvents and concentrations are tested to study the behaviour of each influence to evaluate the effect.

At last, when an optimal system is found which is able to improve the viscosity of a solvent, the challenge is to transfer this effect into very unpolar solvents like motor oil. Here, the cooperation partner Evonik Oil Additives suggested three different oils with different polarities in which the VI improver effect is highly desired. The final aim is to generate a system which is able to improve the viscosity index of an unpolar motor oil significantly.

[82] B. J. B. Folmer, R. P. Sijbesma and E. W. Meijer, *J. Am. Chem. Soc.* **2001**, *123*, 2093-2094.

4. Results and Discussion

4.1 Creating a new Viscosity Index Improver

4.1.1 First Generation: Recreating the Viscosity Index Effect

Any progress in this project is divided into generations. Each generation is dealing with a problem of the previous one with the aim of solving it. In total, six generations of VI improver will be presented and their application will be described. The first generation is dealing with results of the literature known investigations of *E. W. Meijer* and co-workers.[82] This project is evolving within each generation to achieve the final goal of a supramolecular VI improver in oil.

4.1.1.1 State of the Art

The first generation is based on a monomeric unit which is known from the publication of *E. W. Meijer* and co-workers (Figure 41).[82] While studying supramolecular polymers based on ureidopyrimidone units they observed an unexpected effect. Additionally to an increase of the polymeric structures in higher concentrations, a shift from cyclic to polymeric structures was also observed at elevated temperatures. It was mentioned, that this effect is only available in a precise concentration range and specific functional properties of the compound.

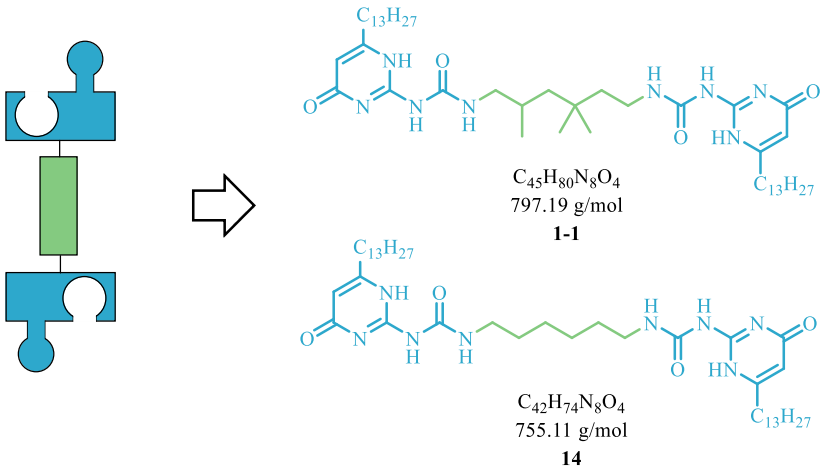

Figure 41: Monomeric units 13-1 and 14 mentioned in the publication of *E. W. Meijer* and co-workers.[82]

The monomeric compound mentioned in the investigations of *E. W. Meijer* and co-workers are based on ureidopyrimidone binding moieties, which are based on a tridecyl-isocytosine unit and a urea unit

that attaches to the linker unit.[82] The binding unit is capable of interacting with itself due to a strong hydrogen bond pattern which leads to a dimerization.[21]

Besides the binding units, the linker unit between the binding units plays a major role. Due to the linker unit, intramolecular interactions are possible and besides the intermolecular interaction (leading to polymerization), intramolecular interaction (leading to cyclic structures) can occur. The exact balance of these two forms is crucial for the desired viscosity effect. While cyclic structures need to be thermodynamically preferred at lower temperatures, the equilibrium needs to shift towards the polymeric form at higher temperatures. Here, the linker has a decisive influence since it can favour or disfavour each form. In Meijer´s work, interestingly only the trimethyl-derivative **1-1** demonstrates the described effect. While the trimethyl-derivative **1-1** and the hexyl derivative **14** are both able to form polymeric structures in higher temperatures, only the trimethyl-derivative **1-1** is capable of cyclic structures at lower temperatures. In the trimethyl-derivative **1-1,** the two methyl groups in the centre of the molecule are introducing a *Thorpe Ingold* effect which is responsible for the pre-coordination.[83] This pre-coordination is responsible for the two binding units to face the same direction to form cyclic structures due to intramolecular interactions. Hexyl-derivative **14** is not able to develop this *Thorpe Ingold* effect. Here, there is no reason for the system to adopt a cyclic structure, since the linear all-*trans* conformation of the hexyl-linker is favoured. This means the polymeric structure is favoured at any temperature. Looking at the trimethyl-derivative **1-1,** the cyclic structure is favoured at lower temperatures due to the pre-coordination of the linker unit. Elevating the temperature leads to an opening of the cyclic structures, resulting in polymerization.

The synthesis of the trimethyl-compound **1-1** was described as a one-step synthesis of the commercially available 6-tridecyl-isocytosine (**18**) and 2,4,4-trimethyl-1,6-diisocyanato-hexane (**19-1**).[82] Due to the reaction of the isocyanate and the amine a urea function is formed, which is necessary to enable the hydrogen bond pattern of the dimerization.

[83] R. M. Beesley, C. K. Ingold and J. F. Thorpe, *J. Chem. Soc., Trans.* **1915**, *107*, 1080-1106.

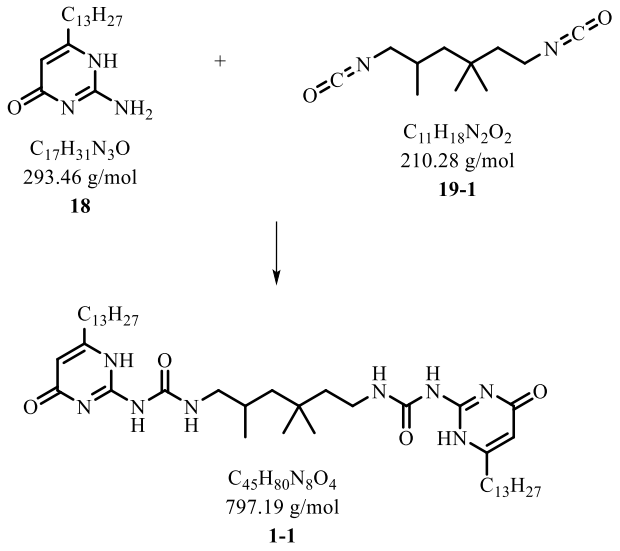

Figure 42: Synthesis of trimethyl-derivative 1-1 according to Meijer.[82]

The investigations of *E. W. Meijer* and co-workers are based on the behaviour of the viscosity within elevated temperatures. It is described, that due to the polymerization at higher temperatures, the hydrodynamic radius and the specific viscosity increases. The described effect was obtainable in chloroformic solutions in a certain concentration (Figure 43).

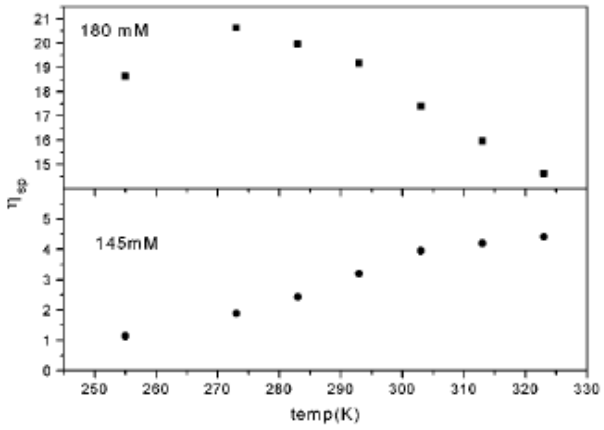

Figure 43: Measurement of the specific viscosity of compound 1-1 at different temperatures according to Meijer.[82] Reprinted with permission from ([82] B. J. B. Folmer, R. P. Sijbesma and E. W. Meijer, *J. Am. Chem. Soc.* 2001, *123*, 2093-2094.). Copyright (2020) American Chemical Society.

E. W. Meijer and co-workers have proven, for the trimethyl-derivative **1-1**, that in a concentration of 145 mM in chloroform a rapid increase of the specific viscosity occurs with increasing temperature. Starting with a specific viscosity at around 1 at 255 K, the viscosity increases to a value of around 4 at 325 K. Looking at the same measurement with a 180 mM solution it stands out, that the effect like this

only occurs at a 145 mM concentration. The 180 mM measurement has a higher specific viscosity at the beginning, increases until 275 K but decreases again at higher temperatures. This is the case because at higher concentrations, the polymeric structures are already favoured at lower temperatures, so that the temperature-induced shift from cyclic to polymeric structures is less pronounced. Therefore, our investigations need to discover the optimal concentration for each derivative to obtain the effect.

The first generation of this project is the 2,4,4-ureidopyrimidone **1-1** derivative. Here, the first challenge is to reproduce the system mentioned in the literature and to investigate and recreate the effect with the analytic methods available in our working group.[82]

4.1.1.2 Calculations

Before the synthesis of the first generation, force field calculations were carried out to prove the ability for ring formation, to compare with other systems. For easier calculation, the C_{13}-alkyl chain was replaced with a methyl group.

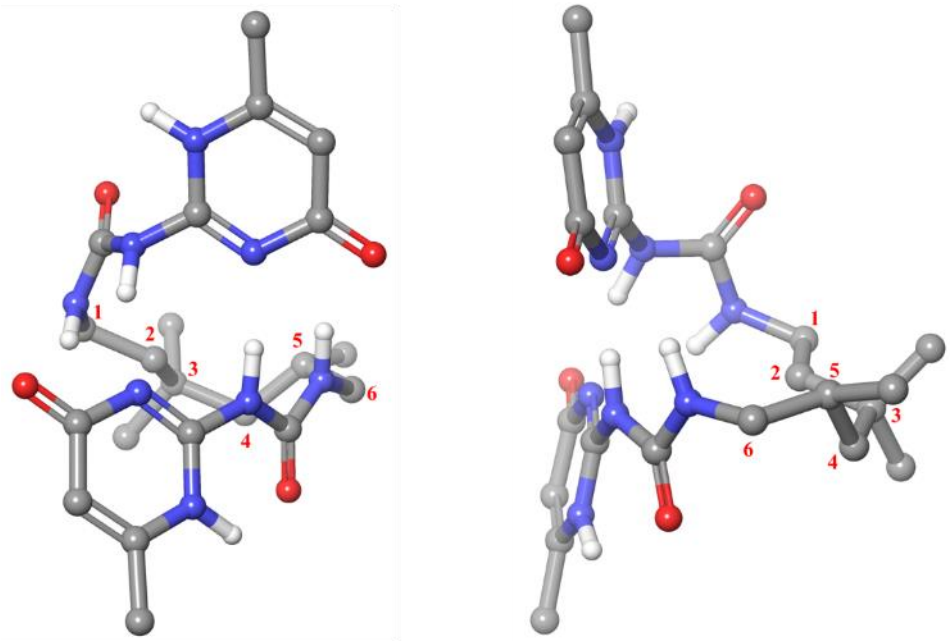

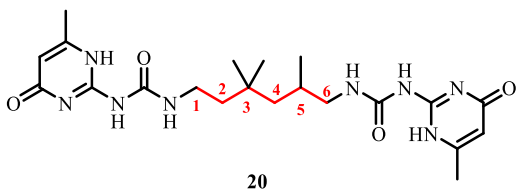

20

Figure 44: Force field calculations of the ureidopyrimidone trimethyl-hexyl derivative 20 (OPLS force field). Left: Front view, Right: Side view.

The calculation is proving the ability of a ring formation. Nevertheless, the formed rings exhibit a high ring tension, since the ureidopyrimidone-units cannot adopt an ideal coplanar arrangement. Similar calculations are used in the following chapters to compare the cyclic structures of each generation.

4.1.1.3 Synthesis

At the beginning of this project, the focus was the evaluation of the results described in the literature and the synthesis of the ureidopyrimidone-hexyl derivative **1-1**. *E. W. Meijer* and co-workers suggested a synthesis via trimethyl-hexyl-diisocyanate **19-1** and tridecyl-isocytosine **18** to build up a urea function via simple coupling reaction.[82] This method was not feasible in our case as the necessary isocyanate **19-1** was not commercially available any more. Therefore, at first, we focused on the synthesis of the isocyanate.

Starting with the commercially available mixture of 2,4,4- and 2,2,4-trimethyl-hexyl-diamine (**21-1**, **21-2**) a mixture of the 2,2,4- and 2,4,4-trimethyl-hexyl-diisocyanate (**19-1**, **19-2**) should be synthesized. After the formation of the urea compound, the two isomers were separated to obtain the final product **1-1**.

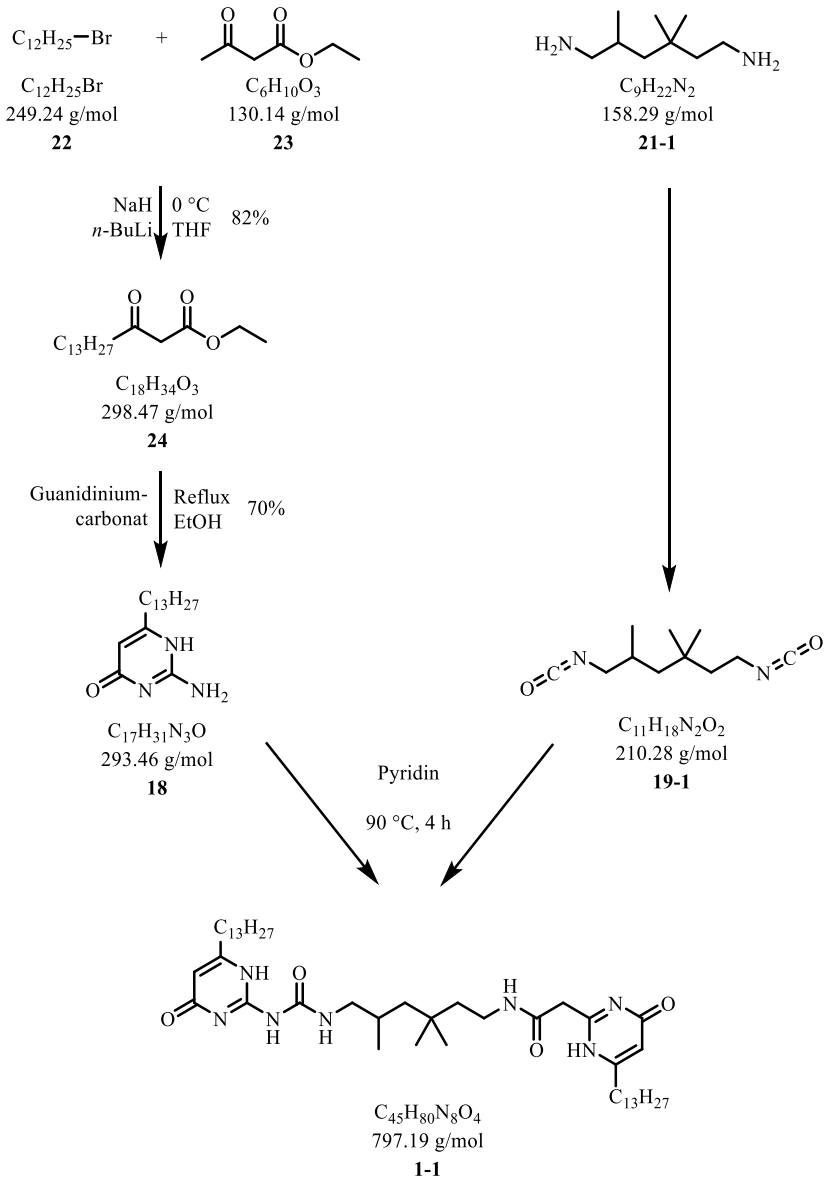

Figure 45: Synthesis of the ureidopyrimidone-hexyl derivative 1-1(compounds 21-2 and 19-2 not shown).

To start the synthesis, 1-bromo-undecane (**22**) and ethyl-3-oxo-butanoate (**23**) were used. The extension with the C_{12} alkyl chain is necessary to achieve better solubility. The substitution of the butanoate was done via the bis-enolate, so that the electrophile reacts with the terminal methyl group. The reaction was carried out at 0 °C with NaH and *n*-BuLi and yielded 82% of the extended product **21**.[84] Continuing the synthesis, guanidinium carbonate was reacted with **24** to yield 70% of the isocytosine **18**.[85] Additional to this reaction, the formation of the diisocyanate **19-1** was carried out achieve the final product **1-1**.

[84] A. Shirai, T. Endo, H. Maseda and T. Omasa, *Biocontrol Sc.* **2013**, *18*, 183-191.

[85] T. F. A. De Greef, M. M. L. Nieuwenhuizen, P. J. M. Stals, C. F. C. Fitié, A. R. A. Palmans, R. P. Sijbesma and E. W. Meijer, *Chem. Commun.* **2008**, 4306-4308.

The synthesis started with a mixture of 2,4,4 and 2,2,4- trimethyl-hexane-1,6-diamine (**21-1**, **21-2**). The first attempt was the reaction via DMAP and Boc_2O.[86]

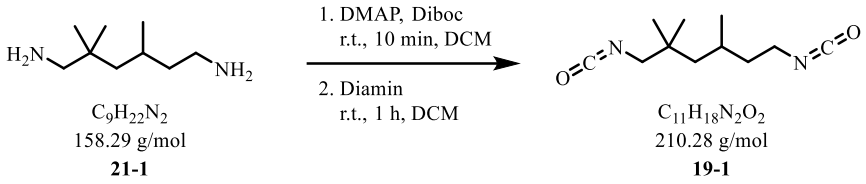

Figure 46: Synthesis of the diisocyanate 19-1 via DMAP and Boc_2O.

The generation of the diisocyanate **19-1** requires the activation of Boc anhydride via DMAP. The reaction was carried out multiple times with different temperatures with no formation of product **19-1**. Unfortunately, the formation of the Boc-protected diamine occurred instead of the formation of the isocyanate. The literature described this reaction as an easy way to generate isocyanates but was mostly successful with tertiary and quarternary α-carbon atoms.[86]

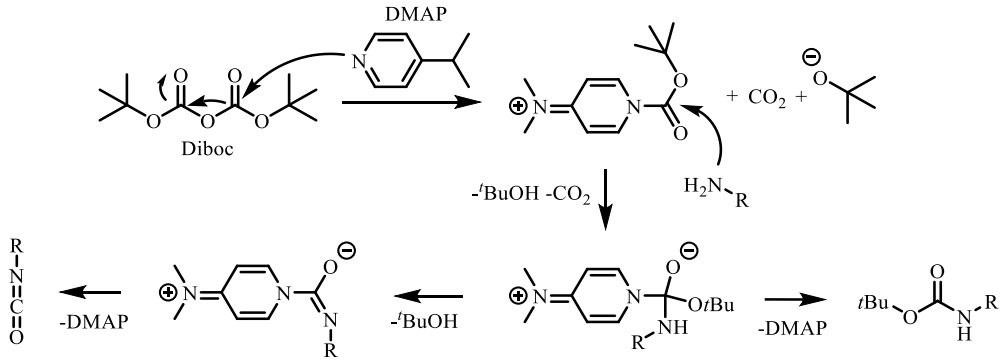

Figure 47: Formation of Boc protection and the isocyanate.[86]

Therefore, primary amines might favour the formation of Boc-protected products. Another method to generate the desired compound **1-1** is the reaction of **21-1** with trichloro-acetyl chloride. Here, synthesis of the isocyanate is skipped to generate a different active compound (**25**, see Figure 48) to subsequently carry out the formation of the urea.[87]

[86] H.-J. Knolker and T. Braxmeier, *Angew. Chem., Int. Ed.* **1995**, *107*, 2746-2749.
[87] C. Schmuck and D. Rupprecht, *Synthesis* **2007**, *20*, 3095-3110.

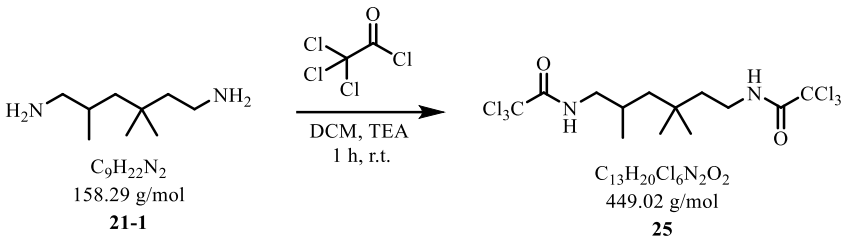

Figure 48: Reaction between diamine 21-1 and the trichloro-acetyl chloride.

The reaction was successful, but another side reaction occurred. Due to the long reaction time, only one amine was transformed and was able to react with another amine. The polymerization could not be stopped, even at lower temperatures, less concentration of the reactants or via adding the diamine **21-1** slowly to the trichloro-acetyl chloride.

Another method to generate isocyanates is the reaction with carbodiimidazoles. The formation of the diisocyanate occurs while two imidazoles are released.[88]

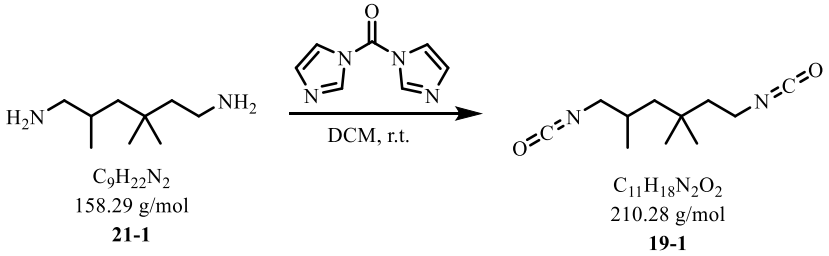

Figure 49: Formation of the diisocyanate 19-1 via carbodiimidazole.

Once again, the carbodiimidazole was added slowly to the diamine **21-1** with a successful formation of the isocyanate. The progress of this reaction could only be obtained via NMR measurements because the isocyanate is highly reactive to water. The isocyanate was obtained in a yield of 10%. Due to the low yield in the reaction with carbodiimidazole, another method was carried out via phosgene (**28**). This reaction was chosen last, due to the high toxicity of this compound. To use a less toxic alternative, instead of phosgene (**28**), triphosgene (**25**) was used, which is in solid-state and easier to handle.[89] Solved triphosgene is capable to release three equivalence of phosgene triggered by elevated temperatures or solving in DCM.

[88] D. D. Chimie, *Starch/Stärke* **2010**, *62*, 90-101.

[89] R. B. Sessions, A. Florey, J. F. Stoddart, D. J. Williams, N. Raja, M. A. Meador, J. F. Stoddart, D. J. Williams, D. J. Cram, A. W. Hanson, V. Boekelheide, D. J. Cram, K. D. Stewart, K. N. Trueblood, T. A. Mirra, J. P. Wepsiec, T. L. Manimardn, N. Raju, M. A. Meador, D. L. Ward and A. V. George, *Angew. Chem., Int. Ed.* **1987**, *26*, 894-895.

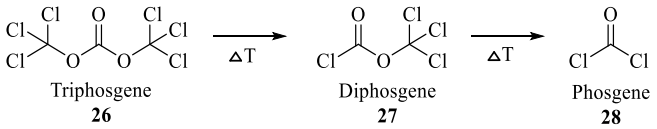

Figure 50: Disintegration of triphosgene 26 into phosgene 28.

The reaction was carried out in DCM at 0 °C with a prepared 1 M solution of triphosgene **26**. It was not necessary to heat up the system to achieve phosgene **28** and to initiate the reaction.[90]

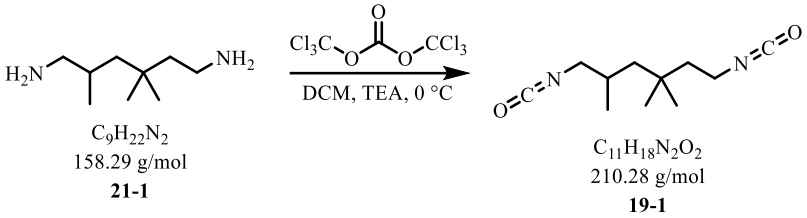

Figure 51: Formation of diisocyanate 19-1 via triphosgene (26).

The reaction with triphosgene **(26**) is highly exothermic. Therefore, the reaction needed to be carried out very slowly and with constant ice-cooling. The formation of the isocyanate was successful, but the purification was difficult, due to the high toxicity of the remaining triphosgene and the reactivity of the isocyanate with water. NMR measurements were indicating a yield of 50%.

To avoid material losses, the diisocyanate **19-1** was not further purified. The reaction was performed as a one-pot reaction after the formation of the isocyanate **19-1** as described in the literature.[82] The reactants were dissolved in pyridine and heated to reflux.

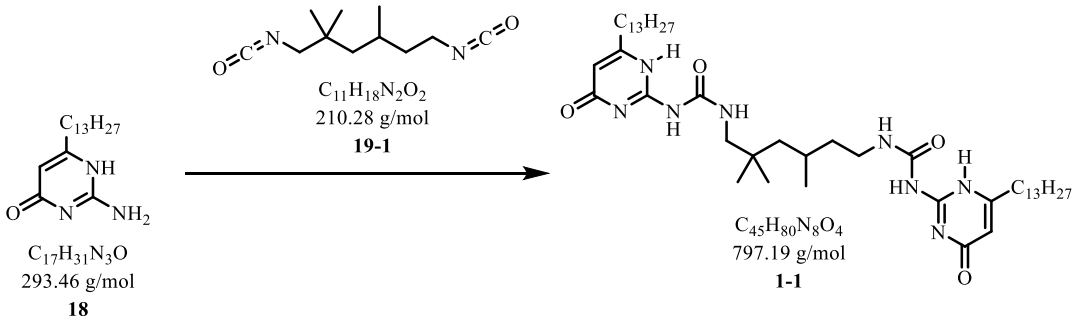

Figure 52: Synthesis of the ureidopyrimidone hexyl derivative 1-1.

[90] N. Kagermeier, K. Werner, M. Keller, P. Baumeister, G. Bernhardt, R. Seifert and A. Buschauer, *Bioorg. Med. Chem.* **2015**, *23*, 3957-3969.

The final compound **1-1** was purified by column chromatography to get the isomeric mixture of compound **1-1** and **1-2**. The final purification was carried out via flash chromatography (RP-18 MeOH/H_2O) to obtain the desired 2,4,4 isomer **1-1**. The desired isomer **1-1** was obtained in a yield of 17% and 16% of the 2,2,4 isomer **1-2** was collected as well.[82]

4.1.1.4 Solubility Tests

The solubility of the developed compounds in unpolar solvents is one of the most important issues in this work. In the following, the solubility was tested in different solvents, like chloroform, toluene, DMSO and the motor oils Nynas NS8, Nexbase 3020 and Nexbase 3043. It was tested if an amount of at least 30 mM concentration is possible in these solvents.

Table 1: Solubility tests of the first generation in different solvents.

Solvent	Max. Concentration
Chloroform	≥ 200 mM
Toluene	15 mM
DMSO	≤ 5 mM
Nynas NS8	≤ 5 mM
Nexbase 3020	≤ 5 mM
Nexbase 3043	≤ 5 mM

The only two solvents able to solve this compound were chloroform and toluene. A good solubility was achieved with chloroform with 200 mM and higher. This confirms the results of *E. W. Meijer* and co-workers where all their investigations took place in chloroform.[82] A toluene solution was only possible up to a concentration of 15 mM which is not enough to see any the effect. All other solvents were not able to solve at least 5 mM and are not tested in viscosity measurements.

4.1.1.5 Measurement of the Viscosity

The measurements of the viscosity were carried out with a falling sphere viscometer. The results of *E. W. Meijer* and co-workers were demonstrating a viscosity improvement with increasing temperature in a concentration of 145 mM in chloroform.[82] Due to these previous results, it was not necessary to find an optimal concentration for this compound. The measurements were carried out in concentrations of 130 mM, 145 mM and 160. Additionally, pure chloroform was measured to evaluate the difference between each solvent and to calculate the specific viscosity.

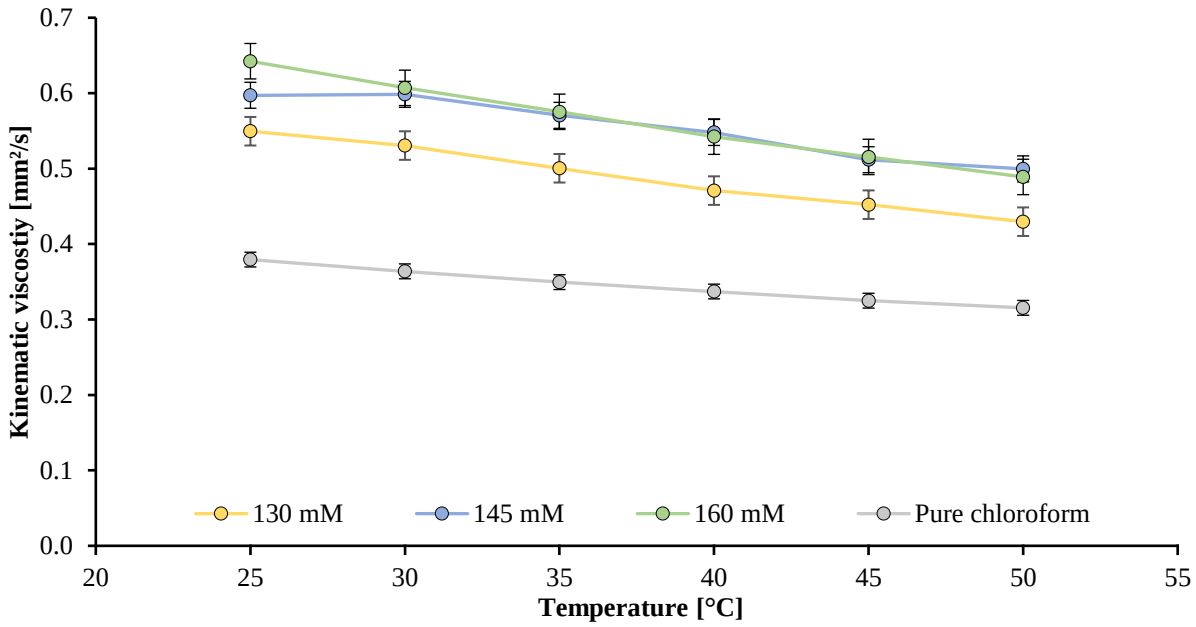

Figure 53: Kinematic viscosity of the ureidopyrimidone hexyl derivative 1-1 at concentrations of 130 mM, 145 mM, 160 mM and chloroform.

At each concentration, increased kinematic viscosities were obtained in comparison to pure chloroform. The kinematic viscosity of pure chloroform starts at 0.37 mm²/s at 25 °C and drops down to 0.32 mm²/s at 50 °C, while the viscosities of the solutions were found to be 0.55 mm²/s and higher at 25 °C. The solutions of 130 mM and 160 mM concentration have a constant decrease of viscosity with temperature. Looking at the 145 mM solution, a non-linear behaviour occurs. Starting with a kinematic viscosity 0.6 mm²/s the viscosity is not decreasing upon heating to 30 °C. Only upon further heating, the kinematic viscosity starts decreasing. This effect was not described by the investigations of *E. W. Meijer* and co-workers because their main focus laid on the specific viscosity.[82] To investigate this effect in detail and to compare the results with the investigations of *E. W. Meijer* and co-workers the specific viscosity was calculated.

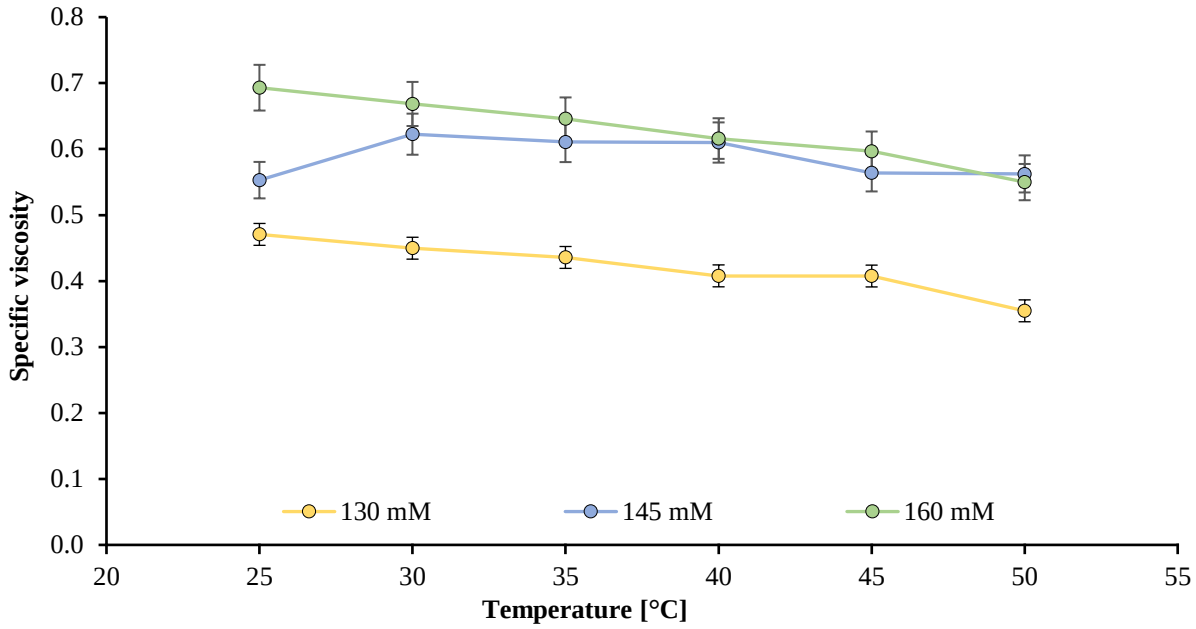

Figure 54: Specific viscosity of the 130 mM, 145 mM and 160 mM solution of the ureidopyrimidone hexyl derivative 1-1.

The specific viscosity is demonstrating the behaviour of the viscosity of the compound **1-1** itself. At the 130 mM concentrated solution a constant loss of specific viscosity with increasing temperatures occurs. The concentration is not high enough to form polymeric structures and only cyclic structures are present. For the 160 mM solution, a similar behaviour is observed. While the starting specific viscosity is 50% higher in comparison to the 130 mM solution, it is still decreasing constantly with increasing temperatures. The high concentration leads to polymerization of the compound even at lower temperatures, so that no ring-chain transition takes place upon increasing the temperature. The 145 mM concentrated solution is behaving different. The specific viscosity is increasing about 13% in comparison to the starting viscosity and staying roughly at the same level for the whole temperature range. Here, the ring-chain transition counteracts the temperature effect, so that at 145 mM, compound **1-1** acts as a viscosity improver.

These results are not identical with those described by *E. W. Meijer* and co-workers, where the specific viscosity seems rising the whole temperature range.[82] But the qualitative trend is similar. All in all, the results of the literature could be recreated and approved.[82] The effect can be measured and needs to be developed further.

Doing the same measurements with the 2,2,4 derivative **1-2**, no viscosity improving concentration can be found, which means, only the 2,4,4 derivative **1-1** features a viscosity improvement at elevated temperatures. This shows that the linker has a crucial influence, which will be investigated using the second generation of compounds.

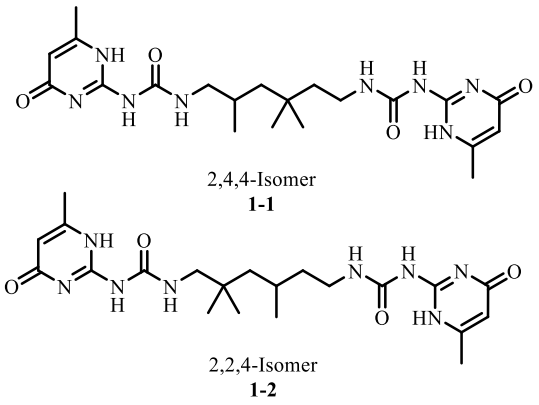

Figure 55: Active 2,4,4 (1-1) and inactive 2,2,4 derivative (1-2) of the ureidopyrimidone hexyl derivative.

4.1.2 Second Generation: Derivatisation of the Linker Unit

The second generation deals with the derivatisation of the linker unit. The investigations of the first generation were demonstrating that an effect is possible with suitable binding units and a pre-coordinating linker unit. While the 2,4,4 isomer **1-1** of the first generation led to an increasing viscosity in elevated temperatures in the first generation, the 2,2,4 isomer **1-2** was not active. This is the reason why this generation is focusing on a way to exchange the linker unit with a more pre-coordinating unit to recreate or maximise the effect.

4.1.2.1 New BINOL-Derivative

For the development of the new VI improver, a system must be found that is capable of changing the conformation in higher temperatures. Additionally, the linker unit should have pre-coordinating properties, so that cyclic structures are possible and ideally favoured at lower temperatures. These two features are given in the building block 1,1'-Binaphthalene-2,2'-diol (BINOL). Here, we have an orthogonally arranged system which is a perfect pre-coordinating candidate.

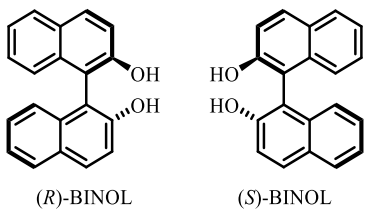

Figure 56: *(R)* and *(S)* conformation of BINOL

Biarylic systems, such as the BINOL, contain two aromatic systems (naphthol) connected by a covalent bond and are axially chiral. BINOL has a rotation barrier of about 150 kJ/mol which means a racemisation only occurs at elevated temperatures of around 200 °C.[35]

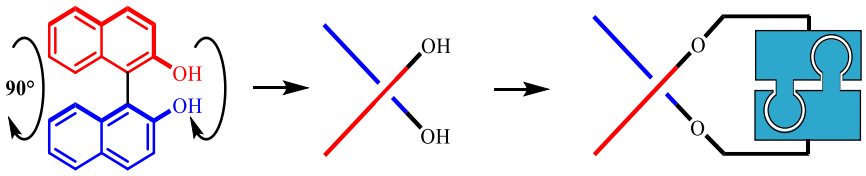

Figure 57: BINOL as rigid, orthogonally arranged pre coordinating linker.

For our purpose, a full rotation is not necessary because a small change of the angle is enough to change the conformation of the compound and to switch between cyclic and open (and possibly polymeric) structure. Because of the high reactivity due to the hydroxy group, coupling reactions like esterification or etherifications are an easy way to synthesise new derivatives of new VI improver candidates.

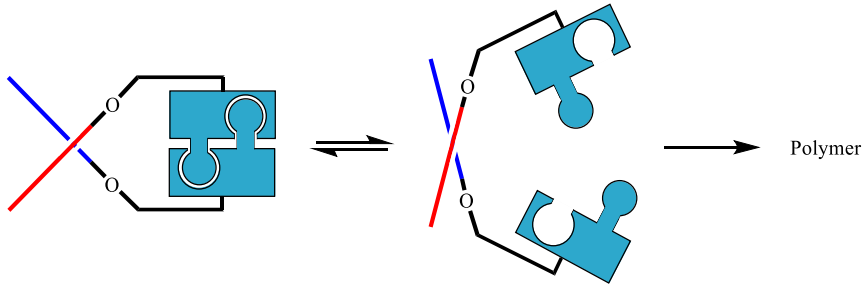

Figure 58: BINOL as new linker unit in a new VI-improver candidate.

Additionally, the influence of the distance between the BINOL and the binding unit must be investigated because this has a major effect on the behaviour of the system. If the distance is too large, the ring formation is less favoured, as the system is too flexible and a cyclization is no longer favoured entropically. If the distance is too small, a cyclization might not take place due to ring-strain. The basic structure of the second generation includes BINOL as a linker unit and the ureidopyrimidones as binding units. As a coupling method, etherification was chosen.

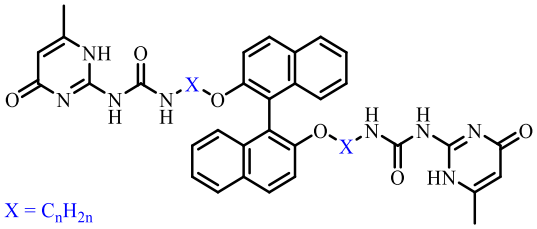

Figure 59: Basic structure of the second generation.

Force field calculations were conducted to determine the optimal length of the alkylene-linker X. For these calculations, two different derivatives were chosen to get a similar structure as in the first generation and to find an optimal system for the BINOL derivative. At first, a propyl chain was chosen, to see if a ring formation is possible for this system.

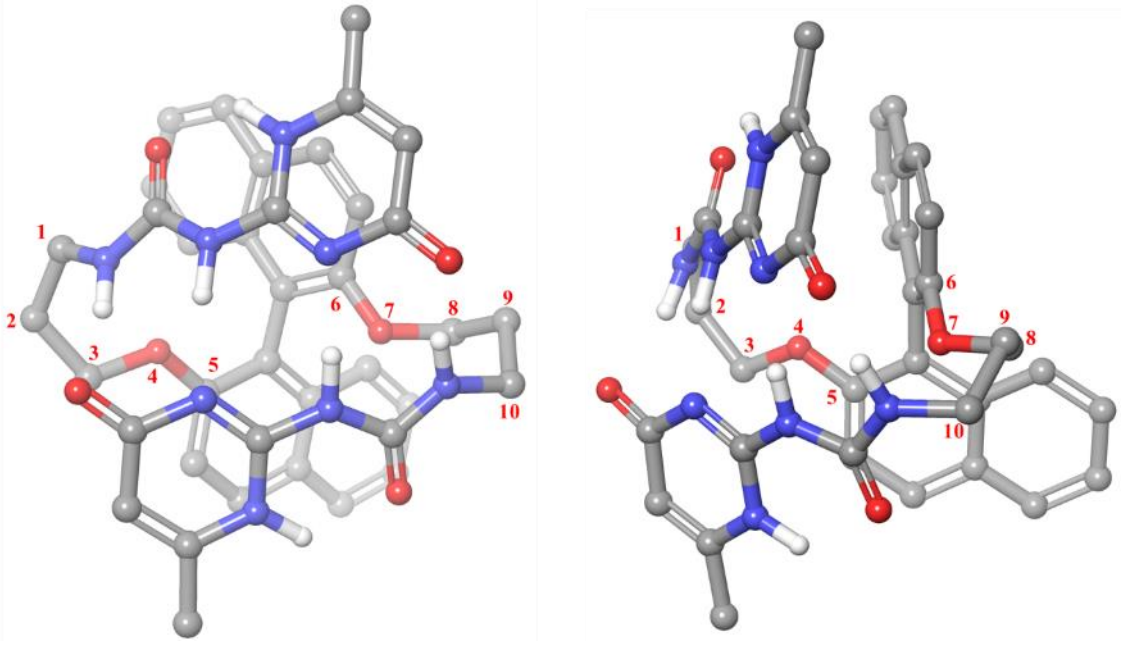

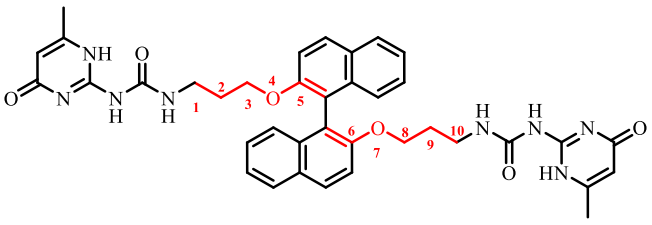

29

Figure 60: Force field calculations of the ureidopyrimidone propyl BINOL derivative 29 (OPLS force field). Left: Front view, Right: Side view.

The calculations are representing that the propyl derivative **29** is capable of forming a ring structure. This ring structure is based on the cyclic form of the BINOL and the alkyl chain to have a main cycle build of ten centres. However, the two ureidopyrimidone units are almost coplanar, so that the ring-tension might not be sufficient to allow for a ring-chain equilibrium. Therefore, the ethyl derivative **2** was calculated too, to see if a cyclic structure with a higher ring tension is possible.

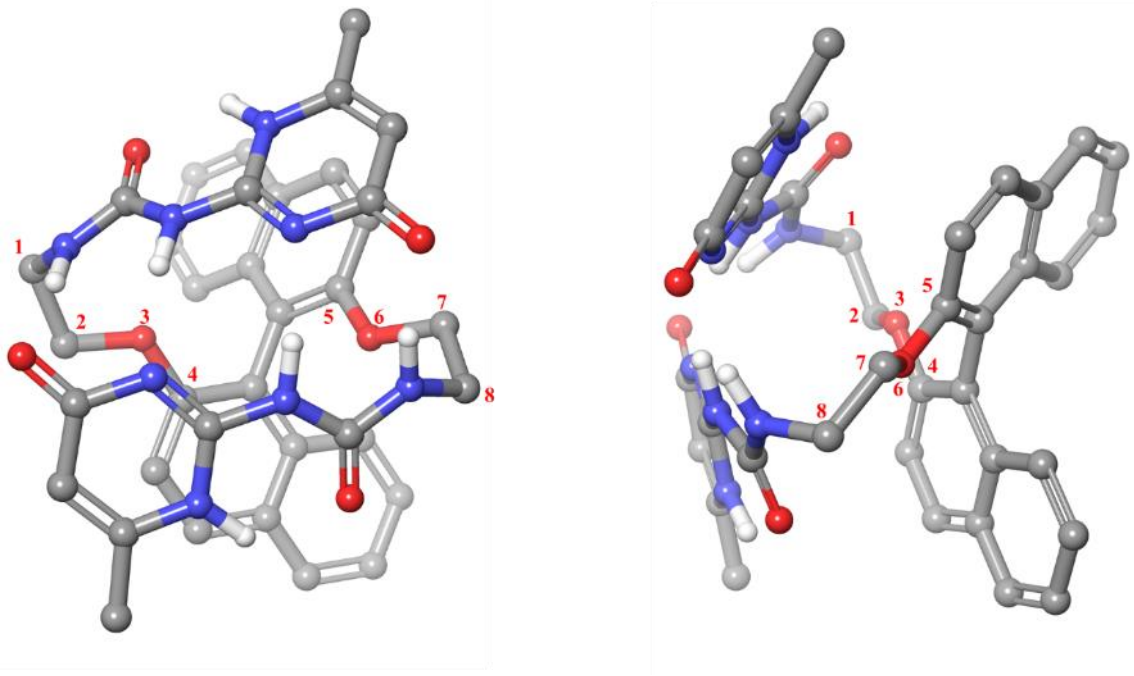

2

Figure 61: Force field calculations of the ureidopyrimidone ethyl BINOL derivative 2 (OPLS force field). Left: Front view, Right: Side view.

The calculations are representing a possible ring formation of the ethyl derivative **2**. Here, a cyclic structure is made with eight centres. The arrangement of the ureidopyrimidone-dimer is significantly distorted from planarity, indicating a higher ring-tension. This is the reason why the ethyl derivative **2** was chosen for the second generation, to be investigated on any viscosity improving effect.

4.1.2.2 Structure of the Monomeric Unit

The calculations indicated that a system containing a BINOL-ethyl ether **2** and ureidopyrimidone binding units is capable of forming cyclic structures. Therefore, this compound was investigated as the second generation.

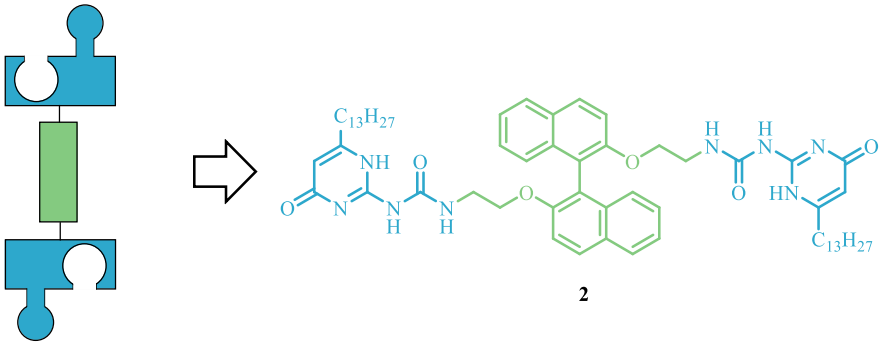

2

Figure 62: Structure of the second generation.

For the binding units, the same units were chosen as in the first generation, to compare both generations and to achieve similar solubilities as the first. For the analysis of the viscosity improvement in elevated temperatures, it was not necessary to investigate which enantiomer of the BINOL would result in a major effect. For the investigations, the *(S)*-enantiomer was chosen and for all following structures.

4.1.2.3 Synthesis

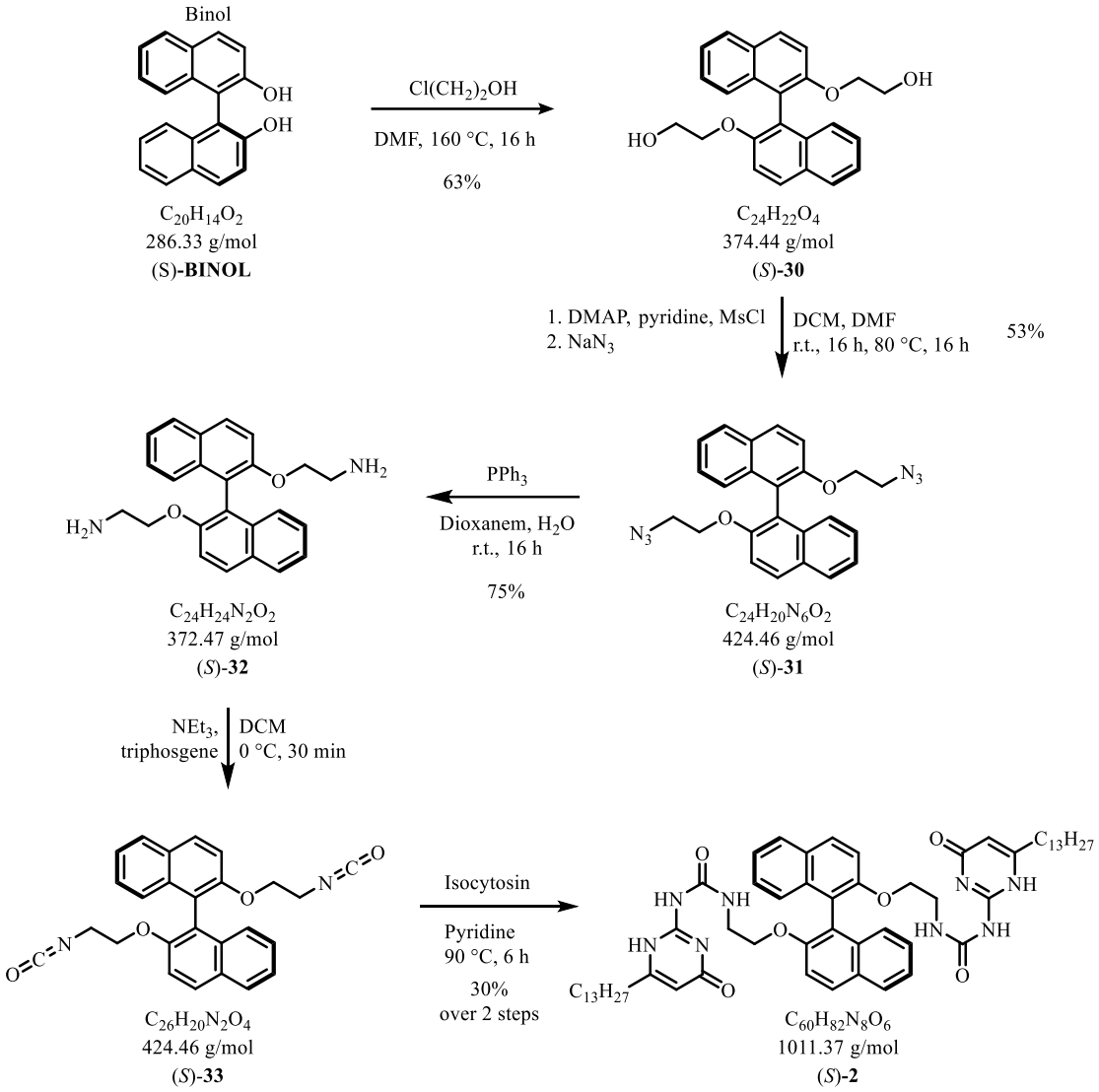

Figure 63: Synthesis of the second generation.

The synthesis is based on the synthesis of the first generation. Starting with *(S)*-BINOL, an etherification was carried out. Using 2-chloroethane-1-ol the diol compound *(S)*-**30** was obtained in a yield of 63%.[91] Subsequently, the diamine *(S)*-**32** was synthesized via the azide *(S)*-**31**, followed by a Staudinger reaction (40% yield over two steps).[92] Continuing the synthesis with the formation of the isocyanate, triphosgene was used as in the first generation, followed by the coupling of the isocytosine *(S)*-**33**. The final product *(S)*-**2** was obtained with a yield of 30% over these two steps. In the ^{1}H-NMR the signal of

[91] T. Taniguchi, T. Suzuki, H. Satoh, Y. Shichibu, K. Konishi and K. Monde, *J. Am. Chem. Soc.* **2018**, *140*, 15577-15581.

[92] C. Schmuck, D. Rupprecht, C. Urban and N. Walden, *Synthesis* **2006**, 89-96.

the NH-CH_2 of the ethyl function is shifted to 3.53 ppm in comparison to the previous compound the diamine at 4.25 ppm, which indicates the formation of the urea function in product *(S)*-**2**. The NMR spectra for the final compound of the second generation are shown in Figure 64.

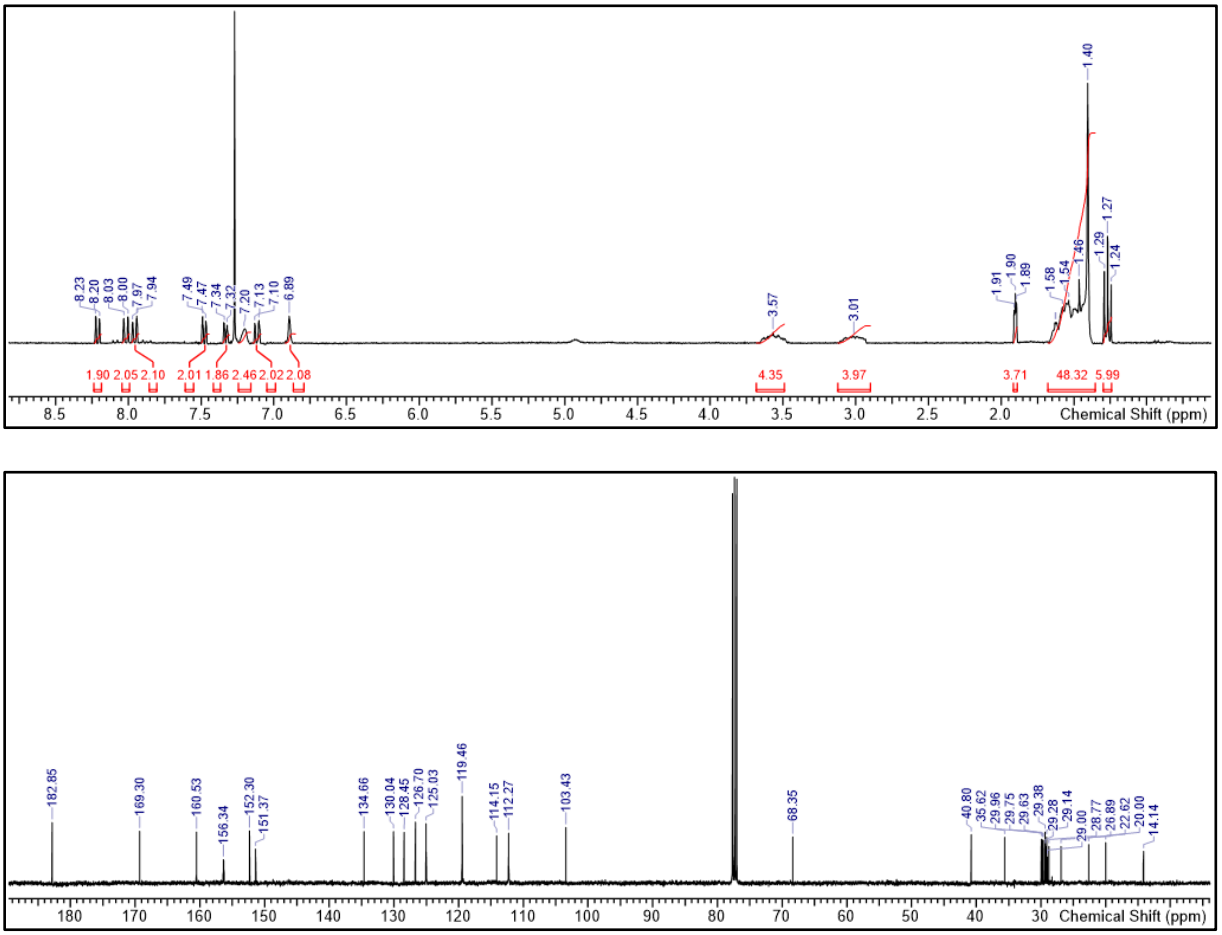

Figure 64: ^{1}H- and ^{13}C-NMR of *(S)*-2 in $CDCl_3$.

4.1.2.4 Measurement of the Viscosity

Before the measurement of the viscosity, another solubility test was carried out. Similar results were observed as in the first generation (Table 2).

Table 2: Solubility tests for the second generation in different solvents.

Solvent	Max. Concentration
Chloroform	≥ 200 mM
Toluene	≤ 5 mM
DMSO	≤ 5 mM
Nynas NS8	≤ 5 mM
Nexbase 3020	≤ 5 mM
Nexbase 3043	≤ 5 mM

Only a solution in chloroform is possible. Therefore, the viscosity of the compound *(S)*-**2** was measured in chloroform, like the first generation. For this purpose, a series of concentrations were set up and measured at different temperatures. The concentration values were chosen based on the measurements of the first generation. The samples were prepared in 130 mM, 145 mM and 160 mM in Chloroform.

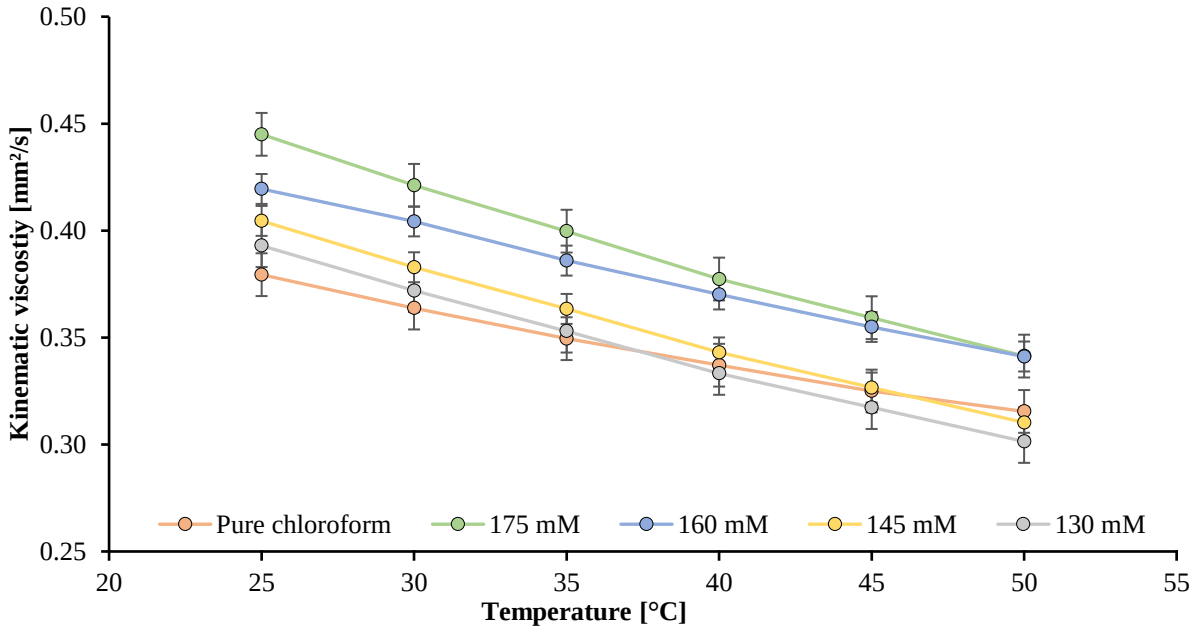

Figure 65: Kinematic viscosity of the ureidopyrimidone BINOL derivative *(S)*-2 at 130 mM, 145 mM, 160 mM, 175 mM and chloroform.

In addition, another solution of 175 mM was prepared to see the same behaviour of a high concentrated solution like in the first generation (Figure 65). The solutions of *(S)*-**2** obtain a higher viscosity than pure

chloroform at 25 °C. However, a stronger decrease of viscosity occurs with increasing temperature in comparison to the pure chloroform, so that the 130 mM and 145 mM solution even have lower viscosities at 50 °C. A positive effect might occur in the 160 mM solution. There is still a loss of viscosity but compared to all other concentrations and in comparison to pure chloroform a different behaviour occurs. This means the optimal concentration for a positive effect is shifted due to the derivatisation of the BINOL. At the 175 mM concentrated solution a higher loss of viscosity occurs than the 160 mM solution, probably due to the fact that the high concentration favours a polymerization even before heating up the system. Remarkable is, that the solutions with no effect are much worse than in the first generation. To compare the viscosities with the first generation, a calculation of the specific viscosity was necessary (Figure 66).

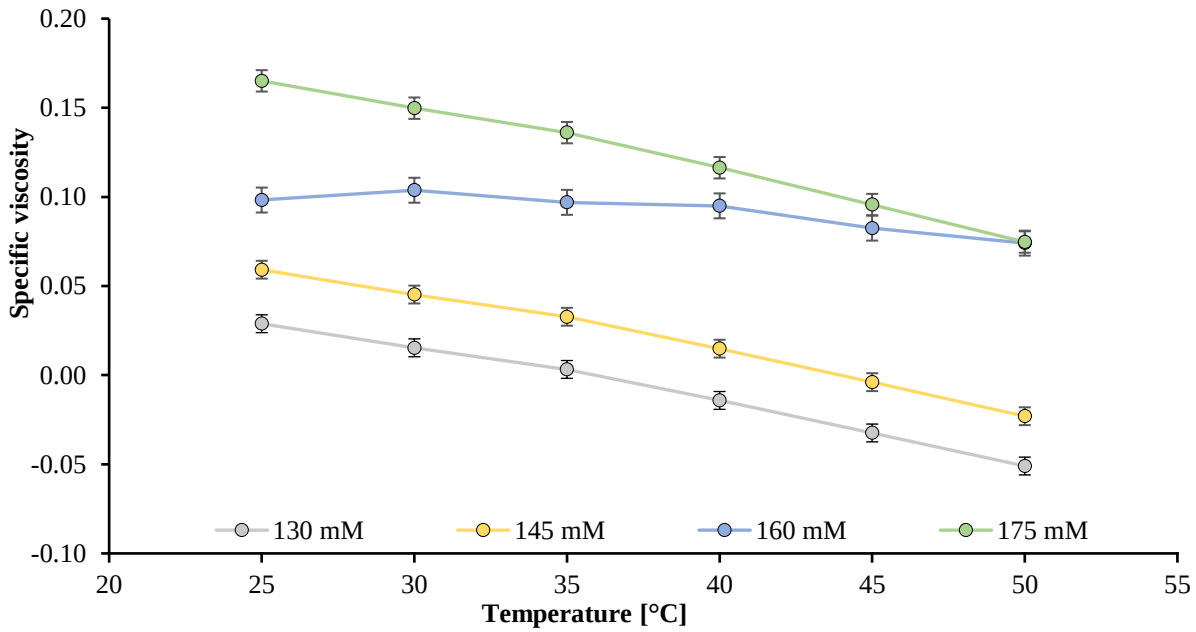

Figure 66: Specific viscosity of the 130 mM, 145 mM, 160 mM and 175 mM solution of the ureidopyrimidone BINOL derivative *(S)*-2.

The measurements of the specific viscosity are demonstrating a similar result as in the kinematic viscosity. Looking at the 160 mM concentrated solution, we see that the viscosity is increased by 5% between 25 °C and 30 °C and is staying on the same level until around 40 °C until the specific viscosity starts decreasing. The specific viscosity of the solutions with 130 mM, 145 mM and 160 mM of *(S)*-**2** are decreasing over the entire temperature range.

Comparing the first and second generation, the first generation obtains a greater effect in improving the specific viscosity in elevated temperatures because here almost no loss of viscosity occurred within the whole temperature range of 25 °C to 50 °C of the 145 mM solution of **1-1**. Nevertheless, the

measurements of the second generation were successful, demonstrating that it is possible to replace parts of the compound without losing the VI improver effect. Thus, BINOL as linker unit was proved to be a suitable alternative.

4.2 Improving the Viscosity Index Improver

4.2.1 Third Generation: Improving VI Properties

After the investigations of literature known compounds of possible VI-improver systems and the derivatization of the linker unit with a BINOL linker unit, the derivatisation of the binding units is put forward. Due to the supramolecular interactions, which are necessary for the desired effect, we were choosing a well-known system based on the GCP-motif **7** which is established in our working group.

4.2.1.1 New GCP-Derivative

Since the GCP motif **7** is capable to form very strong dimers it might be an optimal binding unit for the desired system.[25]

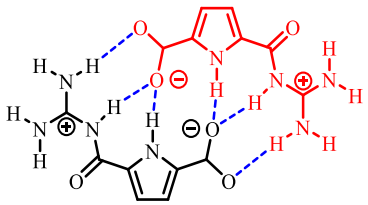

7

Figure 67: Zwitterionic GCP motif 7 forming strong dimers with itself.[92]

In comparison to the second generation, we are only exchanging the binding units to see the influence of the GCP motif **7**. The linker unit remains as a BINOL to connect the two self-complementary binding units.

To discover if the suggested system is suitable as a VI improver, we first carried out force field calculations. These calculations are proving the ability of cyclization of the system, based on the BINOL linker and the GCP binding motifs.

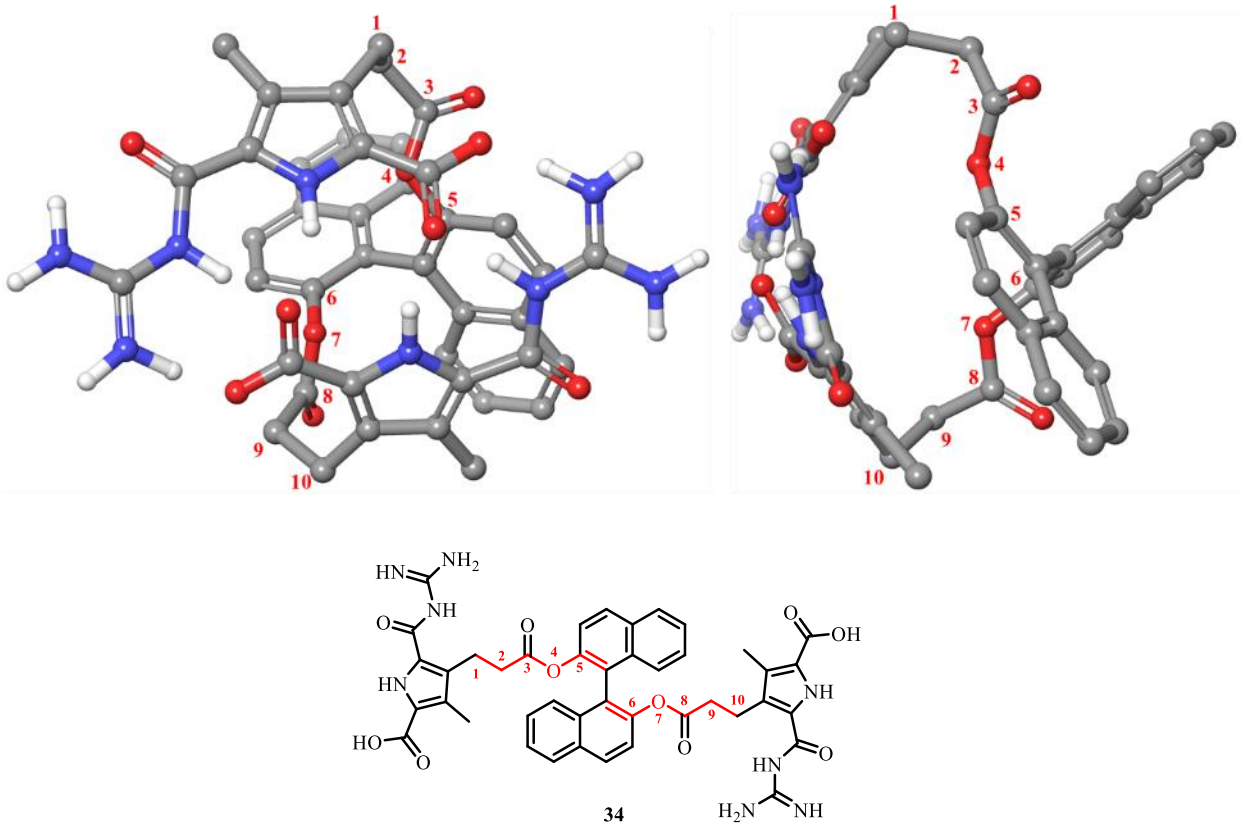

Figure 68: Force field calculation of the BINOL GCP system 34 to form cyclic structures (OPLS force field). Left: Front view, Right: Side view.

The distance between the linker and the binding unit is almost the same as in the calculations of the second generation. There are ten centres between the two binding units, therefore a similar ring tension of the cyclic structure as in the second generation can be assumed. The calculations reveal the ability of the BINOL GCP motif **34** to form cyclic structures as needed.

4.2.1.2 Structure of the Monomeric Unit

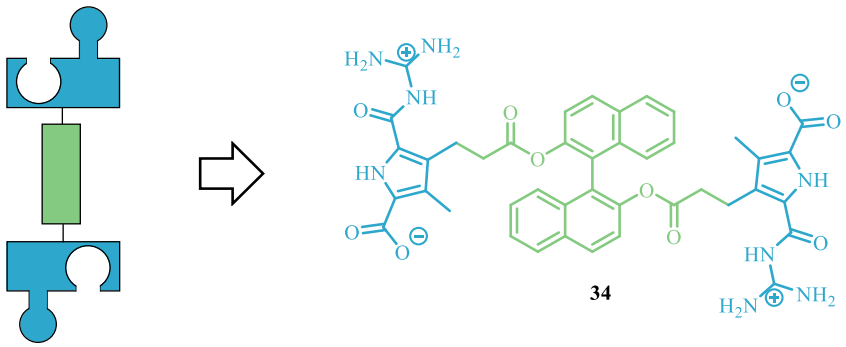

Figure 69: Third generation. GCP-BINOL motif 34.

In contrast to generations 1 and 2, the GCP-BINOL **34** derivative is only working in a pH range between 5 and 8. Therefore, the zwitterionic character of the GCP binding unit leads to a strong dimerization but ensures that the compound obtains a high polarity which might influence the solubility.[32]

4.2.1.3 Synthesis

Starting the synthesis of the third generation, the main reaction to generate the final compound of the third generation is the coupling of the linker with the binding unit. While the linker, BINOL, is commercially available, the binding unit requires more synthetic effort. Nevertheless, the GCP motif **7** is well known in our working group and the synthesis is established.[92] In this synthesis, a GCP derivative **34** is used, which occurs with an additional carboxylic acid.

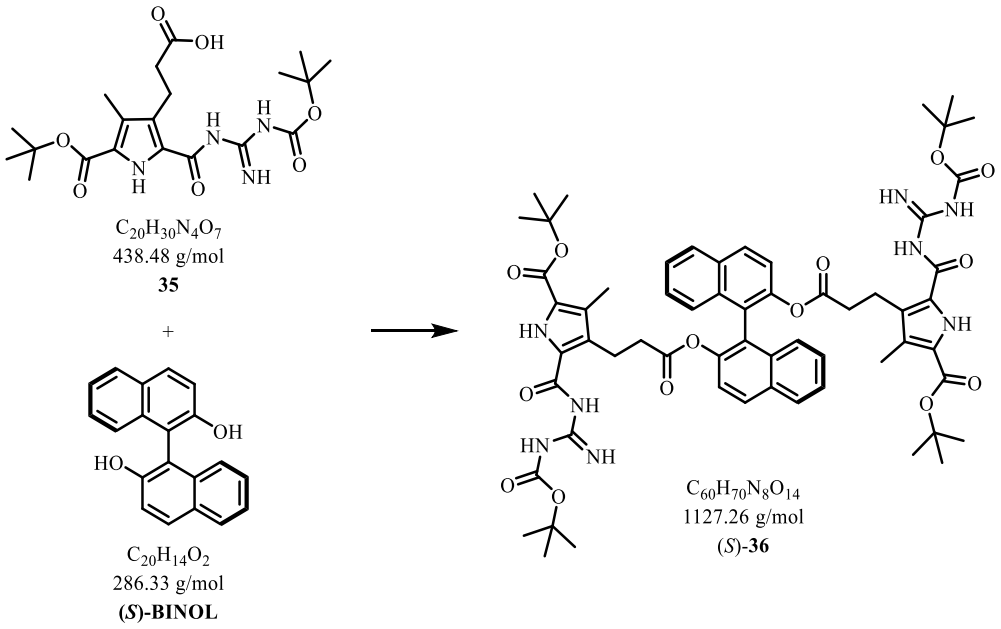

Figure 70: Main synthesis step of the formation of the third generation.

The binding motif contains a pyrrole centre which not only carries the carboxylate- and the guanidiniocarbonyl-groups in the 2- and 5-positions, but is additionally functionalized with a methyl-group in the 3-position and a propionic acid moiety in the 4-position. To generate this intermediate, we first synthesized precursor **37**. The synthesis was carried out as described in the literature.[32]

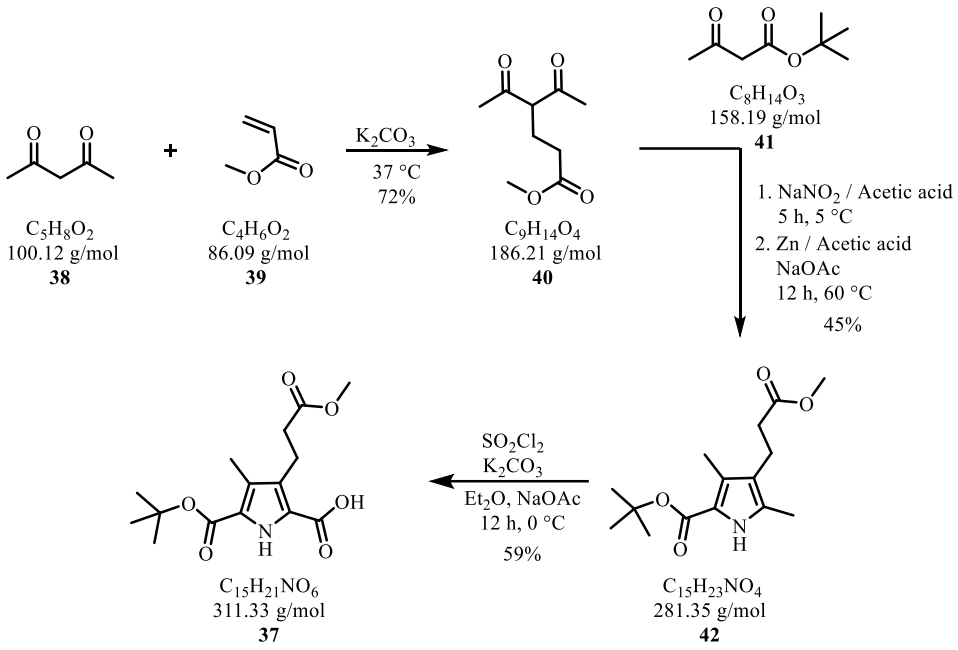

Figure 71: Synthesis of the motif 37.

Starting the synthesis with the extension of the acetylacetone (**38**) by Michael addition to acrylic acid methyl ester, the product **40** was obtained in a yield of 72%. The synthesis was continued by generating the pyrrole compound **42** with a yield of 45%. In this step the functional groups in the 2- and 4-position are generated. To functionalize the methyl-group in the 5-position, a free carboxylic acid was introduced via oxidation with sulfuryl chloride in 59% yield. This led to the final compound (**37**) with two protected and one free carboxylic acids.[32] After generating compound **37**, the GCP building block **35** can be synthesized. In this case, the following reaction is the coupling of the guanidine group.

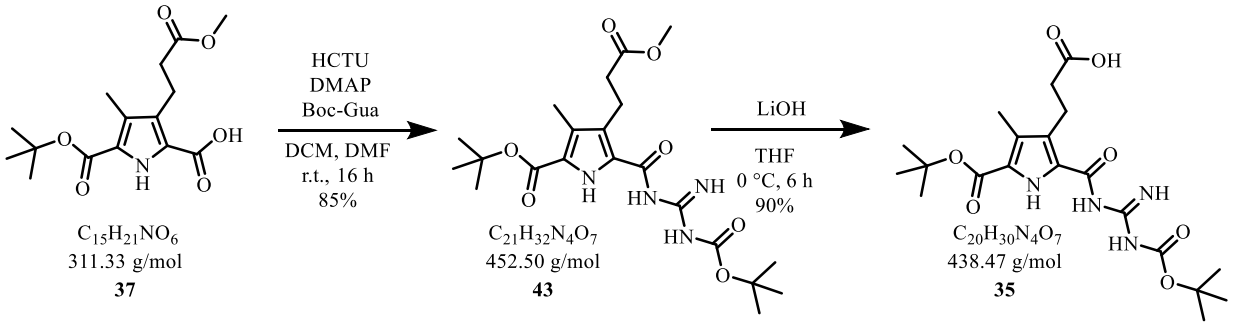

Figure 72: Generating the binding unit of the third generation 34 by coupling with Boc-guanidine and methyl ester deprotection.

Using HCTU and DMAP, the guanidine group was coupled successfully to compound **37**. In this reaction a yield of 63% was obtained. After this, the deprotection of the methyl-ester was done using

lithium hydroxide to obtain compound **35** in a yield of 90%.[92] In the next step, the esterification with the BINOL was carried out. The reaction was done with DCC and DMAP, with the aim of synthesizing the diester **44**.

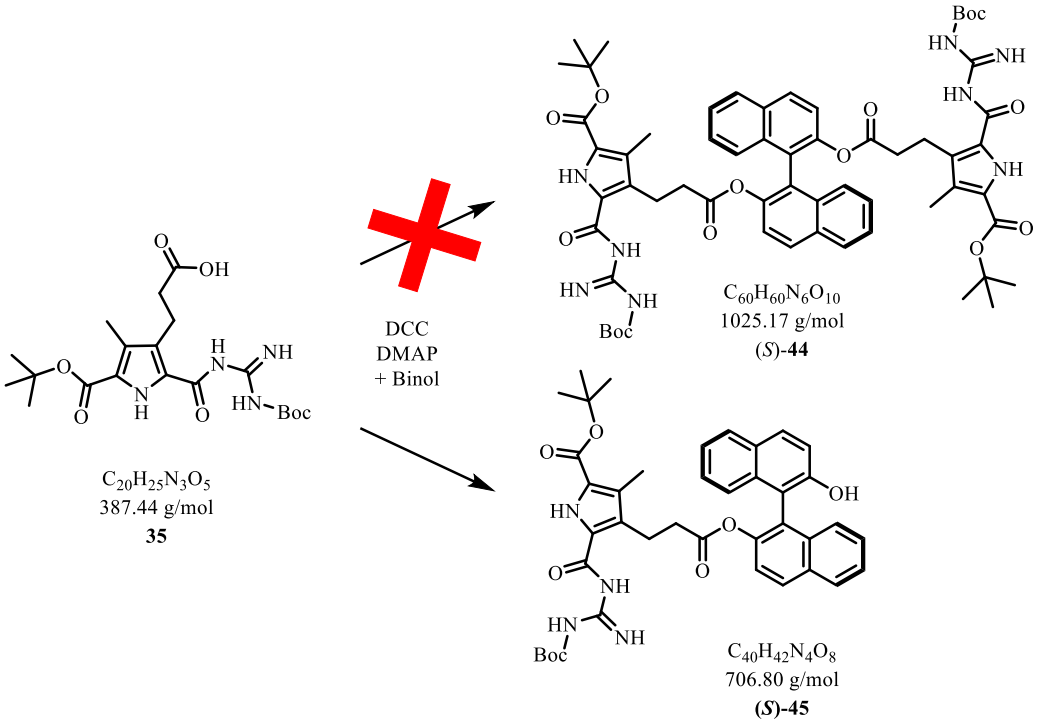

Figure 73: Esterification of the compound 35 with BINOL.

It turned out, that a direct double esterification was not possible, independent of the stoichiometry of reactants or reaction time. NMR measurements were indicating that the reaction stopped with the single substitution and there was no further reaction to the desired product *(S)*-**44**. The reaction mixture was stirred for a total of 3 days until the maximum conversion to the single-substituted product *(S)*-**45** was achieved. It was found that a second coupling has to be carried out to obtain the double-substituted derivative *(S)*-**44**. Various coupling reagents were used to optimize the yield for the single and double substitution. The reactions were observed over three days to determine the completion of the reaction. The use of oxalyl chloride gave the highest yields for the coupling with the GCP to obtain the desired coupled compound *(S)*-**44**.

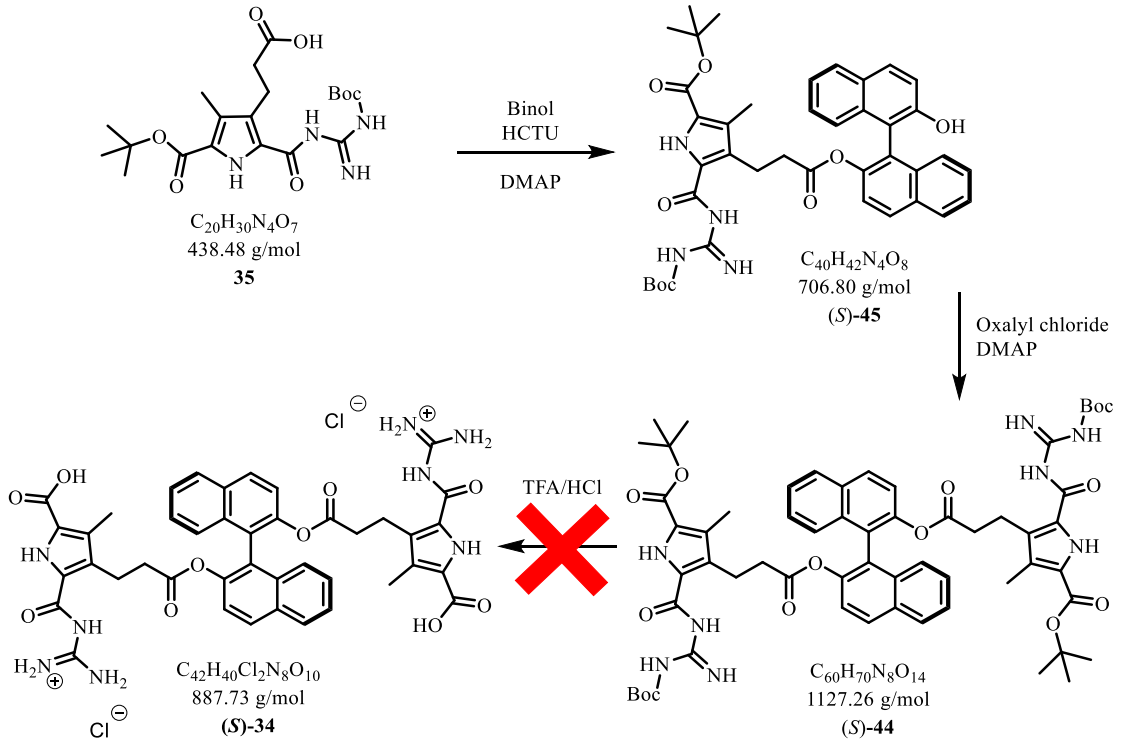

Figure 74: Double esterification of the third generation.

However, the last step of the synthesis of the third generation is the Boc- and *t*-butyl deprotection. Nevertheless, while carrying out the final step a decomposition of compound *(S)*-**34** occurred. NMR measurements were indicating a cleavage of the ester functions due to the acidic conditions. Cooling down the reaction and or slowing down the addition of the acid did not prevent the compound from decomposing. A new synthetic plan was developed for an alternative structure of the third generation.

To solve the problem of acid-induced bond-cleavage, the [1,1'-binaphthalenes]-2,2'-diamine (BINAM) was introduced instead of the BINOL. Using this building block, amide bonds can be generated when the compound **35** is linked.[45]

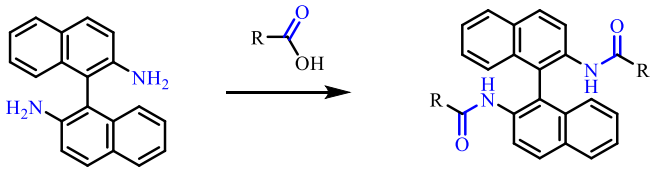

Figure 75: BINAM coupling to generate amides.

By using BINAM as a linker unit of the third generation, the structure of the compound changes slightly. To be sure that the new compound is capable of generating a cyclic structure, another force field calculation was carried out.

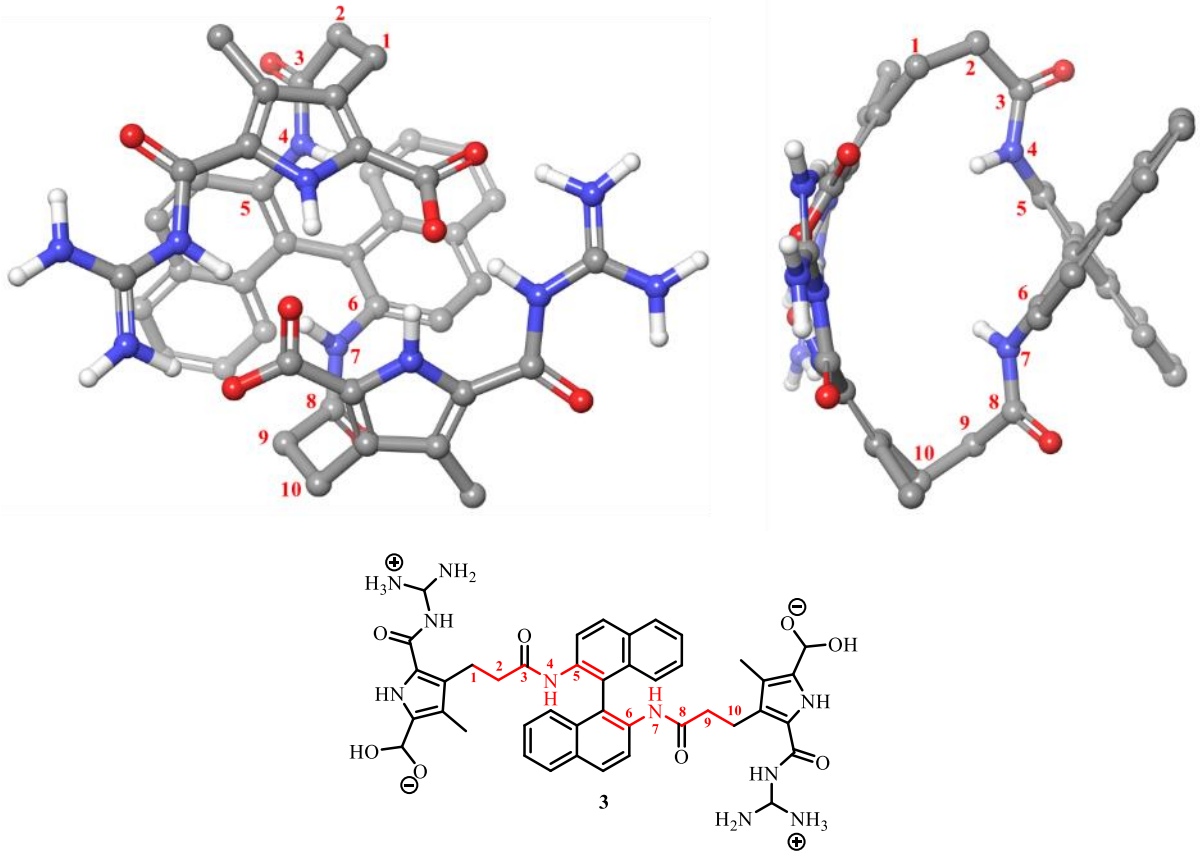

Figure 76: Force field calculation of the BINAM GCP system 3 to form cyclic structures (OPLS force field). Left: Front view. Right: Side view.

The distance between the two binding units is similar to the distance calculated before. Therefore, the same ability to generate cyclic structures is assumed. With these new results, an updated version of the third generation is the new aim for synthesis.

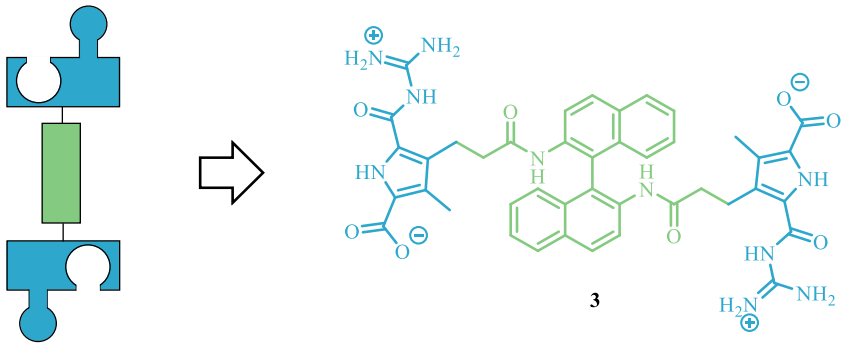

Figure 77: Updated third generation, BINAM GCP derivative 3.

The coupling between BINAM and the compound **35** works much better than the reaction with BINOL. It is now possible to do the double substitution without an additional step in between.

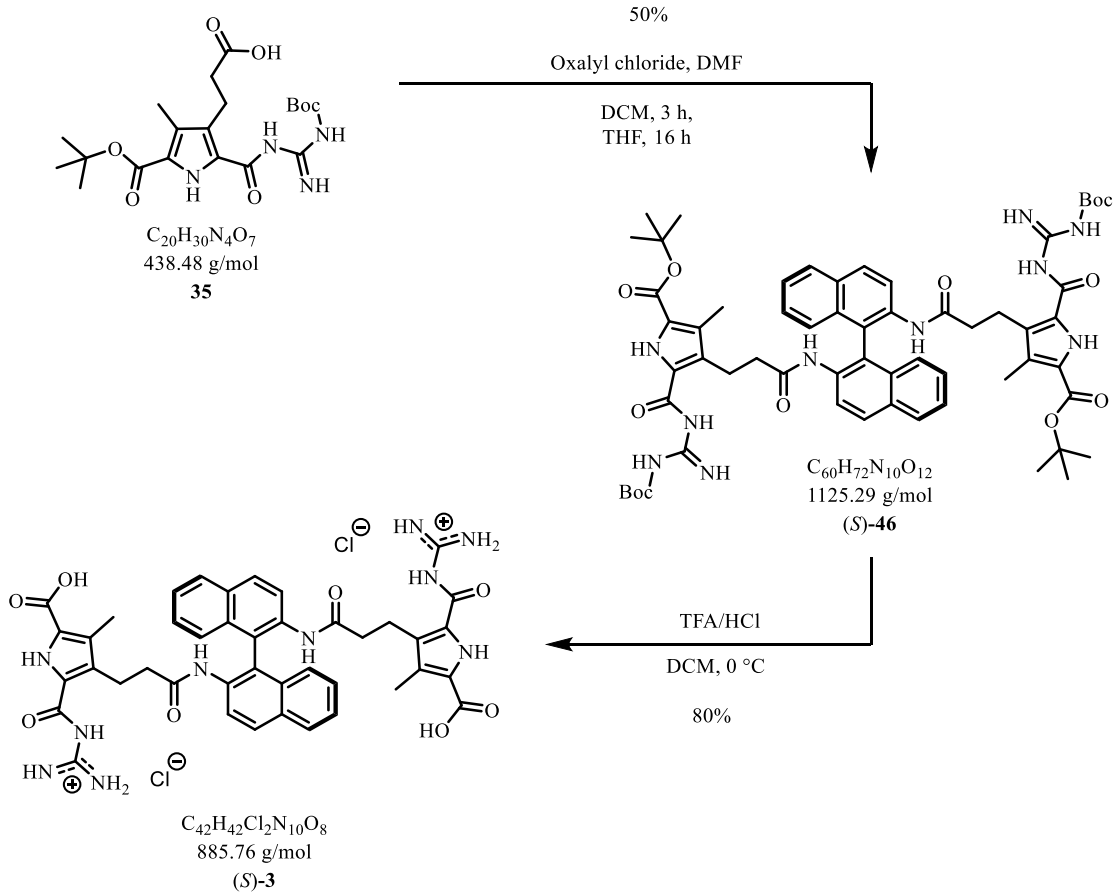

Figure 78: Third generation with BINAM linker unit *(S)*-3.

The coupling reaction of the GCP motif **35** and the BINAM was carried out similar to the synthesis of the BINOL derivative. The reaction was carried out successfully, all NMR signals are matching the

compound *(S)*-**46**. The deprotection of the Boc- and *t*-butyl-group was carried out with standard deprotection conditions with TFA and yielded 80% of the final compound *(S)*-**3**. All signals in the NMR measurements were assigned to the structure of *(S)*-**3**. The signals of the *t*-butyl and Boc-protecting groups have vanished in the ^{1}H and ^{13}C NMR. Additionally, all signals of the ^{1}H NMR which are connected to any heteroatom were assigned to the molecule, which is why a cleavage of the BINAM can be excluded. The NMR spectra for the final compound of the third generation are shown in Figure 79.

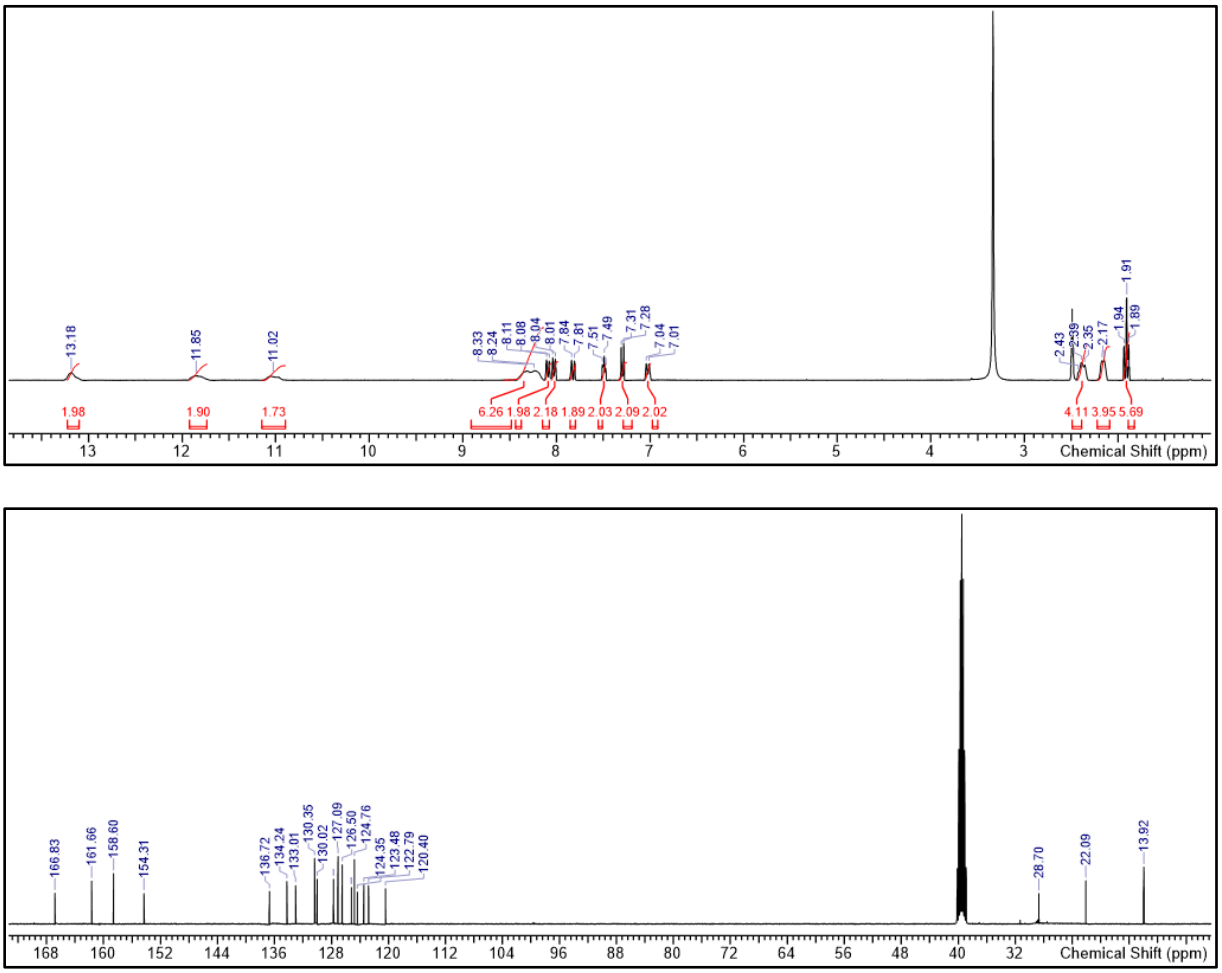

Figure 79: ^{1}H- and ^{13}C-NMR of 3 In DMSO-d_6.

4.2.1.4 Solubility Tests

For the third generation, another solubility test was carried out. Once again, the same solvents as in the first generation were chosen to compare the solubility.

Table 3: Solubility test for the GCP BINAM derivative *(S)*-3.

Solvent	Max. Concentration
Chloroform	10 mM
Toluene	20 mM
DMSO	≥ 200 mM
Nynas NS8	≤ 5 mM
Nexbase 3020	≤ 5 mM
Nexbase 3043	≤ 5 mM

The solubility of the third generation in chloroform is worse than the solubility of the first and second generation. But the solubility in DMSO increases to 200 mM and higher. This is helpful because solutions in DMSO can be measured with temperatures over 100 °C to investigate a possible effect in the viscosity over a broader temperature range.

4.2.1.5 Measurement of the Viscosity

After the successful synthesis and solubility tests of the GCP-BINAM derivative *(S)*-**3**, viscosity experiments were carried out. In this case, DMSO was chosen as a solvent to carry out the viscosity measurements between 25 °C and 100 °C. Different concentrations were chosen to find out in which concentration range a positive effect on the viscosity can be observed. Concentrations from 30 mM to 200 mM were chosen.

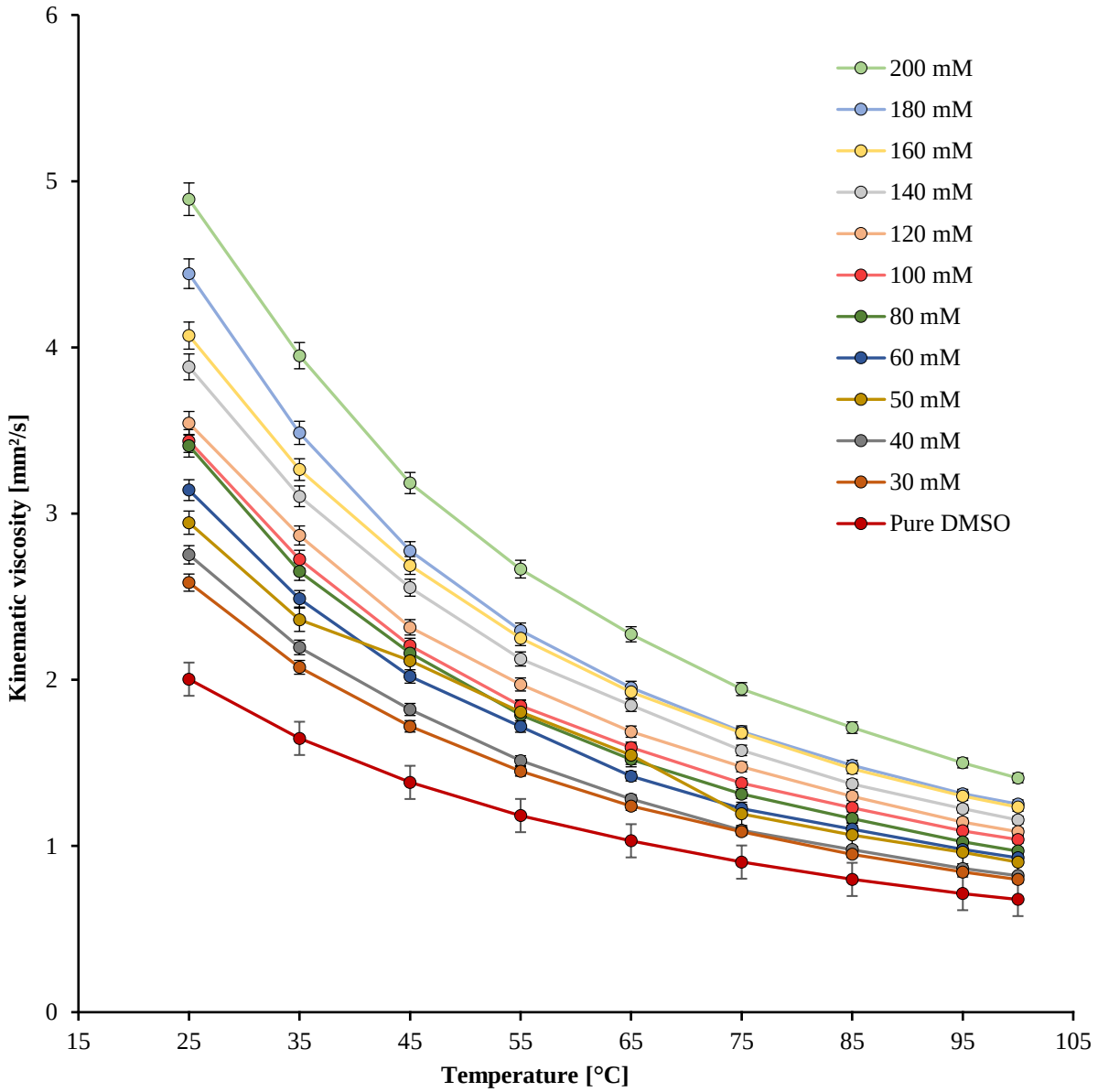

Figure 80: Screening of the kinematic viscosity in dependence of temperature and concentration of the GCP-BINAM derivative *(S)*-3 in DMSO.

The screening of compound *(S)*-**3** is demonstrating the kinematic viscosity in dependence of the concentration and temperature. The viscosity decreases at higher temperatures and at lower concentrations. An irregularity can be observed at a concentration of 50 mM. Here, the kinematic viscosity is behaving differently compared to all other concentrations, since it is not decreasing the same way with higher temperatures. Figure 81 represents the comparison of the 50 mM concentrated solution and pure DMSO.

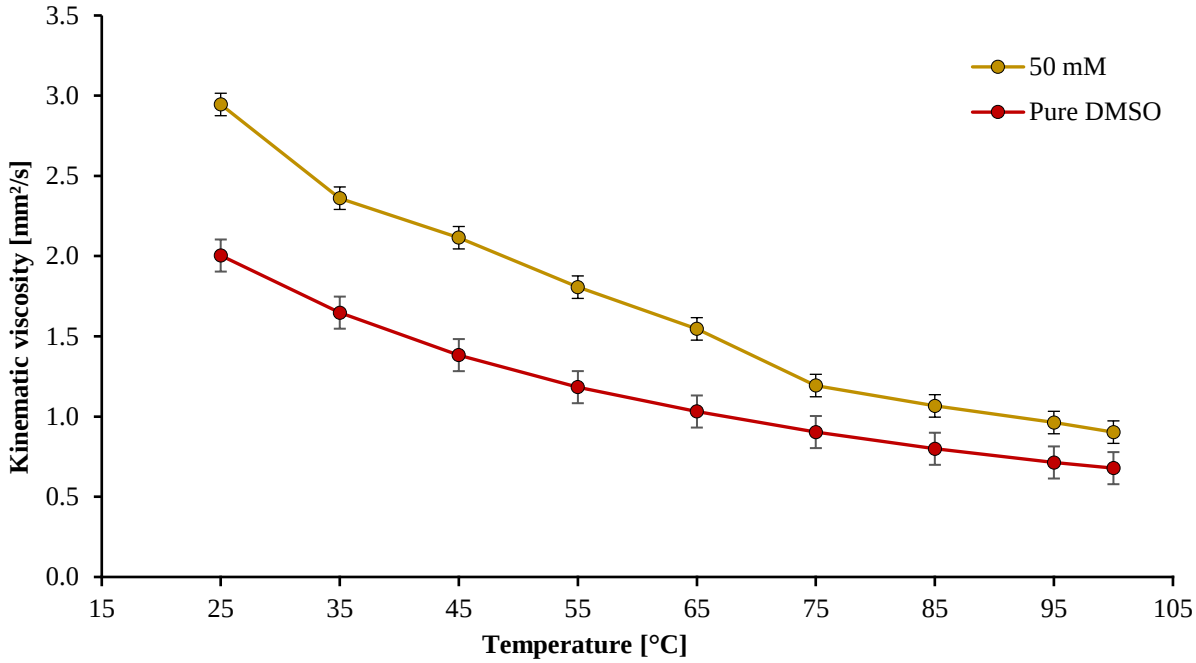

Figure 81: Kinematic viscosity of the third generation in DMSO at a concentration of 50 mM in comparison to pure DMSO.

To investigate the effect of the additive in detail, the specific viscosity was calculated (Figure 82).

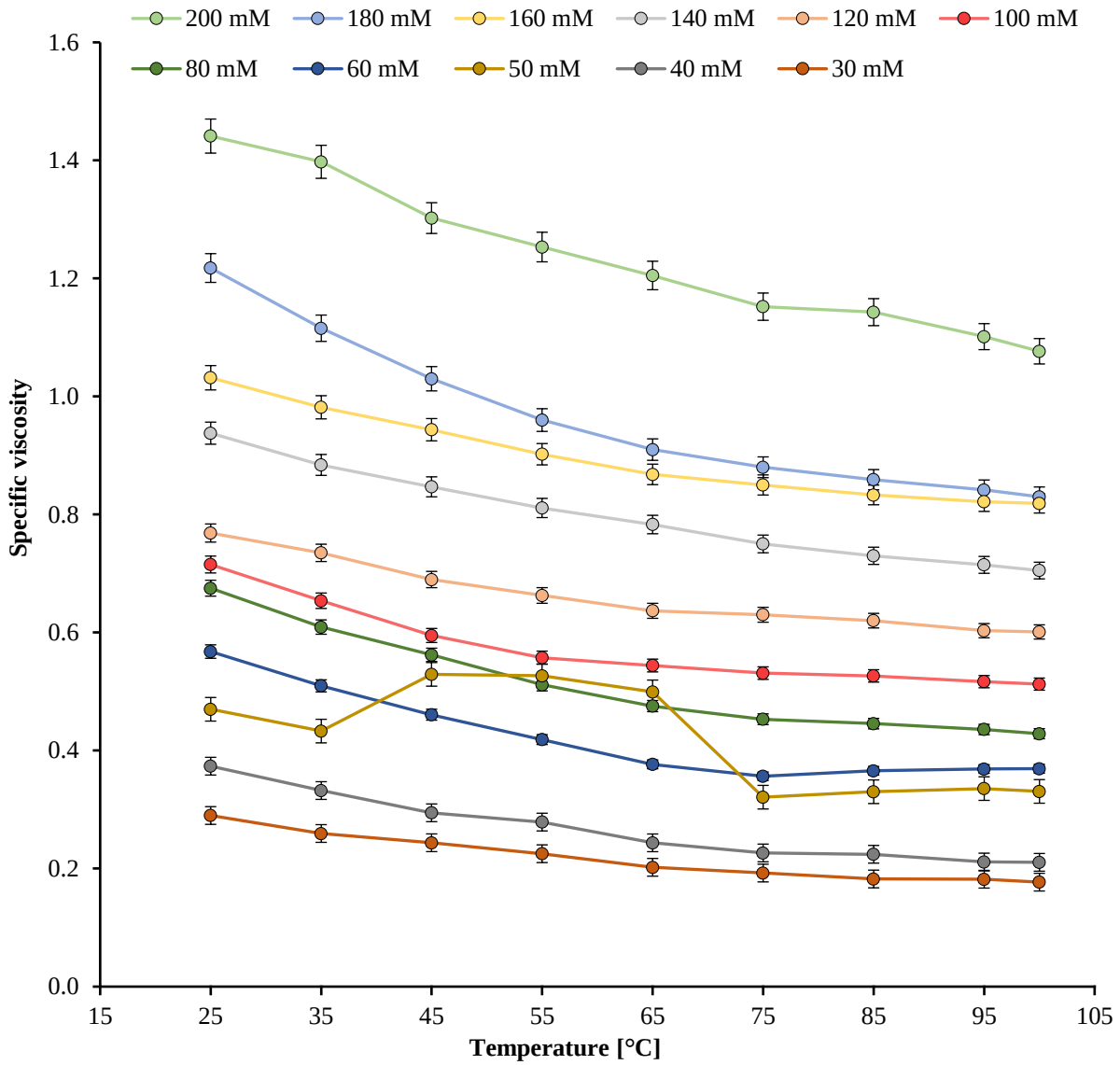

Figure 82: Screening of the specific viscosity, temperature and the concentration of the GCP BINAM derivative *(S)*-3 in DMSO.

At a concentration of 50 mM a major irregularity occurs, due to an increase of the specific viscosity of 13% between 35 °C and 45 °C, and with a decrease at 75 °C. While all other concentrations are decreasing with elevated temperatures, this is the only concentration an improvement of the viscosity within elevated temperatures is obtainable. Nevertheless, the effect seems to be ending at temperatures higher than 75 °C.

4.2.1.6 DLS Measurements

After the results of the viscosity measurements, the results were verified using a DLS measurement. For this purpose, the hydrodynamic radius of a 50 mM solution of *(S)*-**3** in DMSO was determined at 25 °C, 60 °C and 100 °C.

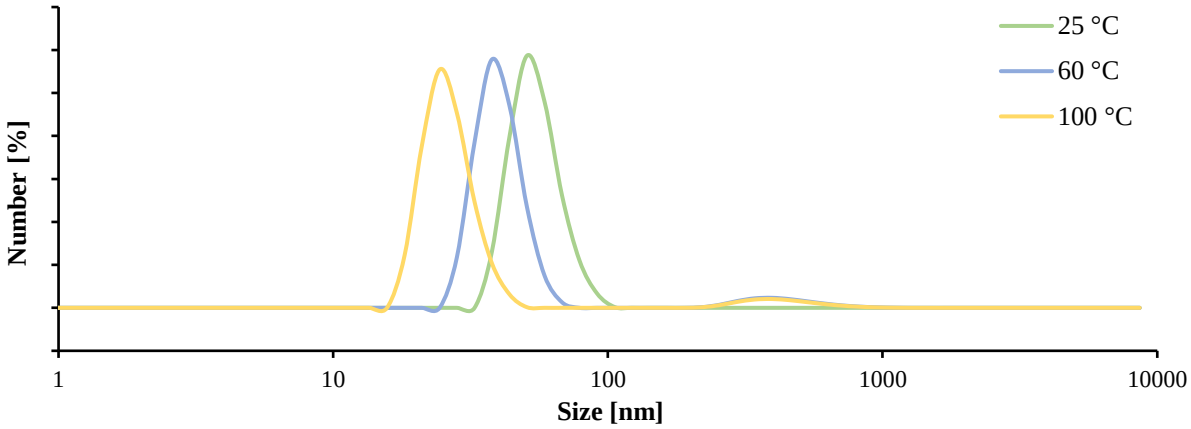

Figure 83: Comparison of standardized DLS measurements of the GCP-BINAM *(S)*-3 at a concentration of 50 mM in DMSO.

The first DLS measurement at 25 °C demonstrates the average hydrodynamic radius of 50 nm. There is only one peak with a signal number of 100%. Elevating the temperature results in a second peak with an average hydrodynamic radius of 396 nm. At 60 °C this peak has a signal number of 6.3% in comparison to the first peak (93.7%) while the first peak is decreasing in size. At 100 °C the first peak decreases further in size and the second peak has a signal number of 5.5%. This increase of the signal number of the second peak until 60 °C and decrease until 100 °C fits to the viscosity measurements before, where a viscosity improving effect occurred until a temperature of 75 °C. To explain the results of the DLS-measurements, the cyclization of the monomeric units needs to be observed. An approach of explanation is the occurrence of multiple cycles in different sizes within the solution (Figure 84).

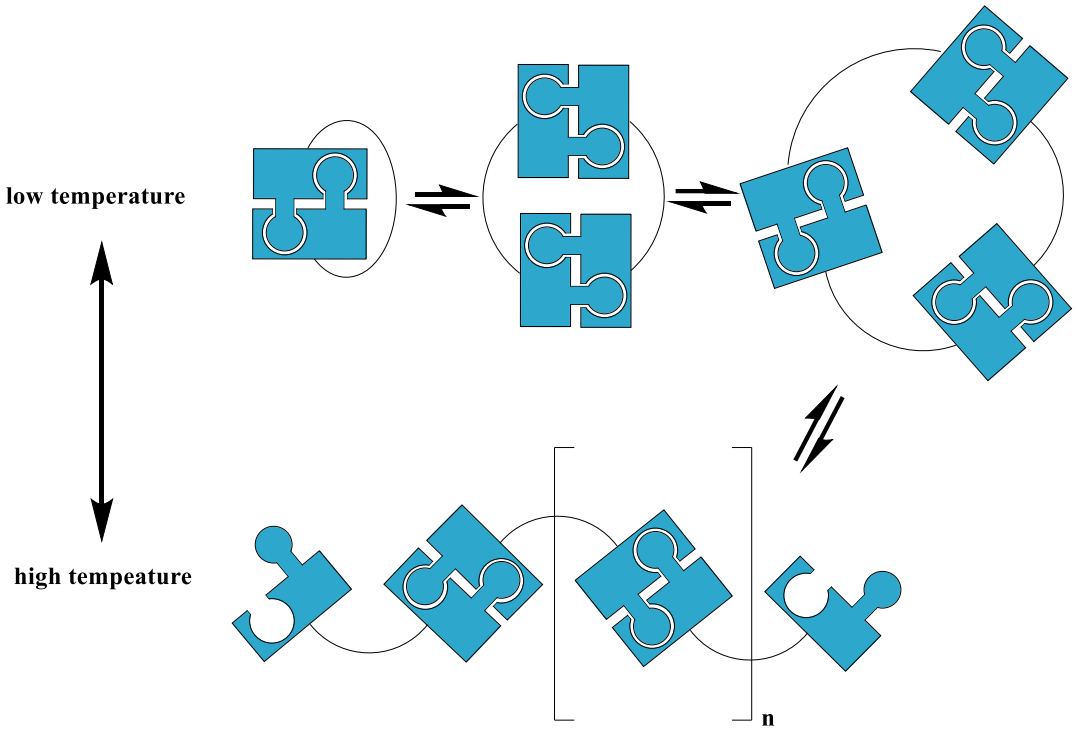

Figure 84: Approach of explanation for DLS-measurements, different cyclic and polymeric structures of monomeric unit *(S)*-3.

In this approach of explanation, the first peak of the DLS measurement is representing the cyclic structures formed of a few monomeric units. Here, even bigger structures of more than one or two monomeric units are involved, due to the average signal size of 50 nm. Therefore, the first peak involves different kinds of cyclic structures and the hydrodynamic radius represents the average radius of all these structures. Elevating the temperature leads to the formation of bigger structures, that can be pictured in the second peak. Here, polymers or large cycles might be responsible for the second peak. But by generating larger structures, the average hydrodynamic radius of the first peak decreases due to less amount of cycles. Increasing the temperature to 100 °C might lead to a decrease of the number of cycles in the first peak and no formation of larger structures. Therefore, the overall hydrodynamic radius is decreasing, as seen in the viscosity measurements.

4.2.2 Fourth Generation: Implementation of the Effect in Oil

The main problem of the generations 1-3 is the lack of solubility in unpolar solvents. The first and second generation were only soluble in chloroform and the third generation was only soluble in DMSO due to the high polarity and the charged properties of the GCP motif **7**. To improve the solubility in unpolar solvents like motor oils, structural modifications are necessary. The idea of the fourth generation is to use another binding motif, ACP. The ACP motif **8** uses similar interactions as the GCP motif **7** but is not charged in a neutral pH range. In the fourth generation, an increase of the solubility was the focus.

4.2.2.1 Improvement of the Solubility with the ACP-Motif

Since the GCP motif **7** yielded promising results as a VI improver, this effect needs to be implemented in different solvents. Therefore, the ACP motif **8**, a neutral analogue of the GCP motif **7** is the focus.[33] Exchanging the GCP binding units with the ACP motif should lead to similar behaviour of the ring-chain transition and might have a positive effect on the solubility.[29]

For this system, another force field calculation was carried out to investigate the behaviour of the cyclic structure.

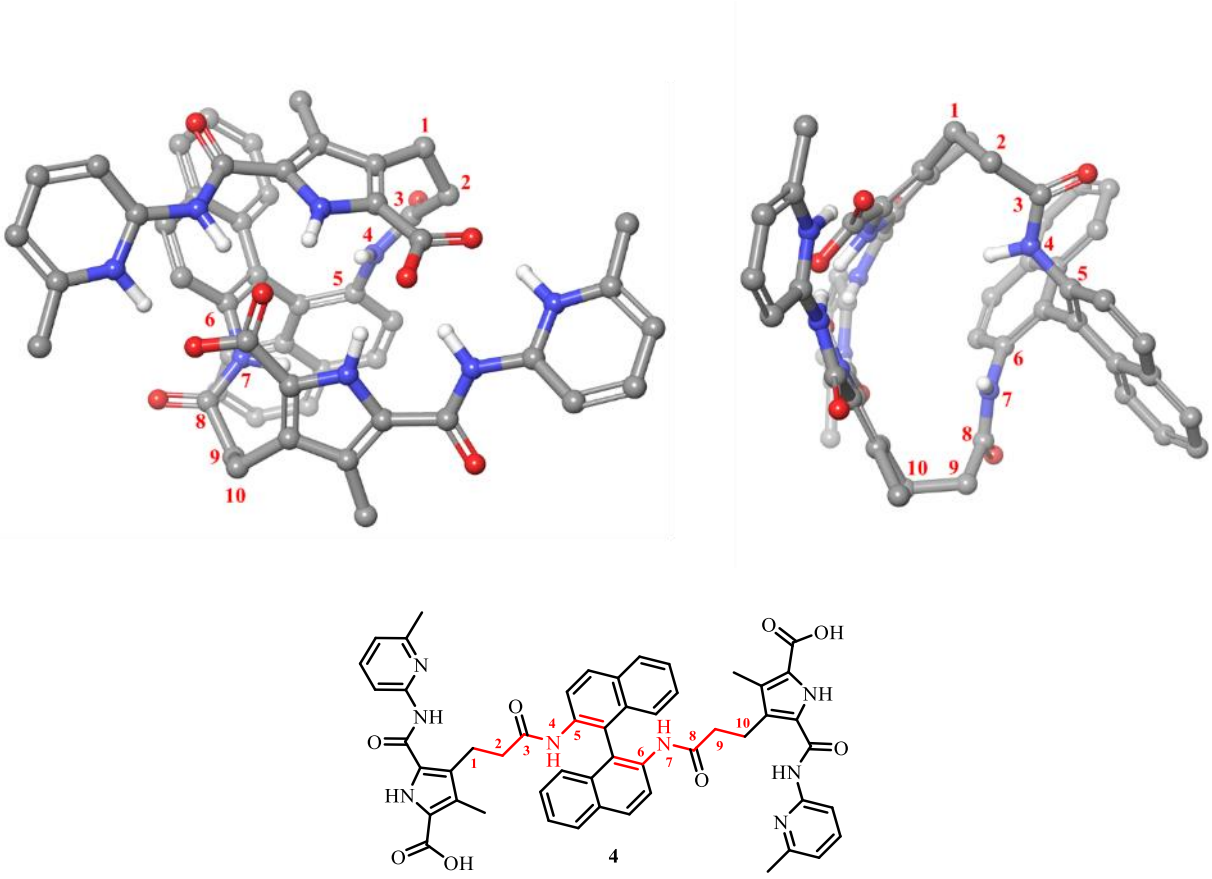

Figure 85: Force field calculation of the BINAM ACP system 4 to form cyclic structures (OPLS force field). Left: Front view. Right: Side view.

Despite the pyridine function in the binding unit, there is no change in comparison to the third generation. Therefore, no differences in the ability of a cyclization are expected to be in the fourth generation.

4.2.2.2 Structure of the Monomeric Unit

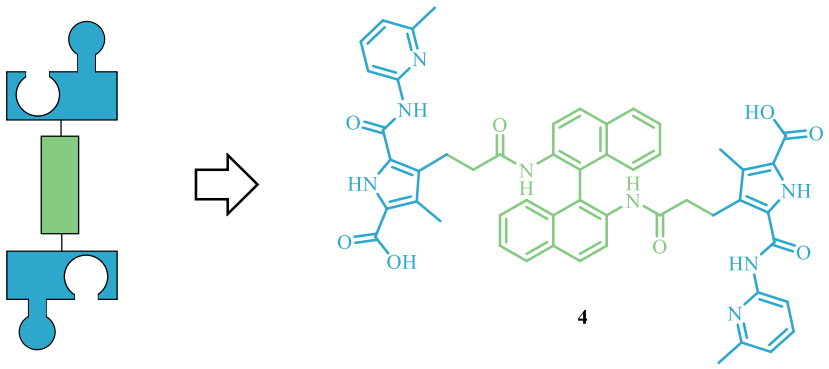

Figure 86: Fourth generation. ACP-BINAM derivative 4.

The structure of the fourth generation is similar to the structure of the third generation.

4.2.2.3 Synthesis

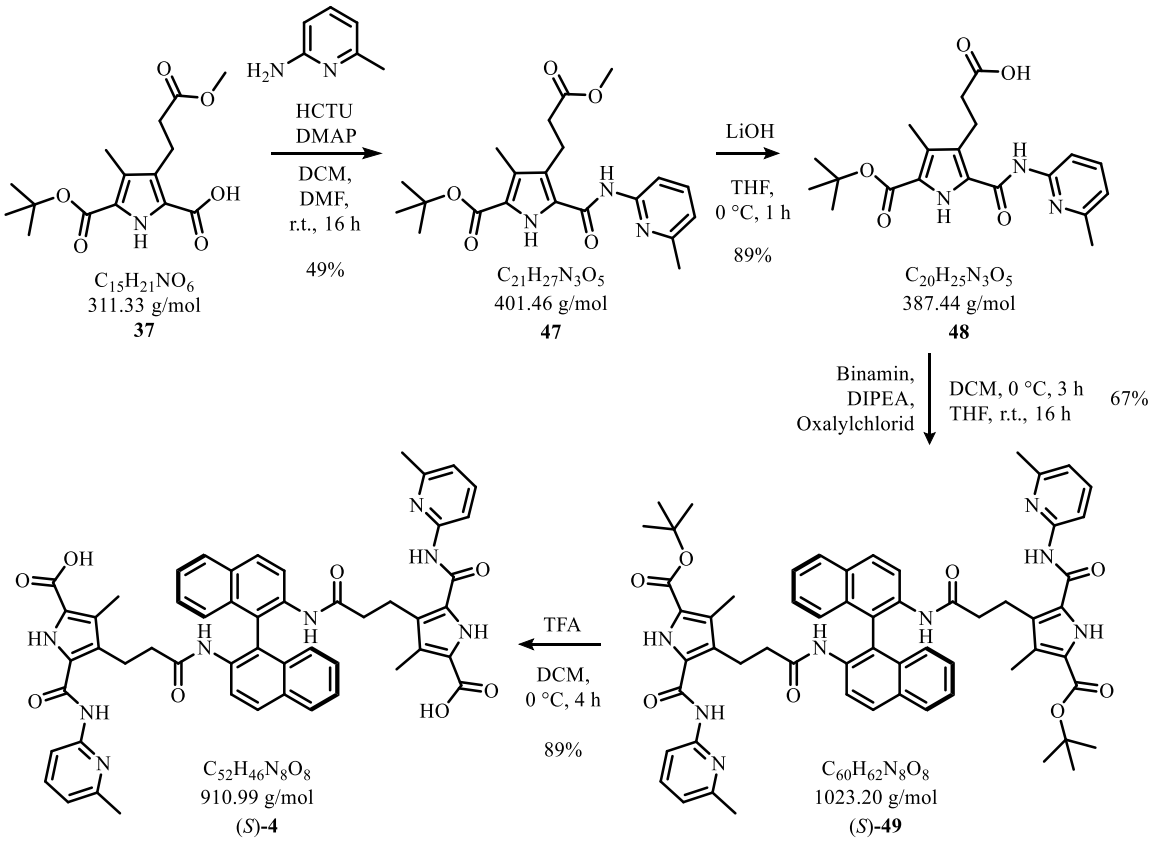

Figure 87: Synthesis of the fourth generation compound *(S)*-4.

The synthesis was carried out similar to the synthesis of the GCP-BINAM derivative **3**. Starting with the precursor **37**, the ACP motif **48** was synthesized via coupling reactions. The formation of compound **47** was based on the reaction of **37** with 2-amino-6-methylpyridine, using HCTU and DMAP as coupling reagents like in the third generation. The product was obtained with a yield of 49%. The methyl deprotection was carried out with LiOH in a quantitative yield. The signal of the methyl ester vanished at the ^{1}H and ^{13}C NMR spectrum. In this case, the coupling with the BINAM was carried out in similar conditions like in the third generation, the optimized synthetic conditions turned out to be suitable for this system too. The protected product *(S)*-**49** was obtained in a yield of 67%. A subsequent Boc-deprotection led to the final product *(S)*-**4** with a yield of 89%. Especially, the signals in the NMR measurements of the signals of the *t*-butyl protecting group have vanished. The NMR spectra for the final compound of the fourth generation are shown in Figure 88.

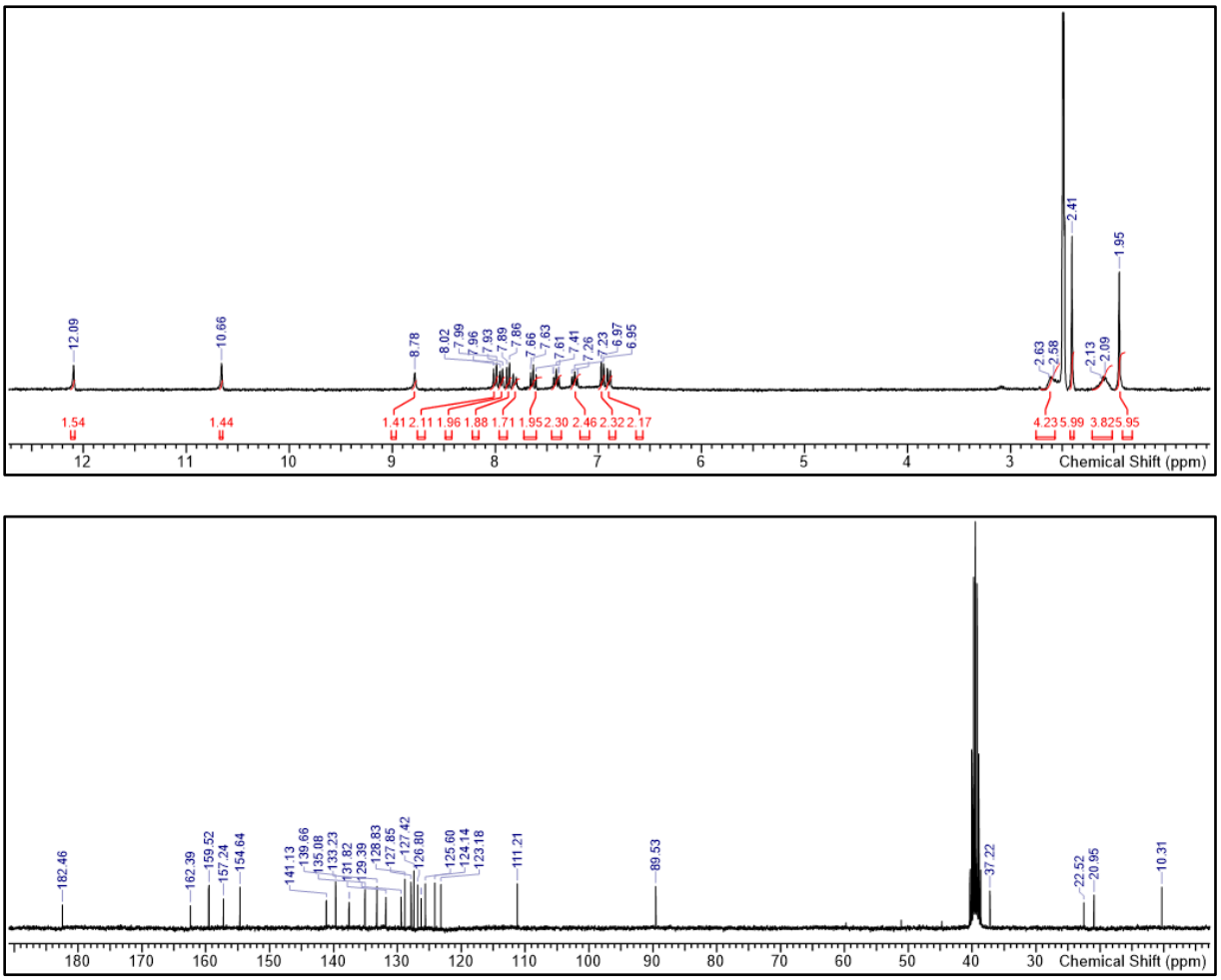

Figure 88: ^{1}H- and ^{13}C-NMR of 4 in DMSO-d_6.

4.2.2.4 Solubility Tests

For the fourth generation, another solubility test was carried out to investigate how the new binding unit is affecting the solubility. The same solvents as in the examples before were chosen to compare each generation.

Table 4: Solubility test for the ACP BINAM derivative *(S)*-4.

Solvent	Max. concentration
Chloroform	≥ 200 mM
Toluene	≥ 200 mM
DMSO	≥ 200 mM
Nynas NS8	60 mM
Nexbase 3020	≤ 5 mM
Nexbase 3043	≤ 5 mM

Once again it can be seen that the binding unit has an extremely high influence on the solubility of the whole compound. The fourth generation is, in contrast to the third generation, able to be dissolved in unpolar solvents like chloroform and toluene. Even in Nynas NS8, one of the thinner motor oils, it is possible to make solutions up to 60 mM. The viscosity measurements will start with the DMSO solution, to allow a comparison between the third and fourth generation.

4.2.2.5 Measurements in DMSO

After the synthesis and enhanced solubility of the fourth generation, the viscosity measurements were continued. To start these measurements, the DMSO solution was chosen for the first viscosity measurements to enable measurements in a temperature range of 25 °C to 100 °C and to compare these results with the data of the third generation. Due to the new binding unit, another screening of the viscosity in different concentrations was made to investigate the kinematic viscosity in dependence of temperature and concentration. For the concentration, a similar range was chosen as in the third generation.

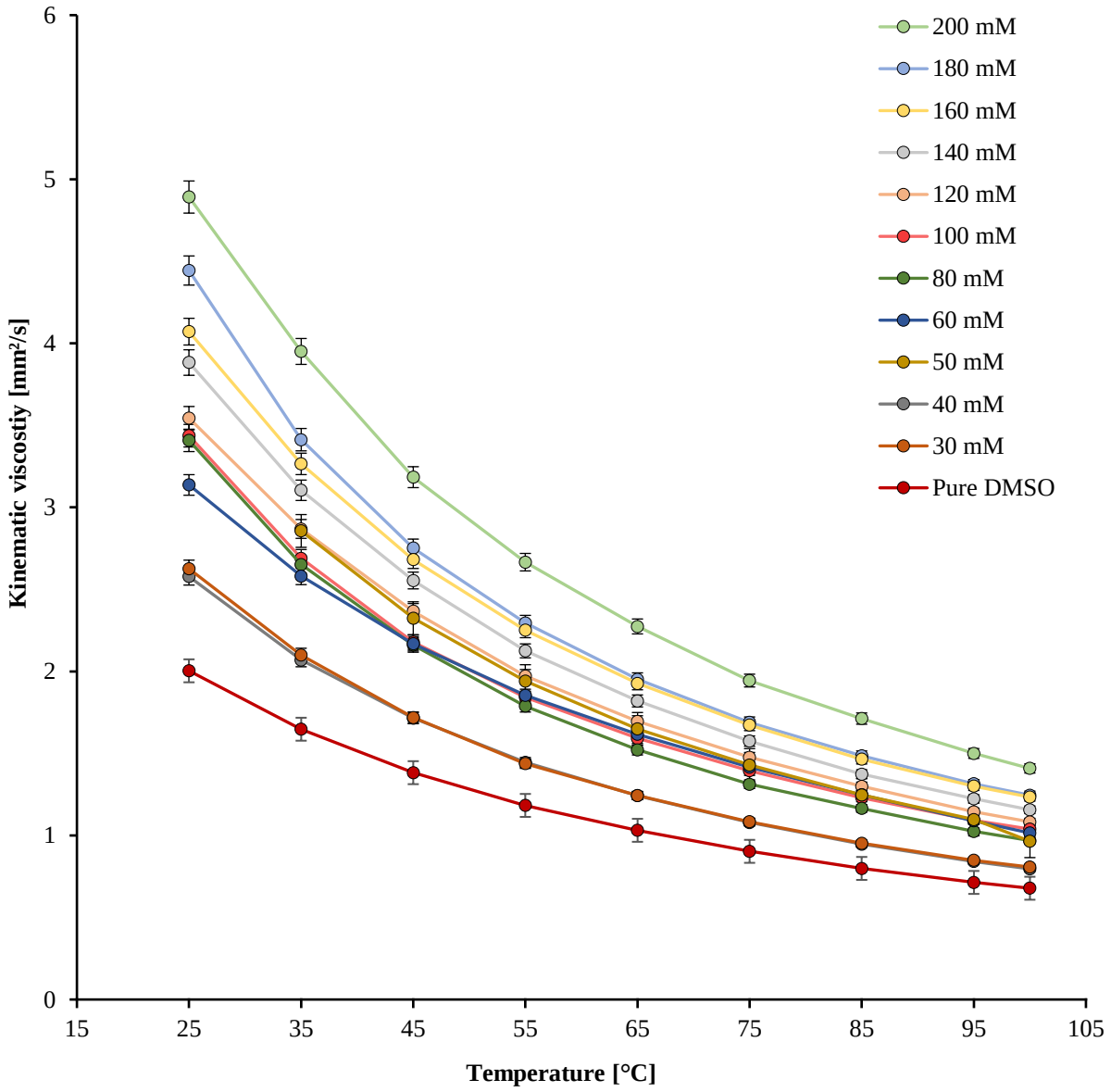

Figure 89: Screening of the kinematic viscosity in dependence of temperature and concentration of the ACP BINAM derivative *(S)*-4.

The screening demonstrates the kinematic viscosity in dependence of the concentration and the temperature. Like in all viscosity measurements, the viscosity drops down at higher temperatures and lower concentrations. An irregularity like in the third generation is hard to observe but in a range of 60 mM to 80 mM some effects are taking place.

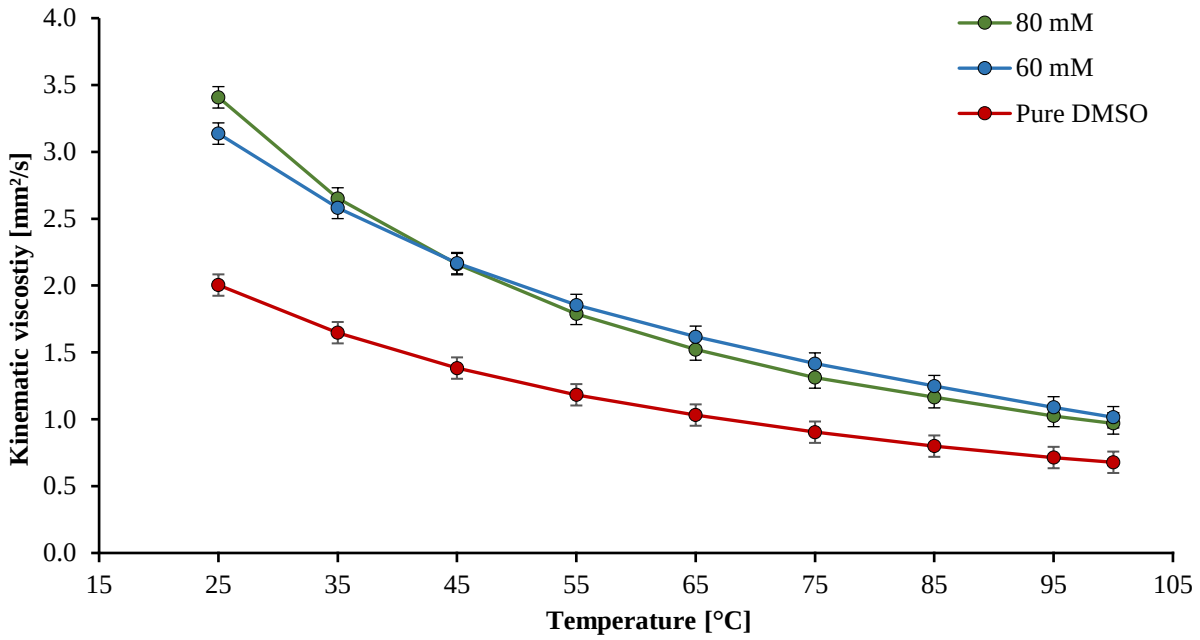

Figure 90: Comparison of the kinematic viscosity of the third generation in concentrations of 60 mM, 80 mM and pure DMSO.

While the viscosity of the 80 mM solution is decreasing steadily with increasing temperatures, the viscosity of the 60 mM solution decreases less significantly, up to a point where its viscosity is even higher than that of the 80 mM solution (for temperatures > 45 °C). To investigate the effect and give a closer look at the concentrations of the effect, the specific viscosity was calculated.

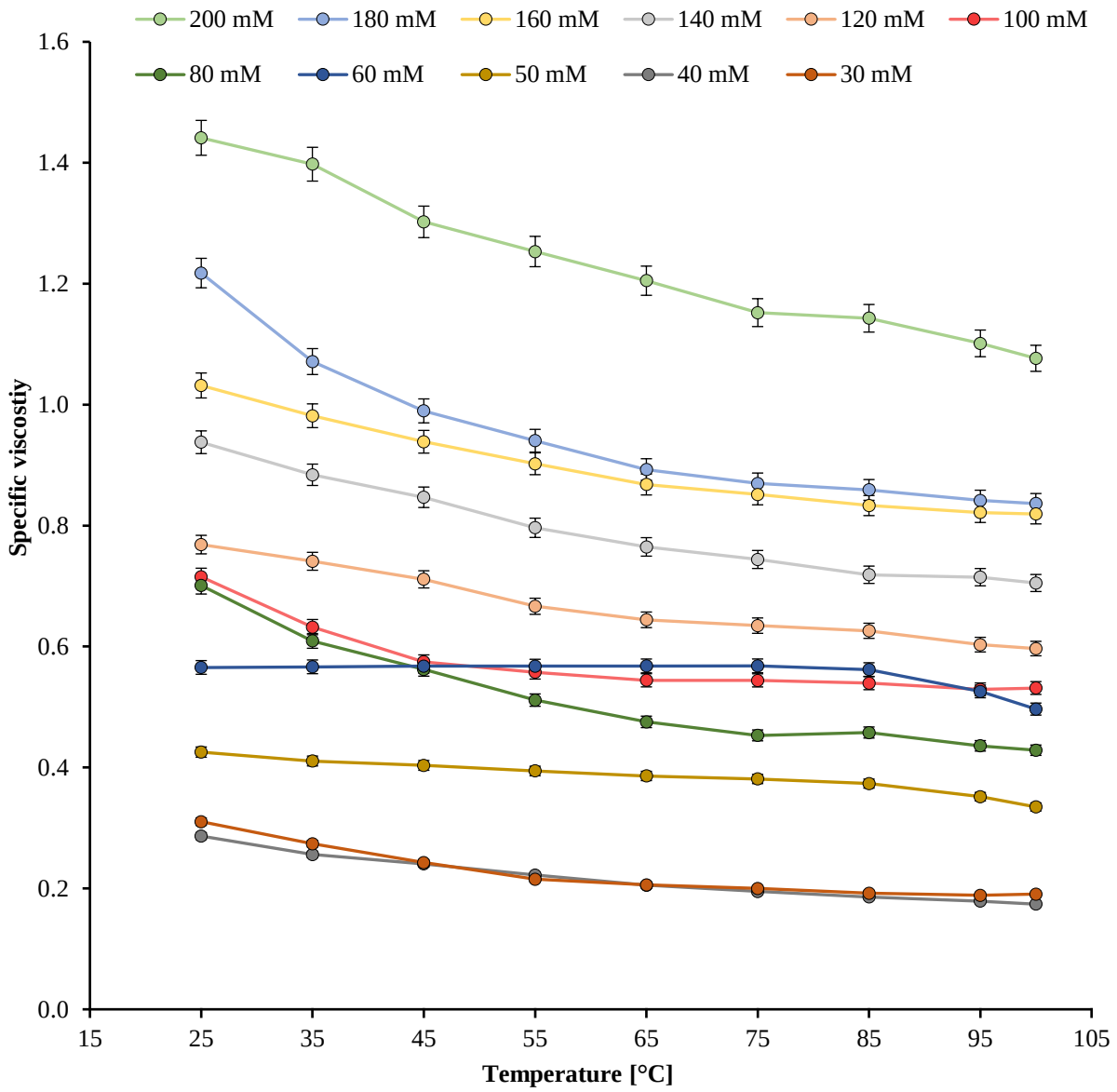

Figure 91: Screening of the specific viscosity, temperature and the concentration of the GCP-BINAM derivative *(S)*-4.

The screening of the specific viscosity demonstrates similar results to the third generation. Looking at all concentrations, an irregularity can be seen at a concentration of 60 mM. Here, in contrast to all other concentrations, a slight increase of the specific viscosity can be seen in a range of 25 °C to 85 °C. Only at higher temperatures, the specific viscosity decreases again.

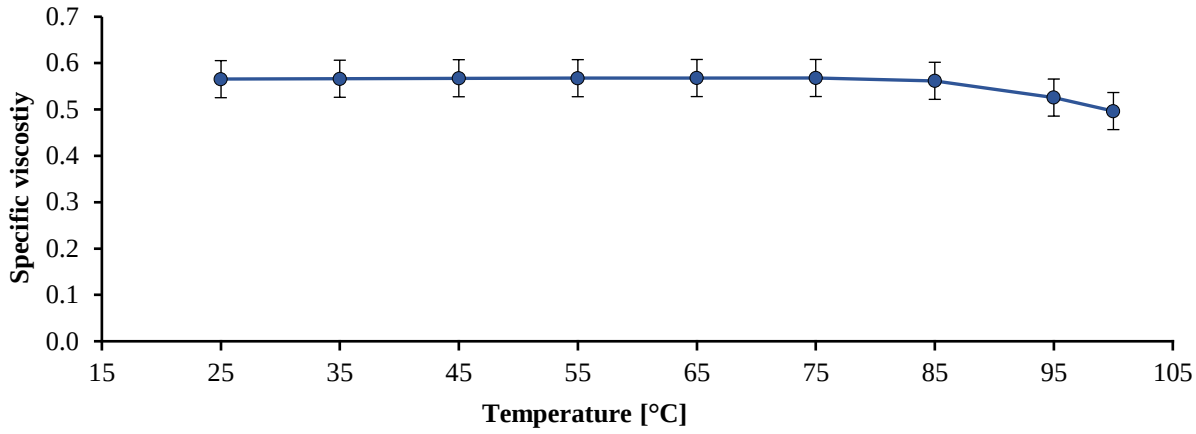

Figure 92: Specific viscosity of the fourth generation in a concentration of 60 mM in DMSO.

Comparing this finding to the effect of the third generation, the fourth obtains only increases up to 0.5% within the whole temperature range in comparison to 13% of the third generation. However, the specific viscosity remains almost constant between 25 °C and 85 °C, while the viscosity improvement for the third generation could only be seen in a temperature range of 40 - 70 °C.

After the successful measurement of the viscosity, measurements of the hydrodynamic radii were carried out. To see if the increased viscosities go along with increased hydrodynamic radii. A 60 mM solution in DMSO was prepared to investigate the effect in DLS measurements. Once again, the measurements were carried out in temperatures of 25 °C, 60 °C and 100 °C to compare the data to the other generations.

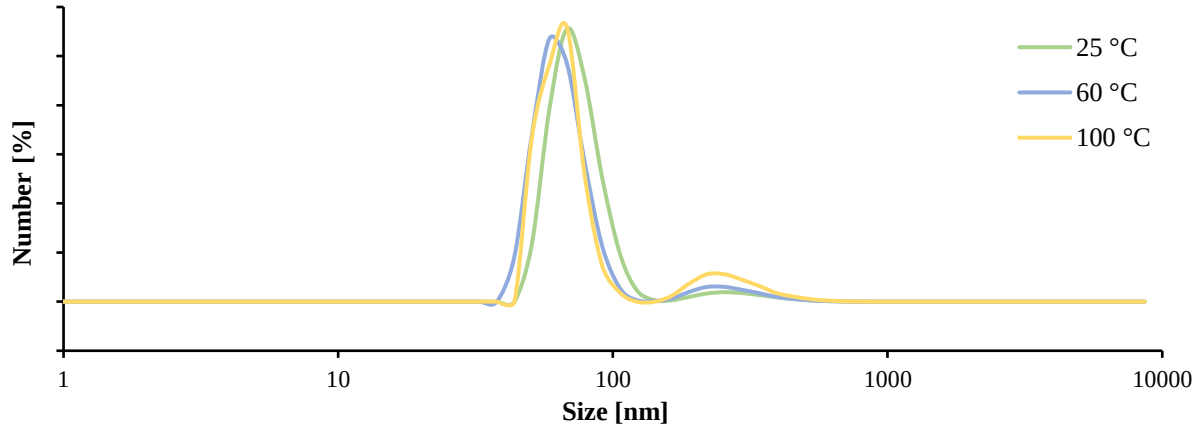

Figure 93: Hydrodynamic radius of the fourth generation in DMSO (60 mM).

Looking at the DLS measurements of the DMSO solution a similar behaviour to the third generation is observed. Once again, there are two peaks of different signal sizes. Despite the measurements in the third generation, even in the 25 °C measurement is developing a first peak of an average hydrodynamic

radius of 78 nm with a signal number of 95.1% and a second peak with a hydrodynamic radius of 255 nm. Despite in the third generation, increasing the temperature to 60 °C and 100 °C leads to an increase of the signal number of the second peak to 13.6%, while the signal number of the first peak is only changing slightly (68 nm at 100 °C). The constant increase of the second peak is related to the increase of the specific viscosity, while the specific viscosity was almost unchanged until 85 °C. With the same approach of explanation as in the third generation, this effect might occur due to the presence of a mixture of different sized cyclic structures, that are observed in the first peak. Elevating the temperature, initiates a polymerization or formation of larger cyclic structures which can be seen in the second peak. In contrast to the third generation, the formation of larger structures does not stop at temperatures below 100 °C.

Since the dimerization of the ACP binding motif is weakened due to DMSO which can act as a competitive solvent for hydrogen-bonding, different solvents need to be tested for this generation. Luckily, the fourth generation is soluble und chloroform, toluene and Nynas NS8. Therefore, the dimerization of the ACP motif should be favoured in these solvents in comparison to DMSO. This is the reason why in the following chapters different solvents are used, to investigate the effect of the fourth generation.

4.2.2.6 Measurements in Chloroform

The next measurement of the viscosity was carried out in chloroform. Therefore, another screening was carried out at different concentrations and temperatures. Due to the boiling point of chloroform of 60 °C the temperature was only increased to 50 °C. Because of the successful measurements in DMSO a similar concentration range of the effect was chosen so that only a range of 40 mM to 100 mM was investigated.

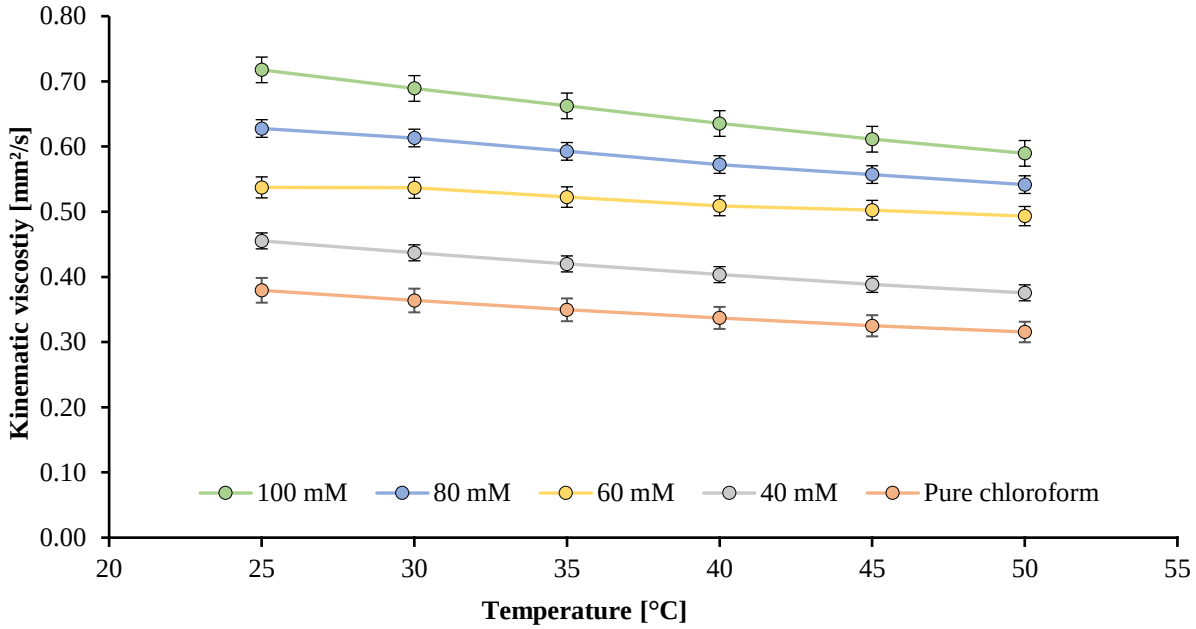

Figure 94: Screening of the kinematic viscosity in dependence of temperature and concentration of the ACP-BINAM derivative *(S)*-4 in chloroform.

These measurements are demonstrating an effect at a concentration of 60 mM similar to the one in DMSO solution. Therefore, the effect occurs in the same concentration and is not changed with changing the solvent, due to the occurring irregularity at the 60 mM solution. Therefore, the assumption, that this effect only is dependent on the concentration and not the solvent, seems accurate. To investigate the effect in detail, another calculation of the specific viscosity was carried out.

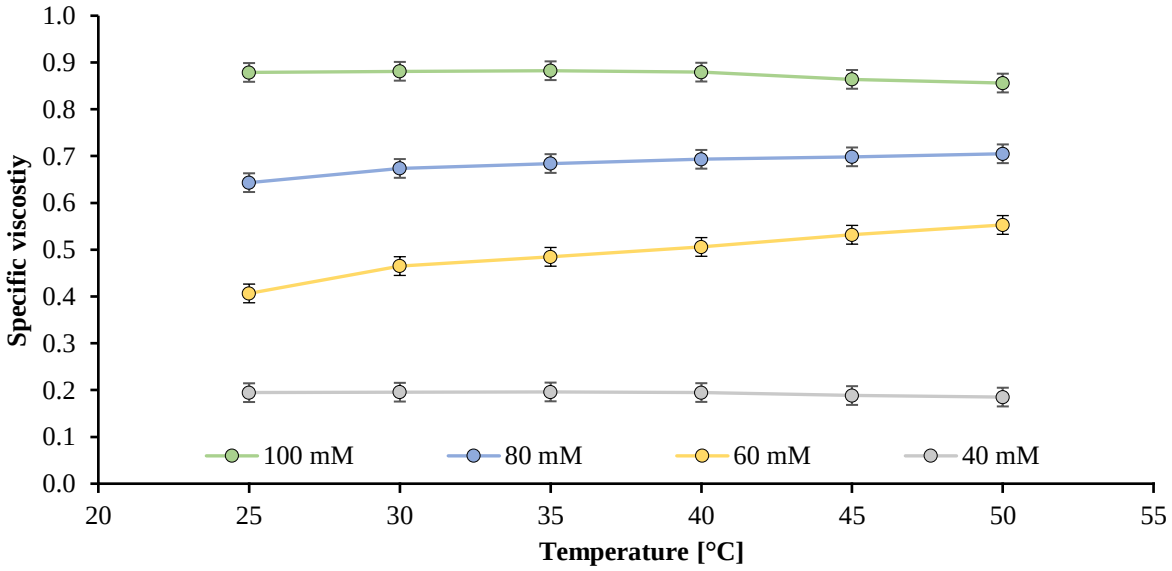

Figure 95: Screening of the specific viscosity in dependence of temperature and concentration of the ACP-BINAM derivative *(S)*-4 in chloroform.

The 60 mM and 80 mM concentrations are indicating an increase of the specific viscosity with the temperature. The specific viscosity is increasing with elevating temperature over the whole temperature range of 25 °C to 100 °C. Especially the viscosity of the 60 mM concentrated solution of compound *(S)*-**4** is increased by 36% between 25 °C and 50 °C, which is the highest increase of all previously investigated generations. One possible reason might be the stronger pairing of the ACP motif in the non-competitive chloroformic solution, which leads to an increased viscosity at elevated temperatures. This behaviour leads to the assumption of a greater effect in more unpolar solvents. This behaviour would be beneficial for an application in highly unpolar oils.

To prove the effect on the viscosity, DLS measurements were performed as well. Therefore, the 60 mM solution in chloroform was measured at 25 °C, 37 °C and 50 °C to observe the behaviour of the hydrodynamic radius at increased temperature.

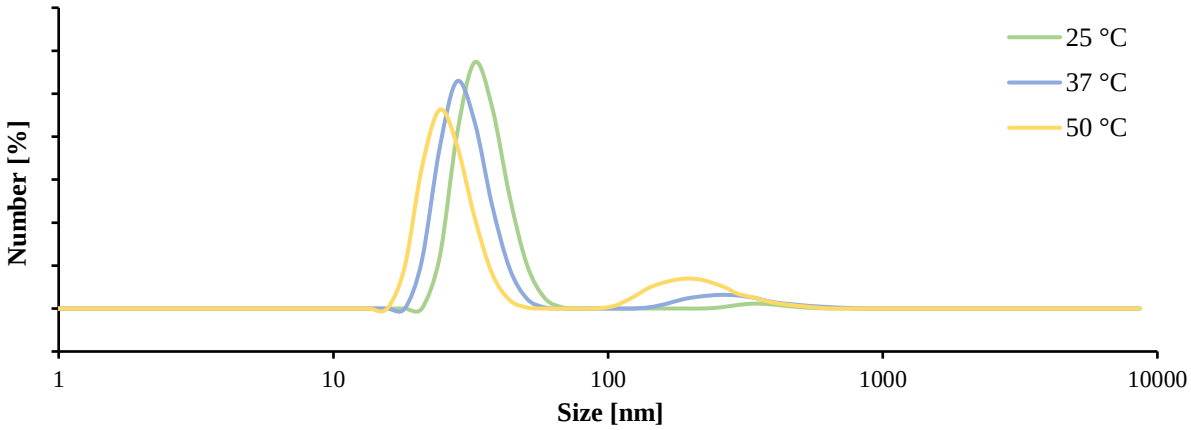

Figure 96: DLS measurement of the fourth generation.

The DLS measurements highlight a similar effect as in the measurements in DMSO. While at 25 °C the second signal has a signal number of 2.0% the 37 °C and 50 °C measurements are developing larger signal numbers of 9.5% and 20.8%. While the first peak obtains hydrodynamic radii of around 30 nm, the second peak has radii around 300 nm. Once again, the first peak is decreasing in the hydrodynamic radius and the signal number within higher temperatures. Noticeable is the behaviour of the second peak, where a decrease of the hydrodynamic radius occurs but an increase of the signal number. Once again, this behaviour might be explained by the occurrence of different cyclic structures represented by the first signal, while in contrast to the measurement in DMSO smaller cycles are present. The formation of larger structures represented by the second peak fits to the results of the viscosity measurements, where an increase of the specific viscosity occurred in the whole temperature range.

4.2.2.7 Measurements in Toluene

The next measurements were taking place in toluene. Here the same conditions (40 mM to 100 mM) were chosen as in the measurements of chloroform but with a higher temperature range.

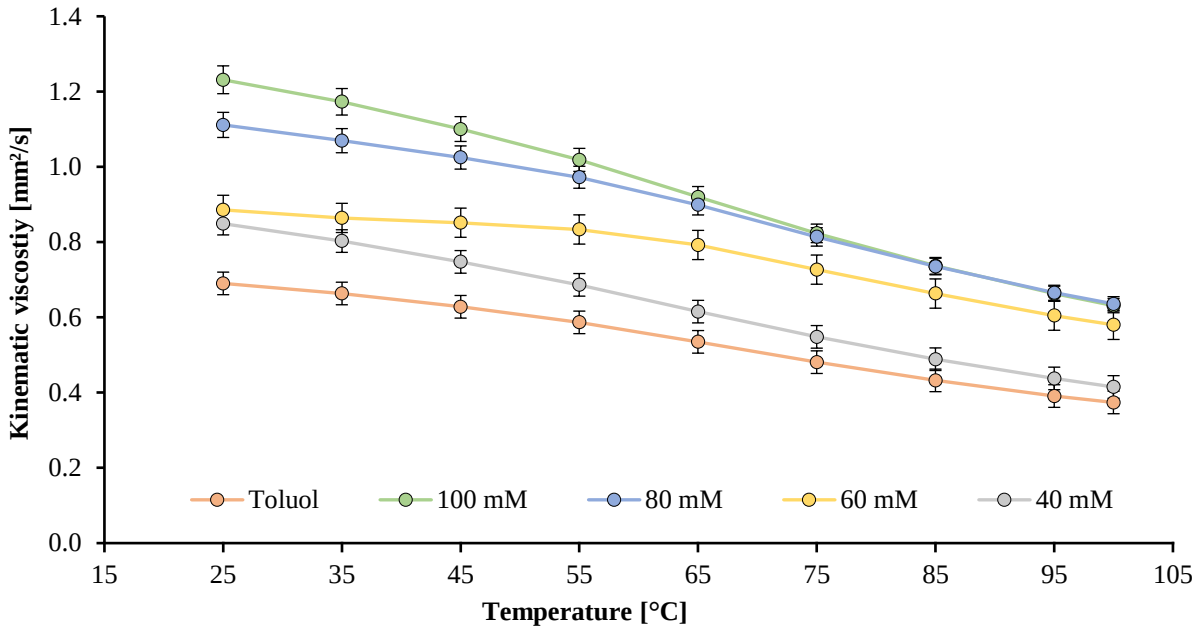

Figure 97: Screening of the kinematic viscosity, temperature and the concentration of the ACP-BINAM derivative *(S)*-4 in toluene.

The irregularity of the kinematic viscosity is once again observable at the concentrations 60 mM and 80 mM. Especially the effect of the 60 mM solution can be seen over a large temperature range. Here, the kinematic viscosity does not decrease as distinct as all other concentrations until 85 °C which highlights, how dominant the effect in more unpolar solvents is. All other concentration except for the 80 mM concentration are behaving similar to the solvent and have a rapid decrease of the kinematic viscosity at elevated temperatures. To investigate this effect in detail, the calculation of the specific viscosity was carried out.

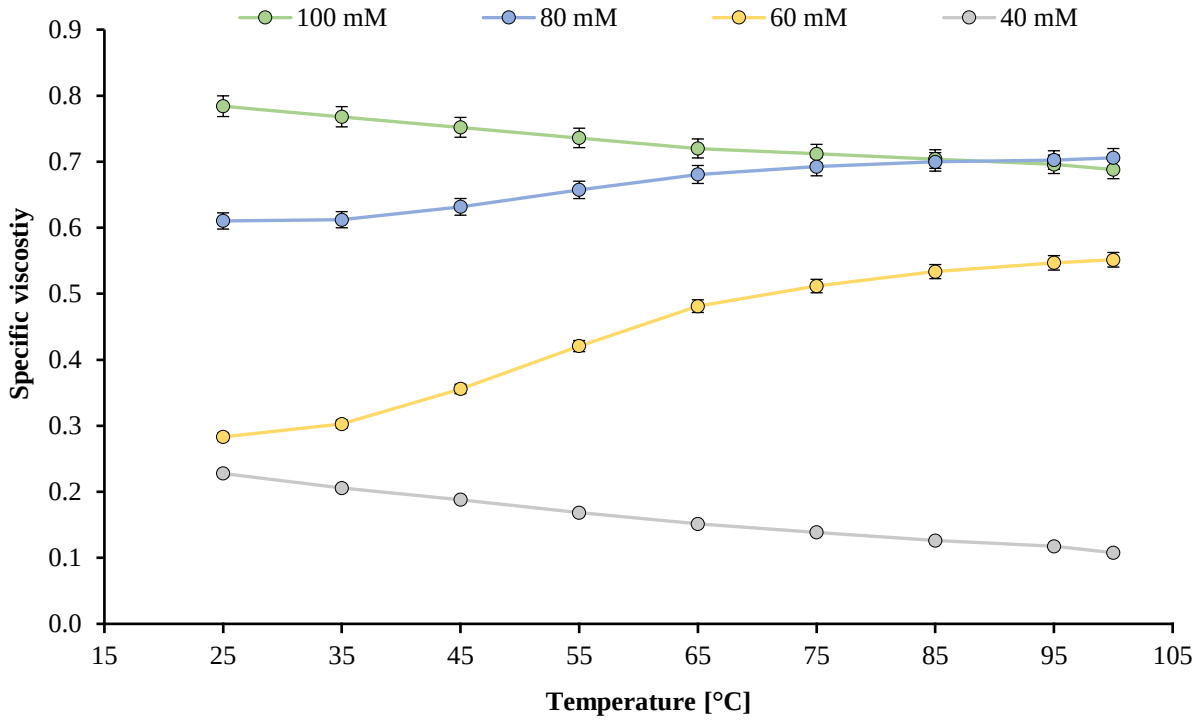

Figure 98: Screening of the specific viscosity, temperature and the concentration of the ACP-BINAM derivative *(S)*-4 in toluene.

The results of these measurements in toluene are indicating the most significant effects observed so far. While the specific viscosities of the 100 mM and 40 mM solution are decreasing rapidly, the 80 mM and 60 mM solutions are significantly increasing. While the specific viscosity of the 80 mM solution is increasing by 16%, it increases by 96% for the 60 mM solution. Due to the unpolar solvent toluene, the formation of the ACP dimers is favoured, so that an optimal balance between the preferred formation of cyclic structures at room temperature and polymeric structures at elevated temperatures seems to be found. This once again demonstrates that a more unpolar solvent leads to a greater effect due to stronger dimerization of the binding units. The specific viscosity, especially at a concentration of 60 mM, increases over the whole temperature range. This means the effect might occur at even higher temperatures than 100 °C.

According to the results of the viscosity measurements, DLS measurements were carried out. Therefore, the 60 mM solution was heated up to 25 °C, 60 °C and 100 °C to investigate the hydrodynamic radii.

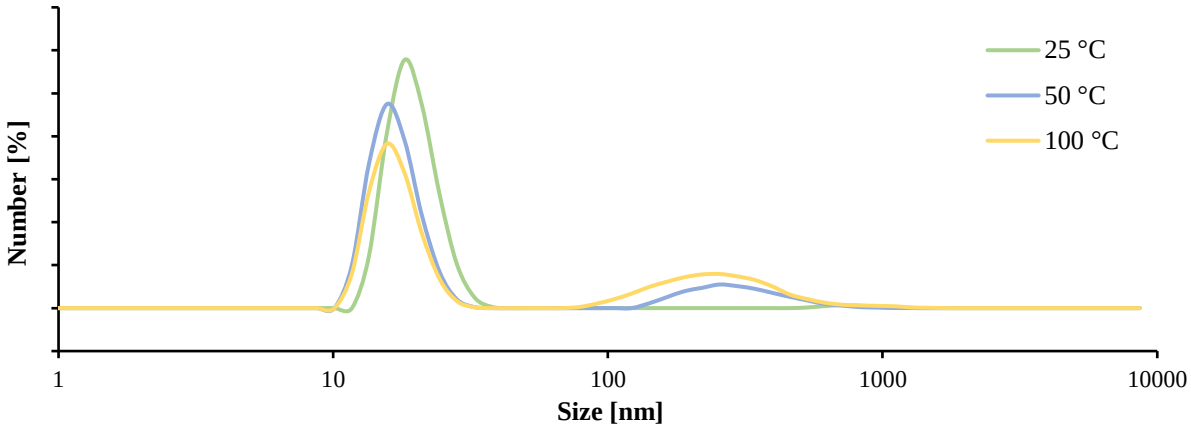

Figure 99: DLS measurement of the fourth generation 60 mM in toluene.

The results of the DLS measurements match with the viscosity measurements. Starting at 25 °C with a second peak that obtains a signal number of 1.1%, elevating the temperature to 60 °C the signal number increases to 18.7% which is fitting to the viscosity measurements, due to higher specific viscosities at elevated temperatures. Therefore, the formation of larger structures is related to the development of higher specific viscosities. Elevating the temperature even more to 100 °C, the signal number increases to 34.6%. Using the same approach of explanation as in the third generation, that means roughly a third of all molecules are included in larger structures. With hydrodynamic radii of around 255 nm of the second peak, and around 20 nm of the first peak, the high improvement of the specific viscosity can be explained, due to the large difference of the hydrodynamic radii and highly increased signal number of the second peak.

4.2.2.8 Measurements in Nynas NS8

The last measurement of the fourth generation was carried out in the first motor oil Nynas NS8. Due to the limited solubility, the measurement was carried out in a concentration of 60 mM, while this concentration happens to be the most promising as seen in previous solvents.

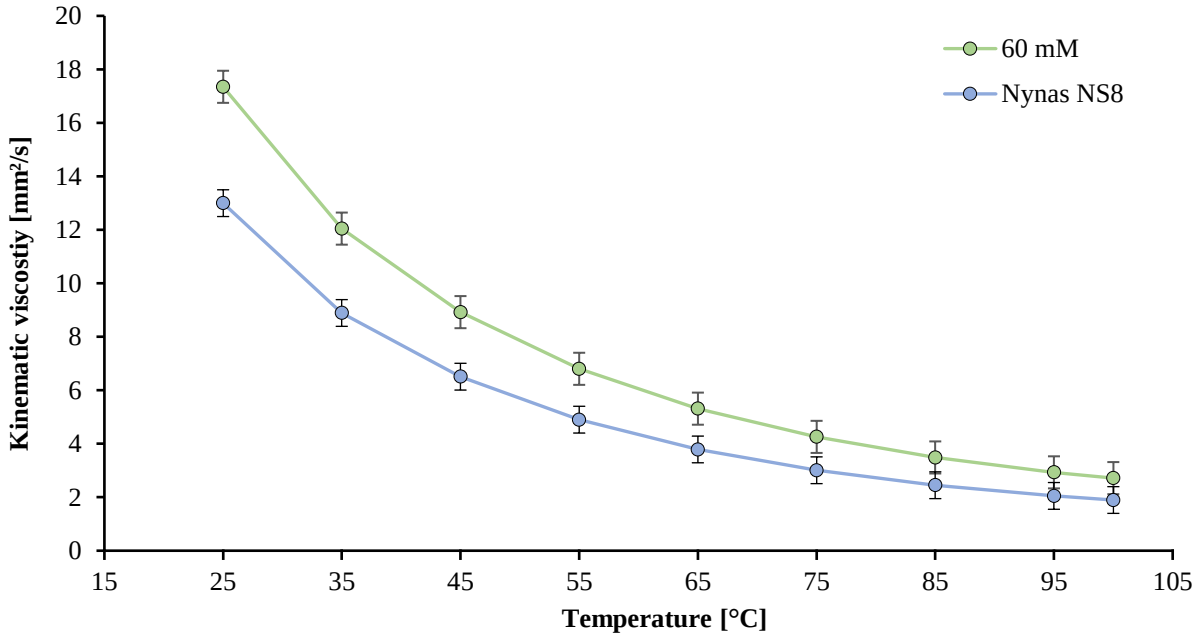

Figure 100: Measurement of the kinematic viscosity, the temperature of the ACP-BINAM derivative *(S)*-4 in Nynas NS8.

Looking at the measurement of the 60 mM concentration, it is hard to guess if an effect takes place or not. There still is a difference between the pure oil and the solution. An increase of the kinematic viscosity occurs over the whole temperature range in comparison to the oil. Therefore, the specific viscosity was calculated.

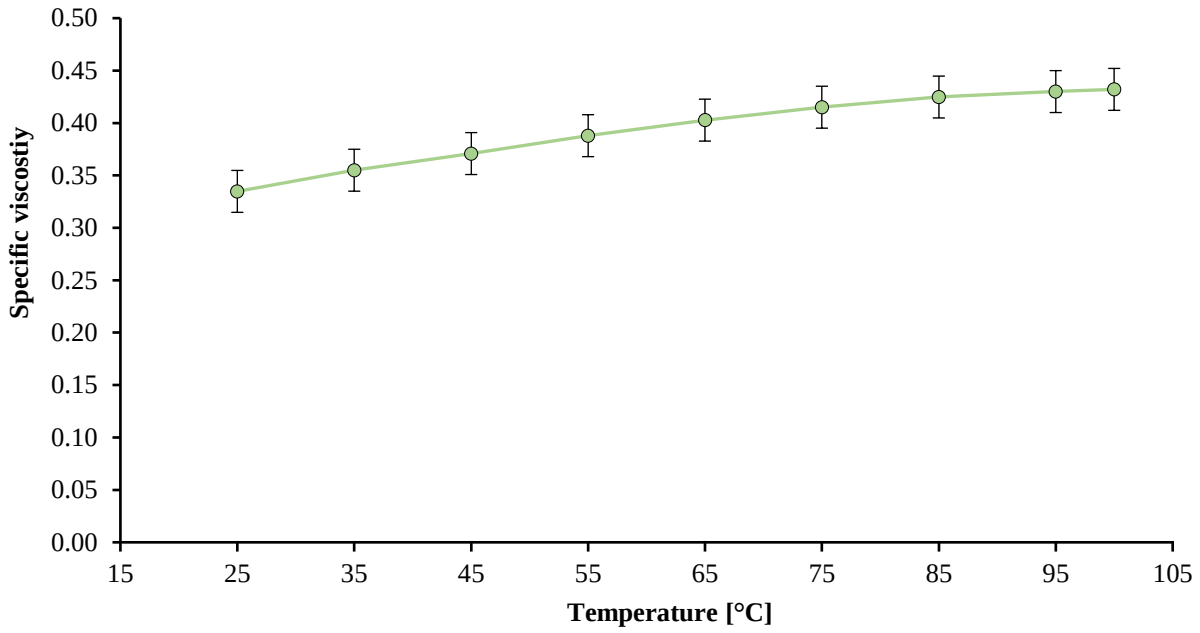

Figure 101: Measurement of the specific viscosity, the temperature of the ACP-BINAM derivative *(S)*-4 in Nynas NS8.

The specific viscosity of the fourth generation in Nynas NS8 demonstrates an increase of the viscosity over the whole temperature range. The specific viscosity increases by 30% between 25 °C and the maximum temperature of 100 °C. This is slightly less than the increase in the toluene solution, but still a significant increase of the specific viscosity. This is the first successful measurement in oils which proves the possibility of the supramolecular VI improver. It is possible with our system to decrease the loss of viscosity with increased temperature.

Unfortunately, no DLS measurements were possible in oil solutions but since an oil was used, the viscosity index can be calculated. The viscosity index is a characteristic of oils, which indicates how big the impact of increased temperature is on the viscosity. The higher the viscosity index, the less is the decrease of the viscosity at elevated temperatures. To determine the viscosity index, only two values are important, the kinematic viscosity at 40 °C and 100 °C.

Table 5: Calculation of the viscosity index of the 60 mM solution of the fourth generation in Nynas NS8.

	Viscosity at 40 °C	Viscosity at 100 °C	Viscosity Index
60 mM Solution	10.48 mm²/s	2.71 mm²/s	94
Pure Nynas NS8	7.35 mm²/s	2.02 mm²/s	47

While the pure oil Nynas NS8 has a viscosity index of 47, the viscosity index of the solution of the fourth generation is increased to 97. With the addition of the fourth generation, the viscosity index was doubled. With these results of the different measurements in different solvents, the fourth generation can be called a VI-improver.

4.3 Increasing the Solubility

4.3.1 Fifth Generation: Increased Solubility with Molecular Extension

After the promising results of the fourth generation in viscosity and DLS measurements, in solvents like chloroform, toluene and Nynas NS8, the aim is now to transfer this effect into even more unpolar solvents. There are two oils of the Evonik left, Nexbase 3020 and Nexbase 3043 which are extremely unpolar and do not have good solubilizing properties. Therefore, modifications of the fourth generation need to be done to increase the solubility in these motor oils. The fifth generation deals with the solubility in motor oils due to modifications into a more unpolar compound.

4.3.1.1 Extension of the Monomeric Unit

Since the ACP motif of the fourth generation demonstrates a significant increase in specific viscosity with increasing temperatures, the binding motif stays the same in the fifth generation. The task is to attach more unpolar functional groups on the monomeric unit to achieve a higher solubility the oils. The idea behind the fifth generation is to extend the linker unit with a functional group which has another binding site, to attach more unpolar functional groups to the whole system.

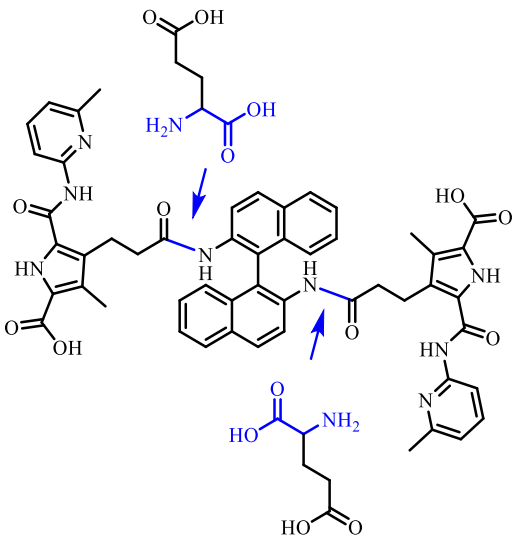

Figure 102: Introduction of glutamic acid to the fourth generation.

To investigate the behaviour of the cyclisation of this compound, another force field calculation was carried out, to find out if the compound is capable of forming cyclic structures.

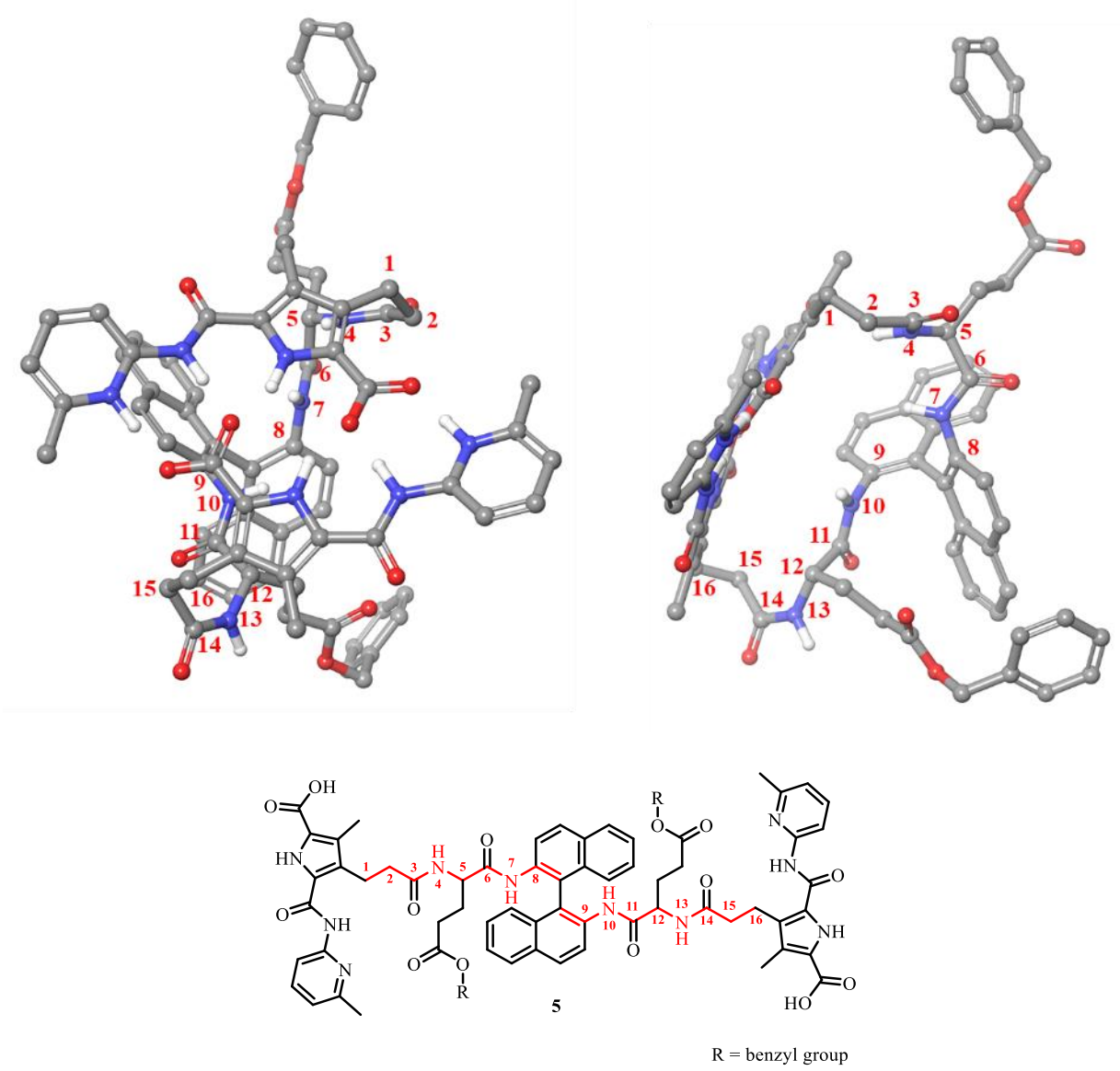

Figure 103: Force field calculation of the BINAM-GLU-ACP system 5 to form cyclic structures (OPLS force field).

The calculation proves that a cyclisation is possible. Since the distance increases from 10 centres in the fourth generation to 16 centres in the fifth generation, this might disfavour the intramolecular cyclization.

4.3.1.2 Structure of the Monomeric Unit

For the extension of the linker unit glutamic acid was chosen. Here all the necessary functional groups are present to introduce a new binding site. The carboxyl group of the amino acid can be coupled with

the BINAM and the amino function with the ACP binding motif **48**. The side chain of the amino acid can be functionalised with different amines with unpolar functional groups.

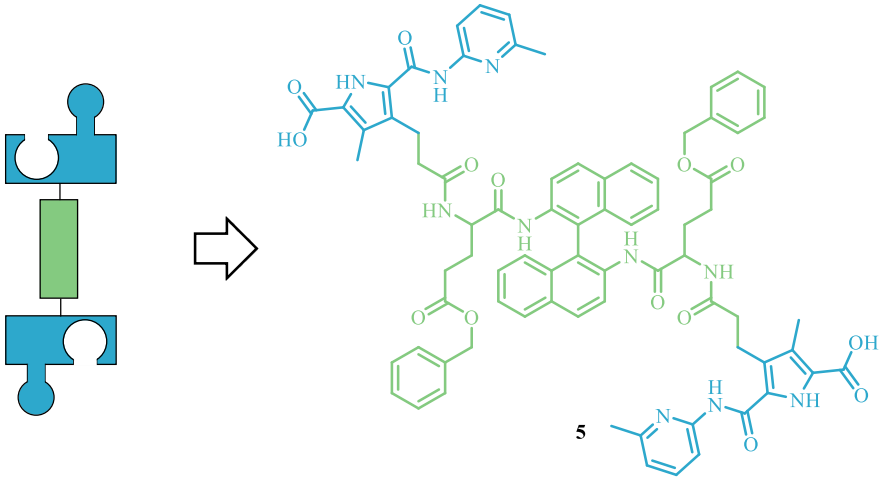

Figure 104: Fifth generation. ACP BINAM glutamic acid derivative 5.

The first aim is to synthesize and measure the benzylic protected derivative **5**. After successful measurements, derivatizations can be done to increase the solubility. Therefore, the benzyl protecting group can be cleaved and different amines with different alkyl chains can be attached by coupling reactions.

4.3.1.3 Synthesis

The synthesis was carried out following the synthesis route of the fourth generation. The reaction started with the coupling of the amino acid to BINAM. This generation was dealing with the coupling of L-glutamic acid, while the influence of the stereo centre was not further investigated.

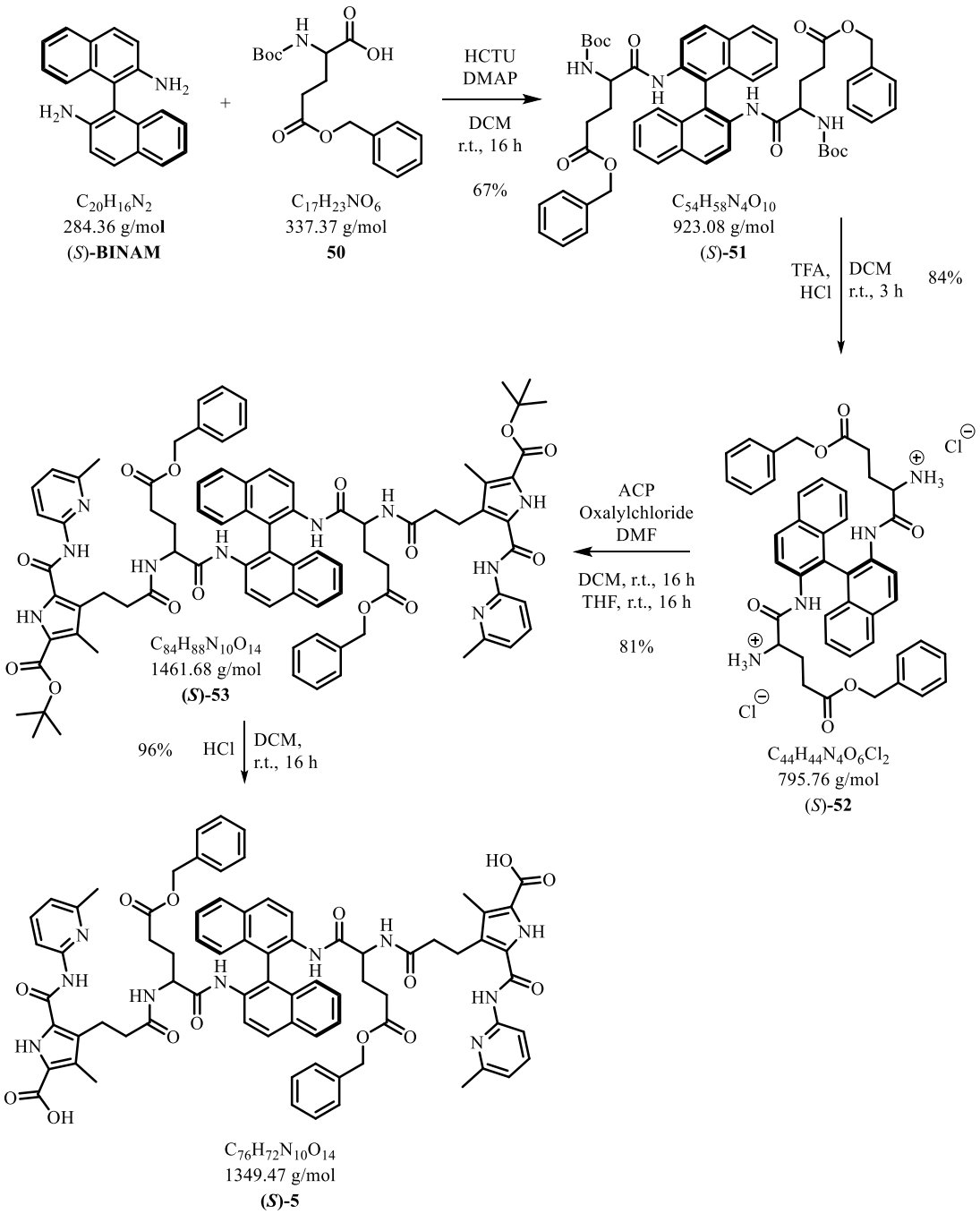

Figure 105: Synthesis of the fifth generation.

Surprisingly, the coupling reaction between the BINAM and the glutamic acid **50** was possible when using HCTU and DMAP as coupling reagents. This has not been successful for the third and fourth generation. The coupling was carried out in a yield of 67% to achieve the extended linker *(S)*-**51**. While the signal of the carboxylic acid disappeared in the ^{1}H-NMR, the amino signal of the BINAM was shifted to 8.90 ppm. The Boc deprotection was carried out using HCl and led to the deprotected compound *(S)*-**52** in a yield of 84%. The coupling of the ACP binding motif was carried out using the same conditions as in the last two generations. Using oxalyl chloride a yield of 81% of compound *(S)*-**53** was achieved

which is a significant improvement, compared to the low yields of the third and fourth generation. The new signals of the *t*-butyl protecting group at 1.56 ppm in the ^{1}H NMR are proving the successful synthesis of *(S)*-**53**. The final deprotection was carried out using TFA and yielded in 96% of the final compound *(S)*-**5**. The NMR spectra for the final compound of the fifth generation are shown in Figure 106.

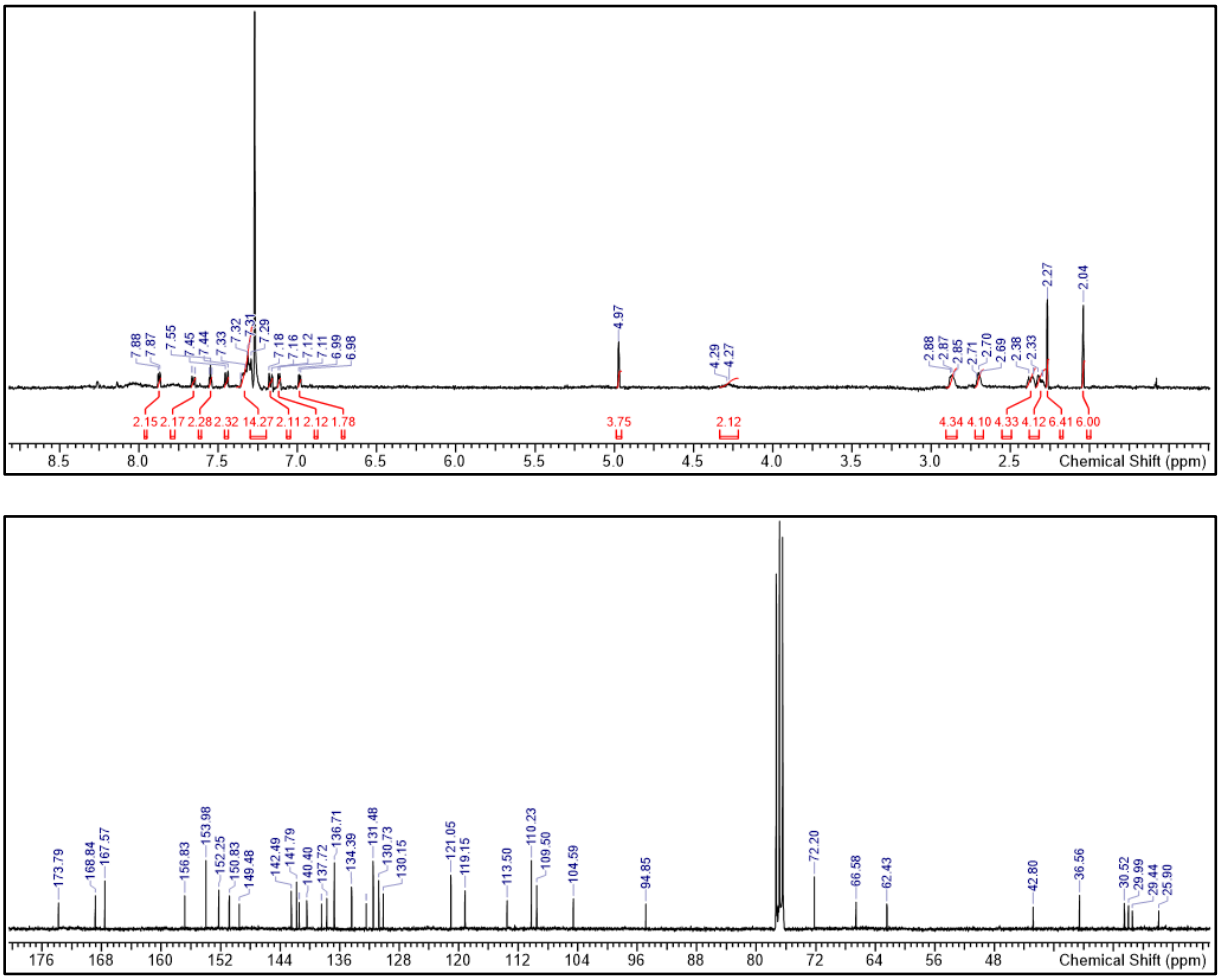

Figure 106: ^{1}H- and ^{13}C-NMR of 5 in $CDCl_3$.

4.3.1.4 Solubility Tests

For the fifth generation, another solubility test was carried out to see if the extension of the linker unit results in the desired higher solubility in oils.

Table 6: Solubility test for the ACP-BINAM glutamic acid derivative *(S)*-5.

Solvent	Max. Concentration
Chloroform	≥ 200 mM
Toluene	≥ 200 mM
DMSO	≥ 200 mM
Nynas NS8	100 mM
Nexbase 3020	40 mM
Nexbase 3043	≤ 5 mM

The fifth generation reveals an increased solubility regarding unpolar solvents. While the fourth generation was only soluble in Nynas NS8 in a concentration of 60 mM, the solubility was increased to 100 mM in the same oil. The solubility in Nexbase 3020 was increased to 40 mM. This means even with the benzylic protection of the amino acid an increased solubility can be achieved. Therefore, we did not carry out further substitution of the benzyl-groups for other unpolar substituents (as originally planned) but used compound *(S)*-**5** directly for further investigations.

4.3.1.5 Measurement in Nynas NS8

After the promising results of the increased solubility of the fifth generation, the viscosity measurements were continued. For the first measurement, Nynas NS8 was chosen to compare the results with the measurements of the fourth generation. A new screening was done to find the optimal concentration. Therefore, a screening in Nynas NS8 was carried out, in a concentration range of 20 mM to 100 mM.

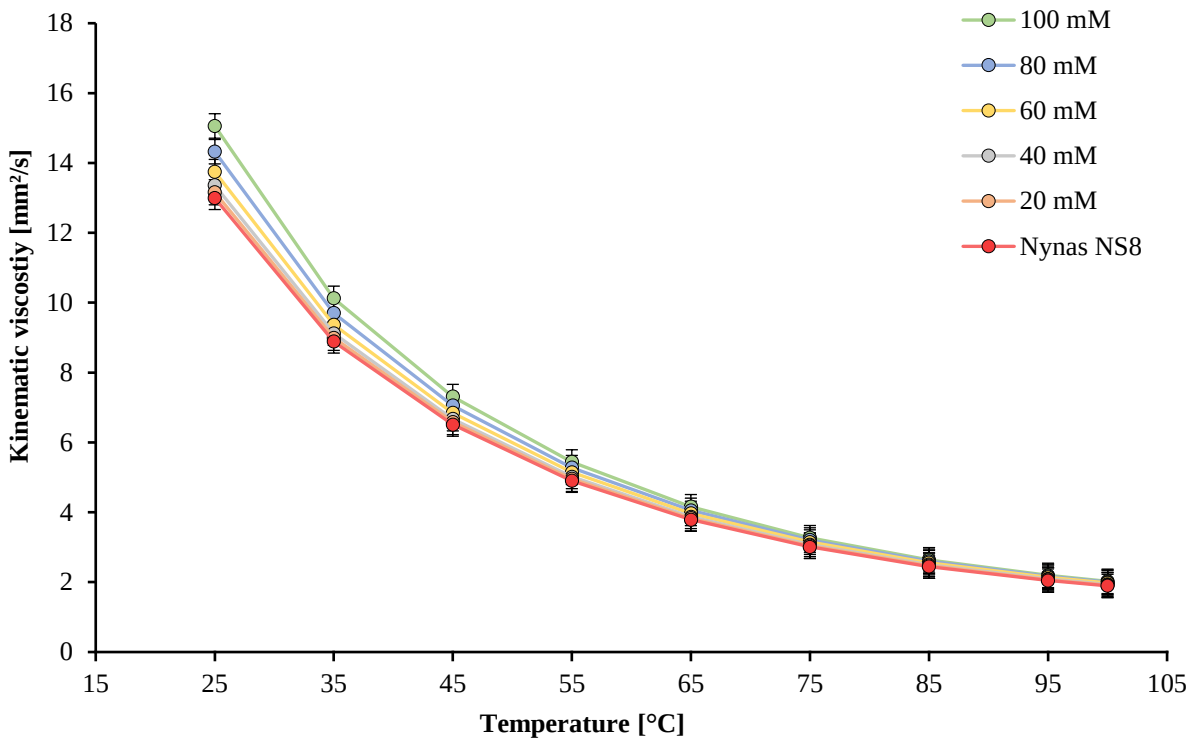

Figure 107: Screening of the kinematic viscosity of the fifth generation in Nynas NS8.

The screening demonstrates the kinematic viscosity as a function of the concentration and the temperature. All concentrations are indicating a decrease of the viscosity within elevated temperatures and lower concentrations. Surprisingly, there is no irregularity in any concentration and the thickening of the solution is less than in all other viscosity measurements. All concentrations are representing a similar behaviour in the viscosity. Therefore, the specific viscosity was calculated to investigate if the effect occurs in the fifth generation.

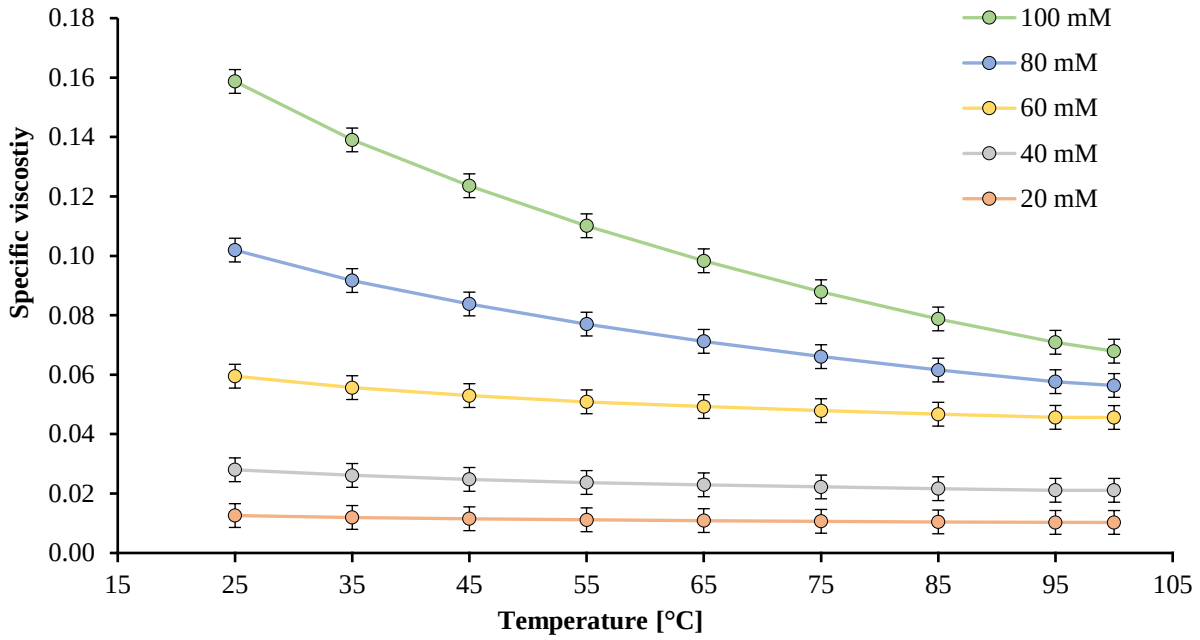

Figure 108: Screening of the specific viscosity of the fifth generation in Nynas NS8.

The screening of the specific viscosity demonstrates a similar result as the kinematic viscosity. In every single concentration, the specific viscosity is decreasing with higher temperatures and lower concentrations. For the measurements in Nynas NS8, it is only possible to solve the compound up to a concentration of 100 mM but even in different solutions like DMSO (not shown here), no effect was obtained for the fifth generation.

4.3.1.6 Measurement in Nexbase 3020

If no improvement of the viscosity behaviour is occurring in Nynas NS8, it might be observable in more unpolar solvents like Nexbase 3020. Here a stronger effect might be found due to a stronger ACP-dimerization.

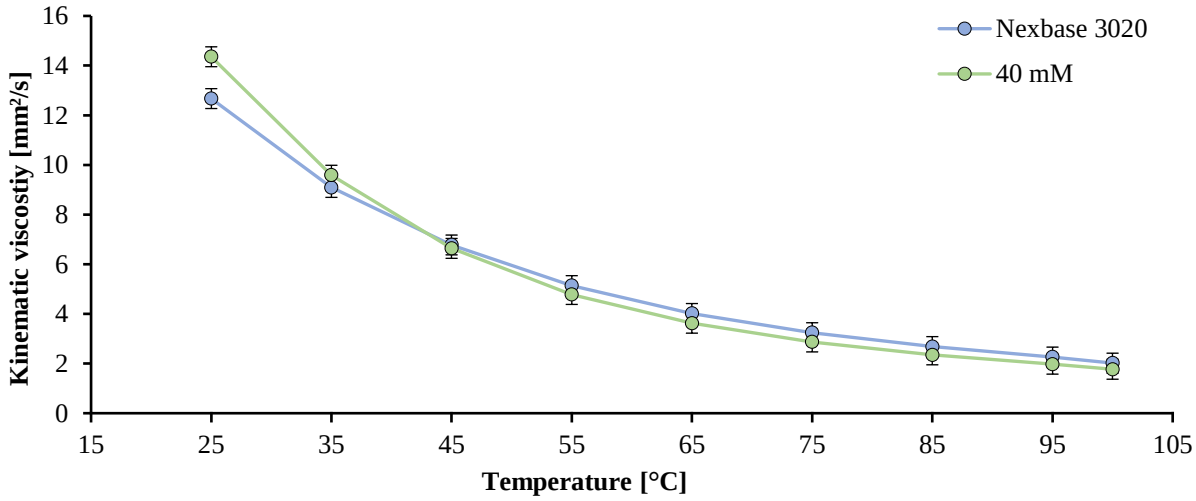

Figure 109: Kinematic viscosity of the fifth generation in Nexbase 3020.

Surprisingly the viscosity decrease in Nexbase 3020 becomes even worse. Comparing the 40 mM solution and the pure Nexbase 3020, the solution decreases to kinematic viscosities below the pure solvent. This means the fifth generation induces a loss of viscosity at elevated temperatures in this solvent. This behaviour becomes clear in the calculation of the specific viscosity.

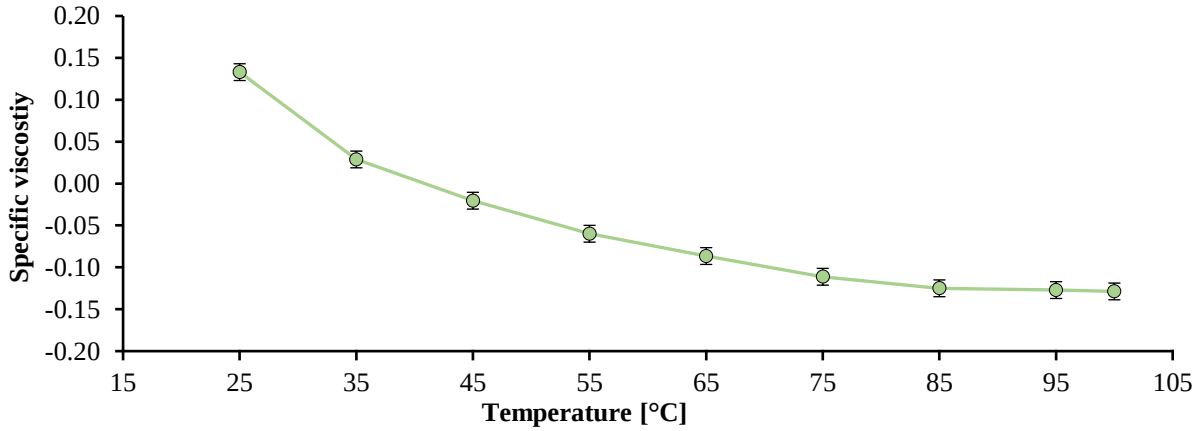

Figure 110: Specific viscosity of the fifth generation on a 40 mM solution in Nexbase 3020.

The specific viscosity decreases within the whole temperature range. Here, at 45 °C, the specific viscosity decreases to values below 0, which means that the viscosity of the solution is below that of the pure solvent. In summary, all measurements prove that the fifth generation has no ability to act as a VI-improver.

4.3.1.7 Loss of Effect with extended Linker Motif

Comparing the fourth and fifth generation, the only difference is the distance between the two binding units. Like the force field calculations were demonstrating, a cyclic formation is possible for both compounds.

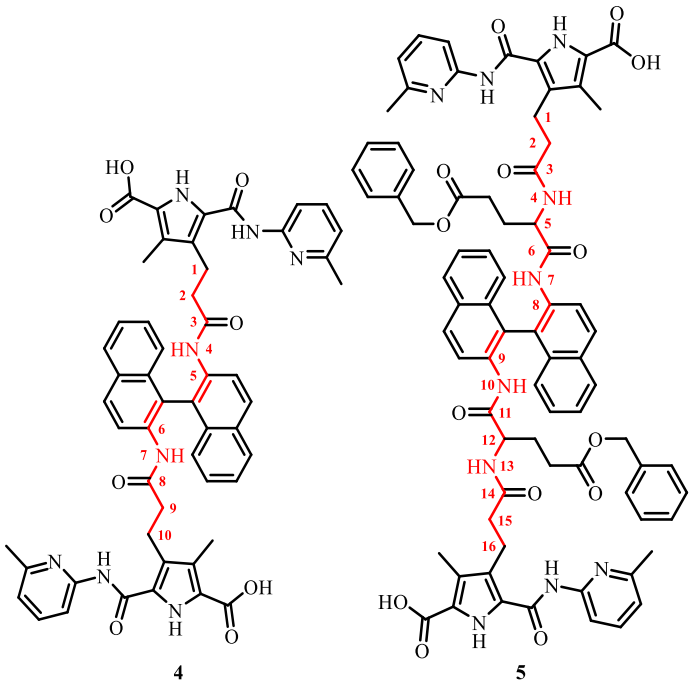

Figure 111: Comparison of the fourth and fifth generation regarding ring tension.

While the fourth generation has 10 centres between the two ACP binding units, the fifth generation has 16 centres. Thus, we might expect a lower ring tension, so that elevating the temperature does not lead to an effective ring-chain transition.

4.3.2 Sixth Generation

Since the fifth generation demonstrated good solubilities but lost the effect of the viscosity improvement due to the extension of the linker unit, another method to increase the solubility was introduced. While the fourth generation resulted a good effect even in the first oil Nynas NS8, the solubility was increased without changing the core structure of the fourth generation. Therefore, the sixth generation deals with the substitution of the BINAM to increase the solubility.

4.3.2.1 Increasing Solubility with Substitution

The fourth generation was demonstrating the best effects on the viscosity. What we learned from the fifth generation is, that the core structure of the fourth generation should not be changed. For this reason, we envisaged a different structural variation to improve the solubility. A direct substitution of the BINAM in the 6-position might lead to better solubility, while it does not influence the supramolecular aggregation behaviour via the ACP-units.

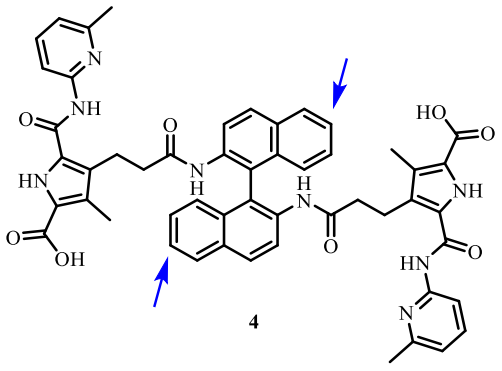

4

Figure 112: Possible substitution positions at the fourth generation.

It is possible to carry out a bromination at the 6,6’ position of the BINAM to achieve a further substitution. This intermediate can then be used with different methods to attach an alkyl chain or other unpolar functional groups to the system. In this case, we chose a hexyl group to increase the solubility for the oils.

While the force field calculations of the fourth generations were indicating a cyclisation of the system, another calculation was carried out, to investigate any hindrance due to an attached alkyl chain.

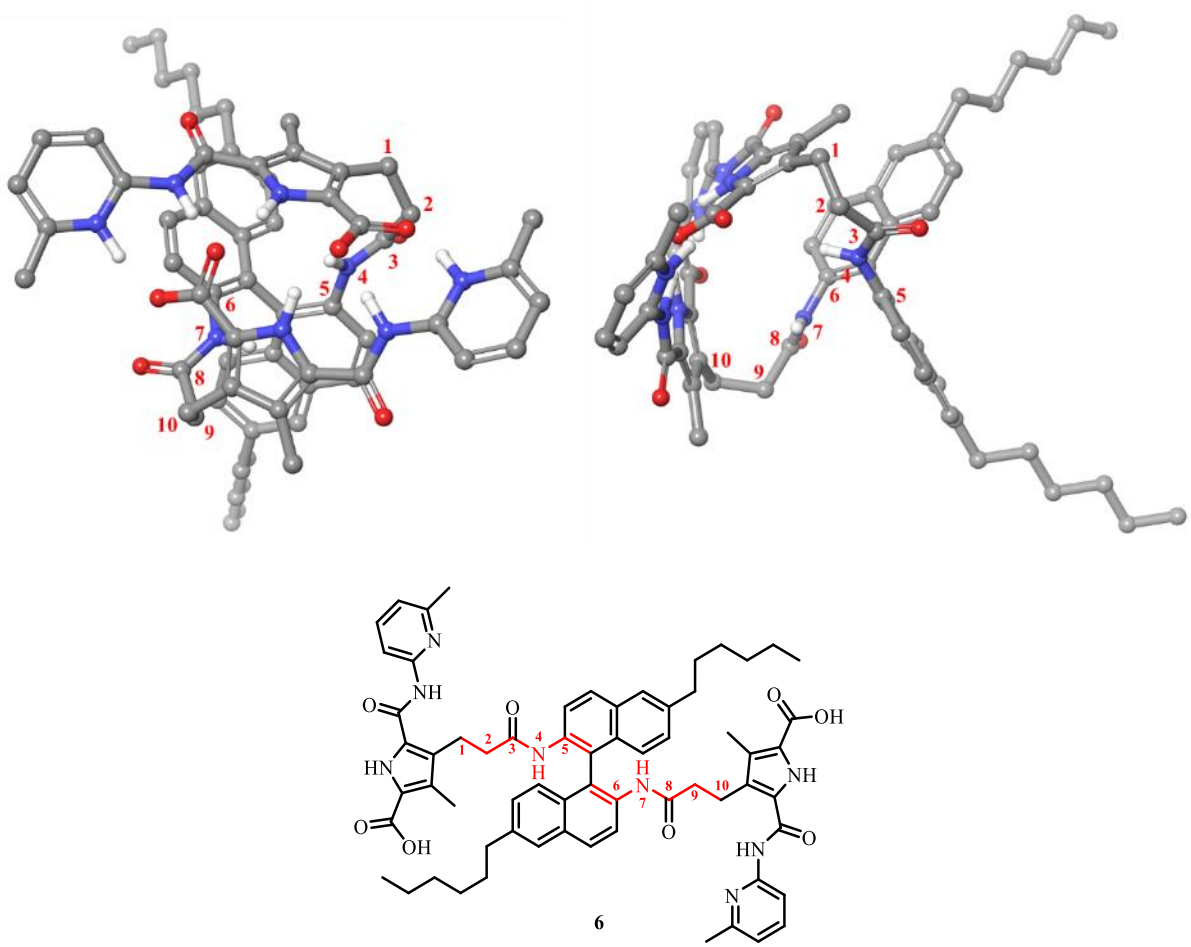

Figure 113: Force field calculation of the alkyl-substituted BINAM-ACP system 6 to form cyclic structures (OPLS force field).

Because the core structure of the fourth generation has not changed, the same ability to form cyclic structures remains. Therefore, the structure of the sixth generations VI improver was found.

4.3.2.2 Structure of the Monomeric Unit

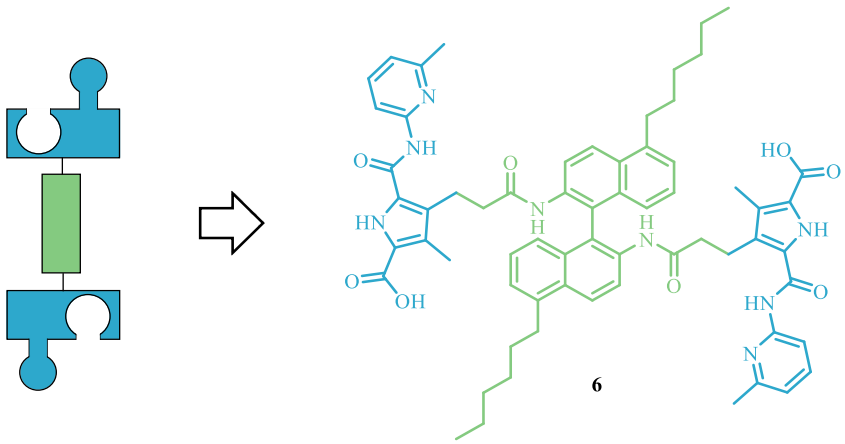

Figure 114: Sixth generation. ACP-BINAM hexyl derivative 6.

For the alkyl chain, the hexyl chain was chosen, because it should have a sufficient influence on the solubility and can easily be introduced.

4.3.2.3 Synthesis

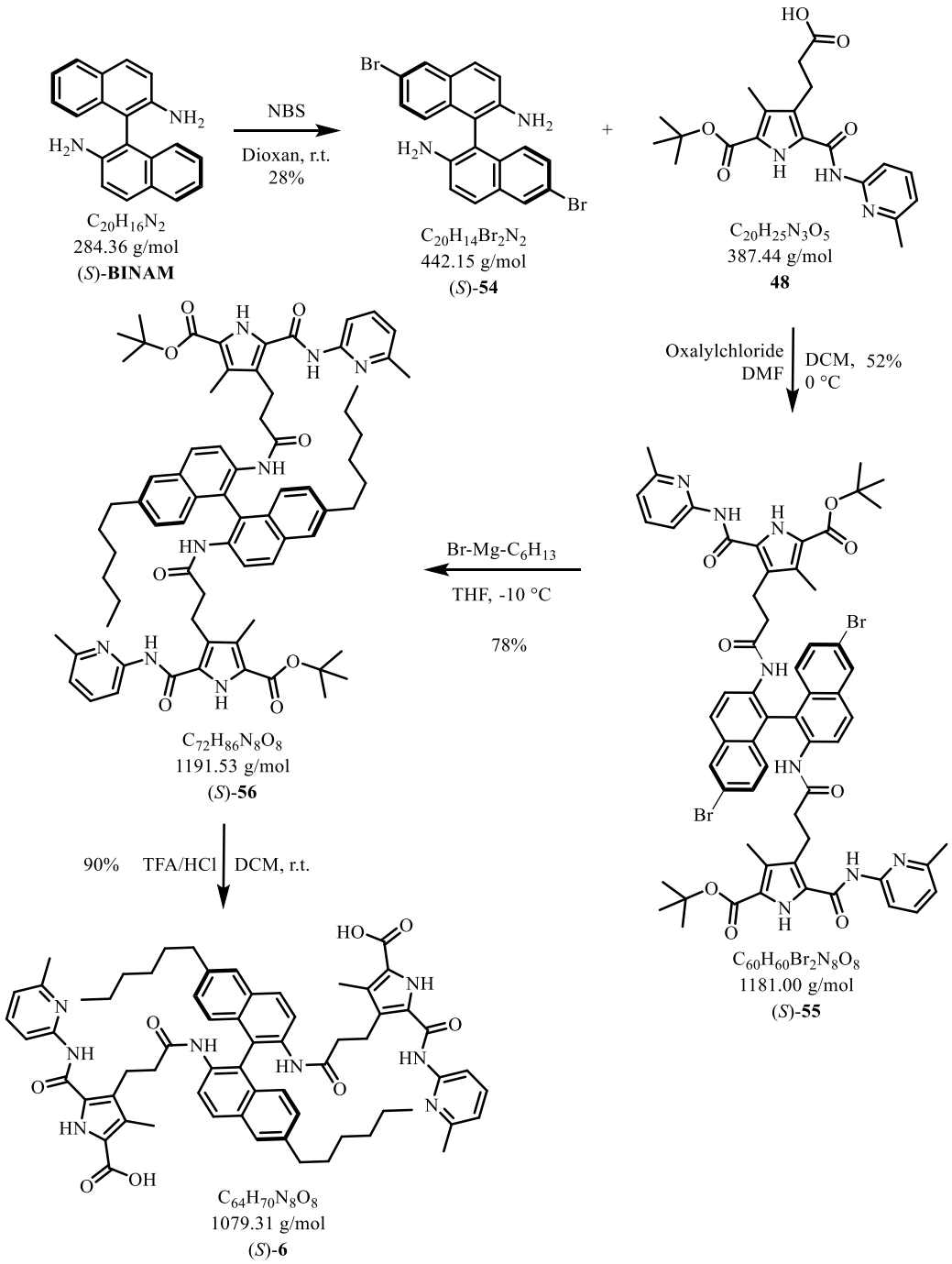

Figure 115: Synthesis of the sixth generation.

The synthesis starts with the bromination of the BINAM. The bromination is known in the literature and yields 28% of compound *(S)*-**54** due to the difficult purification due to many bromination side reactions.[36] After this, the synthesis is similar to the fourth generation where the synthesis of the ACP motif **48** was described. The synthesis continues with the ACP motif coupling with oxalyl chloride as in the generations before that yields 52% of compound *(S)*-**55**. The amide signal shifts to 8.20 ppm in the ^{1}H-NMR was remarkable. Subsequently, a commercially available hexyl-Grignard compound was

used to substitute the bromide. This reaction was carried out with a 78% yield of compound *(S)*-**56**. The benzylic methylene-group appears at 2.79 ppm in the ^{1}H NMR. The final compound of the sixth generation was obtained with a deprotection with a yield of 90%. The absence of the signals at 1.55 ppm in the ^{1}H NMR representing the *t*-butyl protecting group proves the successful synthesis of the final compound *(S)*-**6**. The NMR spectra for the final compound of the sixth generation are shown in Figure 116.

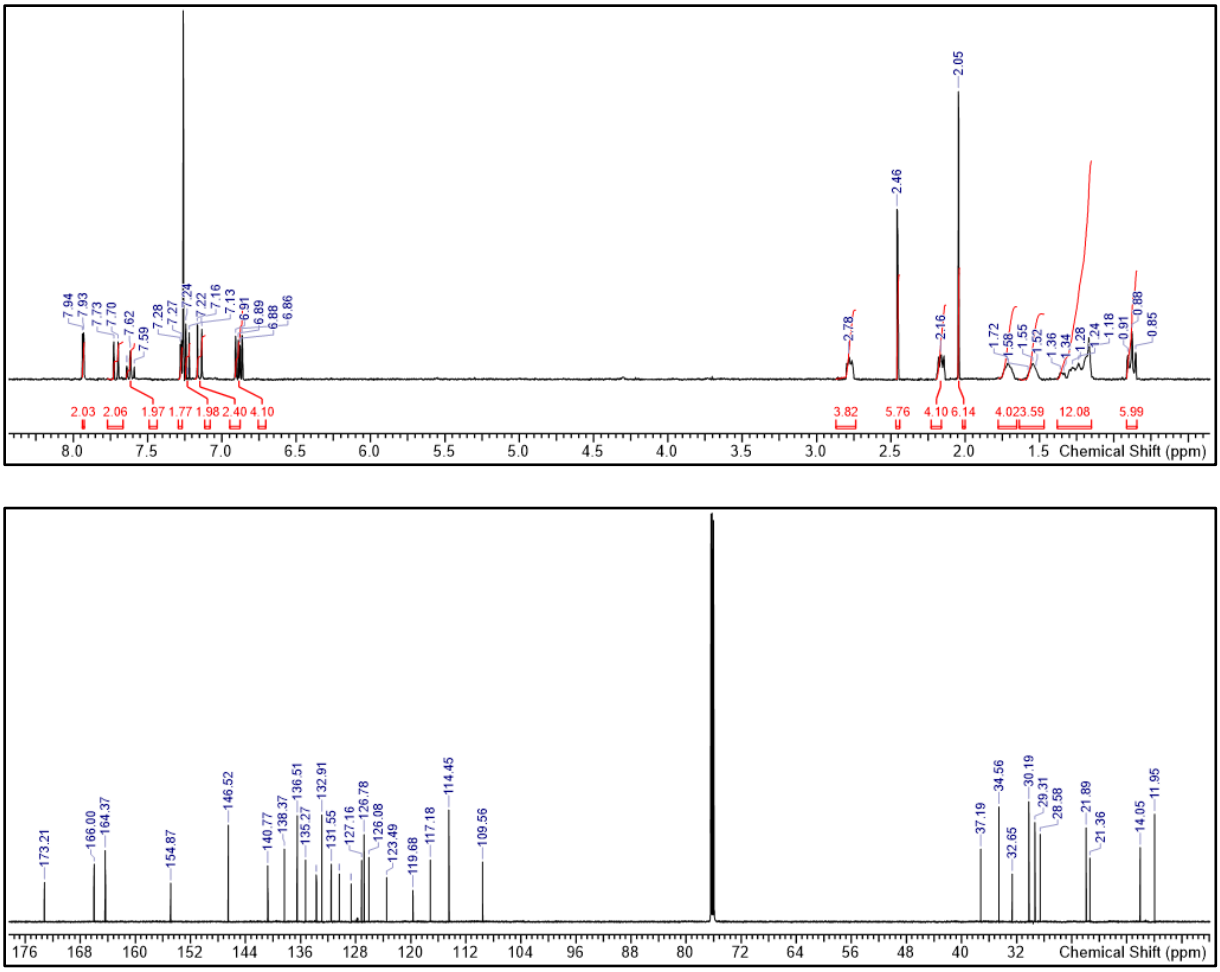

Figure 116: ^{1}H- and ^{13}C-NMR of 6 in $CDCl_3$.

4.3.2.4 Solubility Tests

Table 7: Solubility test for ACP BINAM hexyl derivative *(S)*-6.

Solvent	Max. Concentration
Chloroform	≥ 200 mM
Toluene	≥ 200 mM
DMSO	≥ 200 mM
Nynas NS8	≥ 200 mM
Nexbase 3020	90 mM
Nexbase 3043	≤ 5 mM

The solubility tests of the sixth generation prove an increased solubility, especially in the motor oils. While the solubility in Nynas NS8 was at 60 mM for the fourth generation and 100 mM for the fifth generation, the sixth generation demonstrates a perfect solubility of over 200 mM in Nynas NS8. And even in Nexbase 3020, the solubility could be increased to 90 mM concentration. Only a solution in Nexbase 3043 was not possible with the sixth generation. Nexbase 3043 seems to be too unpolar due to the long alkyl chains of C_{20} to C_{50}.

4.3.2.5 Measurement in Nynas NS8

The solubility tests were demonstrating good results in the solubility in the two oils Nynas NS8 and Nexbase 3043. Therefore, the measurements of the viscosity are starting with Nynas NS8 to have a direct comparison to the fourth generation. Here, another screening of the viscosity, temperature and concentration was carried out, to investigate a possible different behaviour in comparison to the fourth generation.

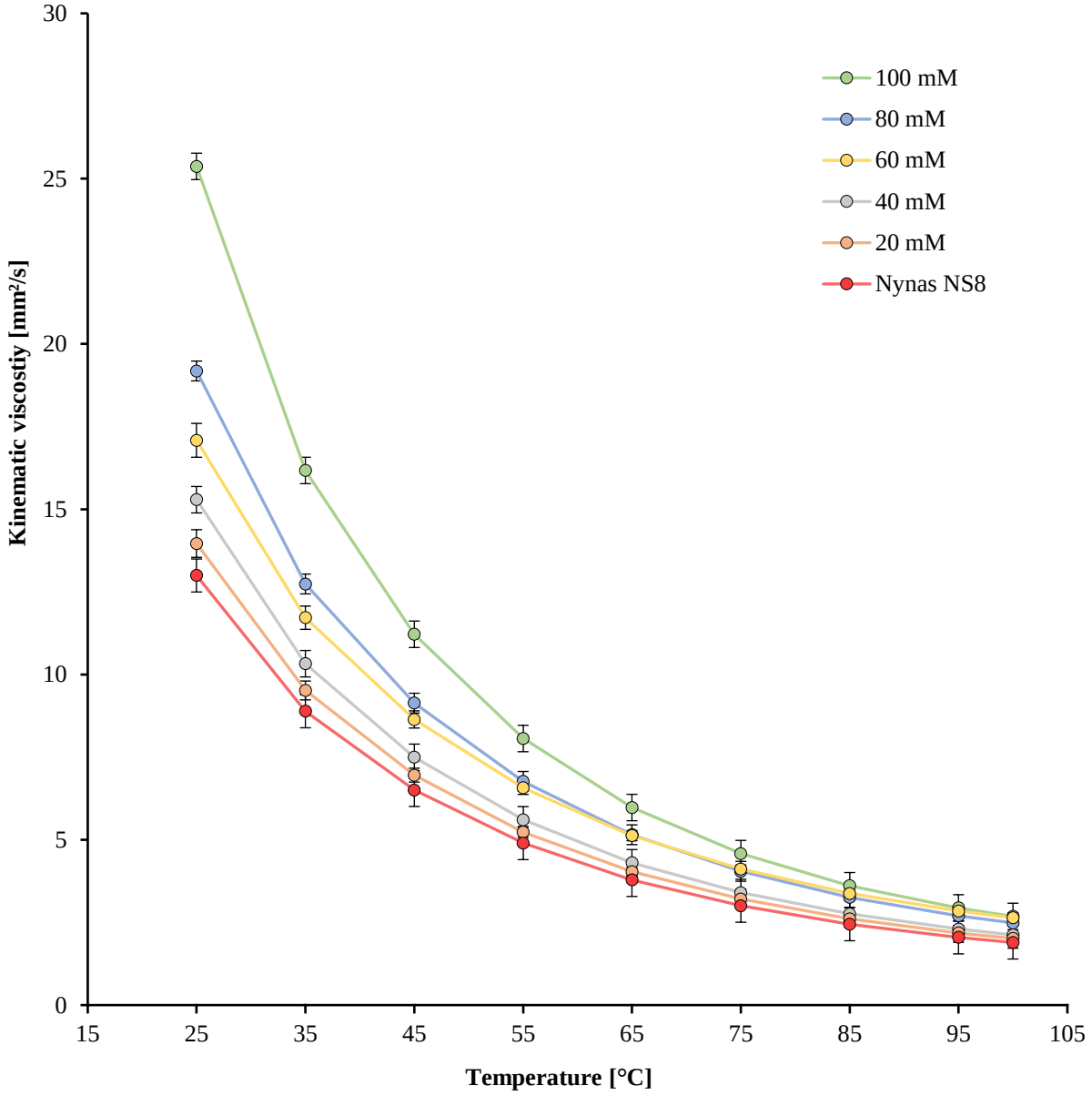

Figure 117: Screening of the kinematic viscosity in dependence of concentration and temperature of the sixth generation in Nynas NS8.

The screening demonstrates the kinematic viscosity as a function of the concentration and the temperature. The range of concentration was chosen from 20 mM to 100 mM because it was assumed, that the effective concentration needs to be similar to the best concentration of the fourth generation, even though, higher concentrations would be possible. Once again it is hard to see where an irregularity occurs in the kinematic viscosity, but in the case of the 60 mM solution a slower decrease in kinematic viscosity occurs. To investigate the real viscosity behaviour of the compound the specific viscosity was calculated.

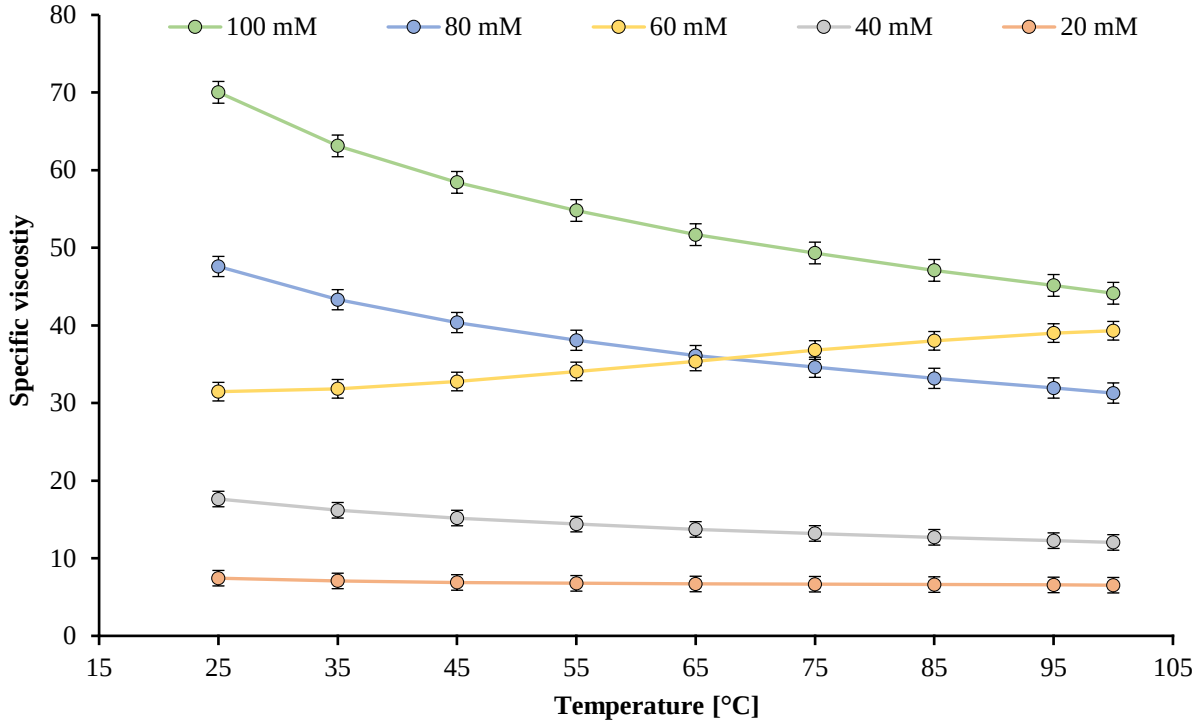

Figure 118: Screening of the specific viscosity of the sixth generation in Nynas NS8.

The screening of the specific viscosity demonstrates a clear effect in the 60 mM solution. In all other concentrations, a decrease of the specific viscosity occurs with elevated temperatures. While the 60 mM solution increases the specific viscosity by 26% between 25 °C and 100 °C, which is similar to the results of the measurements of the fourth generation in Nynas NS8. This means, that a positive effect is obtainable at the same concentration for the fourth and sixth generation. Additionally, there is no major influence of the hexyl chain. To see the influence of the sixth generation to the viscosity index, it was calculated for a better comparison to the fourth generation.

Table 8: Calculation of the viscosity index of the sixth generation in Nynas NS8.

	Viscosity at 40 °C	Viscosity at 100 °C	Viscosity Index
60 mM Solution	10.18 mm²/s	2.64 mm²/s	89
Pure Nynas NS8	7.35 mm²/s	2.02 mm²/s	47

The viscosity index of the Nynas NS8 oil was increased by adding the sixth generation VI-improver. The pure oil has a viscosity index of 47 which increases to 89. This proves the ability to be used as a VI improver, as the viscosity index is almost doubled. Also, the change in VI is very similar to that observed for the fourth generation (VI of 97 for a 60 mM solution).

4.3.2.6 Measurement in Nexbase 3020

To prove the ability of improving the VI in different oils, the same measurement was carried out in Nexbase 3020 to see, if the VI properties are increased by a more unpolar solvent. Here, the same concentration as in the measurements in Nynas NS8 was chosen, since in the fourth and sixth generation the highest improvements where obtained in a 60 mM concentration.

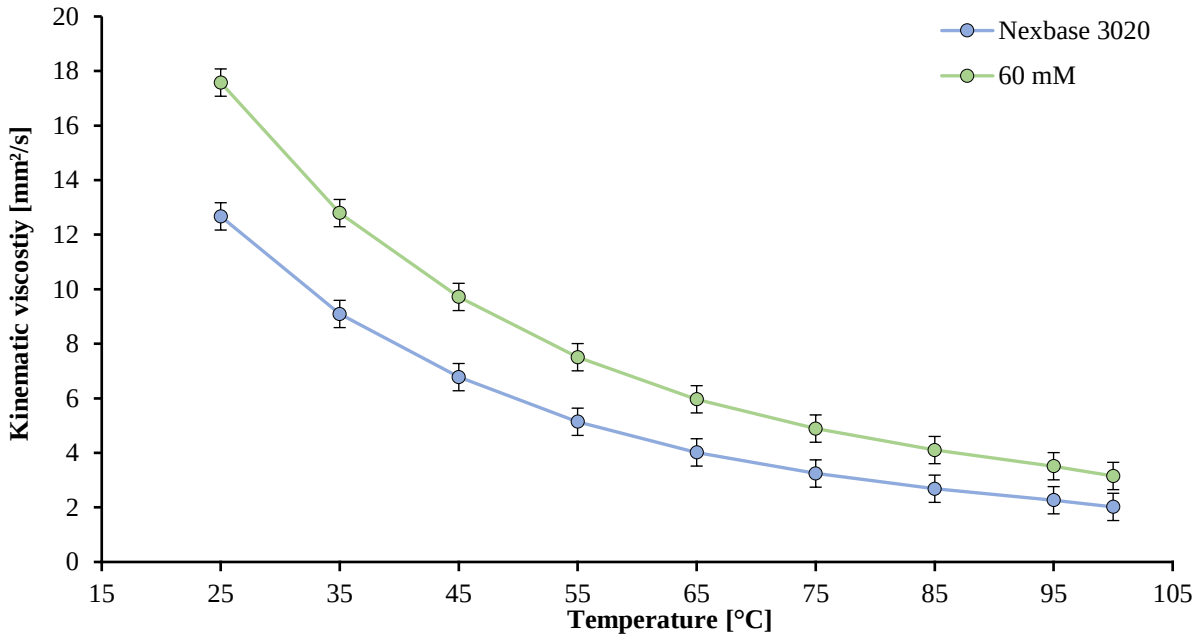

Figure 119: Kinematic viscosity of the sixth generation in Nexbase 3020.

For the sixth generation, the kinematic viscosity is higher than that of pure Nexbase 3020 over a whole temperature range. For a better understanding, the specific viscosity was calculated.

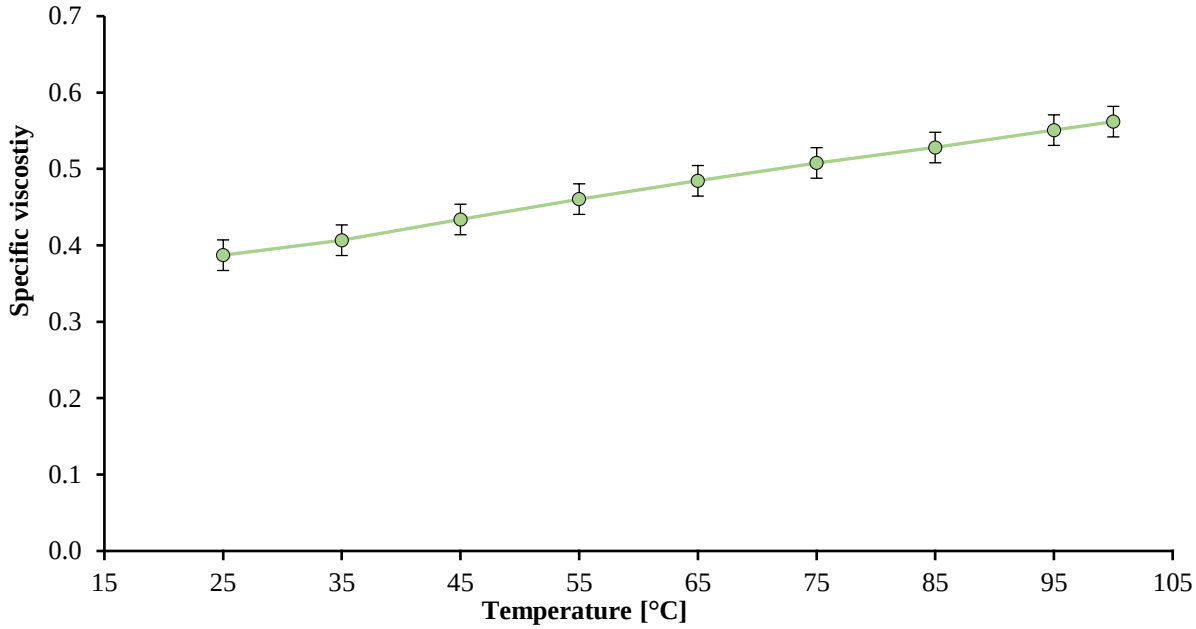

Figure 120: Specific viscosity of the sixth generation in a 60 mM solution in Nexbase 3020.

The specific viscosity for the sixth generation in Nexbase 3020 demonstrates one of the best results of all generations. The specific viscosity increases by 44% between 25 °C 100 °C (for Nynas NS8, an increase of 26% had been observed). This underlines the trend that more unpolar solvents favour, an increase of the specific viscosity with increasing temperature. Finally, the viscosity index of the solution in Nexbase 3020 was calculated.

Table 9: Calculation of the viscosity index of the sixth generation in Nexbase 3020.

	Viscosity at 40 °C	Viscosity at 100 °C	Viscosity Index
60 mM Solution	11.25 mm²/s	3.15 mm²/s	152
Pure Neybase 3020	7.86 mm²/s	2.24 mm²/s	88

While the sixth generation demonstrates the highest increase of the specific viscosity in motor oils, it also leads to the greatest increase of the viscosity index. While the pure Nexbase 3020 obtains a viscosity index of 88 without any addition, the 60 mM solution of the sixth generation almost doubles this value to 152 and obtains the highest measured VI. This proves how successful the implementation of the supramolecular viscosity index improver is.

4.4 Comparison of the Generations

Comparing all generations with each other is not easy, due to the ability to improve the viscosity behaviour in different concentrations and different solvents. Nevertheless, the best candidates of each generation were chosen to compare the specific viscosity. Generation one and two are working best in a chloroformic solution in a concentration of 145 mM and 160 mM. The third was only tested in DMSO and the viscosity improving effect was occurring at a concentration of 50 mM. The fourth generation proved a significant effect in different solvents, but the strongest effect was obtained in a toluene solution of 60 mM. The fifth generation was not developing any effect at all, but here, the 60 mM solution in Nynas NS8 was chosen to compare a negative effect. At last, the sixth generation showed a viscosity improving effect in both motor oils, where the 60 mM solution in Nexbase 3043 the strongest improvement could be observed.

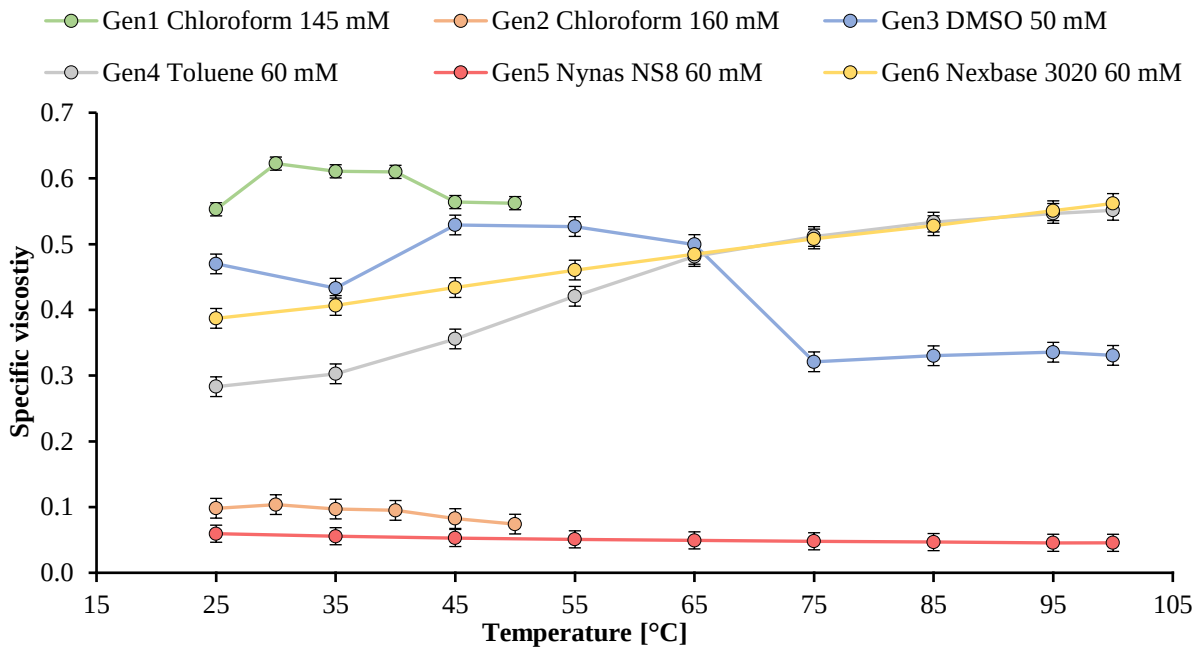

Figure 121: Comparison of the specific viscosity of the most promising candidates of all generations.

Since the viscosity of the first two generations was measured in a chloroformic solution, the temperature was only elevated to 50 °C. Comparing all generations with each other, the first generation obtains the highest specific viscosity of 0.55 at 25 °C and therefore is the most thickening additive. This specific viscosity is increasing to 0.62 and is decreasing again. The viscosity improving effect is occurring in a temperature range between 25 °C and 40 °C. Thickening of the additives is not the aim of this thesis. Here, improving the viscosity index is the focus and an increased specific viscosity at elevated

temperatures is needed. The first generation is increasing the specific viscosity by 13%. This is the same increase, the third generation is showing within the measurements in DMSO. But here, the viscosity improving effect is occurring in a broader temperature range of 40 °C to 70 °C. The activation of the effect is initialized at a higher temperature but is decreasing at even higher temperatures. The thinnest additives are the second and fifth generation. While the fifth generation is not developing any effect on improving the viscosity, the second generation is demonstrating the least effect. Here, the specific viscosity is increased by 4% in a temperature range of 25 °C to 35 °C. Nevertheless, the implementation of the BINOL function of the second generation was a success, which was proven in the fourth and sixth generation. While the fourth generation in toluene is starting at a lower specific viscosity of 0.28 than the sixth generation, the increase of the specific viscosity of the fourth generation is greater. The specific viscosity of the fourth generation in toluene is increasing by 96%, while the viscosity for the sixth generation in Nexbase 3020 increases by 44%. Therefore, the fourth and sixth generation are showing similar results, but additional to all measured solvents, the sixth generation is capable of improving the viscosity of Nexbase 3020 in elevated temperatures. The final aim of this thesis was the implementation of the viscosity improving additives in motor oils. Therefore, comparing all measurements in oils were used to investigate the behaviour of the effect within different conditions.

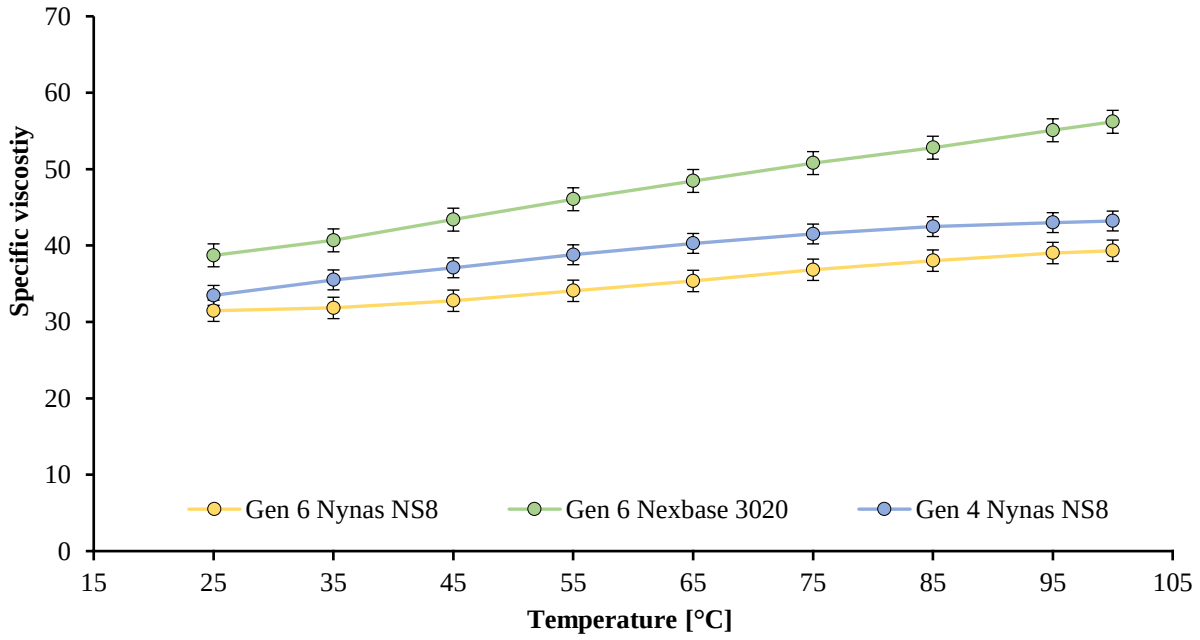

Figure 122: Specific viscosity of 60 mM solutions of generation six in Nynas NS8 and Nexbase 3020 and generation four in Nynas NS8.

Looking at the specific viscosity of the sixth generation in Nynas NS8 and Nexbase 3020, an increase of the effect was found in the more unpolar Nexbase 3020. But comparing the measurements in Nynas

NS8 for both generations, there is a loss of viscosity improvement in the sixth generation, due to the hexyl substitution. This effect can be compensated with the usage of a more unpolar solvent, due to the higher solubility of the sixth generation. Here the greatest improvement in oils of the specific viscosity is observed. Additionally, these results can be seen by comparing all improvements of the VI.

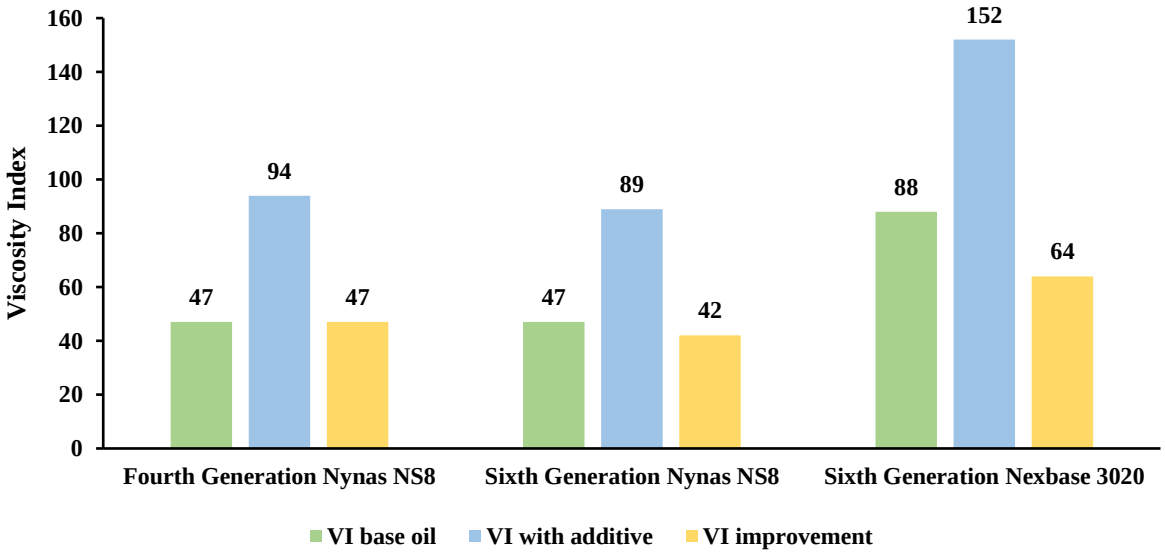

Figure 123: Comparison of all VI improvements of oil measurements.

While the VI of Nynas NS8 is similar improved by the fourth and sixth generation, a major increase of the VI in Nexbase 3020 occurs. Here, the increase of the VI is 64 and is therefore 50% higher than all other VI improvements. Therefore, the sixth generation is a perfect candidate in improving the VI to counteract the loss of viscosity at elevated temperatures. Therefore, the development of a VI improver based on supramolecular interactions was successful.

5. Summary and Outlook

This thesis aimed to develop an additive for different solvents and oils to improve the VI. This aim was achieved within the development of six generations.

Table 10: Schematic illustration of the progress of all generations.

Generation	**1**	**2**	**3**	**4**	**5**	**6**
Solubility in unpolar solvent	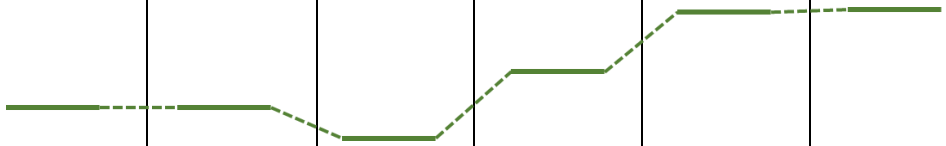					
Viscosity Improvement	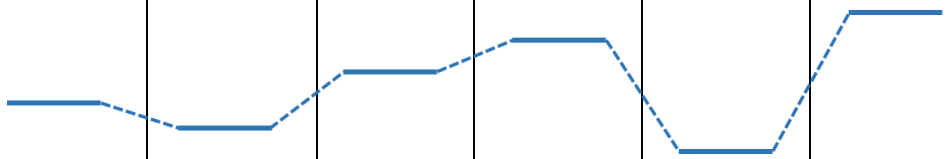					

While the sixth generation is improving the viscosity index significantly and obtained a major effect on kinematic and specific viscosity, all other generations were important to develop the final compound. Retrospective, the first three generations were dealing with generating a viscosity improving effect with different binding and linker units, while the last three generations were dealing with the improvement of the solubility.

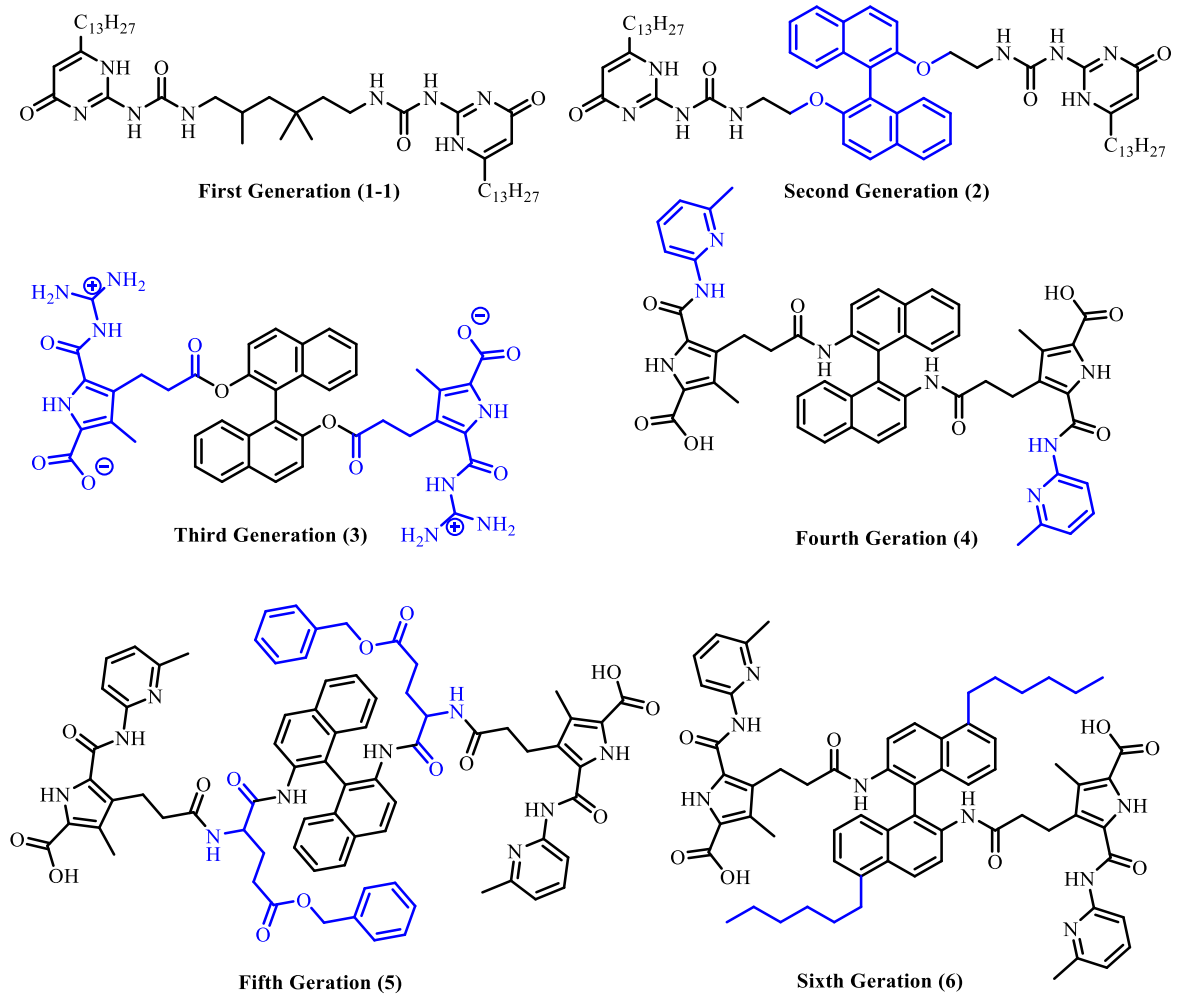

Figure 124: Final structures of all six generations.

The investigation started with a literature known system, the hexyl ureidopyrimidone **1-1**.[82] While the synthesis was carried out within four steps, the most challenging formation of the isocyanate **19-1** was finally carried out using triphosgene. The system demonstrated a good improvement of the viscosity in elevated temperatures in a 145 mM concentrated chloroformic solution, where the specific viscosity was increased by 13%. Nevertheless, the solubility was limited to chloroformic solutions.

Subsequently, the second generation was used to implement the BINOL unit as a linker unit, to investigate the influence of different linkers. The synthesis was carried out within five steps, where the formation of the isocyanate was already investigated in the first generation. Here, the solubility and the effect on the viscosity were similar to the results of the first generation, where an increased specific viscosity by 4% occurred at a 160 mM concentrated solution. The measurements of the viscosity were still limited to chloroformic solutions.

To increase the solubility in other solvents than chloroform, and to investigate the influence on another binding unit, the GCP motif **35** was implemented in the third generation. The synthesis was carried out with seven steps, where a change of the BINOL linker unit to a BINAM linker unit was introduced, due

to deprotection problems. Here, the solubility in DMSO increased, which enabled measurements up to 100 °C. Viscosity measurements were demonstrating that the effect increased again, due to the improvement of the specific viscosity by 13%. However, the increasing specific viscosity occurred in a small temperature range. These results were proven with DLS measurements, which were indicating an increase of larger molecules in higher temperatures. But the third generation was only soluble in DMSO, while the final aim was to improve the viscosity of unpolar solvents like oils.

The ACP motif enabled an increased solubility in unpolar solvents, due to the neutral structure of the ACP motif in comparison to the GCP motif. The synthesis of the fourth generation was carried out in seven steps. This enabled the measurement of the viscosity in chloroform, toluene and the oil Nynas NS8. Here, good results were obtained due to the positive effect of the fourth generation on the viscosity in higher temperatures. While the viscosity measurements in DMSO were generating almost no change in the specific viscosity, more unpolar solvents demonstrated an increased specific viscosity. In chloroform and toluene, the specific viscosity increased 36% and 96% which was additionally substantiated by DLS measurements, where a major increase of large structures occurred. Measurements in the motor oil Nynas NS8 demonstrate an increased specific viscosity by 30%. The calculated viscosity index indicates that it is possible to increase the VI by using a supramolecular viscosity index improver, due to the increased VI of Nynas NS8 from 47 to 94. These results are representing the first ever reported use of a supramolecular system, that is able to increase the VI of a motor oil.

To achieve even higher solubilities in more unpolar solvents like motor oils, the fifth generation was started to investigate the effect of the extension with an amino acid. The synthesis was carried out in eight steps. This generation failed to increase the viscosity in elevated temperatures. It was possible to increase the solubility in Nynas NS8 and Nexbase 3020, but all effects with regard to viscosity improvement were lost.

Therefore, the sixth generation was generated to substitute the fourth generation without further changes in the core structure. The synthesis was carried out in eight steps. This modification was a success. While the kinematic and specific viscosity were improved at elevated temperatures, the solubility in Nynas NS8 and Nexbase 3020 was improved as well. While the specific viscosity in Nynas NS8 and Nexbase 3020 were increased by 26% and 44%, the VI's were increased too, from 47 to 89 and from 88 to 152. For the first time, an application of a supramolecular viscosity improver was possible in Nexbase 3020.

Nevertheless, the sixth generation is not yet prepared for applicational use in motor oil or industrial use. Due to the limited solubility, the use is not possible for any motor oil or solvent. Because of this, further structural modifications might be necessary in order to achieve solubility in more unpolar solvents. For example, the simple addition of a longer alkyl chains would increase the solubility and thus the applicability of this system.

6. Zusammenfassung

Ziel dieser Arbeit war die Generierung von Lösungsmittel- und Öl-Additiven, die in der Lage sind, den Viskositätsindex zu erhöhen. Dieses Ziel wurde im Verlauf von sechs synthetischen Generationen erreicht.

Table 11: Entwicklung der Ergebnisse in dieser Arbeit.

Generation	**1**	**2**	**3**	**4**	**5**	**6**
Löslichkeit in unpolaren Lösungsmitteln						
Viskositäts-verbesserung	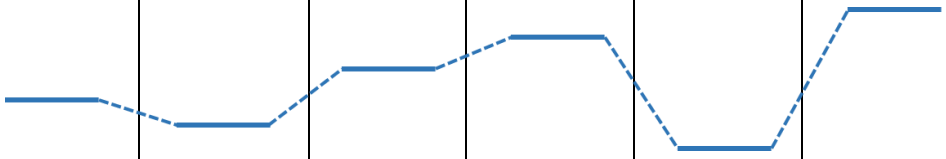					

Während die sechste Generation den Viskositätsindex signifikant erhöht hat und einen großen Einfluss auf die spezifische Viskosität zeigte, waren alle anderen Generationen für die Entwicklung des finalen Additivs notwendig. Rückblickend beschäftigten sich die ersten drei Generationen mit der Entwicklung eines Systems, das die Viskosität in erhöhten Temperaturen positiv beeinflusst. In den letzten drei Generationen stand die Verbesserung der Löslichkeit im Vordergrund.

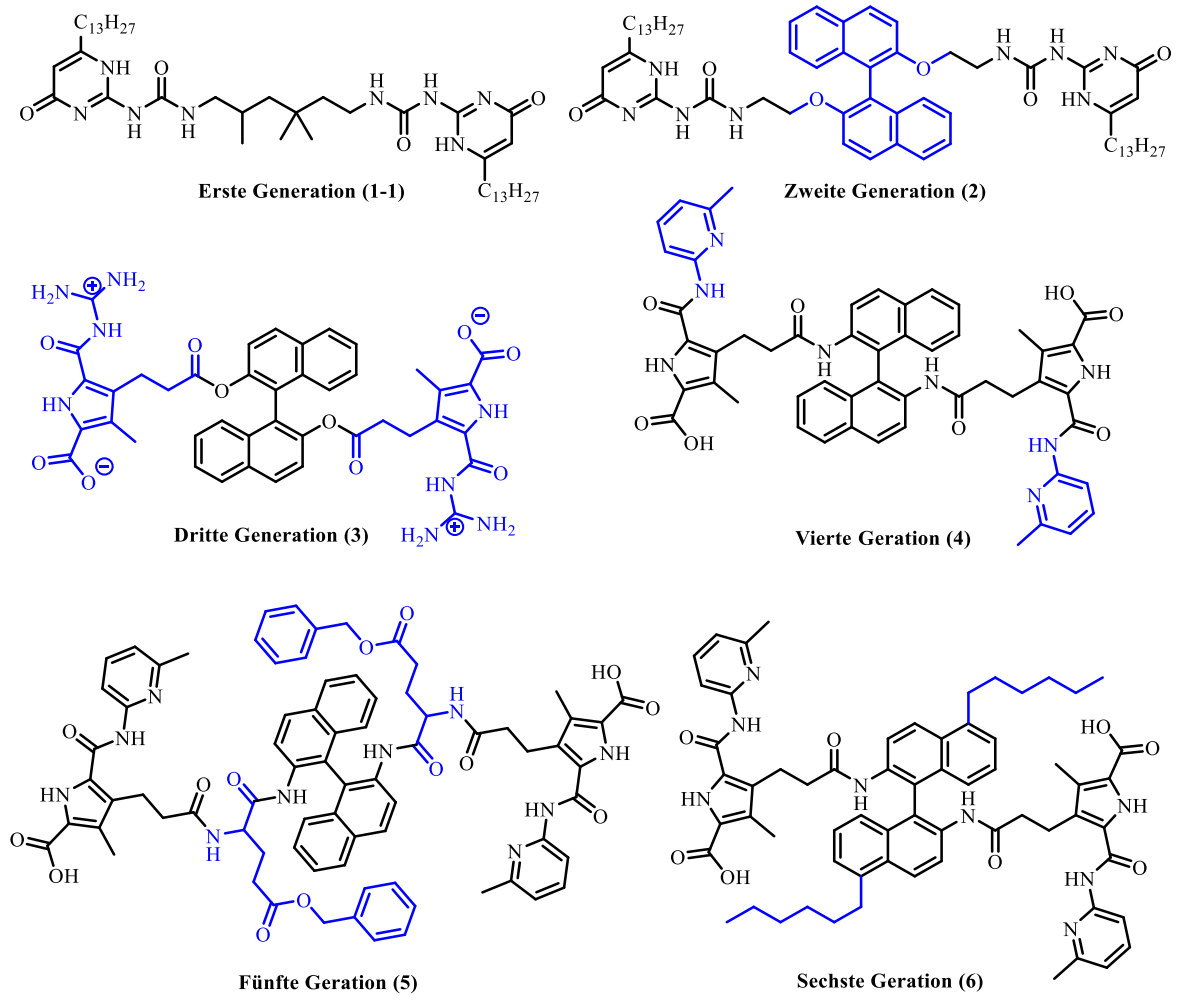

Figure 125: Finale Strukturen aller Generationen.

Die Untersuchungen starteten mit einem literaturbekannten System, dem Hexyl-ureidopyrimidon **1-1**.[82] Dieses System konnte in vier Syntheseschritten synthetisiert werden, wobei sich herausstellte, dass die Erstellung des Isocyanats die größte Herausforderung darstellen würde. Dieses Problem konnte letztendlich unter der Verwendung von Triphosgen gelöst werden. Das dargestellte System zeigte gute viskositätsverbessernde Eigenschaften in einer 145 mM Lösung in Chloroform. Die spezifische Viskosität konnte in erhöhten Temperaturen um 13% im Vergleich zu der spezifischen Viskosität bei Raumtemperatur erhöht werden. Die Löslichkeit des Systems der ersten Generation war jedoch ausschließlich auf Chloroform begrenzt.

Anschließend wurde die zweite Generation synthetisiert, um eine BINOL-Einheit in das System einzubauen. Die BINOL-Einheit sollte den Linker der ersten Generation ersetzen, um den Einfluss der Linkereinheit zu untersuchen. Die Synthese wurde in fünf Schritten durchgeführt, wobei die Erfahrung aus der Synthese der ersten Generation genutzt werden konnte. Die Löslichkeit und der Effekt auf die Viskosität waren ähnlich zu der ersten Generation. Die Konzentration der viskositätsverbessernden

Lösung wurde auf 160 mM verschoben, wodurch die spezifische Viskosität um 4% erhöht wurde. Weiterhin konnten die Messungen lediglich in Chloroform durchgeführt werden.

Um die Löslichkeit in anderen Lösungsmitteln als Chloroform zu erhöhen, wurde in der dritten Generation der Einfluss einer neuen Bindungseinheit untersucht, indem die GCP-Einheit in das System eingeführt wurde. Die Synthese wurde in sieben Schritten durchgeführt und die BINOL-Einheit durch eine BINAM-Einheit ausgetauscht. Hierdurch konnte die Löslichkeit in DMSO erheblich verbessert werden, wodurch nun Messungen von bis zu 100 °C möglich wurden. Die Messungen der Viskosität zeigten einen erhöhten Effekt auf die Viskositätsverbesserung. Hier konnte die spezifische Viskosität um 13% verbessert werden. Dieser Effekt zeigte sich jedoch in einen kleinen Temperaturfenster. Die Ergebnisse der Viskositätsmessungen konnte mit DLS-Messungen bestätigt werden. Hier konnte die Bildung von großen Polymerteilchen in erhöhten Temperaturen und ein Zerfall dieser Strukturen bei weiterer Erhöhung der Temperaturen beobachtet werden. Jedoch war die dritte Generation nur in DMSO löslich, während das finale Ziel der Arbeit die Verbesserung der Viskosität von unpolaren Lösungsmitteln (Öle) war.

Das ACP Motiv konnte die Löslichkeit des Systems durch die neutrale Struktur erheblich verbessern. Nun war es möglich Messungen in Chloroform, Toluol, DMSO und dem ersten Motoröl Nynas NS8 durchzuführen. Die Synthese der vierten Generation wurde in sieben Schritten durchgeführt. Messungen der Viskosität zeigten, dass die Viskosität von Lösungsmitteln in erhöhten Temperaturen erheblich beeinflusst wurde. Während die spezifische Viskosität sich in Messungen in DMSO kaum änderte, konnten unpolare Lösungsmittel einen deutlichen Anstieg der spezifischen Viskosität erreichen. In Chloroform und Toluol konnte die spezifische Viskosität um 36% und 96% erhöht werden. Dieser Effekt konnte zudem in DLS-Messungen gezeigt werden. Zusätzlich konnte in Nynas NS8 die spezifische Viskosität um 30% erhöht werden und der Viskositätsindex von 47 auf 94 verbessert werden. Somit wurde erstmals gezeigt, dass ein Viskositätsindex-Verbesserer auf Basis von supramolekularen Interaktionen erfolgreich eingesetzt werden kann.

Um weiterhin die Löslichkeit des Systems zu steigern und weitere Messungen in anderen Ölen durchführen zu können, sollte in der fünften Generation die Löslichkeit durch die Erweiterung der Linkereinheit um eine Aminosäure erhöht werden. Die Synthese wurde in Acht Schritten durchgeführt. Die Löslichkeit wurde erfolgreich verbessert und Lösungen in Nexbase 3020 waren nun möglich. Leider zeigte die fünfte Generation keinen Effekt in der Verbesserung der Viskosität in erhöhten Temperaturen. Sämtliche Eigenschaften, hinsichtlich der Verbesserung der Viskosität, der vierten Generation gingen verloren.

Somit wurde die sechste Generation synthetisiert. Die vierte Generation sollte derivatisiert werden, ohne die Grundstruktur zu verändern. Hierzu wurde an die Linkereinheit eine Hexylgruppe substituiert. Die Synthese wurde in acht Schritten durchgeführt. Diese Modifikation war ein großer Erfolg. Während sowohl die spezifische Viskosität erheblich verbessert werden konnte, konnte auch die Löslichkeit in

Nynas NS8 und Nexbase 3020 ebenfalls gesteigert werden. Die spezifische Viskosität in Nynas NS8 konnte um 26% in erhöhten Temperaturen verbessert werden und in Nexbase 3020 sogar um 44% erhöht werden. Des weiteren, konnte durch die sechste Generation der Viskositäts Index der Öle Nynas NS8 und Nexbase 3020 von 47 auf 89 bzw. von 88 auf 152 erhöht werden. Im Vergleich zu der vierten Generation wurde der Effekt leicht vermindert, aber dadurch das nun Lösungen in noch unpolaren Lösungsmitteln möglich waren, konnte dies durch den gesteigerten Effekt in Nexbase 3020 kompensiert werden. Es konnte zum ersten Mal gezeigt werden, dass ein Viskositäts Index Verbesserer auf Basis von supramolekularen Eigenschaften erfolgreich in Ölen wie Nexbase 3020 eingesetzt werden kann.

7. Experimental Section

7.1 Material and Methods

7.1.1 General Remarks and analytical Methods

Each commercially available chemical mentioned was used without any purification unless specified. All reactions were carried out in argon atmosphere in a pre-heated flask and all chemicals were added in argon flow. The solvents THF, DCM and DMF were always freshly dried and distilled under argon and only used in previously heated out flasks with an argon atmosphere. The solvents were never stored for longer than 48 hours under argon atmosphere. The milli-Q water was made by a Micropure apparatus from TKA.

Thin-layer chromatography (TLC) was carried out an TLC plates of Polygram® SIL G/UV254 (silica gel 0.2 mm, 40 x 80 mm) purchased from Macherey-Nagel GcbH & Co. KG.

Diisopropylamin was dried over CaH_2 and refluxed for 72 h until it was distilled under argon atmosphere and stored with molecular sieve under argon.

7.1.1 NMR-Spectroscopy

^{1}H NMR and ^{13}C NMR spectra were measured by:

- Bruker DMX 300
    - ^{1}H: 300 MHz, ^{13}C: 75 MHz
- AV Neo 400 NMR
    - ^{1}H: 400 MHz, ^{13}C: 151 MHz
- Bruker DMX 600
    - ^{1}H: 600 MHz, ^{13}C: 151 MHz

All measurements were carried out at room temperature in DMSO-d_6 and $CDCl_3$ as a solvent. For software analysis, ACD-Labs 2018 – Spectrus Processor was used. All chemical shifts were standardized with the signals of the solvent (DMSO-d_6 = 2.50 ppm, $CDCl_3$ = 7.26 ppm).

The J-coupling was measured in Hertz. The multiplicity of all signals the following abbreviations were used: s = singlet, br s = broad singlet, d = doublet, t = triplet, m = multiplet (denotes complex pattern). For some measurements, it was necessary to add TFA (0.1 N) to the solution to hinder the system in aggregation.

7.1.2 Mass Spectrometry

The high-resolution mass spectrometry was carried out in Essen and in Münster. The measurements in Essen were carried out in Bruker maXis 4G (ESI) and were measured in MeOH or DCM. The concentrations of the solutions were 10^{-4} to 10^{-5} M.

The measurements in Münster were carried out on a Thermo Scientific Orbitrap LTQ-XL mass spectrometer. For software analysis, Brukers Compass DataAnalysis 4.1 was used.

7.1.3 Viscometer

The viscosity measurements were carried out via "Rolling-ball viscometer Lovis 2000 M" by Anton paar with a sample amount of 100 µL to 200 µL and a temperature range of −30 °C to 100 °C. All viscosity measurements were done in neutral pH value, which was adjusted if necessary, by adding 0.1 N NaOH or 0.1 N HCl aqueous solution, monitored via pH-Meter 766 from Knickarray.

For each sample (compound and concentration) three different solutions were prepared and filtered through syringe filters (0.4 µm). Each solution was measured heating up at 25 °C, 35 °C, 45 °C, 55 °C, 65 °C, 75 °C, 85 °C, 95 °C and 100 °C and cooling down at the same temperatures except for chloroform solutions where the maximum temperature was 50 °C. Each measuring point was measured by the viscometer in a sequence of six times switching the angle to let the sphere fall and each sequence was done three times. After every measurement session, the sample holder was completely cooled down to room temperature and washed with acetone and cyclohexane and dried with compressed air. With this method, falling time, kinematic viscosity and dynamic viscosity were measured.

7.1.4 Specific Viscosity

The specific viscosity was calculated with the kinematic viscosity of each solution and the pure solvent. Therefore, the viscosity of the pure solvent was measured the same way as described before. By the formula of the specific viscosity the percentage behaviour was obtained.

$$\eta_{Sp} = \frac{\eta_C - \eta_0}{\eta_0} \qquad \text{(equation 5)}$$

The specific viscosity (η_{Sp}) results out of the dynamic viscosity of each concentration (η_C) and the equivalent dynamic viscosity of the solvent (η_0) at each temperature.

7.1.5 Viscosity Index

The viscosity index (VI) was calculated by VI tables of Evonik Oil Additives.[93] Therefore, the kinematic viscosities of the liquid of 40 °C and 100 °C were set and compared to oils with similar VI's to achieve the VI of the measurement.

7.1.5 DLS-Measurements

Dynamic Light Scattering (DLS) was measured via Zetasizer-Nano ZS from Malvern in different Temperatures (25 °C, 50 °C, 60 °C, 100 °C). All DLS measurements were carried out with a HeNe Laser at a wavelength of 633 nm and a back-scatter angle of 173° (non-invasive backscatter technology). Samples were equilibrated for 3 min at each temperature before each measurement.

7.1.6 FT-IR-Measurements

For IR measurements a FT-IR 430 Spectrometer by Jasco was used. All signals were ordered from small to large.

7.1.7 Melting Point

The melting point was measured with B-540 from Büchi. All solid compounds were heated up until 300 °C, until the melting or decomposition of the compound occurs. Reported melting points are not corrected.

7.1.6 Force Field Calculations

The Schrödinger Maestro Suite (11.8) was used for the molecular modelling studies. The structures were calculated using MacroModel and OPLS 2005 force field choosing chloroform as the solvent.

[93] *12.06.2020* **https://oil-additives.evonik.com/product/oil-additives/resources/viscosity-index-en.html**, *Evonik Oil Additives*

Energy minimization was performing using the PCRG-method (maximum 50000 steps, convergence threshold 0.01).

7.1.7 Elemental Analysis

The measurements of the elemental analysis were carried out on an EA-CHNSO Analyser from HEKAtech GmbH.

7.2 Synthesis

7.2.1 Synthesis of Tridecane-Isocytosine 18

Described experiment: JO-005. Repeated: JO-047.

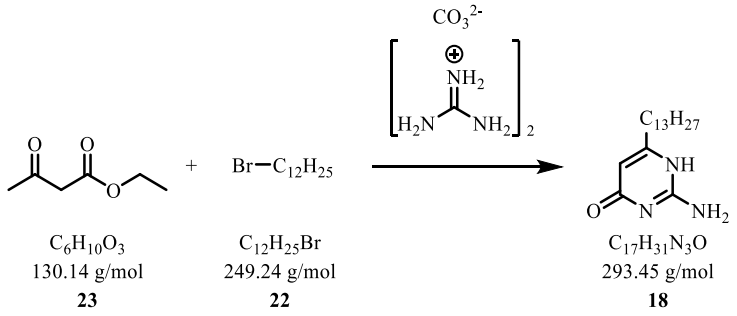

Figure 126: Synthesis of Tridecane-Isocytosine 18.

The synthesis was carried out as described in the literature.[85] In a dry flask sodiumhydride (1.49 g, 37.4 mmol, 1.1 eq) was dissolved in dry tetrahydrofuran (100 mL) and cooled down to −10 °C. Ethylacetoacetate (**23**) (4.30 mL, 4.42 g, 1.0 eq, 34.0 mmol) was added slowly until a strongly exothermic reaction was observed. After 30 minutes *n*-butyllithium (13.6 mL, 34.0 mmol, 2.5 M in tetrahydrofuran, 1 eq) was added at the same temperature within 15 minutes and the mixture was stirred additional 15 minutes. Afterwards 1-bromododecane (**22**) (6.39 mL, 9.31 g, 37.4 mmol, 1.1 eq) was added slowly at 0 °C and the mixture was allowed to reach room temperature within one hour.

The reactions mixture was diluted with diethylether (350 mL) acidified with 0.5 M HCl (200 mL). The organic layer was separated and the aqueous layer was extracted with diethylether (3 x 100 mL). The combined organic layers were washed with brine (3 x 100 mL) and dried over sodiumsulfate. The solvent was removed in vacuum to give the intermediate (8.09 g, 27.6 mmol, 81%) as a colourless oil which was pure enough to continue the synthesis.

In a dry flask guanidiniumcarbonate (1.10 g, 6.13 mmol, 0.18 eq) was dissolved in ethanol (100 mL). Ethyl-3-oxohexadecanoate (3.00 g, 10.2 mol, 0.3 eq) was added and the mixture was refluxed for 24 hours. The solvent was removed until 20% remained and the mixture was refluxed additional two hours.

After cooling down to room temperature *n*-hexane (150 mL) and water (50 mL) were added to precipitate the product. The solid was filtered of and washed with *n*-hexane (100 mL), acetone (100 mL) and water (100 mL). The pure product **18** was obtained as a white solid (2.10 g, 7.15 mmol, 70%, overall yield 57%) by recrystallisation in ethanol.

Sum formula: $C_{17}H_{31}N_3O$

Molar mass: 293.45 g/mol

R_f: 0.67 (cyclohexane:ethylacetate = 1:1)

^{1}H-NMR: (300 MHz, DMSO-d_6) δ [ppm] = 0.85 (t, 3 H, J^3 = 6.88 Hz, CH_2-CH_3), 1.23 (s, 20 H, (CH_2)$_{10}$), 1.47 - 1.54 (m, 2 H, CH_2-CH_2-CH_2), 2.21 (t, J^3 = 7.66 Hz, 2 H, C_q-CH_2-CH_2), 5.36 (s, 1 H, C*H*), 6.42 (br s, 2 H, NH_2), 10.56 (br s, 1 H, N*H*).

^{13}C-NMR: (75 MHz, DMSO-d_6) δ [ppm] = 13.96, 22.09, 27.52, 28.64, 28.70, 28.86, 28.97, 29.01, 30.70, 31.28, 37.06, 38.68, 40.36, 119.52, 155.53, 162.81, 169.78.

FT-IR: (ATR): $\tilde{\nu}$ [cm^{-1}] = 3360, 3162, 2878, 2720, 1601, 1592, 1554, 1489, 1437, 1400.

Melting point: 145 °C

7.2.2 Synthesis of Trimethyl-hexyl-Ureidopyrimidone 1-1

Described experiment: JO-006. Repeated: JO-009.

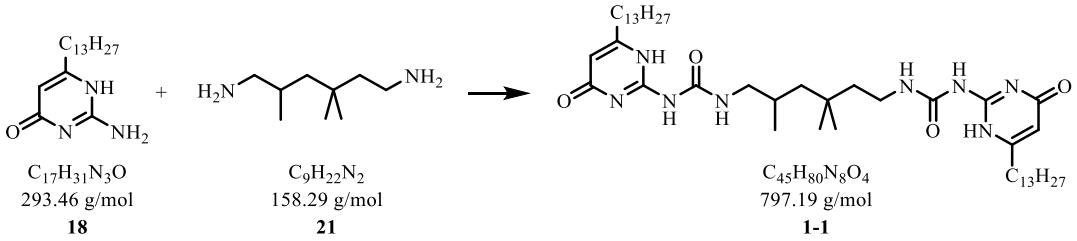

Figure 127: Synthesis of Trimethyl-hexyl-Ureidopyrimidone 1-1.

A mixture of 2,4,4-trimethylhexane-1,6-diamine (**21-1**) and 2,2,4-trimethylhexane-1,6-diamine (**21-2**) (0.367 mL, 0.318 g, 2.01 mmol, 0.5 eq) and triethylamine (1.68 mL, 1.22 g, 12.1 mmol, 3 eq) were dissolved in dry dichloromethane (50 mL) and stirred for 20 minutes at room temperature. Meanwhile triphosgene (**23**) (1.19 g, 4.02 mmol, 1 eq) was weighed in a dry flask, dissolved in dry dichloromethane (20 mL) and the solution was cooled down to 0 °C. Following the diamine solution was added slowly to the triphosgene solution which resulted in a yellow-orange solution. After 30 minutes the solvent was removed in vacuum and the residue was dissolved in pyridine (40 mL). A solution of tridecane-isocytosine (**18**) (1.18 g, 4.02 mmol, 1 eq) in pyridine (20 mL) was added and the mixture was heated to reflux for six hours.

The reaction mixture was quenched with water (50 mL) and the solvent was removed in vacuum. The remaining white solid was purified with column chromatography (ø = 5 cm, h = 40 cm, chloroform: methanol = 3:1) and MPLC (ø = 3 cm, h = 60 cm, RP18, methanol:water = 1:10 to pure methanol) to give the pure product (0.54 g, 0.68 mmol, 17%) as a white solid, while only the 2,4,4-isomer was collected as a final product **1-1**.

Sum formula: $C_{45}H_{80}N_8O_4$

Molar mass: 797.19 g/mol

R_f: 0.71 (cyclohexane:ethylacetate = 1:2)

^{1}H-NMR: (300 MHz, $CDCl_3$ + TFA - 12:1) δ [ppm] = 0.88 - 1.00 (m, 15 H, 5 x C*H*$_3$), 1.22 - 1.53 (m, 44 H, 2 x (C*H*$_2$)$_{11}$), 1.60 - 1.70 (m, 4 H, 2 x C_q-C*H*$_2$-CH$_2$), 1.82 (m, 1 H, C*H*), 2.69 (m, 2 H, C*H*$_2$), 2.78 (m, 2 H, C*H*$_2$), 3.08 (m, 2 H, C*H*$_2$), 3.23 (m, 2 H, C*H*$_2$), 6.27 (s, 2 H, 2 x C*H*), 6.83 (br.s., 2 H, 2 x N*H*).

^{13}C-NMR: (75 MHz, $CDCl_3$ + TFA) δ [ppm] = 13.99, 20.04, 22.66, 26.79, 26.99, 28.72, 29.00, 29.05, 29.30, 29.34, 29.50, 29.58, 29.63, 31.91, 32.71, 32.90, 37.14, 40.60, 45.82, 47.89, 105.38, 105.65, 113.66 151.42, 151.67, 153.21, 153.67, 158.50.

HR-MS: (ESI): m/z = 797.6389 ($[M+H]^+$), calcd. 797.6375(for $[C_{45}H_{81}N_8O_4]^+$).

FT-IR: (ATR): $\tilde{\nu}$ [cm^{-1}] = 3054, 2925, 2825, 1721, 1645, 1609, 1580, 1511, 1461, 1239, 797.

Melting point: 211 °C

7.2.3 Synthesis of BINOL-Ethyl-Ether *(S)*-30

Described experiment: JO-022.

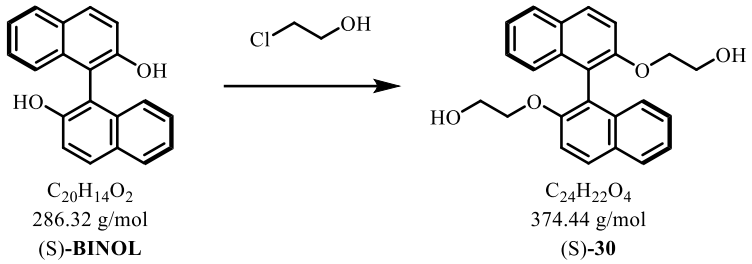

Figure 128: Synthesis of BINOL-Ethyl-Ether *(S)*-30.

The synthesis was carried out as described in the literature.[91] *(S)*-1,1'-binaphthalene-2,2'-diol (0.2 g, 0.7 mmol, 1 eq) was solved in dimethylformamide (10 mL) and $Cl(CH_2)_2OH$ (0.19 mL, 0.225 g, 2.79 mmol, 4 eq) and potassium carbonate (0.386 g, 2.79 mmol, 4 eq) were added, and the mixture was refluxed for 16 h. The mixture was diluted with ethylacetate (10 mL) and washed sequentially with water, 2 M NaOH (3 x 5 mL) and brine (3 x 10 mL) and dried over $MgSO_4$. After the removal of the solvent, the crude product was purified via column chromatography (ø = 3 cm, h = 60 cm, cyclohexane:ethylacetate = 1:2) to give the product *(S)*-**30** (0.17 g, 0.44 mmol, 63%) as a white solid.

Sum formula: $C_{24}H_{22}O_4$

Molar mass: 374.44 g/mol

R_f-value: 0.34 (cyclohexane:ethylacetate = 1:1)

^{1}H-NMR: (300 MHz, DMSO-*d_6*) [ppm] δ = 3.43 (m, 4 H, 2 x C*H_2*), 3.74 (m, 4 H, 2 x C*H_2*), 6.98 (d, J^3 = 8.6 Hz, 2 H, 2 x BINOL-*H*), 7.21 (m, 2 H, 2 x BINOL-*H*), 7.30 (m, 2 H, 2 x BINOL-*H*), 7.38 (m, 2 H, 2 x BINOL-*H*), 7.88 (d, J^3 = 8.0 Hz, 2 H, 2 x BINOL-*H*), 8.03 (d, J^3 = 9.2 Hz, 2 H, 2 x BINOL-*H*).

^{13}C-NMR: (75 MHz, DMSO-d_6) δ [ppm] = 38.95, 68.52, 117.90, 123.18, 124.51, 126.33, 127.99, 128.04, 128.55, 129.21, 133.81, 153.32.

HR-MS: (ESI): m/z = 375.1587 ($[M+H]^+$), calcd. 375.1591 (for $[C_{24}H_{23}O_4]^+$).

Melting point: 168 °C

7.2.4 Deprotection of BINOL-Ethyl-Amine *(S)*-32

Described experiment: JO-022.5.

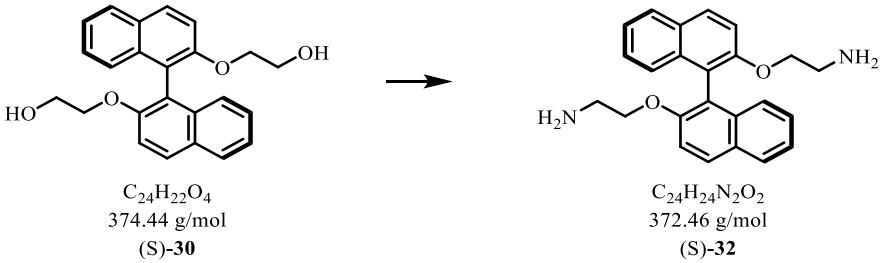

$C_{24}H_{22}O_4$
374.44 g/mol
(S)-**30**

$C_{24}H_{24}N_2O_2$
372.46 g/mol
(S)-**32**

Figure 129: Deprotection of BINOL-Ethyl-Amine *(S)*-32.

The synthesis was carried out as described in the literature.[91] *(S)*-BINOL-ethanol [*(S)*-**30**] (0.1 g, 0.267 mmol, 1 eq) was dissolved in dichloromethane (3 mL) when DMAP (3.26 mg, 0.0267 mmol, 0.1 eq), pyridine (0.110 mL, 0.110 g, 1.34 mmol, 5 eq) and MsCl (0.103 mL, 0.153 g, 1.34 mmol, 5 eq) were added and the mixture was stirred at room temperature for 16 h. To the mixture chloroform (3 mL) was added and then washed with water (3 x 5 mL) and brine (3 x 5 mL) and dried with $MgSO_4$. After removing the solvent in vacuum, the crude product was dissolved in dimethylformamide (3 mL) and NaN_3 (0.130 g, 2.00 mmol, 7.5 eq) was added and the mixture was refluxed at 80 °C for another 16 h. The mixture was diluted with chloroform and washed with water (3 x 5 mL) and brine (3 x 5 mL) and dried with $MgSO_4$. After the removal of the solvent in vacuum, the crude intermediate was purified by column chromatography (ø = 3 cm, h = 30 cm, cyclohexane:ethylacetate = 5:1) to give the azide *(S)*-**31** as a yellow oil.

The azide intermediate (0.06 g, 0.14 mmol, 53%) was dissolved in dioxane (3 mL) and water (0.6 mL) and PPh_3 (0.280 g, 1.07 mmol, 4 eq) was added and the mixture was stirred for 16 h. After the removal of the solvent in vacuum, the product was purified by column chromatography (ø = 3 cm, h = 30 cm, chloroform:methanol = 8:1) to give the product *(S)*-**32** (0.0418 g, 0.112 mmol, 75%, overall yield 42%) as a white solid.

Sum formula: $C_{24}H_{24}N_2O_2$

Molar mass: 372.46 g/mol

R_f: 0.12 (cyclohexane:ethylacetate = 1:1).

^{1}H-NMR: (300 MHz, DMSO-*d*$_6$) δ [ppm] = 3.28 (m, 4 H, 2 x C*H*$_2$), 3.56 (m, 4 H, 2 x C*H*$_2$), 6.87 (m, 2 H, 2 x BINOL-*H*), 7.08 (m, 2 H, 2 x BINOL-*H*), 7.33 (m, 2 H, 2 x BINOL-*H*), 7.43 (m, 2 H, 2 x BINOL-*H*), 7.79 (m, 2 H, 2 x BINOL-*H*), 7.97 (d, J^3 = 9.2 Hz, 2 H, 2 x BINOL-*H*).

^{13}C-NMR: (75 MHz, DMSO-*d*$_6$) δ [ppm] = 31.41, 68.54, 117.83, 123.00, 124.32, 125.83, 126.27, 126.97, 127.12, 130.14, 134.23, 154.31.

HR-MS: (ESI): m/z = 373.1943 ($[M+H]^+$), calcd. 373.1911(for $[C_{24}H_{25}N_2O_2]^+$).

Melting point: Decomposition at 213 °C

7.2.5 Synthesis of BINOL-Ethyl-Ureidopyrimidone 2

Described experiment: JO-030.

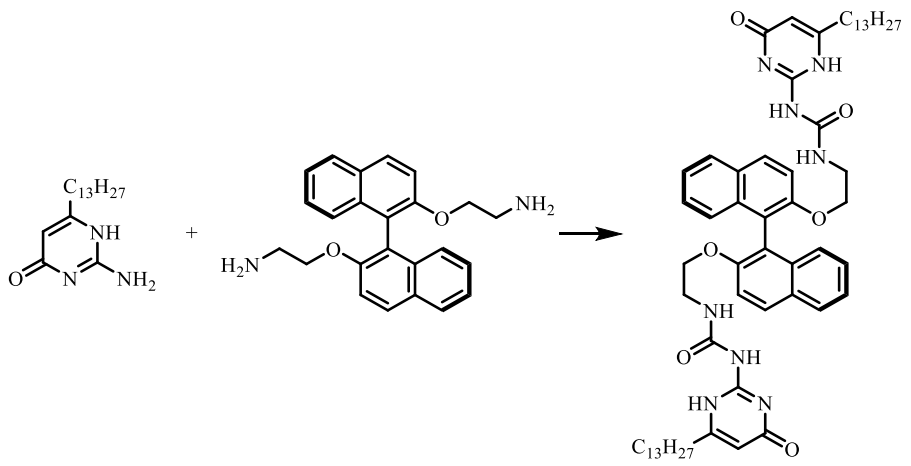

$C_{17}H_{31}N_3O$ | 293.46 g/mol | **18**

$C_{24}H_{24}N_2O_2$ | 372.46 g/mol | (*S*)-**32**

$C_{60}H_{82}N_8O_6$ | 1011.37 g/mol | (*S*)-**2**

Figure 130: Synthesis of BINOL-Ethyl-Ureidopyrimidone 2.

Diethylamino-*(S)*-BINOL (***[S]*-32**) (50.3 mg 0.135 mmol, 0.5 eq) and triethylamine (0.112 mL, 81.5 mg, 0.81 mmol, 3 eq) were dissolved in dry dichloromethane (20 mL) and stirred for 20 minutes at room temperature. Meanwhile triphosgene (79.7 mg, 0.27 mmol, 1 eq) was weight in a dry flask, dissolved in dry dichloromethane (10 mL) and cooled down to 0 °C. Following the diamine solution was added slowly to the triphosgene solution which resulted in a yellow solution. After 30 minutes the solvent was removed in vacuum and the residue was dissolved in pyridine (20 mL). A solution of tridecane-isocytosine (**18**) (78.8 mg, 0.266 mmol, 1 eq) in pyridine (10 mL) was added and the mixture was heated to reflux for six hours.

The reaction mixture was quenched with water (10 mL) and the solvent was removed in vacuum. The remaining white solid was purified with column chromatography (ø = 3 cm, h = 30 cm, chloroform:methanol = 5:1) to give the pure product *(S)*-**2** (82.0 mg, 0.0811 mmol, 30%) mmol as a white solid.

Sum formula: $C_{60}H_{82}N_8O_6$

Molar mass: 1011.37 g/mol

R_f: 0.67 (cyclohexane:ethylacetate = 1:2)

^{1}H-NMR: (300 MHz, $CDCl_3$ + TFA - 12:1) δ [ppm] = 1.27 (t, J^3 = 7.19 Hz, 6 H, 2 x C*H*$_3$), 1.40 – 1.63 (m, 44 H, 2 x $(CH_2)_{11}$), 1.90 (m, 4 H, C_q-C*H*$_2$), 3.01 (m, 4 H, 2 x C*H*$_2$), 3.57 (m, 4 H, 2 x C*H*$_2$), 6.89 (s, 2 H, 2 x C*H*) 7.11, (d, J^3 = 8.44 Hz, 2 H, 2 x BINOL-*H*), 7.2 (br s, 2 H, 2 x N*H*), 7.33 (d, J^3 = 5.94 Hz, 2 H, 2 x BINOL-*H*), 7.48 (d, J^3 = 7.82 Hz, 2 H, 2 x BINOL-*H*), 7.96 (d, J^3 = 8.44 Hz, 2 H, 2 x BINOL-*H*), 8.02 (d, J^3 = 8.76 Hz, 2 H, 2 x BINOL-*H*), 8.21 (d, J^3 =8.13 Hz, 2 H, 2 x BINOL-*H*).

^{13}C-NMR: (75 MHz, $CDCl_3$ + TFA) δ [ppm] = 14.14, 20.00, 22.62, 26.89, 28.77, 29.00, 29.14, 29.28, 29.38, 29.63, 29.75, 29.96, 35.62, 40.80, 68.35, 103.43, 112.27, 114.15, 119.46, 125.03, 126.70, 128.45, 130.04, 134.66, 151.37, 152.30, 156.34, 160.53, 169.30, 182.85.

HR-MS: (ESI): m/z = 1011.6428 ($[M+H]^+$), calcd. 1011.6430 (for $[C_{60}H_{82}N_8O_6]^+$).

FT-IR: (ATR): $\tilde{\nu}$ [cm^{-1}] = 3531, 3054, 2627, 2867, 2825, 1721, 1691, 1660, 1650, 1223, 1120, 1074, 1070, 815, 795, 776.

Melting point: 256 °C

7.2.6 Synthesis of the GCP Binding Motive 43

Described experiment: JO-057. Repeated: JO-063, JO-067.

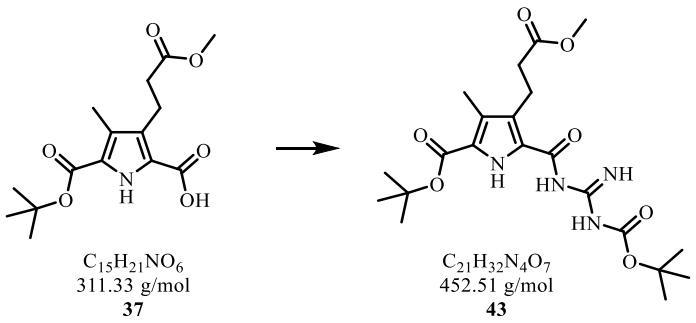

Figure 131: Synthesis of the GCP Binding Motive 40.

The synthesis of building block **37** and the GCP binding motif **43** were carried out as described in the literature.[92] The building block **37** (1.00 g, 3.21 mmol, 1 eq), HCTU (1.62 g, 3.85 mmol, 1.2 eq) and DMAP (0.784 g, 6.42 mmol, 2 eq) were dissolved in dichloromethane (50 mL) and dimethylformamide (10 mL). After stirring for 30 minutes to build the active ester, Boc-guanidine (0.766 g, 4.81 mmol, 1.5 eq) was added and the mixture was stirred another 16 hours at room temperature. The mixture was separated from all solvent in vacuum and resolved in dichloromethane (20 mL). After washing with water (3 x 20 mL) and brine (3 x 20 mL) the product was purified via column chromatography (ø = 5 cm, h = 40 cm, cyclohexane:ethylacetate = 3:1). The product **43** (0.919 g, 2.03 mmol, 63%) was obtained as a white solid.

Sum formula: $C_{21}H_{32}N_4O_7$

Molar mass: 452.51 g/mol

R_f: 0.60 (SiO_2, cyclohexane:ethylacetate = 3:1)

^{1}H NMR: (300 MHz, $CDCl_3$) δ [ppm] = 1.53 (s, 9 H, C-(CH_3)$_3$), 1.56 (s, 9 H, C-(CH_3)$_3$), 2.26 (s, 3 H, CH_3), 2.6 (t, J^3 = 8.4 Hz, 2 H, CH_2), 3.11 (t, J^3 = 7.82 Hz, 2 H, CH_2), 3.70 (s, 3 H, CH_3), 8.38 (br s, 1 H, N*H*), 8.93 (br s, 2 H, 2 x N*H*) 9.49 (s, 1 H, N*H*).

^{13}C-NMR: (100 MHz, DMSO-*d6*) δ [ppm] = 9.67, 19.71, 27.73, 27.99, 34.12, 51.32, 72.92, 80.67, 80.81, 123.31, 124.95, 125.23, 129.30, 158.45, 159.83, 160.13, 161.05.

FT-IR: (ATR): $\tilde{\nu}$ [cm^{-1}] = 3456, 3392, 3277, 2979, 1737, 1636, 1311, 1154, 1075, 848, 753, 539.

Melting point: 115 °C

7.2.7 Deprotection of the GCP Building Block 35

Described experiment: JO-059. Repeated: JO-063, JO-067.

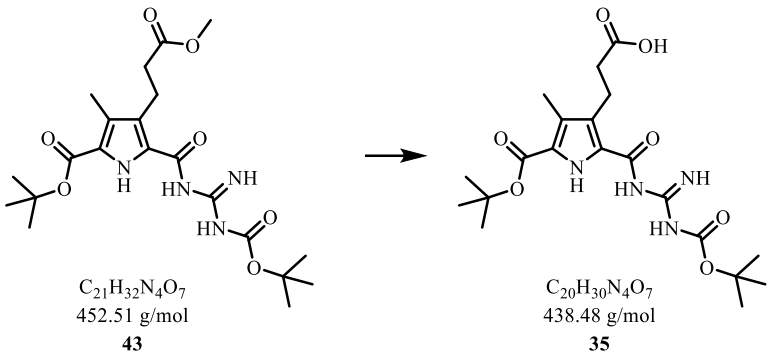

Figure 132: Deprotection of the GCP building block 35.

To a solution of the protected GCP building block **43** (0.7 g, 1.55 mmol, 1 eq) in tetrahydrofuran (50 mL) was LiOH Monohydrat (0.151 g, 6.19 mmol, 4 eq) in water (20 ml) added and stirred for six hours at 0 °C. The solvent tetrahydrofuran was removed in vacuum and the residue was diluted with water (20 mL). The solution was acidified with 5% HCl aq. and directly extracted with ethylacetate (3 x 30 mL). All organic layers were collected, washed with brine (3 x 10 mL) and dried with $MgSO_4$. The product **35** (0.612 g, 1.39 mmol, 90%) was obtained as a white powder.[92]

Sum formula: $C_{20}H_{30}N_4O_7$

Molar mass: 438.48 g/mol

R_f: 0.25 (SiO_2, cyclohexane:ethylacetate = 4:1)

^{1}H-NMR: (400 MHz, DMSO-*d6*) δ [ppm] = 1.35 (s, 9 H, C-(C*H*$_3$)$_3$), 1.45 (s, 9 H, C-(C*H*$_3$)$_3$), 2.10 (s, 3 H, C*H*$_3$), 2.21 (t, J^3 = 7.73 Hz, 2 H, C*H*$_2$), 2.98 (t, J^3 = 7.21 Hz, 2 H, C*H*$_2$), 8.74 (s, 1 H, N*H*), 9.47 (s, 1 H, N*H*), 10.38 (s, 1 H, N*H*), 11.21 (s, 1 H, O*H*), 11.36 (s, 1 H, N*H*).

^{13}C-NMR: (100 MHz, DMSO-*d6*) δ [ppm] = 8.98, 17.45, 27.45, 28.41, 34.58, 80.13, 80.90, 122.38, 125.47, 125.83, 130.22, 156.44, 158.72, 160.20, 160.54, 174.91.

FT-IR: (ATR): $\tilde{\nu}$ [cm^{-1}] = 3371, 3310, 2979, 2931, 1707, 1634, 1274, 1133, 840, 779, 592.

Melting point: 188 °C

7.2.8 Synthesis of the GCP-BINAM Motif 44

Described experiment: JO-064. Repeated: JO-065, JO-073, JO-075.

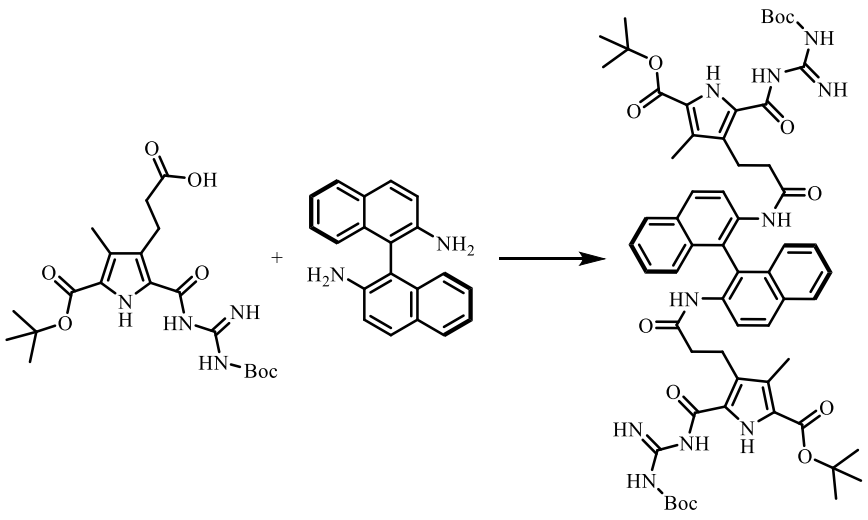

Figure 133: Synthesis of the GCP-BINAM motif 46.

A dry schlenk tube was filled with a solution of the deprotected GCP building block **35** (0.10 g, 0.228 mmol, 2.5 eq) in dry dichloromethane (20 mL). *N*,*N*-Dimethylformamid (0.5 mL) was added and the solution was cooled down to 0 °C. At this temperature oxalyl chloride (23.5 µL, 34.7 mg, 0.273 mmol, 3 eq) was slowly added to give a red solution. The solution was stirred for three hours while it was brought to room temperature.

Subsequently the solvent was removed in vacuum to give a light red foam which was dissolved in dry tetrahydrofuran (20 mL). This solution was added to a solution of *(S)*-1,1'-binaphthalene-2,2'-diamine (25.98 mg, 0.09 mmol, 1 eq) and Diisopropylamine (76.6 µL, 55.4 mg, 0.547 mmol, 6 eq) in tetrahydrofuran (20 mL) at room temperature and was stirred for 16 hours until a yellow suspension was build.

The solvent was removed in vacuum and the residue was solved in dichloromethane (20 mL). The organic layer was washed with water (3 x 10 mL) and brine (3 x 10 mL) and dried over $MgSO_4$. The product was purified via column chromatography (ø = 3 cm, h = 30 cm, cyclohexane:ethylacetate = 2:1) to give the pure product *(S)*-**46** (51.2 mg, 0.0455 mmol, 50%) as a white solid.

Sum formula: $C_{60}H_{72}N_{10}O_{12}$

Molar mass: 1125.273 g/mol

R_f: 0.34 (cyclohexane:ethylacetate = 2:1)

^{1}H-NMR: (400 MHz, $CDCl_3$) δ [ppm] = 1.52 (s, 18 H, 2 x C-(CH_3)$_3$), 1.57 (s, 18 H, 2 x C-(CH_3)$_3$), 2.03 - 2.04 (m, 6 H, 2 x CH_3), 2.19 - 2.27 (m, 4 H*H*), 2.64 - 2.71 (m, 4 H, 2 x CH_2), 7.10 (d, J^3 = 8.54 Hz, 2 H, 2 x BINOL-*H*), 7.27 - 7.30 (m, 2 H, 2 x BINOL-*H*), 7.39 - 7.46 (m, 2 H, 2 x BINOL-*H*), 7.91 (d, J^3 = 8.09 Hz, 2 H, 2 x BINOL-*H*), 7.98 (d, J^3 = 9.00 Hz, 2 H, 2 x BINOL-*H*), 8.36 (d, J^3 = 8.85 Hz, 2 H, 2 x BINOL-*H*).

^{13}C-NMR: (151 MHz, $CDCl_3$) δ [ppm] = 9.66, 21.36, 27.95, 28.39, 38.42, 81.25, 83.23, 121.49, 121.86, 122.47, 125.17, 125.56, 125.93, 127.18, 127.74, 127.94, 128.28, 129.47, 131.32, 132.26, 134.87, 153.03, 158.03, 160.35, 171.27, 172.88.

HR-MS: (ESI): m/z = 1125.5397 ($[M+H]^+$), calcd. 1125.5404 (for $[C_{60}H_{73}N_{10}O_{12}]^+$).

FT-IR: (ATR): $\tilde{\nu}$ [cm^{-1}] = 3508, 3267, 3062, 2925, 2630, 1845, 1771, 1675, 1621, 1141, 1130, 1141, 1078, 895, 830, 681, 524.

Melting point: 138 °C

7.2.9 Deprotection of the BINAM-GCP-Motive to achieve Compound *(S)*-3

Described experiment: JO-064. Repeated: JO-065, JO-073, JO-075.

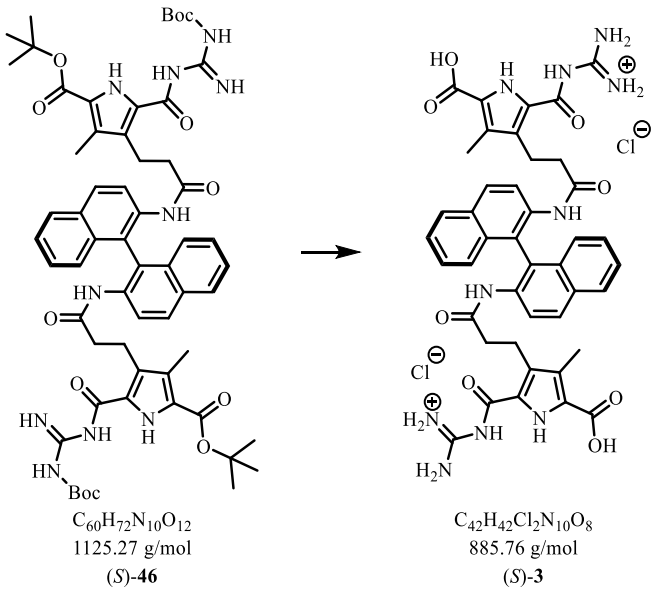

Figure 134: Deprotection of the BINAM-GCP-Motive *(S)*-46.

The *(S)*-BINAM-GCP-motif ***(S)*-46** (100 mg, 0.0889 mmol) was dissolved in dichloromethane (5 mL) and cooled down to 0 °C. Trifluoroacetic acid (2.5 mL) was added slowly and the mixture was allowed to thaw to room temperature within one hour. The mixture was stirred at room temperature additional four hours and the solvent was removed in vacuum. 10 mL of hydrochloric acid were added and the resulted solution was dried in vacuum. The pure product ***(S)*-3** (63.3 mg, 0.0715 mmol, 80%) was obtained via MPLC (ø = 3 cm, h = 60 cm, RP18, methanol:water = 1:10 to pure methanol) as a white solid.

Sum formula: $C_{42}H_{42}N_{10}O_8$

Molar mass: 885.76 g/mol

R_f: 0.08 (cyclohexane:ethylacetate = 1:1)

^{1}H-NMR: (300 MHz, DMSO-*d6*) δ [ppm] = 1.89 - 1.94 (m, 6 H, 2 x CH_3), 2.15 - 2.17 (m, 4 H, 2 x CH_2), 2.35 - 2.43 (m, 4 H, 2 x CH_2), 7.03 (d, J^3 = 9.07 Hz, 2 H, 2 x BINOL-*H*), 7.29 (d, J^3 = 7.82 Hz, 1 H, 2 x BINOL-*H*), 7.49 (t, J^3 = 6.57 Hz, 2 H, 2 x BINOL-*H*), 7.82 (d, J^3 = 9.38 Hz, 2 H, 2 x BINOL-*H*), 8.03 (d, J^3 = 8.44 Hz, 1 H, 2 x BINOL-*H*), 8.09 (d, J^3 = 9.07 Hz, 2 H, 2 x BINOL-*H*), 8.24 - 8.33 (m, 4 H, 2 x NH_2), 11.02 (br s, 1 H, N*H*), 11.85 (br s, 1 H, N*H*), 13.18 (br s, 1 H, N*H*).

^{13}C-NMR: (151 MHz, DMSO-*d6*) δ [ppm] = 13.92, 22.09, 28.70, 120.40, 122.79, 123.48, 124.35, 12468, 125.21, 126.50, 127.09, 127.70, 130.02, 130.35, 133.01, 134.24, 136.72, 154.31, 158.60, 161.66, 166.83.

HR-MS: (ESI): m/z = 813.3115 ([M+H^+-2HCl]$^+$), calcd. 813.3103 (for [$C_{42}H_{41}N_{10}O_8$]$^+$).

FT-IR: (ATR): ṽ [cm^{-1}] 3531, 3054, 2867, 2627, 1773, 1691, 1660, 1650, 1120,1066, 1074,1070, 815, 777.

Elemental analysis: calcd. (%) for $C_{42}H_{42}Cl_2N_{10}O_8$: C 56.95, H 4.78, N 15.81; found: C 52.80, H 3.91, N 11.20.

Melting point: 166 °C

7.2.10 Synthesis of the ACP Binding Motive 47

Described experiment: JO-044. Repeated: JO-056, JO-062, JO-077.

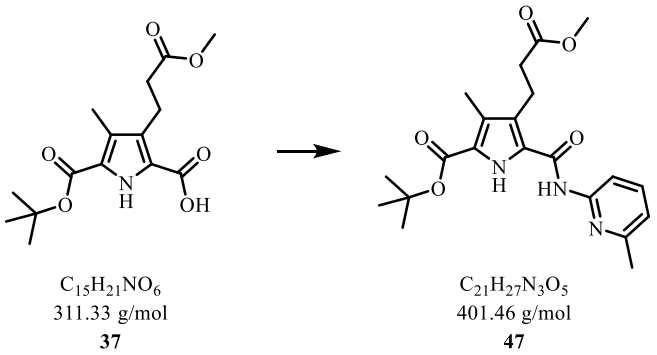

Figure 135: Synthesis of the ACP binding motif 47.

The synthesis of building block **37** was carried out as described in the literature.[92] The building block **37** (1.00 g, 3.21 mmol, 1 eq), HCTU (1.59 g, 3.85 mmol, 1.2 eq) and DMAP (1.17 g, 9.63 mmol, 3 eq) were dissolved in dichloromethane (50 mL) and dimethylformamide (2 mL). After stirring for 30 minutes to build the active ester, 6-methylpyridin-2-amine (0.521 g, 4.81 mmol, 1.5 eq) was added and the mixture was stirred another 16 hours at room temperature. The mixture was separated from all solvent in vacuum and resolved in dichloromethane (20 mL). After washing with water (3 x 10 mL) and brine (3 x 10 mL) the product was purified via column chromatography (ø = 5 cm, h = 40 cm, cyclohexane:ethylacetate = 5:1). The product **47** (0.630 g, 1.57 mmol, 49%) was obtained as a white solid.

Sum formula: $C_{21}H_{27}N_3O_5$

Molar mass: 401.46 g/mol

R_f: 0.61 (cyclohexane:ethylacetate = 5:1)

^{1}H-NMR: (400 MHz, $CDCl_3$) δ [ppm] = 1.55 (s, 9 H, (C-C*H*$_3$)$_3$), 2.30 (s, 3 H, CH_3), 2.47 (s, 3 H, CH_3), 2.73 (t, J^3 = 6.94 Hz, 2 H, CH_2), 3.09 (t, J^3 = 7.02 Hz, 2 H, C*H*$_2$), 3.70 (s, 3 H, C*H*$_3$), 6.91 (d, J^3 = 7.48 Hz, 1 H, pyr-C*H*), 7.63 (t, J^3 = 7.86 Hz,

1 H, pyr-C*H*), 8.10 (d, J^3 = 8.24 Hz, 1 H, pyr-C*H*), 10.04 (s, 1 H, N*H*), 10.21 (br s, 1 H, N*H*).

^{13}C-NMR: (151 MHz, $CDCl_3$) δ [ppm] = 10.36, 20.26, 23.76, 28.48, 33.91, 52.11, 81.75, 112.07, 119.26, 123.36, 124.83, 125.82, 126.49, 139.36, 151.17, 156.13, 159.90, 160.33, 174.16.

HR-MS: (ESI): m/z = 402.2036 ($[M+H]^+$), calcd. 402.2023 (for $[C_{21}H_{28}N_3O_5]^+$).

FT-IR: (ATR): $\tilde{\nu}$ [cm^{-1}] = 3332, 3301, 2923, 1695, 1664, 1604, 1569, 1542, 1438, 1365, 1336, 1303, 1278, 1249, 1213, 1155, 1135, 1078, 983, 842, 779, 709, 609.

Melting Point: 101 °C

7.2.11 Deprotection of the ACP Building Block to achieve Compound 48

Described experiment: JO-044. Repeated: JO-056, JO-062, JO-077.

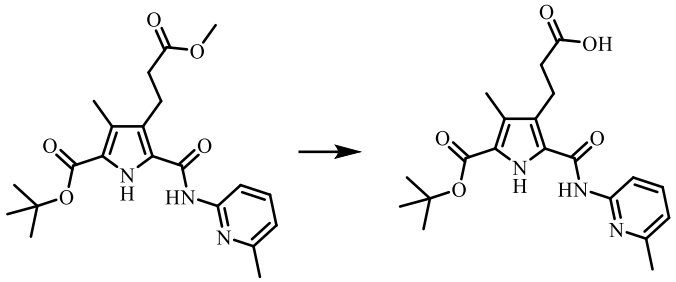

Figure 136: Deprotection of the ACP building block 47.

To a solution of the protected ACP building block **47** (1.00 g, 2.49 mmol, 1 eq) in tetrahydrofuran (50 mL) was $LiOH \cdot H_2O$ (0.418 g, 9.96 mmol, 4 eq) in water (20 ml) added and stirred for 1 hour at 0 °C and additionally 8 hours at room temperature. The mixture was diluted with water (10 mL) and washed with diethylether (3 x 30 mL). The solution was acidified by 0.5 M $NaHSO_4$ (10 mL) and directly extracted with ethylacetate (3 x 30 mL). All organic layers were collected, washed with brine (3 x 30 mL) and dried with $MgSO_4$. The product **48** (0.860 g, 2.22 mmol, 89%) was obtained as a white powder.

Sum formula: $C_{20}H_{25}N_3O_5$

Molar mass: 387.44 g/mol

R_f: 0.22 (cyclohexane:ethylacetate = 3:1)

^{1}H-NMR: (400 MHz, DMSO-d_6) δ [ppm] = 1.55 (s, 9 H, C-(C*H*$_3$)$_3$), 2.20 (s, 3 H, C*H*$_3$), 2.40 (t, J^3 = 7.63 Hz, 2 H, C*H*$_2$), 2.43 (s, 3 H, C*H*$_3$), 2.97 (t, J^3 = 7.78 Hz, 2 H, C*H*$_2$), 6.98 (d, J^3 = 7.32 Hz, 1 H, pyr-C*H*), 7.66 (t, J^3 = 7.86 Hz, 1 H, pyr-C*H*), 8.01 (d, J^3 = 8.39 Hz, 1 H, pyr-C*H*), 10.71 (s, 1 H, N*H*), 12.04 (br s, 1 H, O*H*), 12.07 (s, 1 H, N*H*).

^{13}C-NMR: (151 MHz, DMSO-d_6) δ [ppm] = 9.78, 20.20, 23.60, 28.06, 34.34, 80.76, 111.30, 118.74, 122.08, 123.74, 124.93, 130.27, 138.38, 151.56, 156.49, 158.88, 160.41, 174.22.

HR-MS: (ESI): m/z = 410.1680 ($[M+Na]^+$), calcd. 410.1686 (for $[C_{20}H_{25}N_3O_5Na]^+$).

FT-IR: (ATR): $\tilde{\nu}$ [cm^{-1}] = 3311, 2919, 1704, 1670, 1612, 1571, 1450, 1367, 1319, 1272, 1218, 1159, 1128, 1089, 1000, 923, 890, 844, 800, 779,730, 659, 628, 611.

Melting point: 195 °C

7.2.12 Synthesis of the BINAM-ACP Motive *(S)*-49

Described experiment: JO-070. Repeated: JO-078, JO-116.

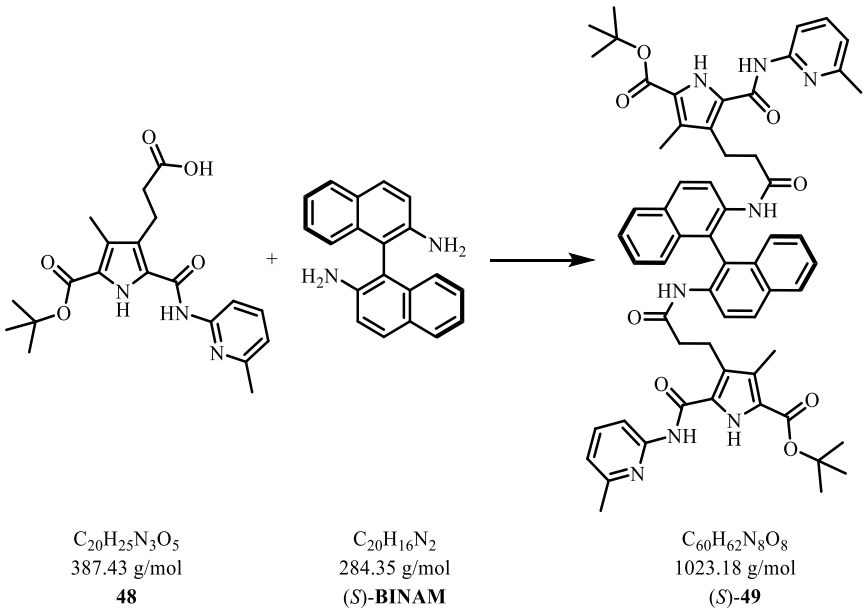

Figure 137: Synthesis of BINAM-ACP Motive *(S)*-49.

A dry schlenk tube was filled with a solution of the deprotected ACP building block **48** (0.1 g, 0.258 mmol, 3 eq) in dry dichloromethane (20 mL). *N*,*N*-Dimethylformamid (0.5 mL) was added and the solution was cooled down to 0 °C. At this temperature oxalyl chloride (22.1 µL, 32.7 mg, 0.258 mmol, 3 eq) was slowly added to give a red solution. The solution was stirred for three hours while it was brought to room temperature.

Subsequently the solvent was removed in vacuum to give a light red foam which was dissolved in dry tetrahydrofuran (20 mL). This solution was added to a solution of *(S)*-1,1'-binaphthalene-2,2'-diamine (24.5 mg, 0.09 mmol, 1 eq) and diisopropylamine (72.3 µL, 52.2 mg, 0.522 mmol, 6 eq) in tetrahydrofuran (20 mL) at room temperature and was stirred for 16 hours until a yellow suspension was build.

The solvent was removed in vacuum and the residue was solved in dichloromethane (20 mL). The organic layer was washed with water (3 x 15 mL) and brine (3 x 15 mL) and dried over $MgSO_4$. The product *(S)*-**49** was purified via column chromatography (ø = 3 cm, h = 30 cm, cyclohexane:ethylacetate = 2:1) to give the pure product (59.2 mg, 58.0 mmol, 67%) as a white solid.

Sum formula: $C_{60}H_{62}N_8O_8$

Molar mass: 1023.18 g/mol

R_f: 0.25 (cyclohexane:ethylacetate = 2:1)

^{1}H-NMR: (300 MHz, DMSO-d_6) δ [ppm] = 1.55 (s, 18 H, 2 x C-(C*H*$_3$)$_3$), 2.00 (s, 6 H, 2 x C*H*$_3$), 2.14 - 2.27 (m, 4 H, 2 x C*H*$_2$), 2.43 (s, 6 H, 2 x C*H*$_3$), 2.65 - 2.84 (m, 4 H, 2 x C*H*$_2$), 6.98 (d, J^3 = 7.50 Hz, 2 H, 2 x pyr-C*H*), 7.04 (d, J^3 = 8.76 Hz, 2 H, 2 x pyr-C*H*), 7.19 (d, J^3 = 8.76 Hz, 2 H, 2 x BINOL-*H*), 7.27 (br t, J^3 = 7.35 Hz, 2 H, 2 x pyr-C*H*), 7.43 (t, J^3 = 7.50 Hz, 2 H, 2 x BINOL-*H*), 7.67 (t, J^3 = 7.82 Hz, 2 H, 2 x BINOL-*H*), 7.91 (d, J^3 = 8.13 Hz, 2 H, 2 x BINOL-*H*), 7.98 (d, J^3 = 9.38 Hz, 2 H, 2 x BINOL-*H*), 8.16 (d, J^3 = 8.44 Hz, 2 H, 2 x BINOL-*H*), 8.23 (br s, 2 H, 2 x N*H*), 10.63 (br s, 2 H, 2 x N*H*), 11.97 (br s, 2 H, 2 x N*H*).

^{13}C-NMR: (75 MHz, DMSO-d_6) δ [ppm] = 10.22, 20.78, 22.96, 31.69, 35.21, 87.27, 108.34, 120.46, 122.79, 125.20, 126.81, 127.12, 127.93, 129.11, 130.55, 131.08, 131.87, 132.64, 133.66, 135.89, 137.12, 138.21, 142.10, 156.50, 157.87, 158.72, 161.09, 181.47.

HR-MS: (ESI): m/z = 1023.4752 ($[M+H]^+$), calcd. 1023.4763 (for $[C_{60}H_{63}N_8O_8]^+$).

FT-IR: (ATR): $\tilde{\nu}$ [cm^{-1}] = 3452, 3446, 3087, 2866, 2642, 1778 1649, 1646, 1200, 1071, 1057, 868, 795, 624, 531.

Melting point: 210 °C

7.2.13 Deprotection of the BINAM-ACP Motif to achieve Compound *(S)*-4

Described experiment: JO-070. Repeated: JO-078, JO-116.

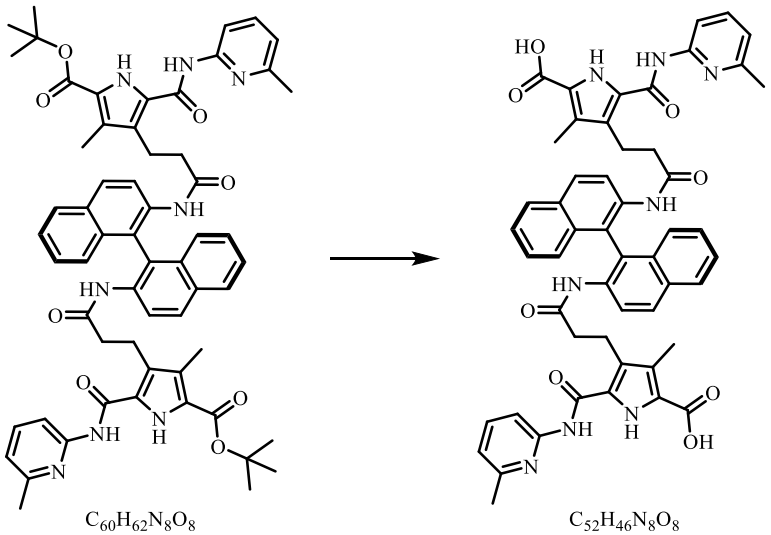

Figure 138: Deprotection of the BINAM-ACP Motive *(S)*-49.

The Boc deprotection of the *(S)*-BINAM GCP motif *(S)*-**49** was carried out with the *(S)*-BINAM GCP motif (100 mg, 0.0977 mmol) solved in dichloromethane (5 mL) with ice cooling to 0 °C. TFA (1 mL) was added and the mixture was stirred for one hour while the temperature was brought to room temperature. Subsequently the mixture was stirred additional four hours. The completion of the reaction was proofed via TLC. The solvent was removed in vacuum and the residue was resolved in 1 M hydrochloric acid (10 mL). The resulted solution was dried in vacuum and the crude product was purified via MPLC (ø = 3 cm, h = 60 cm, RP18, methanol:water = 1:10 to pure methanol). The pure product *(S)*-**4** (79.0 mg, 0.0867 mmol, 89%) was obtained as a white solid.

Sum formula: $C_{52}H_{46}N_8O_8$

Molar mass: 910.97 g/mol

R_f: 0.11 (cyclohexane:ethylacetate = 2:1)

^{1}H-NMR: (300 MHz, DMSO-d_6) δ [ppm] = 1.95 (s, 6 H, 2 x CH_3), 2.09 - 2.13 (m, 4 H, 2 x CH_2), 2.41 (s, 6 H, 2 x CH_3), 2.53 - 2.66 (m, 4 H, 2 x CH_2), 6.90 (d, J^3 = 9.07 Hz, 2 H, 2 x pyr-C*H*), 6.96 (d, J^3 = 7.19 Hz, 2 H, 2 x BINOL-*H*), 7.23 (t, J^3 = 8.13, 2 H, 2 x pyr-C*H*), 7.41 (t, J^3 = 8.13, 2 H, 2 x BINOL-*H*), 7.63 (t, J^3 = 8.13, 2 H, 2 x BINOL-*H*), 7.81 (d, J^3 = 9.07 Hz, 2 H, 2 x pyr-C*H*), 7.87 (d, J^3 = 8.13 Hz, 2 H, 2 x BINOL-*H*), 7.95 (d, J^3 = 8.76 Hz, 2 H, 2 x BINOL-*H*), 8.01 (d, J^3 = 8.76 Hz, 2 H, 2 x BINOL-*H*), 8.78 (br s, 2 H, 2 x N*H*), 10.66 (br s, 2 H, 2 x O*H*), 12.09 (br s, 2 H, 2 x N*H*).

^{13}C-NMR: (75 MHz, DMSO-d_6) δ [ppm] = 10.31, 21.95, 22.52, 37.22, 89.53, 111.21, 123.18, 124.14, 125.60, 126.26, 126.85, 127.39, 127.85, 128.83, 129.39, 131.82, 133.23, 135.08, 137.57, 139.66, 141.13, 154.64, 157.24, 159.52, 162.39, 182.46.

HR-MS: (ESI): m/z = 933.3354 ($[M+Na]^+$), calcd. 933.3331 (for $[C_{52}H_{46}N_8O_8Na]^+$).

FT-IR: (ATR): $\tilde{\nu}$ [cm^{-1}] = 3551, 3522, 3023, 2866, 2474, 1729, 1645, 1635, 1604, 1085, 1052, 1050, 896, 757, 676, 648.

Elemental analysis: calcd. (%) for $C_{52}H_{46}N_8O_8$: C 68.56, H 5.09, N 12.30; found: C 68.40, H 4.77, N 8.55.

Melting point: Decomposition at 265 °C

7.2.14 Synthesis of BINAM-Glutamic Acid *(S)*-51

Described experiment: JO-080. Repeated: JO-087, JO-094.

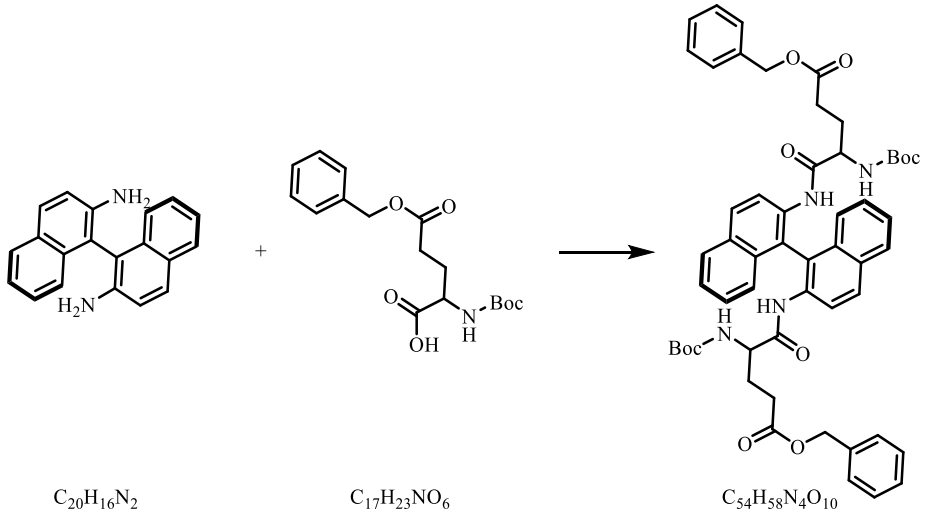

$C_{20}H_{16}N_2$
284.35 g/mol
(*S*)-**BINAM**

$C_{17}H_{23}NO_6$
337.37 g/mol
50

$C_{54}H_{58}N_4O_{10}$
923.06 g/mol
(*S*)-**51**

Figure 139: Synthesis of BINAM-Glutamic acid *(S)*-51.

The protected glutamic acid **50** (7.11 g, 21.1 mmol, 3 eq), HCTU (8.71 g, 21.1 mmol, 3 eq) and DMAP (4.30 g, 35.1 mmol, 5 eq) were dissolved in dichloromethane (100 mL) and dimethylformamide (1 mL) and stirred for one hour to build the active ester. Subsequently *(S)*-BINAM (2.00 g, 7.02 mmol, 1 eq) was added and stirred for 16 hours at room temperature. The solvent was evaporated in vacuum and the residue was resolved in ethylacetate. The organic layer was washed with water (3 x 50 mL) and brine (3 x 50 mL) and dried over $MgSO_4$. The solvent was evaporated and the crude product purified via column chromatography (ø = 6 cm, h = 50 cm, cyclohexane:ethylacetate = 5:1) to obtain the product *(S)*-**51** (4.35 g, 4.71 mmol, 67%) as a white foam.

Sum formula: $C_{54}H_{58}N_4O_{10}$

Molar mass: 923.059 g/mol

R_f: 0.52 (cyclohexane:ethylacetate = 5:1)

^{1}H-NMR: (300 MHz, DMSO-d_6) δ [ppm] = 1.27 - 1.37 (m, 22 H, 2 x C-(CH_3)$_3$ + 2 x CH_2), 1.85 - 1.92 (m, 4 H, 2 x CH_2), 3.76 - 3.84 (m, 2 H, 2 x C*H*), 5.01 (s, 4 H, 2 x CH_2), 6.75 (d, J^3 = 7.82 Hz, 2 H, 2 x BINOL-*H*), 6.85 (d, J^3 = 8.44 Hz, 2 H, 2 x BINOL-*H*), 7.20 (d, J^3 = 7.50 Hz, 2 H, 2 x BINOL-*H*), 7.32 - 7.38 (m, 12 H, 2 x BINOL-*H* + 2 x C$_6H_5$), 7.89 (d, 7.82 Hz, 2 H, 2 x BINOL-*H*), 7.92 (br s, 2 H, 2 x N*H*), 7.99 (d, J^3 = 9.07 Hz, 2 H, 2 x BINOL-*H*), 8.90 (br s, 2 H, 2 x N*H*).

^{13}C-NMR: (75 MHz, DMSO-d_6) δ [ppm] = 17.77, 30.25, 34.28, 54.78, 64.13, 81.50, 120.52, 122.49, 124.98, 125.80, 127.16, 128.86, 129.23, 132.30, 133.54, 136.88, 138.86, 140.67, 142.48, 149.31, 160.71, 176.00, 180.93.

HR-MS: (ESI): m/z = 923.4187 ([M+H]$^+$), calcd. 923.4226 (for [$C_{54}H_{59}N_4O_{10}$]$^+$).

FT-IR: (ATR): $\tilde{\nu}$ [cm^{-1}] = 2979, 1675, 1596, 1496, 1452, 1365, 1247, 1160, 1052, 865, 811, 746, 696.

Melting point: 67 °C

7.2.15 Deprotection of BINAM-Glutamic Acid to achieve Compound *(S)*-52

Described experiment: JO-080. Repeated: JO-095, JO-097, JO-104.

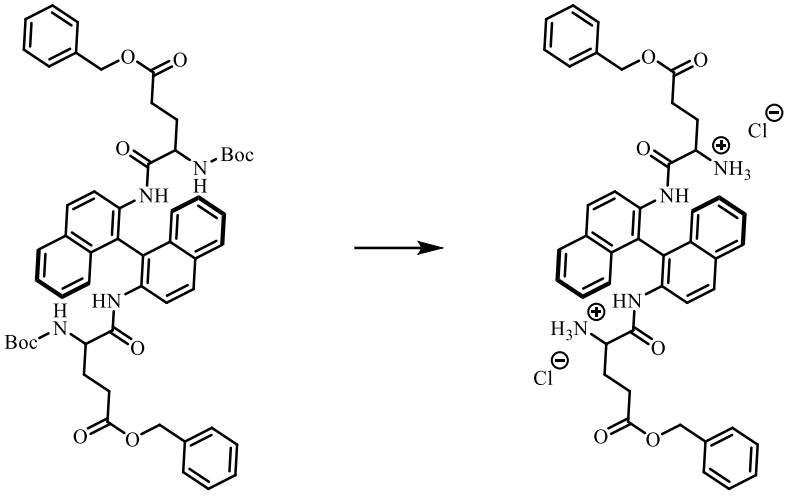

$C_{54}H_{58}N_4O_{10}$
923.08 g/mol
(*S*)-**51**

$C_{44}H_{44}Cl_2N_4O_6$
795.76 g/mol
(*S*)-**52**

Figure 140: Deprotection of BINAM-Glutamic acid *(S)*-51.

The *(S)*-BINAM glutamic acid *(S)*-**51** (200 mg, 0.217 mmol) was dissolved in dichloromethane (6 mL) and TFA (3 mL) was added to initiate the deprotection. The mixture was stirred for three hours at room temperature and the reaction progress was monitored with TLC. The solvent was removed in vacuum and the residue was solved in 10 mL 1M aqueous hydrochloric acid, dried and the crude product was purified via MPLC (ø = 2 cm, h = 30 cm, RP18, methanol:water = 1:10 to pure methanol). The deprotected product *(S)*-**52** (145 mg, 0.182 mmol, 84%) was obtained as a white solid.

Sum formula: $C_{44}H_{44}Cl_2N_2O_6$

Molar mass: 795.76 g/mol

R_f: 0.05 (cyclohexane:ethylacetate = 4:1)

^{1}H-NMR: (300 MHz, DMSO-d_6) δ [ppm] = 1.25 - 1.32 (m, 4 H, 2 x CH_2), 1.42 - 1.70 (m, 4 H, 2 x CH_2), 3.77 - 3.82 (m, 2 H, 2 x C*H*), 5.05 (s, 4 H, 2 x CH_2), 6.94 (d, J^3

= 8.44 Hz, 2 H, 2 x BINOL-*H*), 7.19 (t, J^3 = 7.19 Hz, 2 H, 2 x BINOL-*H*), 7.31 - 7.48 (m, 12 H, 2 x BINOL-*H* + 2 x C_6H_5), 7.68 (d, J^3 = 9.07 Hz, 2 H, 2 x BINOL-*H*), 7.86 (d, J^3 = 8.13 Hz, 2 H, 2 x BINOL-*H*), 7.96 (d, J^3 = 9.07 Hz, 2 H, 2 x BINOL-*H*), 8.14 (br s, 4 H, 2 x NH_2), 9.63 (s, 2 H, 2 x N*H*).

^{13}C-NMR: (75 MHz, DMSO-d_6) δ [ppm] = 18.49, 36.74, 56.26, 66.66, 120.14, 121.60, 122.71, 123.18, 125.59, 126.73, 128.16, 132.36, 133.96, 135.43, 137.88, 140.49, 142.40, 145.93, 165.78, 169.28.

HR-MS: (ESI): m/z = 723.3168 ($[M+H^+-2HCl]^+$), calcd. 723.3177 (for $[C_{44}H_{43}N_4O_6]^+$).

FT-IR: (ATR): $\tilde{\nu}$ [cm^{-1}] = 2983, 1775, 1664, 1597, 1489, 1484, synthe1451, 1356, 1277, 1155, 1048, 852, 801, 702, 680.

Melting point: 98 °C

7.2.16 Synthesis of the BINAM-Glutamic Acid-ACP Motif *(S)*-53

Described experiment: JO-101. Repeated: JO-105, JO-129.

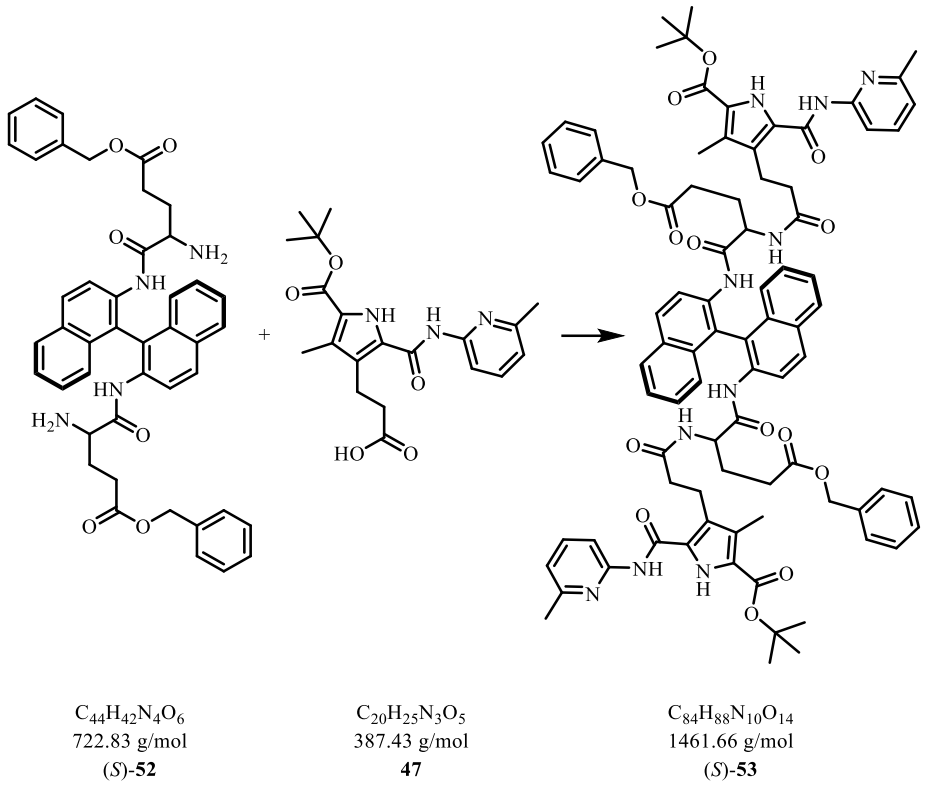

$C_{44}H_{42}N_4O_6$
722.83 g/mol
(*S*)-**52**

$C_{20}H_{25}N_3O_5$
387.43 g/mol
47

$C_{84}H_{88}N_{10}O_{14}$
1461.66 g/mol
(*S*)-**53**

Figure 141: Synthesis of the BINAM-Glutamic acid-ACP Motive *(S)*-53.

A dry schlenk tube was filled with a solution of the deprotected ACP building block **48** (100 mg, 0.258 mmol, 3 eq) in dry dichloromethane (20 mL). *N*,*N*-Dimethylformamid (0.5 mL) was added and the solution was cooled down to 0 °C. At this temperature oxalyl chloride (22.1 µL, 32.7 mg, 0.258 mmol, 3 eq) was slowly added to give a yellow solution. The solution was stirred for 16 hours while it was brought to room temperature.

Subsequently the solvent was removed in vacuum to give a yellow foam which was dissolved in dry tetrahydrofuran (20 mL). This solution was added to a solution of the deprotected *(S)*-BINAM glutamic acid ***(S)*-52** (62.2 mg, 0.0860 mmol, 1 eq) and diisopropylamine (72.3 µL, 52.2 mg, 0.522 mmol, 6 eq) in tetrahydrofuran (20 mL) at room temperature and was stirred for 16 hours until a suspension was built. The solvent was removed in vacuum and the residue was solved in dichloromethane (20 mL). The organic layer was washed with water (3 x 15 mL) and brine (3 x 15 mL) and dried over $MgSO_4$. The product ***(S)*-53** was purified via column chromatography (ø = 3 cm, h = 30 cm, cyclohexane:ethylacetate = 4:1) to give the pure product (102 mg, 0.0698 mmol, 81%) as a white solid.

Sum formula: $C_{84}H_{86}N_8O_{16}$

Molar mass: 1461.656 g/mol

R_f: 0.46 (cyclohexane:ethylacetate = 2:1)

^{1}H-NMR: (300 MHz, $CDCl_3$) δ [ppm] = 1.56 (s, 18 H, 2 x C-(CH_3)$_3$), 2.24 (s, 6 H, 2 x CH_3), 2.52 (s, 6 H, 2 x CH_3), 2.67 - 2.78, (m, 8 H, 4 x CH_2), 3.15 (t, J^3 = 7.82 Hz, 4 H, 2 x CH_2), 3.27 (t, J^3 = 6.88 Hz, 4 H, 2 x CH_2), 3.80 - 3.81 (m, 2 H, 2 x C*H*), 5.08 (s, 4 H, 2 x CH_2), 6.86 (d, J^3 = 7.50 Hz, 2 H, 2 x pyr-C*H*), 6.96 (d, J^3 = 2.81 Hz, 2 H, 2 x pyr-C*H*), 7.07 (d, J^3 = 3.75 Hz, 2 H, 2 x BINOL-*H*), 7.27 - 7.30 (m, 14 H, 2 x BINOL-*H* + 2 x C_6H_5 + 2 x pyr-C*H*), 7.43 (d, J^3 = 3.44 Hz, 2 H, 2 x BINOL-*H*), 7.53 (t, J^3 = 6.25 Hz, 2 H, 2 x BINOL-*H*), 7.69 (d, J^3 = 3.31, 2 H, 2 x BINOL-*H*), 8.07 (d, J^3 = 8.13 Hz, 2 H, 2 x BINOL-*H*).

^{13}C-NMR: (75 MHz, $CDCl_3$) δ [ppm] = 26.17, 27.22, 30.27, 30.83, 31.30, 36.83, 43.08, 62.71, 66.86, 70.71, 94.61, 104.86, 109.78, 112.74, 113.77, 119.43, 121.32, 123.83, 127.02, 131.00, 131.76, 132.71, 134.66, 136.99, 138.00, 138.71, 140.68, 141.70, 142.07, 142.76, 147.22, 149.76, 152.53, 156.05, 157.10, 167.84, 171.36, 174.06.

HR-MS: (ESI): m/z = 1461.6493 ($[M+H]^+$), calcd. 1461.6554 (for $[C_{84}H_{89}N_{10}O_{14}]^+$).

FT-IR: **(**ATR): $\tilde{\nu}$ [cm^{-1}] = 3437, 3266, 3058, 2925, 2710, 1798, 1675, 1666, 1634, 1158, 1058, 1030, 1012, 821, 801, 765, 653, 641.

Melting point: Decomposition at 254 °C

7.2.17 Deprotection of the BINAM-Glutamic acid-ACP Motive to achieve Compound *(S)*-49

Described experiment: JO-129. Repeated: JO-138.

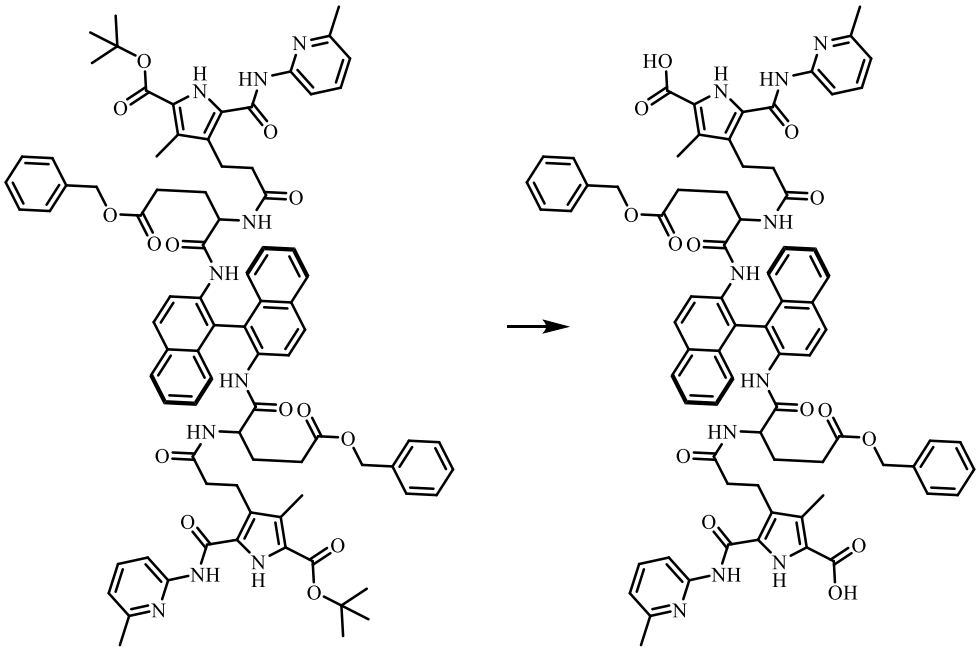

Figure 142: Deprotection of the BINAM-Glutamic acid-ACP Motive *(S)*-53.

The *(S)*-BINAM glutamic acid ACP motif *(S)*-**53** (100 mg, 0.0684 mmol) was dissolved in dichloromethane (5 mL) and TFA (1 mL) was added to initiate the deprotection. The mixture was stirred for 16 hours and the reaction progress was monitored with TLC. The solvent was removed in vacuum, resolved in 10 mL 1 M hydrochloric acid, dried in vacuum and the crude product was purified via MPLC (ø = 2 cm, h = 30 cm, RP18, methanol:water = 1:10 to pure methanol). The deprotected product *(S)*-**5** (88.5 mg, 0.0656 mmol, 96%) was obtained as a white solid.

Sum formula: $C_{76}H_{72}N_{10}O_{14}$

Molar mass: 1349.443 g/mol

R_f: 0.21 (cyclohexane:ethylacetate = 4:1)

^{1}H-NMR: (300 MHz, $CDCl_3$) δ [ppm] = 2.04 (s, 6 H, 2 x C*H*$_3$), 2.27, (s, 4 H, 2 x C*H*$_2$), 2.30 - 2.33 (m, 4 H, 2 x C*H*$_2$), 2.36 - 2.38 (m, 4 H, 2 x C*H*$_2$), 2.69 - 2.71 (m, 4 H, 2 x C*H*$_2$), 2.85 - 2.88 (m, 4 H, 2 x C*H*$_2$), 4.27 - 4.29 (m, 2 H, 2 x C*H*), 4.97 (s, 4 H, 2 x C*H*$_2$), 6.98 (d, J^3 = 3.13 Hz, 2 H, pyr-C*H*), 7.12 (d, J^3 = 2.81 Hz, 2 H, pyr-C*H*), 7.17 (d, J^3 = 5.63 Hz, 2 H, 2 x BINOL-*H*), 7.32 (m, 14 H, , 2 x BINOL-*H* + 2 x C_6H_5 + 2 x pyr-C*H*), 7.45 (d, J^3 = 4.69 Hz, 2 H, 2 x BINOL-*H*), 7.55 (t, J^3 = 3.13 Hz, 2 H, 2 x BINOL-*H*), 7.66 (d, J^3 = 5.63 Hz, 2 H, 2 x BINOL-*H*), 7.87 (d, J^3 = 3.13 Hz, 2 H, 2 x BINOL-*H*).

^{13}C-NMR: (75 MHz, $CDCl_3$) δ [ppm] = 25.90, 29.44, 29.99, 30.52, 36.56, 42.80, 62.43, 66.58, 72.20, 94.85, 104.59, 109.50, 110.23, 113.50, 119.15, 121.05, 130.15, 130.73, 131.48, 132.43, 134.39, 136.71, 137.72, 138.44, 140.40, 141.43, 141.79, 142.49, 149.48, 150.83, 152.25, 153.98, 156.83, 167.57, 168.84, 173.79.

HR-MS: (ESI): m/z = 1371.5078 ($[M+Na]^+$), calcd. 1371.5122 (for $[C_{76}H_{72}N_{10}O_{14}Na]^+$).

FT-IR: **(**ATR): $\tilde{\nu}$ [cm^{-1}] 3415, 3030, 2901, 2891, 1847, 1672, 1621, 1071, 1100, 922, 859, 821, 794, 633.

Elemental analysis: calcd. (%) for $C_{76}H_{72}N_{10}O_{14}$: C 67.64, H 5.38, N 10.38; found: C 67.2, H 4.60, N 8.76.

Melting point: Decomposition at 219 °C

7.2.18 Bromination of BINAM to achieve Compound *(S)*-55

Described experiment: JO-144. Repeated: JO-156, JO-168.

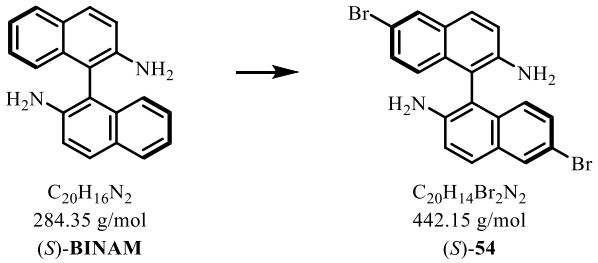

Figure 143: Bromination of *(S)*-BINAM.

The bromination was carried out as described in the literature.[36] *(S)*-BINAM (1.00 g, 3.52 mmol, 1 eq) was dissolved in 1,4-dioxane (100 mL). *N*-bromosuccinimide (1.88 g, 10.6 mmol, 3 eq) was added in portions and stirred at room temperature for five hours to give a black suspension. An 10% aqueous $Na_2S_2O_3$ solution (50 mL) was added to stop the reaction. The mixture was extracted with ethyl acetate (3 x 50 mL) and the combined organic layers were washed with water (3 x 50 mL) and brine (3 x 50 mL) to give a black solution. Activated carbon was added to partially discolour the solution. After filtrating and drying over $MgSO_4$ the solvent was removed in vacuum to give a black residue. The crude product was purified via column chromatography (ø = 6 cm, h = 40 cm, cyclohexane:ethylacetate = 1:4) to give the pure product *(S)*-**54** (431 mg, 0.986 mmol, 28%) as a beige powder.

Sum formula: $C_{20}H_{14}Br_2N_2$

Molar mass: 442.147 g/mol

R_f: 0.45 (cyclohexane:ethylacetate = 1:4)

^{1}H-NMR: (300 MHz, $CDCl_3$) δ [ppm] = 3.65 (br s, 4 H, 2 x N*H*$_2$), 6.79 (d, J^3 = 8.7 Hz, 2 H, 2 x BINOL-*H*),7.27 (d, J^3 = 8.7 Hz, 2 H, 2 x BINOL-*H*), 7.45 (dd, J^3 = 2.1, 8.7 Hz, 2 H, 2 x BINOL-*H*), 7.78 (d, J^3 = 8.7 Hz, 2 H, 2 x BINOL-*H*), 7.91 (d, J^3 = 2.1 Hz, 2 H, 2 x BINOL-*H*).

^{13}C-NMR: (151 MHz, DMSO-d_6) δ [ppm] = 111.87, 116.17, 119.42, 125.59, 128.94, 129.58, 130.13, 130.24, 132.28, 143.04.

HR-MS: (ESI): m/z = 442.9588 ($[M+H]^+$), calcd. 442.9576 (for $[C_{20}H_{15}Br_2N_2]^+$).

Melting point: Decomposition at 201 °C

7.2.19 Synthesis of BINAM-Br-ACP *(S)*-55

Described experiment: JO-203.

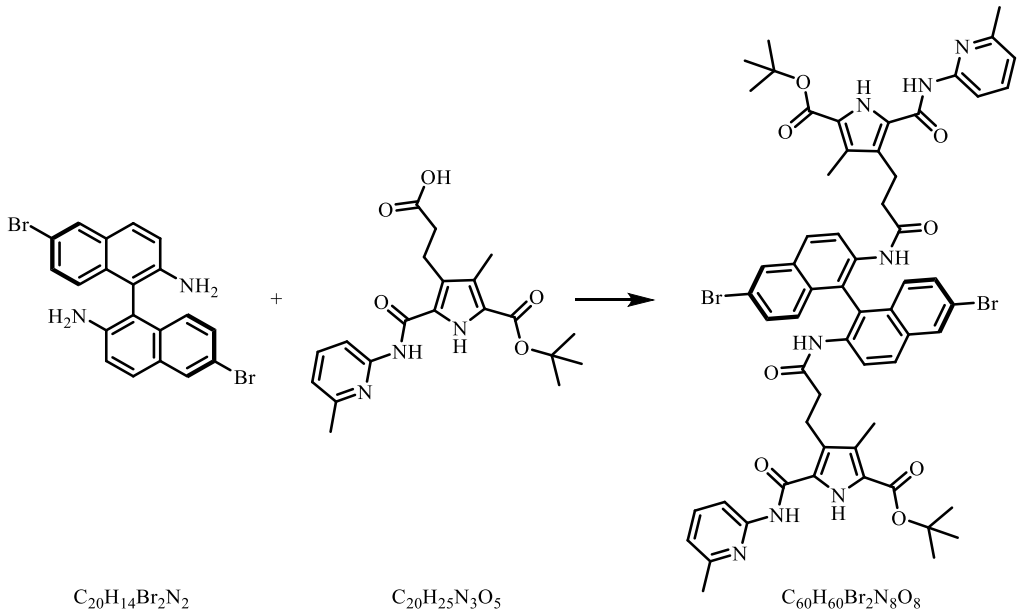

Figure 144: Synthesis of BINAM-Br-ACP *(S)*-55.

A dry schlenk tube was filled with a solution of the deprotected ACP building block **48** (26.0 mg, 0.0671 mmol, 3 eq) in dry dichloromethane (10 mL). *N*,*N*-Dimethylformamid (0.1 mL) was added and the solution was cooled down to 0 °C. At this temperature oxalyl chloride (5.76 µL, 8.52 mg, 0.0671 mmol, 3 eq) was slowly added to give a yellow solution. The solution was stirred for 16 hours while it was brought to room temperature.

Subsequently the solvent was removed in vacuum to give a yellow foam which was dissolved in dry tetrahydrofuran (10 mL). This solution was added to a solution of the brominated *(S)*-BINAM *(S)*-**54** (9.89 mg, 0.0224 mmol, 1 eq) and diisopropylamine (18.8 µL, 13.4 mg, 0.13 mmol, 6 eq) in tetrahydrofuran (20 mL) at room temperature and was stirred for 16 hours until a suspension was built. The solvent was removed in vacuum and the residue was solved in dichloromethane (20 mL). The organic layer was washed with water (3 x 15 mL) and brine (3 x 15 mL) and dried over $MgSO_4$. The product was purified via column chromatography (ø = 3 cm, h = 30 cm, cyclohexane:ethylacetate = 10:1) to give the pure product *(S)*-**55** (13.8 mg, 0.0117 mmol, 52%) as a white solid.

Sum formula: $C_{60}H_{60}Br_2N_8O_8$

Molar mass: 1181.00 g/mol

R_f: 0.56 (cyclohexane:ethylactate = 3:1)

^{1}H-NMR: (300 MHz, DMSO-d_6) δ [ppm] = 1.56 (s, 18 H, 2 x C-(C*H*$_3$)$_3$), 1.98 (s, 6 H, 2 x C*H*$_3$), 2.22 (t, J^3 = 6.88 Hz, 4 H, 2 x C*H*$_2$), 2.41 (s, 6 H, 2 x C*H*$_3$), 2.76 (t, J^3 = 6.57 Hz, 4 H, 2 x C*H*$_2$), 6.66 (d, J^3 = 9.07 Hz, 2 H, 2 x pyr-C*H*), 6.99 (d, J^3 = 8.44 Hz, 2 H, 2 x pyr-C*H*), 7.22 (dd, J^3 = 1.88 Hz, 8.76 Hz, 2 H, 2 x pyr-C*H*), 7.23 (d, J^3 = 8.75 Hz, 2 H, 2 x BINOL-*H*), 7.66 (t, J^3 = 5.94 Hz, 2 H, 2 x BINOL-*H*), 7.74 (d, J^3 = 9.07 Hz, 2 H, 2 x BINOL-*H*), 7.98 (d, J^3 = 1.88 Hz, 2 H, 2 x BINOL-*H*), 8.02 (d, J^3 = 5.94 Hz, 2 H, 2 x BINOL-*H*), 8.20 (br s, 2 H, 2 x N*H*), 10.59 (br s, 2 H, 2 x N*H*), 11.93 (br s, 2 H, 2 x N*H*).

^{13}C-NMR: (151 MHz, $CDCl_3$) δ [ppm] =12.22, 19.27, 23.07, 30.32, 35.18, 88.13, 114.51, 118.57, 120.15, 121.57, 123.27, 123.78, 125.42, 126.83, 127.13, 128.22, 128.68, 129.65, 129.85, 130.73, 132.26, 133.23, 133.92, 135.88, 149.34, 153.48, 162.83, 175.91.

HR-MS: (ESI): m/z = 1181.2826 ($[M+H]^+$), calcd. 1181.2953 (for $[C_{60}H_{61}Br_2N_8O_8]^+$).

FT-IR: **(**ATR): $\tilde{\nu}$ [cm^{-1}] = 3403, 3321, 3061, 2876, 2464, 1843, 1796, 1663, 1629, 1130, 1108, 1034, 864, 753, 585, 572.

Melting point: 204 °C

7.2.20 Synthesis of Hexyl-BINAM-ACP *(S)*-56

Described experiment: JO-204.

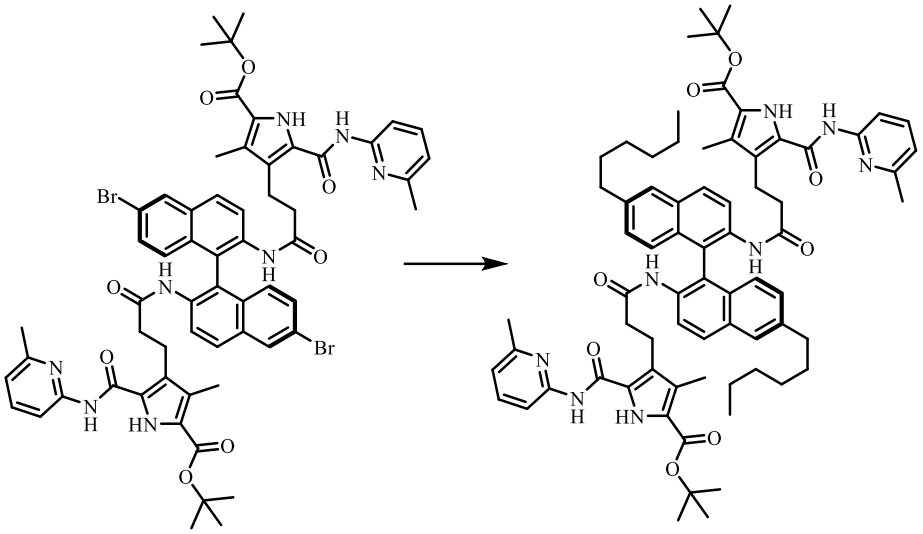

Figure 145: Synthesis of Hexyl-BINAM-ACP *(S)*-56.

The brominated product *(S)*-**55** (20.0 mg, 0.0169 mmol, 1 eq) and 1,3-bis(diphenyl phosphino)-propane nickel(II)chloride (0.220 mg, 0.406 µmol, 2.4 mol%) were dissolved in dry diethylether (20 mL) the mixture was cooled down to −10 °C in an ice/salt bath and a 0.8 M hexyl magnesium bromide in diethylether (0.03 mL, 0.03 mmol, 1.5 eq) was added slowly at this temperature. The mixture was allowed to thaw to room temperature and stirred for 16 hours. The catalyst was filtered of and the organic layer was washed with 0.5 M HCl (2 x 10 mL), water (3 x 15 mL) and brine(3 x 15 mL). After the removal of the solvent in vacuum, the crude product was purified via column chromatography (ø = 3 cm, h = 30 cm, cyclohexane:ethylacetate = 7:1). The pure product *(S)*-**56** (15.8 mg, 0.0133 mmol, 78%) was obtained as a white solid.

Sum formula: $C_{72}H_{86}N_8O_8$

Molar mass: 1191.528 g/mol

R_f: 0.68 (cyclohexane:ethylacetate = 4:1)

^{1}H-NMR: (400 MHz, $CDCl_3$) δ [ppm] = 0.91 (t, J^3 = 6.88 Hz, 6 H, 2 x C*H*$_3$), 1.24 - 1.46 (m, 12 H, 2 x C*H*$_2$-C*H*$_{2-2}$), 1.28 - 1.56 (m, 24 H, 2 x C-(C*H*$_3$)$_3$ + 2 x C*H*$_3$), 2.30 (s, 6 H, 2 x C*H*$_3$), 2.56 (s, 4 H, 2 x C*H*$_2$), 2.61 - 2.67 (m, 8 H, 4 x C*H*$_2$), 2.79 (t, J^3 = 7.50 Hz, 4 H, 2 x C*H*$_2$), 6.89 (d, J^3 = 9.07 Hz, 2 H, pyr-C*H*), 7.02 (d, J^3 = 5.94 Hz, 2 H, 2 x pyr-C*H*), 7.15 (d, J^3 = 8.76 Hz, 2 H, 2 x BINOL-*H*), 7.26 (dd, J^3 = 1.88 Hz, 2.19 Hz, 2 H, 2 x pyr-C*H*), 7.64 (t, J^3 = 7.82 Hz, 2 H, 2 x BINOL-*H*), 7.71 (d, J^3 = 8.76 Hz, 2 H, 2 x BINOL-*H*), 7.93 (d, J^3 = 2.19 Hz, 2 H, 2 x BINOL-*H*), 8.03 (d, J^3 = 6.88 Hz, 2 H, 2 x BINOL-*H*).

^{13}C-NMR: (151 MHz, $CDCl_3$) δ [ppm] = 12.54, 13.90, 22.48, 22.90, 29.16, 30.18, 30.66, 30.78, 31.72, 35.15, 36.12, 81.44, 104.23, 115.49, 117.77, 119.61, 124.08, 125.70, 127.37, 128.50, 129.26, 130.21, 132.14, 132.92, 134.30, 135.34, 137.09, 137.47, 141.36, 149.72, 155.46, 159.95, 160.68, 174.52.

HR-MS: (ESI): m/z = 1191.6701 ($[M+H]^+$), calcd. 1191.6641 (for $[C_{72}H_{87}N_8O_8]^+$).

FT-IR: **(**ATR): $\tilde{\nu}$ [cm^{-1}] = 3462, 3358, 3070, 2872, 2684, 1821, 1742, 1633, 1630, 1172, 1134, 1040, 944, 765, 748, 550.

Melting point: 255 °C

7.2.21 Deprotection of Hexyl-BINAM-ACP to achieve Compound *(S)*-6

Described experiment: JO-205.

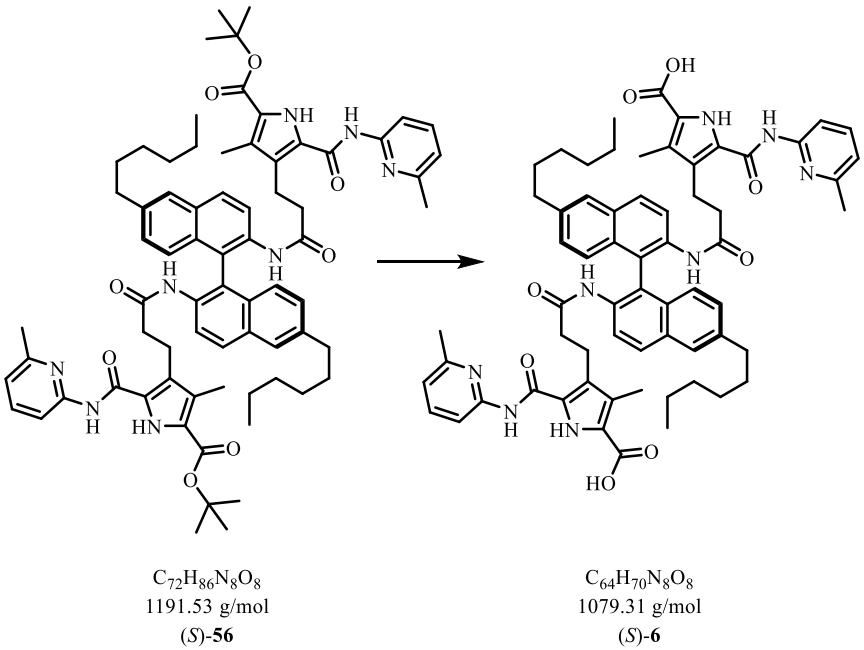

Figure 146: Deprotection of Hexyl-BINAM-ACP *(S)*-56.

The *(S)*-BINAM hexyl ACP motif *(S)*-**56** (12 mg, 0.0101 mmol) was dissolved in dichloromethane (5 mL) and TFA (1 mL) was added to initiate the deprotection. The mixture was stirred for 16 hours and the reaction progress was monitored with TLC. The solvent was removed in vacuum and the crude product was purified via MPLC (ø = 2 cm, h = 30 cm, RP18, methanol:water = 1:10 to pure methanol). The deprotected product *(S)*-**6** (9.80 mg, 0.00908 mmol, 90%) was obtained as a white solid.

Sum formula: $C_{64}H_{70}N_8O_8$

Molar mass: 1079.312 g/mol

R_f: 0.33 (cyclohexane:ethylacetate = 4:1)

^{1}H-NMR: (400 MHz, $CDCl_3$) δ [ppm] = 0.88 (t, J^3 = 7.97 Hz, 6 H, 2 x C*H*$_3$), 1.18 - 1.36 (m, 12 H, 2 x CH$_2$-C*H*$_2$-C*H*$_2$), 1.52 (m, 4 H, 2 x C*H*$_2$), 1.55 (m, 4 H, 2 x C*H*$_2$),

2.05 (s, 6 H, 2 x C*H*$_3$), 2.16 (m, 4 H, 2 x C*H*$_2$), 2.46 (s, 6 H, 2 x C*H*$_3$), 2.78 (m, 4 H, 2 x C*H*$_2$), 6.87 (m, 4 H, 2 x C*H*$_2$), 6.90 (d, J^3 = 5.32 Hz, 2 H, 2 x BINOL-*H* + 2 x pyr-C*H*), 7.15 (d, J^3 = 9.07 Hz, 2 H, 2 x pyr-C*H*), 7.23 (d, J^3 = 6.88 Hz, 2 H, 2 x BINOL-*H*), 7.28 (d, J^3 = 2.19 Hz, 2 H, 2 x BINOL-*H*), 7.62 (t, J^3 = 7.50 Hz, 2 H, pyr-C*H*), 7.71 (d, J^3 = 8.75 Hz, 2 H, 2 x BINOL-*H*), 7.93 (d, J^3 = 2.19 Hz, 2 H, 2 x BINOL-*H*).

^{13}C-NMR: (151 MHz, $CDCl_3$) δ [ppm] = 11.95, 14.05, 21.36, 21.89, 28.58, 29.31. 30.19, 32.65, 34.56, 37.19, 109.56, 114.45, 117.18, 119.68, 123.49, 126.08, 126.78, 127.16, 128.67, 130.36, 131.55, 132.91, 133.71, 135.27, 136.51, 138.37, 140.77, 146.52, 154.87, 164.37, 166.00, 173.21.

HR-MS: (ESI): m/z = 1101.5299 ($[M+Na]^+$), calcd. 1101.5209 (for $[C_{64}H_{70}N_8O_8Na]^+$).

FT-IR: **(**ATR): $\tilde{\nu}$ [cm^{-1}] = 3456, 3121, 3021, 2925, 1756, 1658, 1655, 1635, 1143, 1058, 1066, 955, 791, 764.

Elemental analysis: calcd. (%) for $C_{64}H_{70}N_8O_8$: C 71.22, H 6.54, N 10.38; found: C 69.40, H 6.02, N 10.60.

Melting point: Decomposition at 278 °C

8. Appendix

8.1 Abbreviations

δ	chemical shift
°C	degree celsius
λ	wavelength
µ	micro
π	pi
Å	Ångstrom
AA	amino acid
abs	absolute
Ac	acetyl
AFM	atomic force microscopy
Alloc	allyloxycarbonyl
AMP	adenosine monophosphate
NPs	nanoparticles
BINAM	1,1′-binaphthyl-2,2′-diamine
BINOL	1,1'-binaphthyl-2,2'-diol
Bn	benzyl
Boc	*tert*-butyloxycarbonyl
tBu	*tert*-butyl
br	broad
c	concentration
ca.	circa
calcd.	calculated
$CDCl_3$	deuterated chloroform
cm	centimeter
d	doublet / diameter/ day
DCM	dichloromethane
DIPEA	*N,N´*-diisopropylethyl amine
DLS	dynamic light scattering
DMF	*N,N´*-dimethyl formamide
DMSO	dimethyl sulfoxide
d_6-DMSO	deuterated dimethyl sulfoxide
DNA	deoxyribonucleic acid
DOPE	dioleoylphosphatidyl-ethanolamine
E	glutamic acid
e.g.	for example
eq	equivalent
ESI	electrospray ionization
ESI-MS	electrospray ionization mass spectrometry
Et_3N	triethylamine
Fmoc	9-fluorenylmethyl-oxycarbonyl
FT-IR	fourier transform infrared spectroscopy
g	gram
GCP	guanidiniocarbonyl pyrrole
h	hour (s)
HCTU	1-H-Benzotriazolium 1-[bis(dimethylamino)-methylene]-5chloro-hexafluorophosphate (1-),3-oxide
H-donor	hydrogen bond donor
HOBt	1-hydroxybenzotriazole
HPLC	high performance liquid chromatography

HRMS	high resolution mass spectrometry
Hz	Hertz
kJ	kilo Joule
K_d	dissociation constant
m	milli / multiplett / meter
M	mol/L
m/z	mass per charge
max	maximum
Me	methyl
MeOH	methanol
MHz	megahertz
min	minute (s)
µM	micromolar
mM	millimolar
MPLC	medium performance liquid chromatography
MS	mass spectrometry
n	nano
nm	nanometer
nM	nanomolar
NMM	N-methylmorpholin
NMR	nuclear magnetic resonance
NPs	nanoparticles
p	para
Pd/C	palladium on charcoal
pH	pondus hydrogenii
*p*Ka	logarithmic acid dissociation constant
ppm	parts per million
PyBOP	benzotriazol-1-yl-N-oxy-tris(pyrrolidino)-phosphoniumhexa-fluorophosphate
q	quadruplet
r	radius
rt	room temperature
s	singulett / second(s)
t	time
T	temperature/thymine
TEM	transmission electron microscopy
TFA	trifluoroacetic acid
THF	tetrahydrofuran
TIS	triisopropylsilane
Trt	trityl
Trp	tryptophan
Tyr	tyrosine
U	uracil
UV	ultraviolet
UV/Vis	ultraviolet/ visible
V	volume
VI	viscosity index

8.2 Measurement of Viscosity

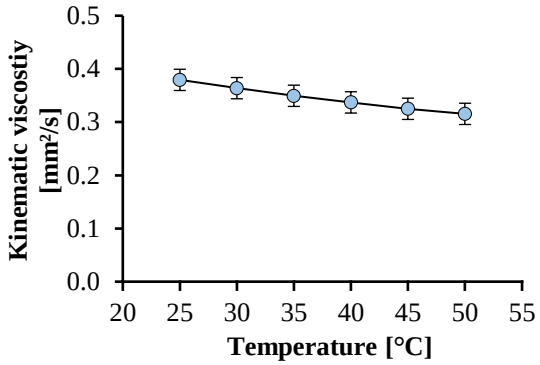

Figure 147: Kinematic viscosity of pure chloroform.

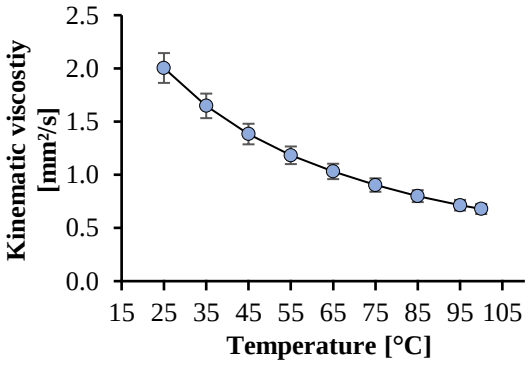

Figure 148: Kinematic viscosity of pure DMSO.

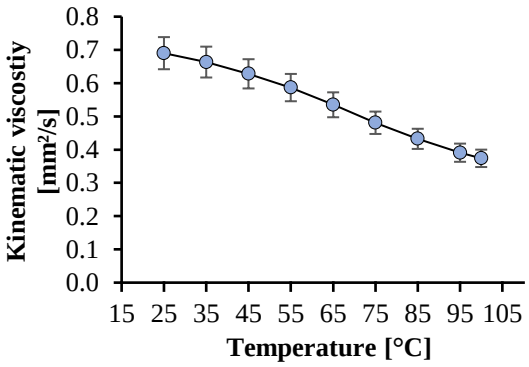

Figure 149: Kinematic viscosity of pure toluene.

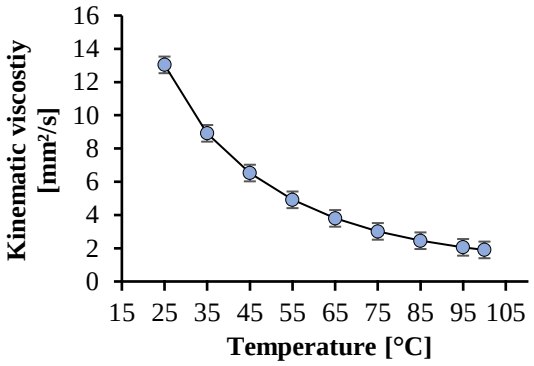

Figure 150: Kinematic viscosity of pure Nynas NS8.

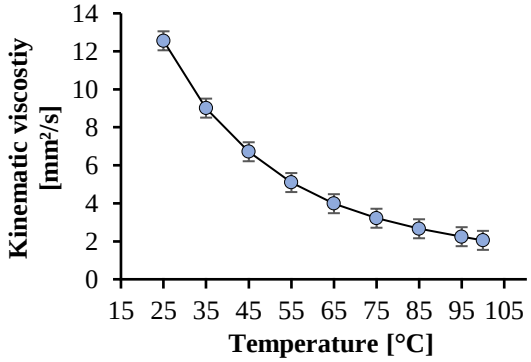

Figure 151: Kinematic viscosity of pure Nexbase 3020.

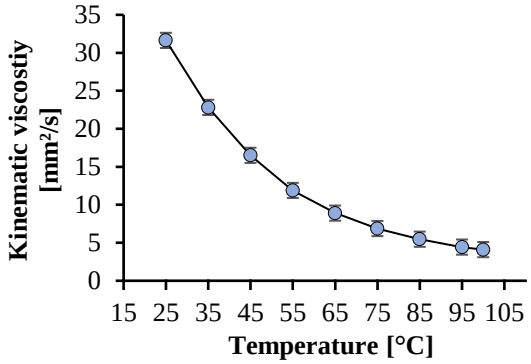

Figure 152: Kinematic viscosity of pure Nexbase 3043.

8.2.1 Viscosity Measurements of Generation 1 in Chloroform

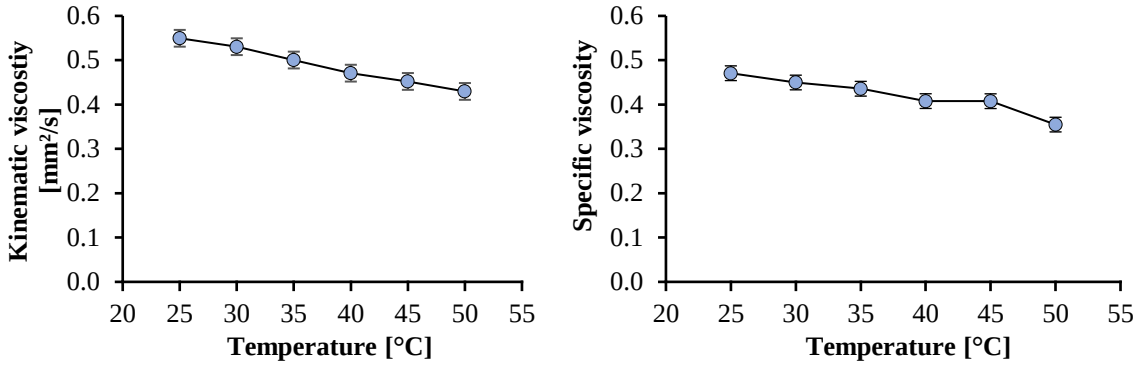

Figure 153: Kinematic (left) and specific (right) viscosity for generation 1 in chloroform at 130 mM.

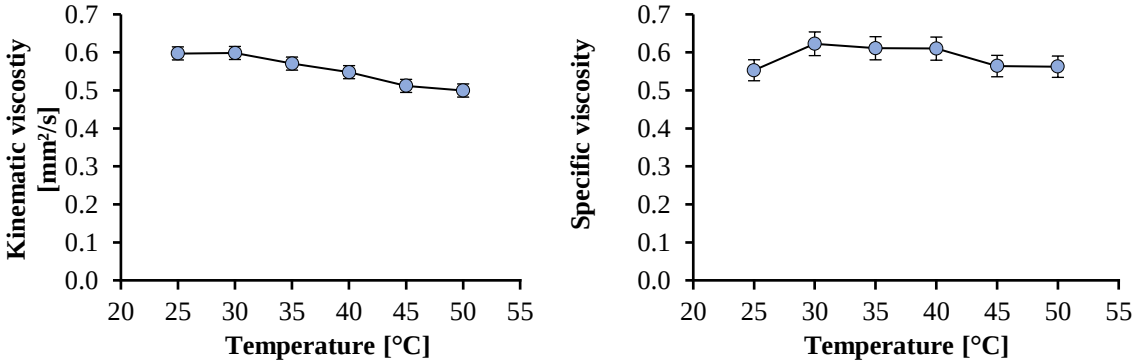

Figure 154: Kinematic (left) and specific (right) viscosity for generation 1 in chloroform at 145 mM.

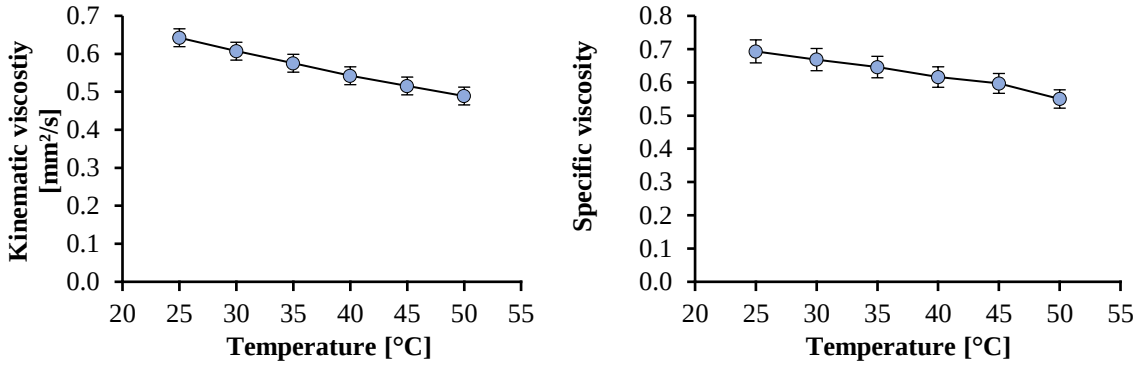

Figure 155: Kinematic (left) and specific (right) viscosity for generation 1 in chloroform at 160 mM.

8.2.2 Viscosity Measurements of Generation 2 in Chloroform

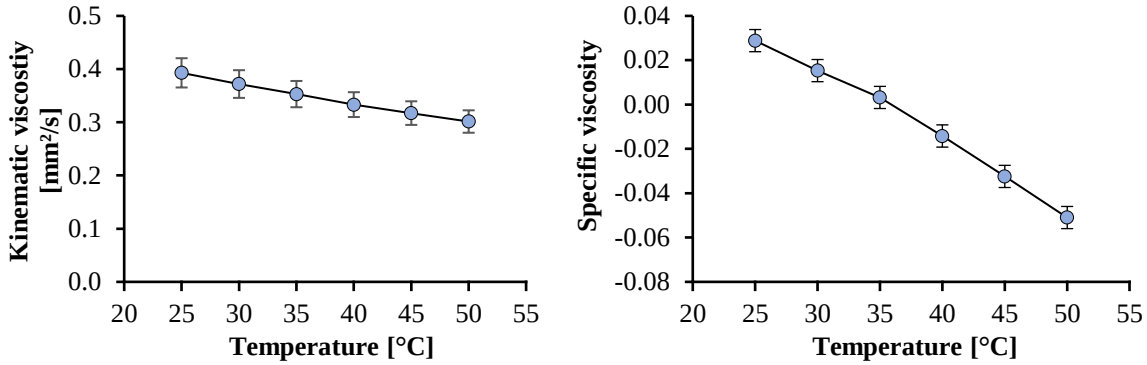

Figure 156: Kinematic (left) and specific (right) viscosity for generation 2 in chloroform at 130 mM.

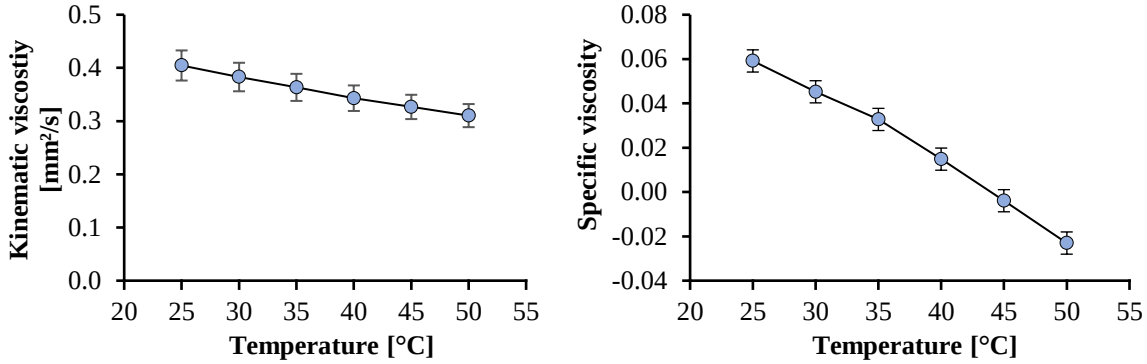

Figure 157: Kinematic (left) and specific (right) viscosity for generation 2 in chloroform at 145 mM.

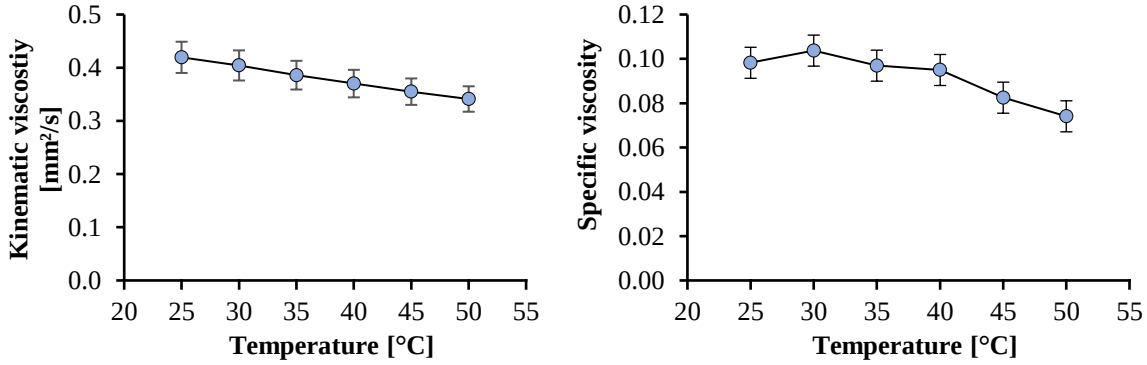

Figure 158: Kinematic (left) and specific (right) viscosity for generation 2 in chloroform at 160 mM.

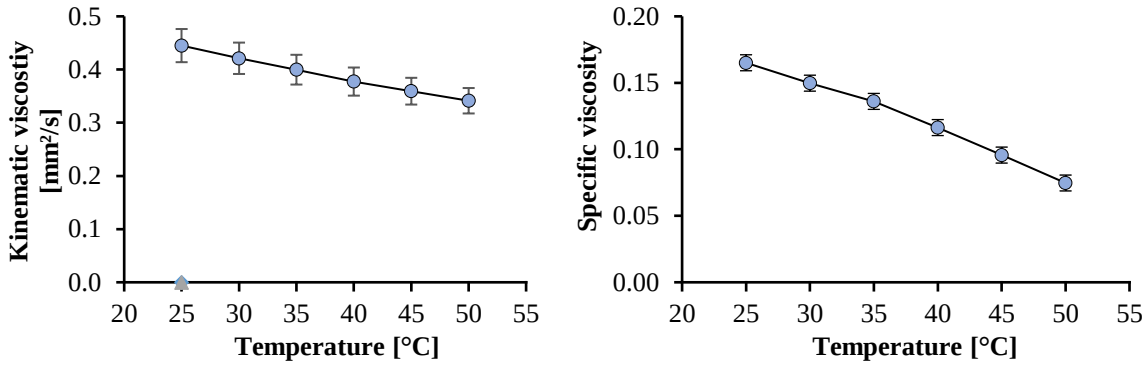

Figure 159: Kinematic (left) and specific (right) viscosity for generation 2 in chloroform at 175 mM.

8.2.3 Viscosity Measurements of Generation 3 in DMSO

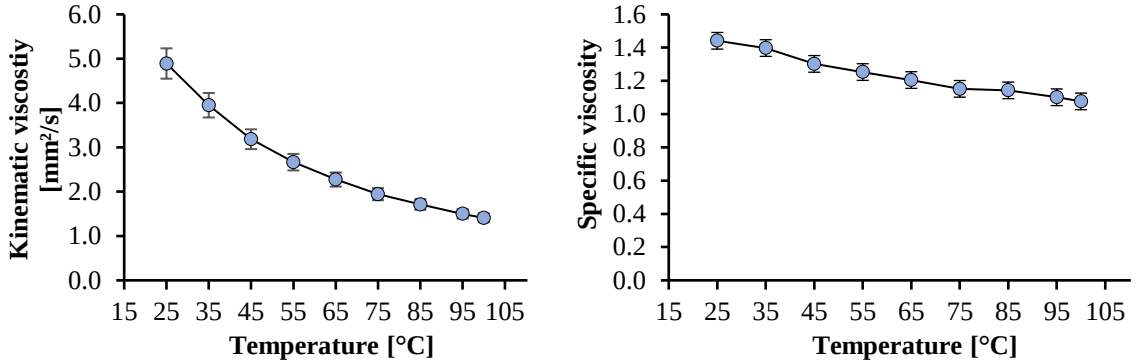

Figure 160: Kinematic (left) and specific (right) viscosity for generation 3 in DMSO at 200 mM.

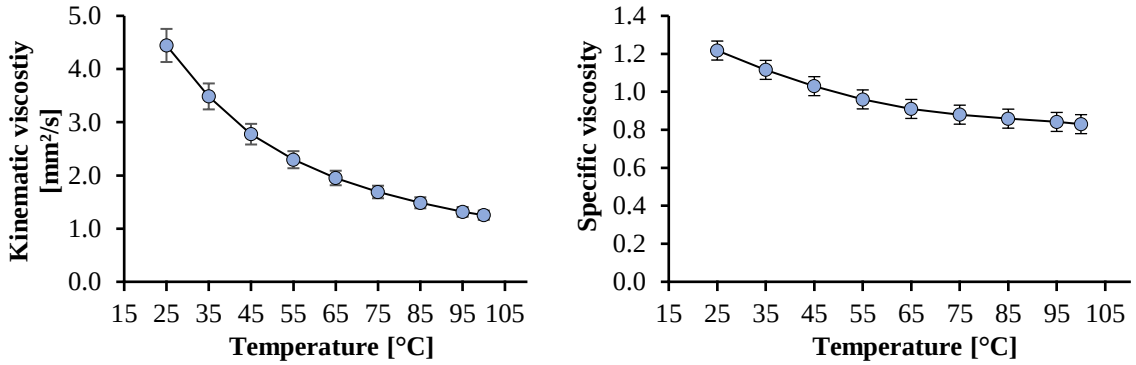

Figure 161: Kinematic (left) and specific (right) viscosity for generation 3 in DMSO at 180 mM.

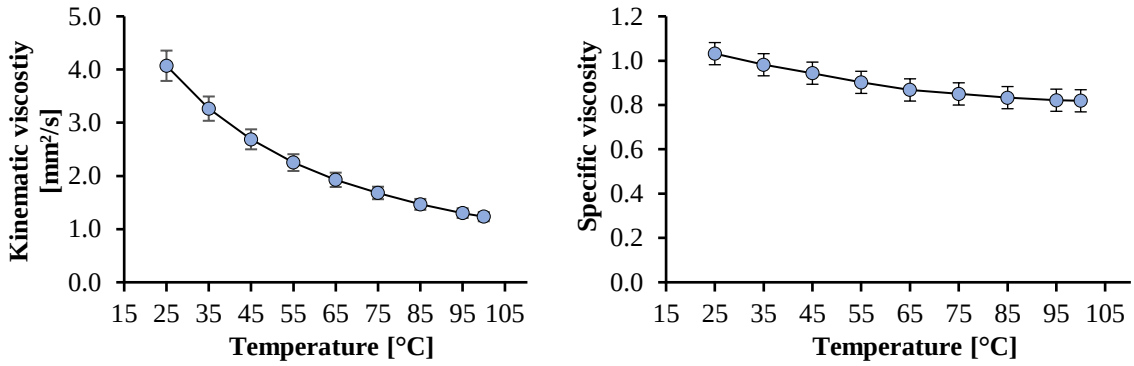

Figure 162: Kinematic (left) and specific (right) viscosity for generation 3 in DMSO at 160 mM.

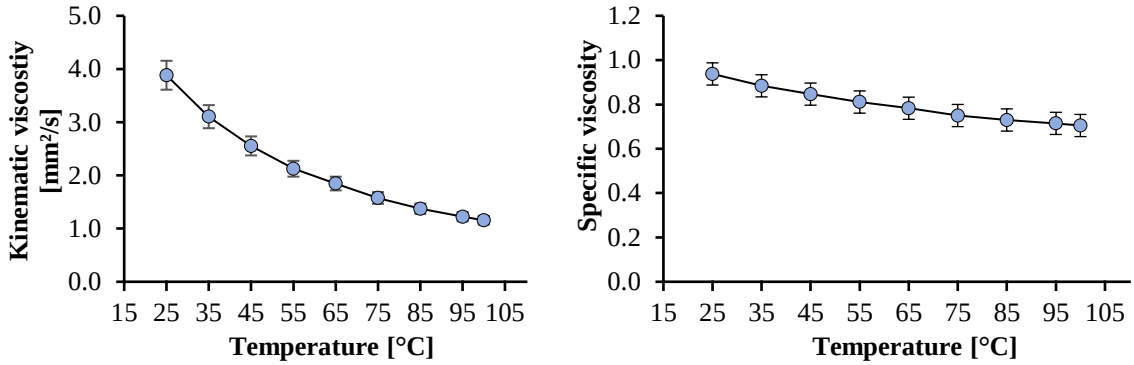

Figure 163: Kinematic (left) and specific (right) viscosity for generation 3 in DMSO at 140 mM.

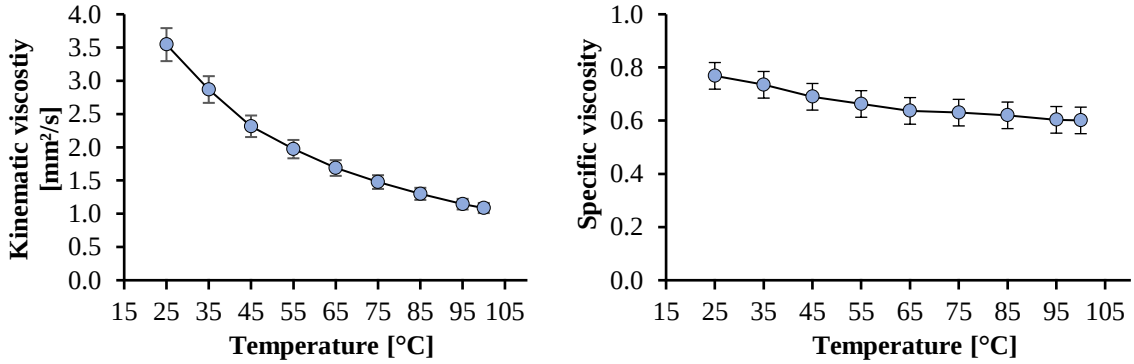

Figure 164: Kinematic (left) and specific (right) viscosity for generation 3 in DMSO at 120 mM.

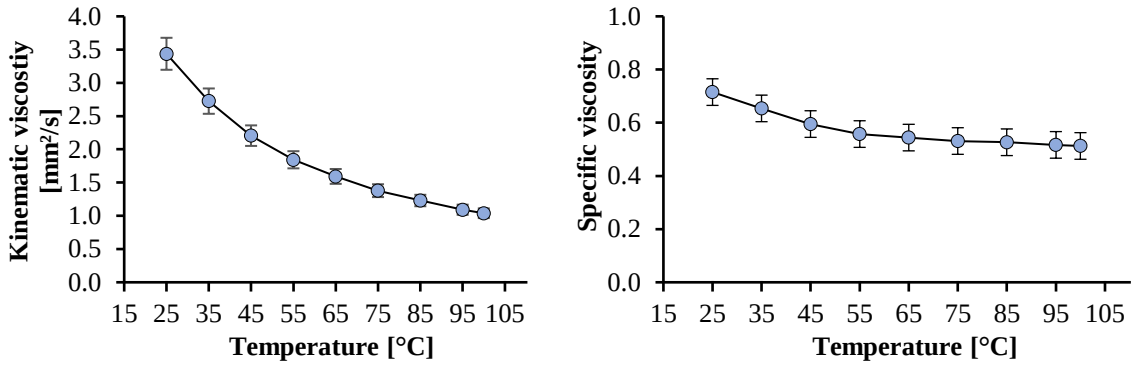

Figure 165: Kinematic (left) and specific (right) viscosity for generation 3 in DMSO at 100 mM.

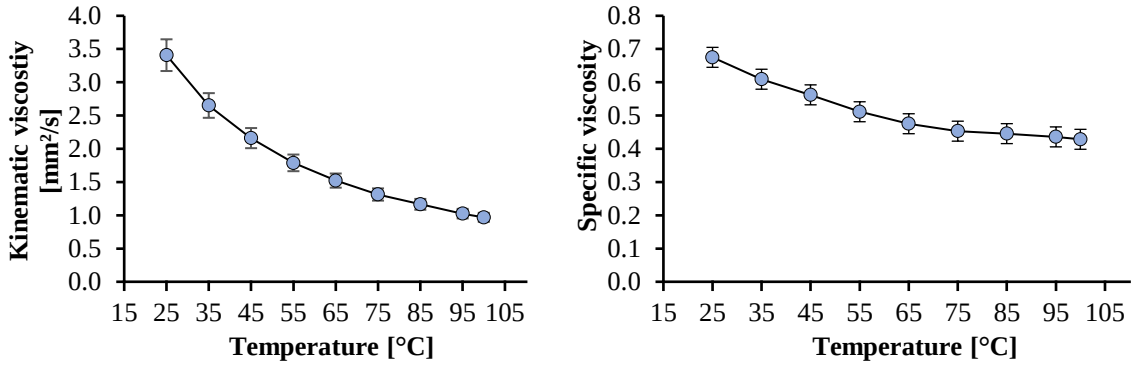

Figure 166: Kinematic (left) and specific (right) viscosity for generation 3 in DMSO at 80 mM.

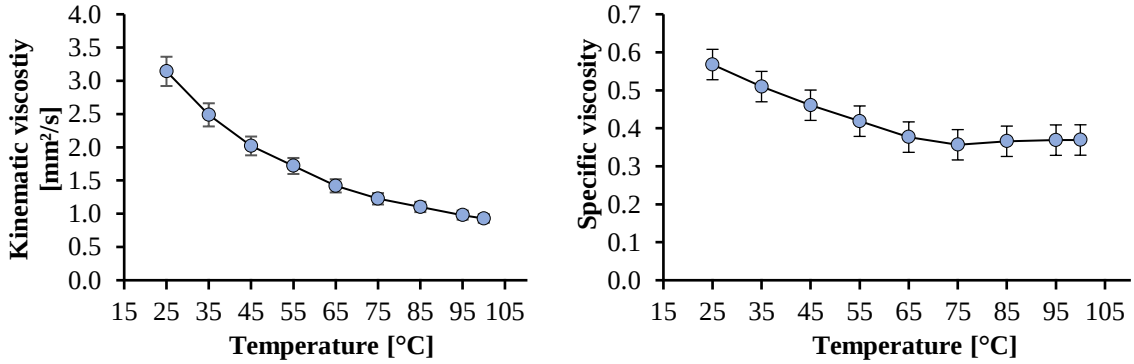

Figure 167: Kinematic (left) and specific (right) viscosity for generation 3 in DMSO at 60 mM.

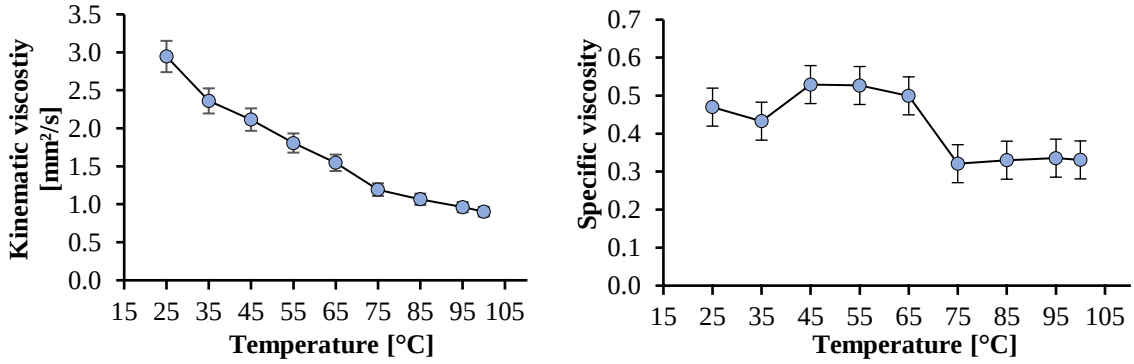

Figure 168: Kinematic (left) and specific (right) viscosity for generation 3 in DMSO at 50 mM.

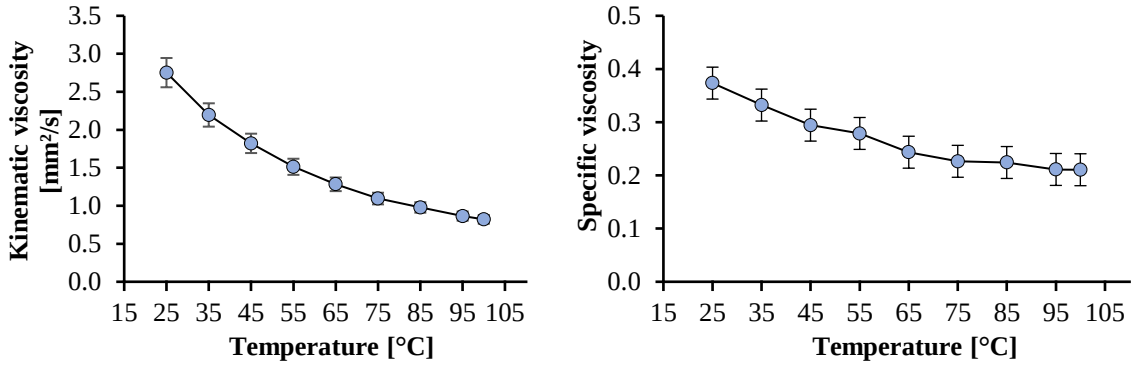

Figure 169: Kinematic (left) and specific (right) viscosity for generation 3 in DMSO at 40 mM.

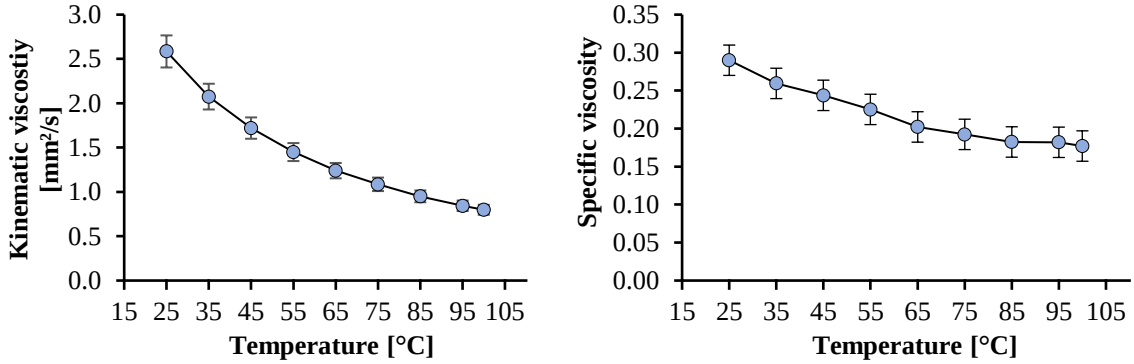

Figure 170: Kinematic (left) and specific (right) viscosity for generation 3 in DMSO at 30 mM.

8.2.4 Viscosity Measurements of Generation 4

8.2.4.1 Measurements in DMSO

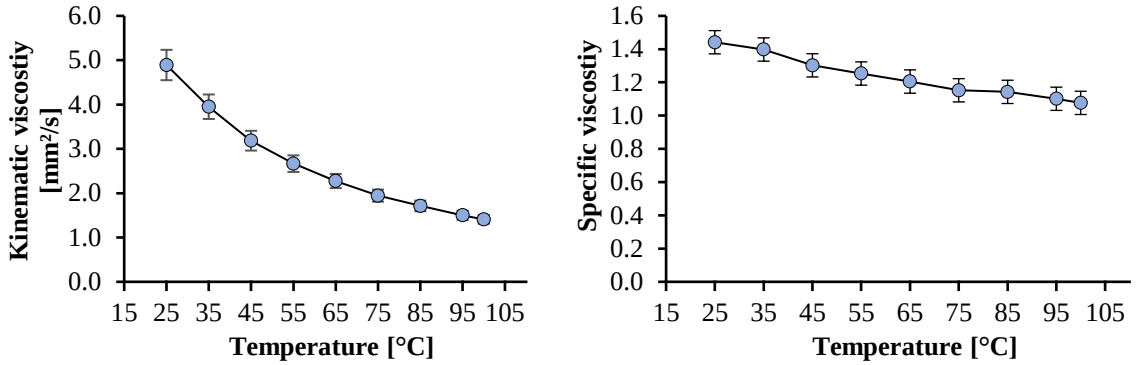

Figure 171: Kinematic (left) and specific (right) viscosity for generation 4 in DMSO at 200 mM.

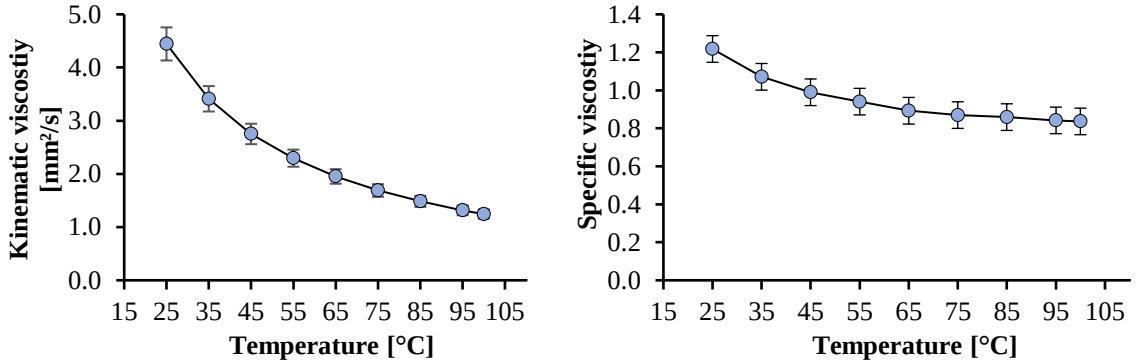

Figure 172: Kinematic (left) and specific (right) viscosity for generation 4 in DMSO at 180 mM.

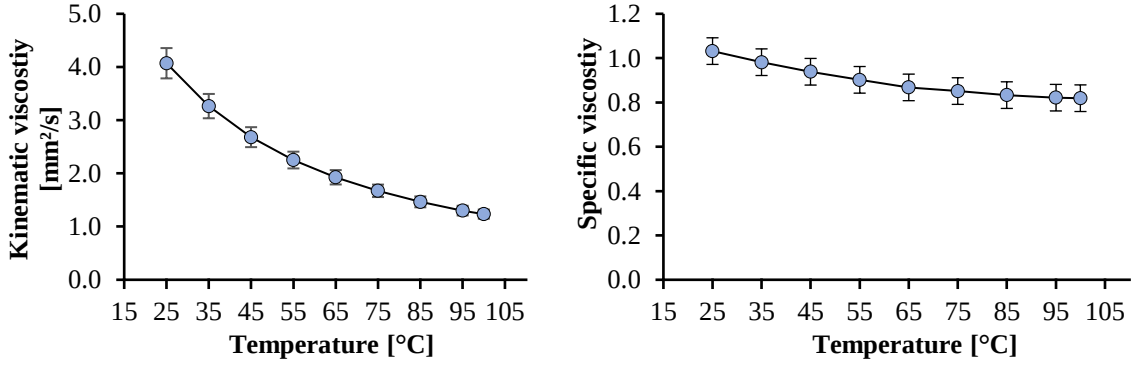

Figure 173: Kinematic (left) and specific (right) viscosity for generation 4 in DMSO at 160 mM.

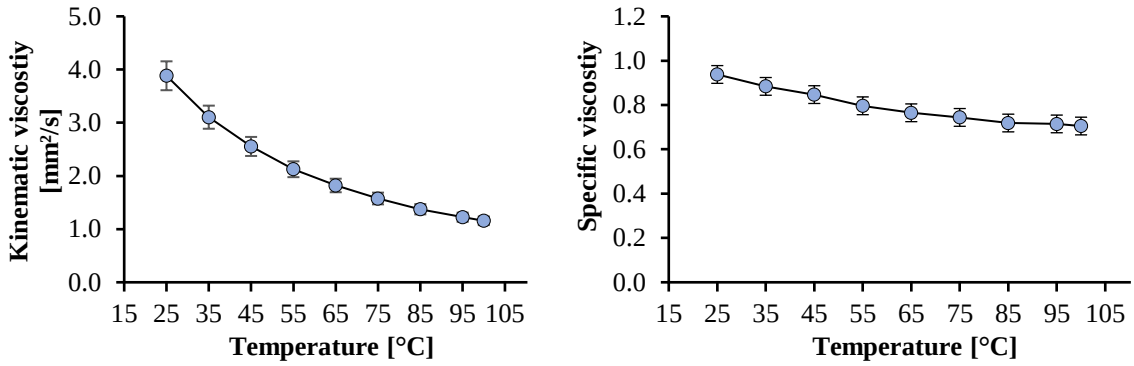

Figure 174: Kinematic (left) and specific (right) viscosity for generation 4 in DMSO at 140 mM.

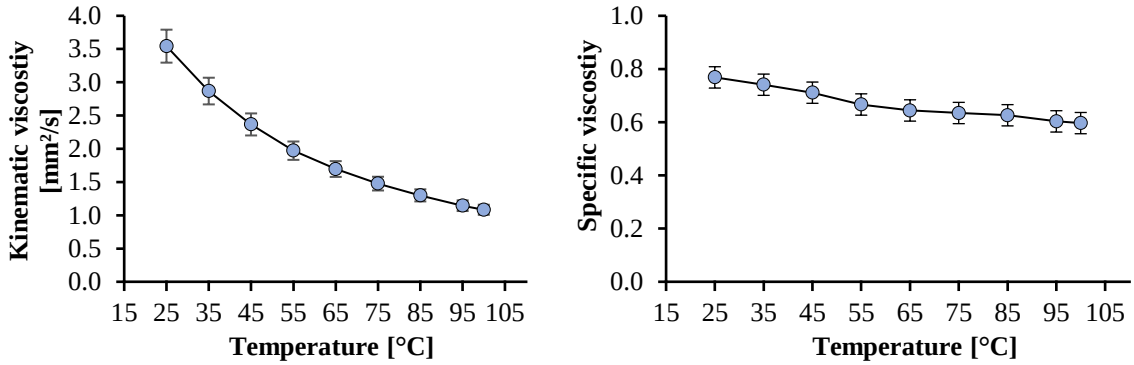

Figure 175: Kinematic (left) and specific (right) viscosity for generation 4 in DMSO at 120 mM.

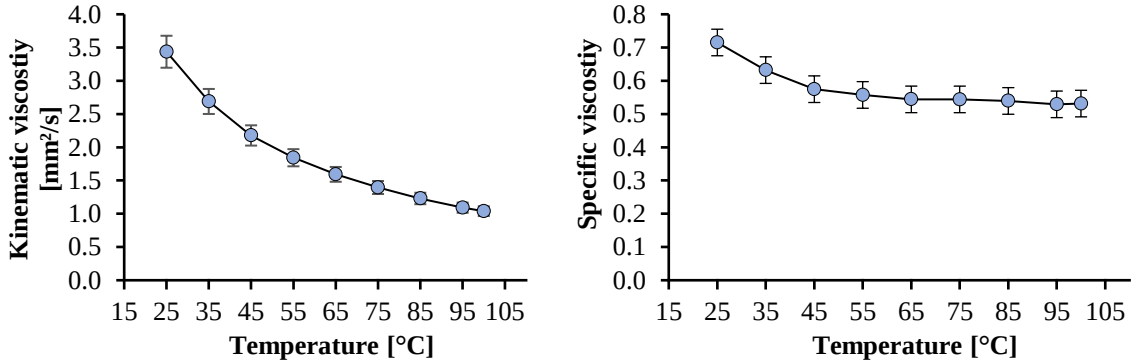

Figure 176: Kinematic (left) and specific (right) viscosity for generation 4 in DMSO at 100 mM.

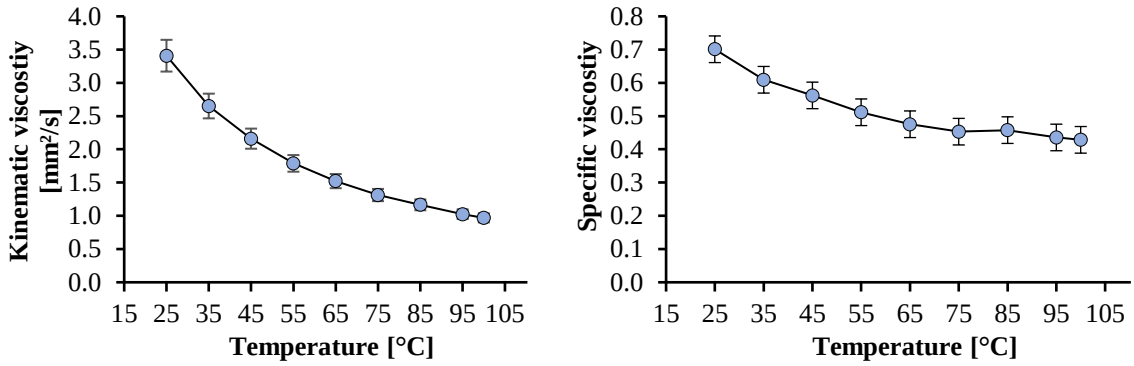

Figure 177: Kinematic (left) and specific (right) viscosity for generation 4 in DMSO at 80 mM.

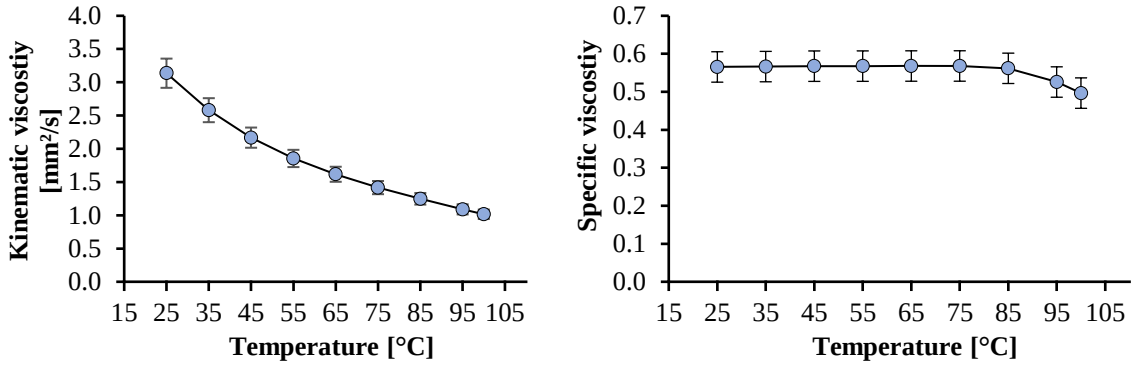

Figure 178: Kinematic (left) and specific (right) viscosity for generation 4 in DMSO at 60 mM.

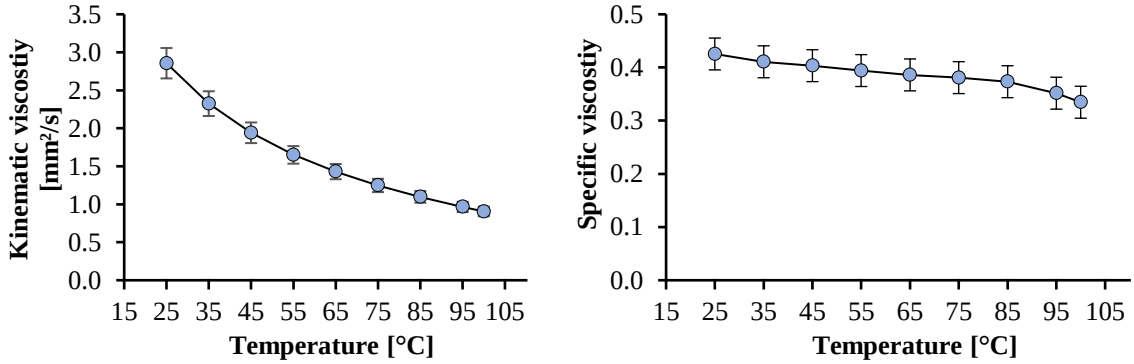

Figure 179: Kinematic (left) and specific (right) viscosity for generation 4 in DMSO at 50 mM.

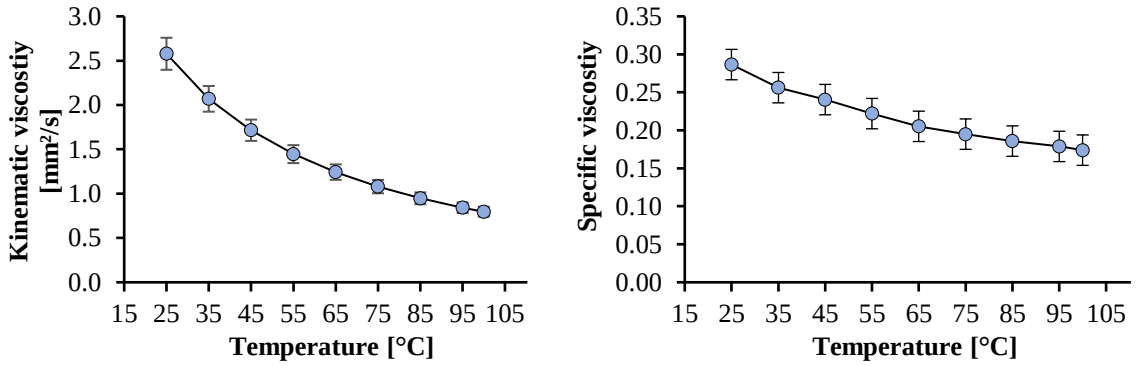

Figure 180: Kinematic (left) and specific (right) viscosity for generation 4 in DMSO at 40 mM.

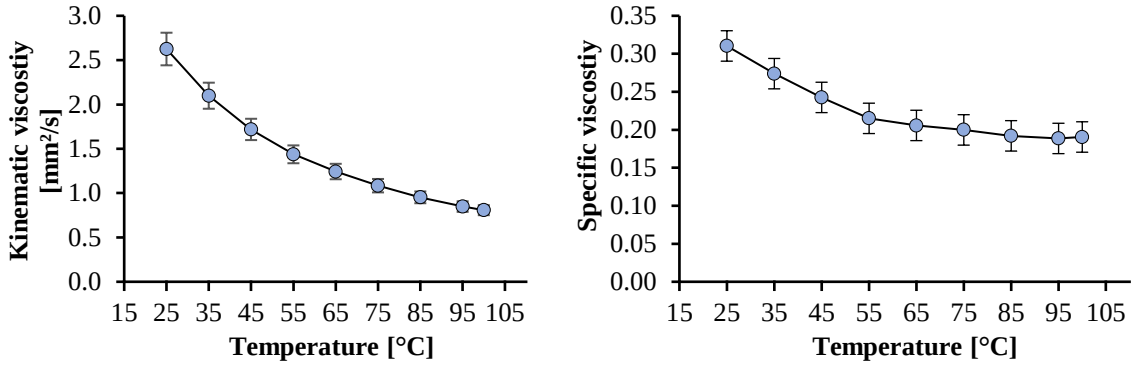

Figure 181: Kinematic (left) and specific (right) viscosity for generation 4 in DMSO at 30 mM.

8.2.4.2 Measurements in Chloroform

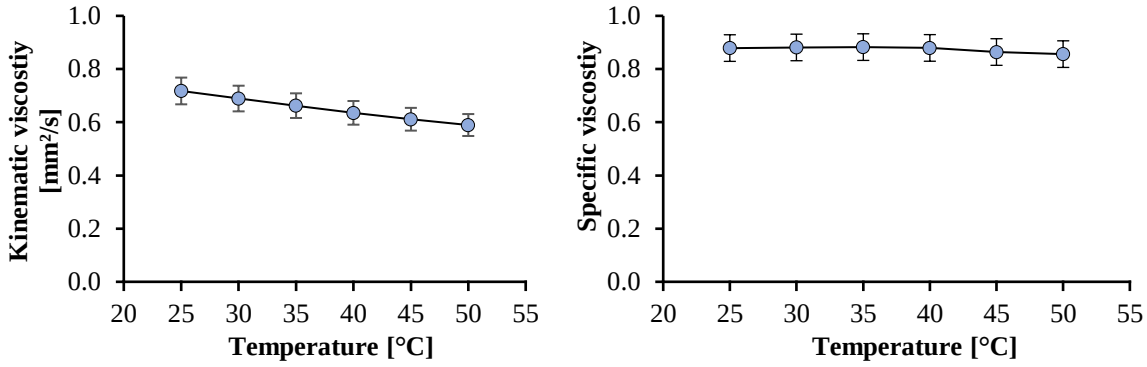

Figure 182: Kinematic (left) and specific (right) viscosity for generation 4 in chloroform at 100 mM.

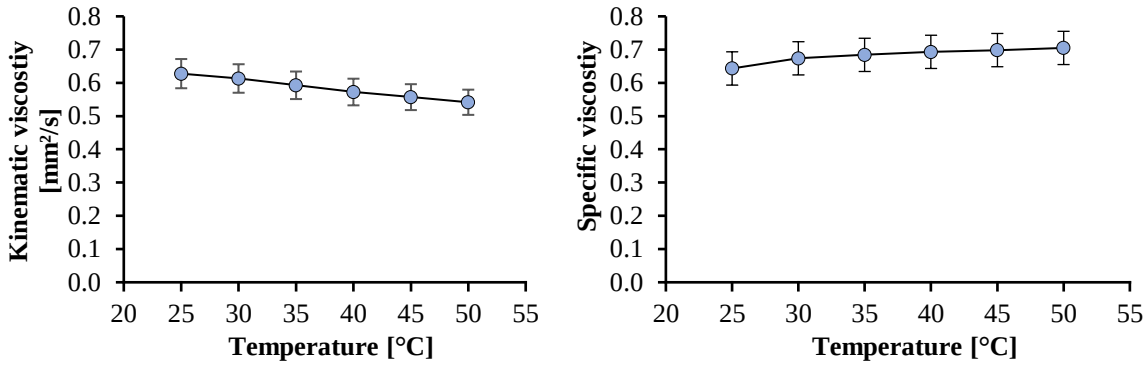

Figure 183: Kinematic (left) and specific (right) viscosity for generation 4 in chloroform at 80 mM.

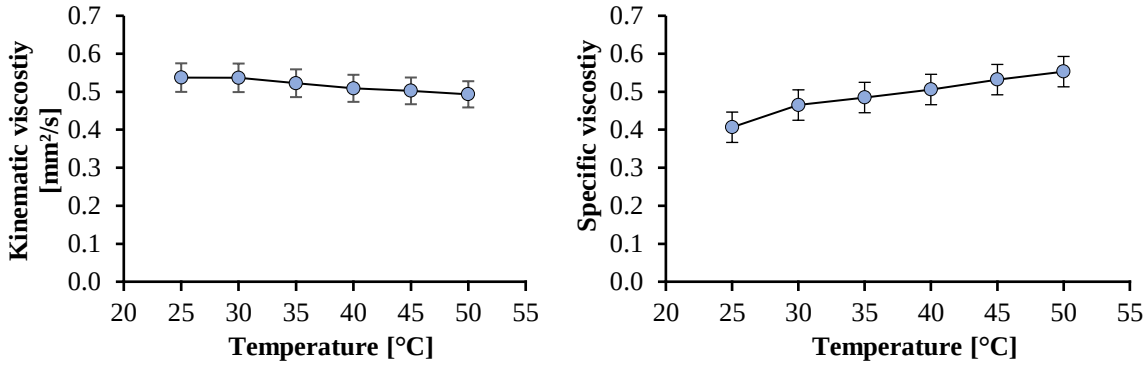

Figure 184: Kinematic (left) and specific (right) viscosity for generation 4 in chloroform at 60 mM.

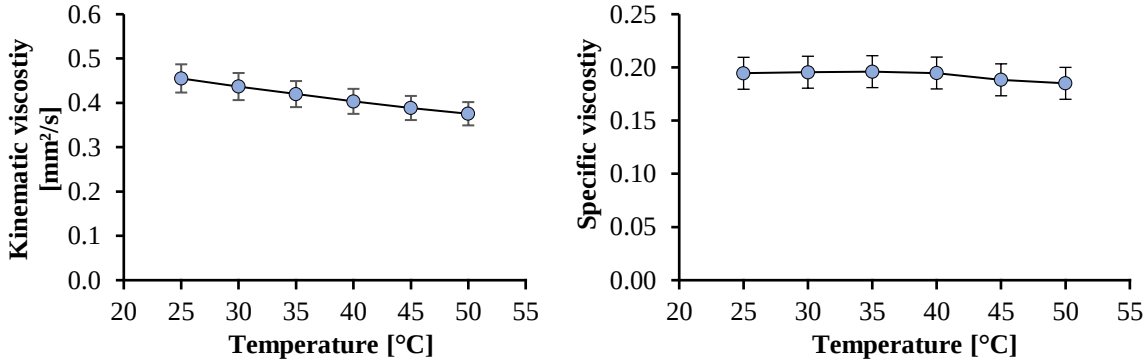

Figure 185: Kinematic (left) and specific (right) viscosity for generation 4 in chloroform at 40 mM.

9.2.4.3 Measurements in Toluene

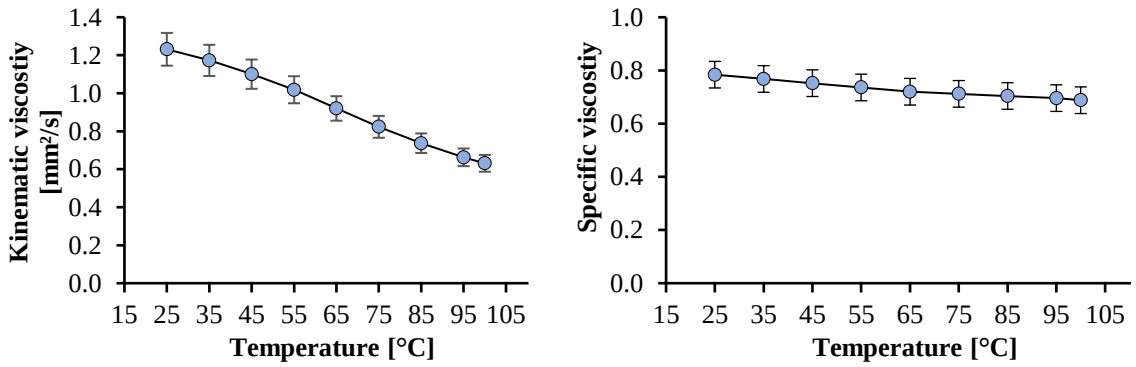

Figure 186: Kinematic (left) and specific (right) viscosity for generation 4 in toluene at 100 mM.

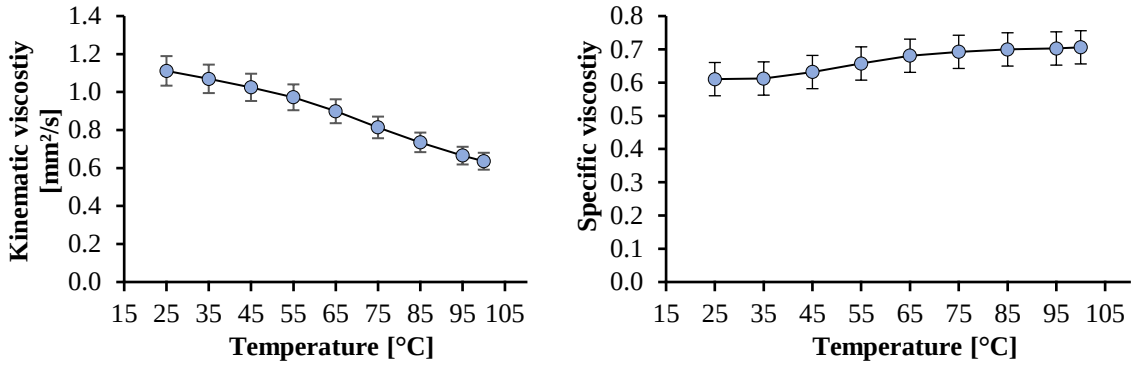

Figure 187: Kinematic (left) and specific (right) viscosity for generation 4 in toluene at 80 mM.

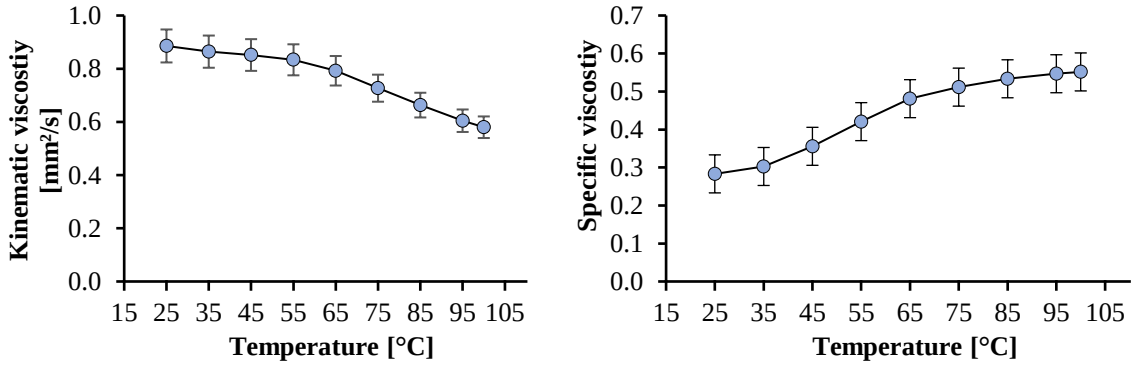

Figure 188: Kinematic (left) and specific (right) viscosity for generation 4 in toluene at 60 mM.

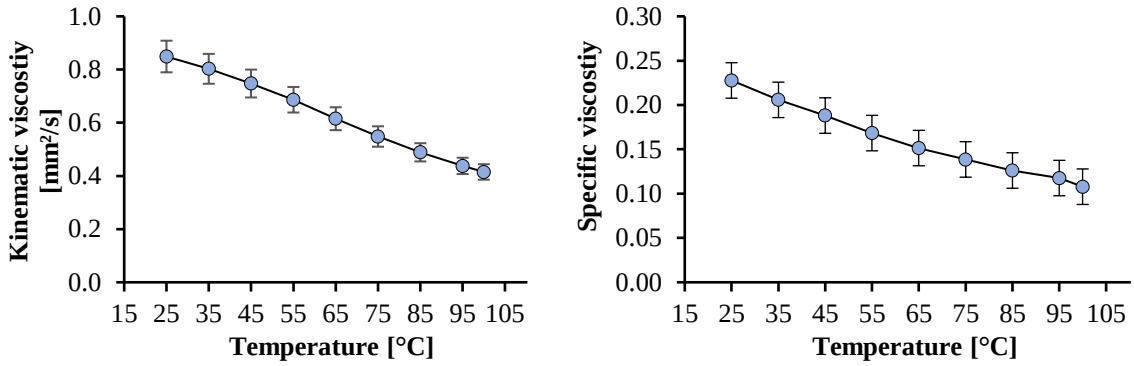

Figure 189: Kinematic (left) and specific (right) viscosity for generation 4 in toluene at 40 mM.

8.2.4.3 Measurement in Nynas NS8

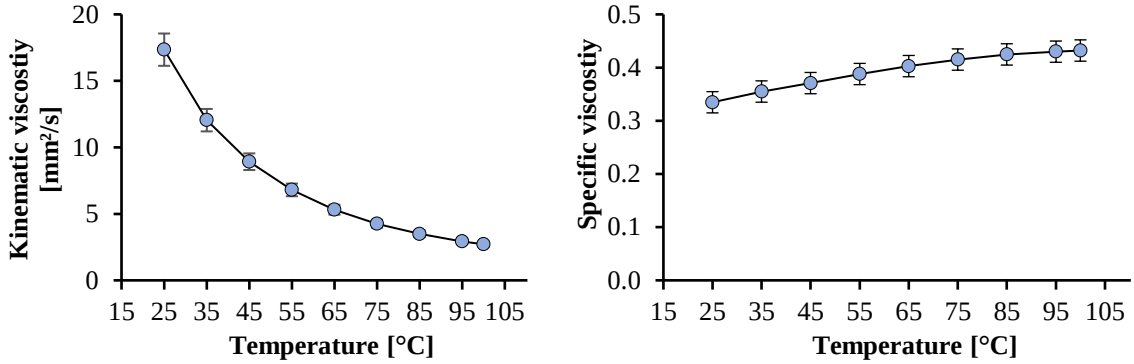

Figure 190: Kinematic (left) and specific (right) viscosity for generation 4 in Nynas NS8 at 60 mM.

8.2.5 Viscosity Measurements of Generation 5

8.2.5.1 Measurements in Nynas NS8

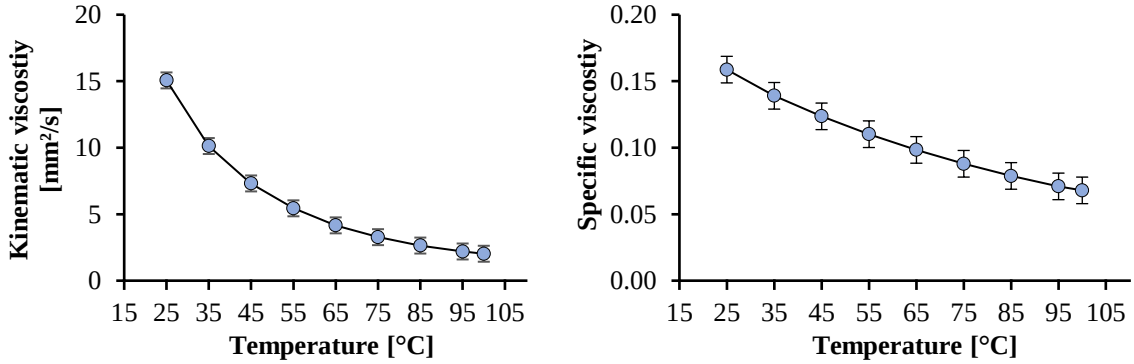

Figure 191: Kinematic (left) and specific (right) viscosity for generation 4 in Nynas NS8 at 100 mM.

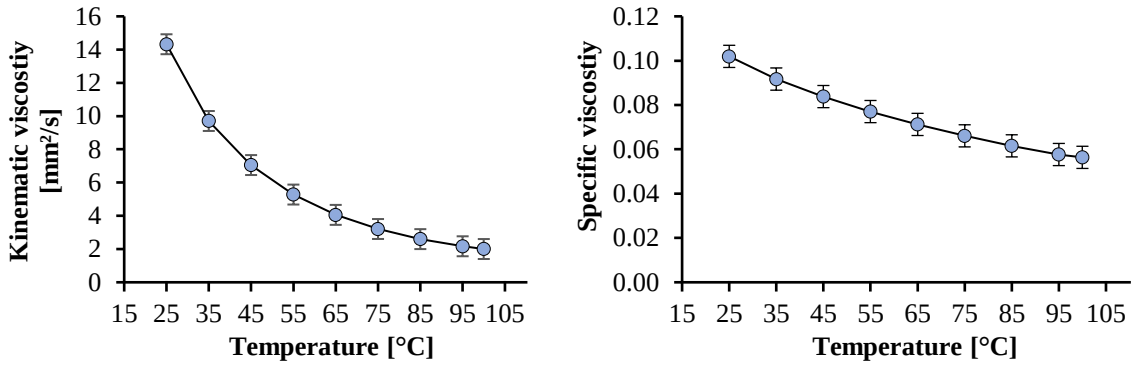

Figure 192: Kinematic (left) and specific (right) viscosity for generation 4 in Nynas NS8 at 80 mM.

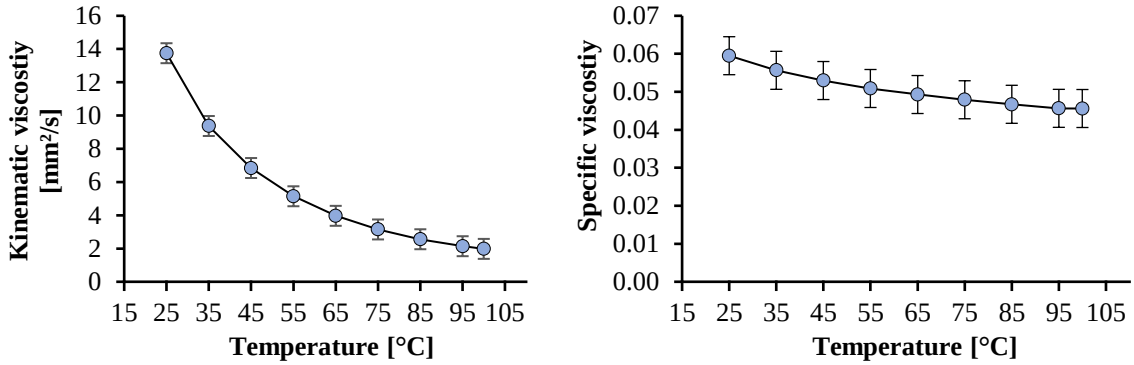

Figure 193: Kinematic (left) and specific (right) viscosity for generation 4 in Nynas NS8 at 60 mM.

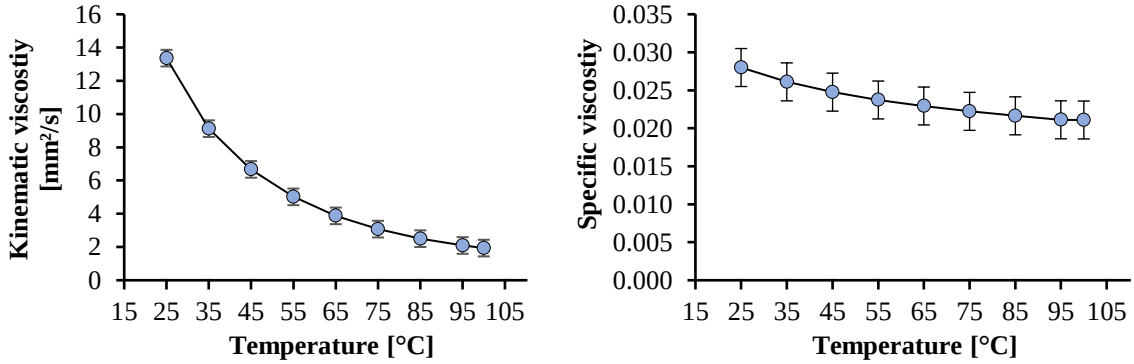

Figure 194: Kinematic (left) and specific (right) viscosity for generation 4 in Nynas NS8 at 40 mM.

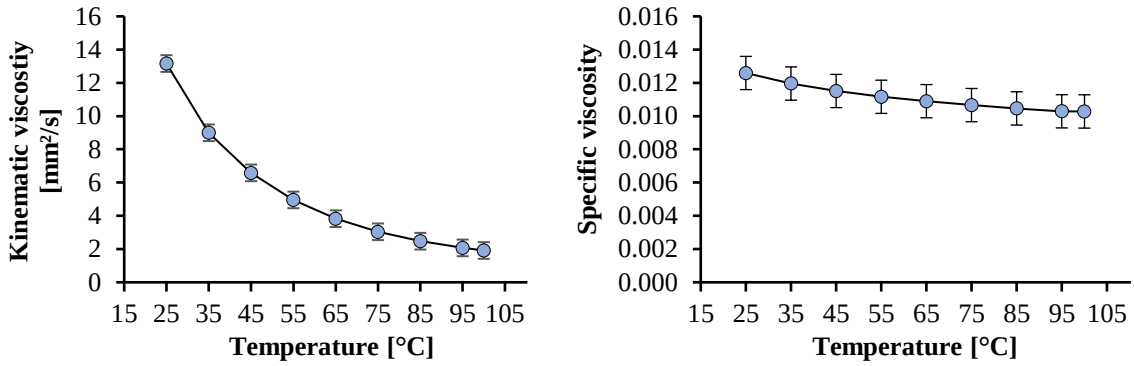

Figure 195: Kinematic (left) and specific (right) viscosity for generation 4 in Nynas NS8 at 20 mM.

8.2.5.1 Measurement in Nexbase 3020

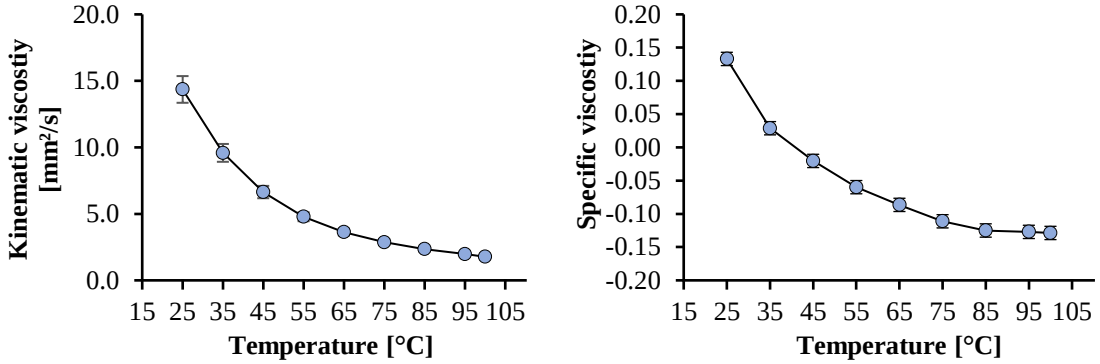

Figure 196: Kinematic (left) and specific (right) viscosity for generation 4 in Nexbase 3020 at 40 mM.

8.2.6 Viscosity Measurements of Generation 6

8.2.6.1 Measurements in Nynas NS8

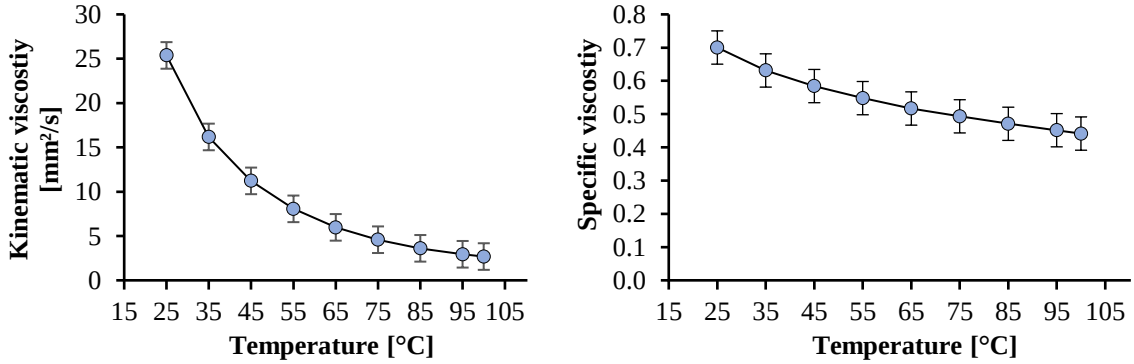

Figure 197: Kinematic (left) and specific (right) viscosity for generation 4 in Nynas NS8 at 100 mM.

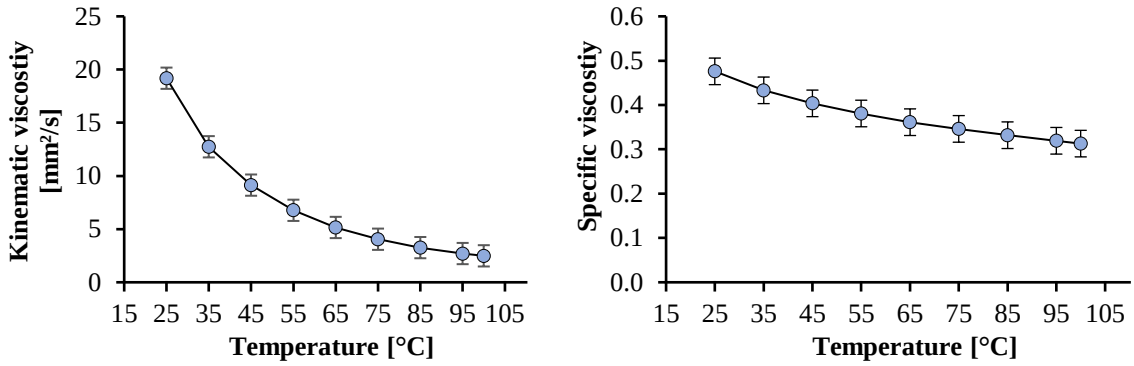

Figure 198: Kinematic (left) and specific (right) viscosity for generation 4 in Nynas NS8 at 80 mM.

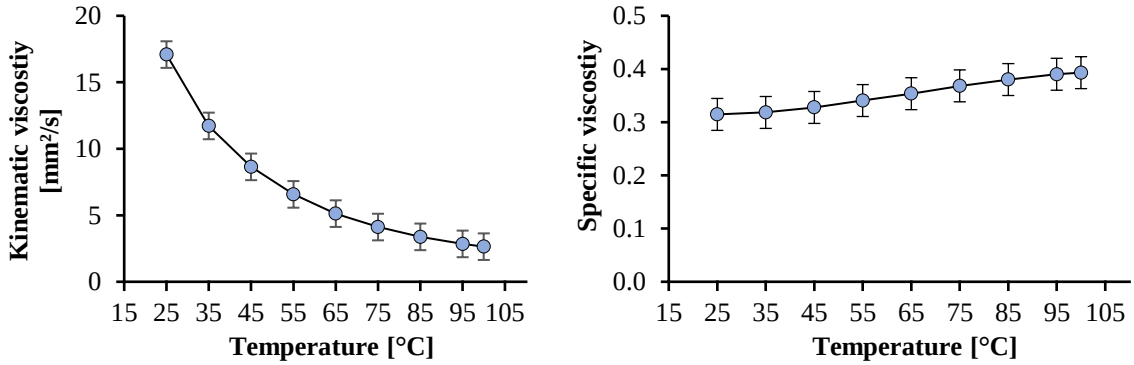

Figure 199: Kinematic (left) and specific (right) viscosity for generation 4 in Nynas NS8 at 60 mM.

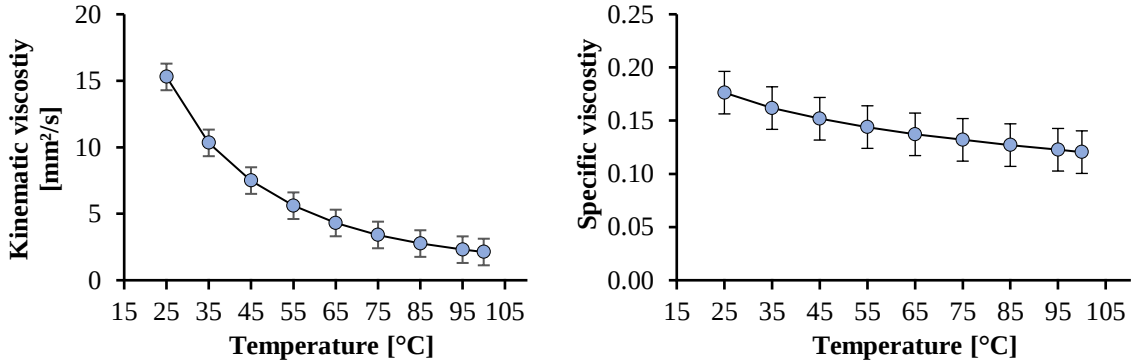

Figure 200: Kinematic (left) and specific (right) viscosity for generation 4 in Nynas NS8 at 40 mM.

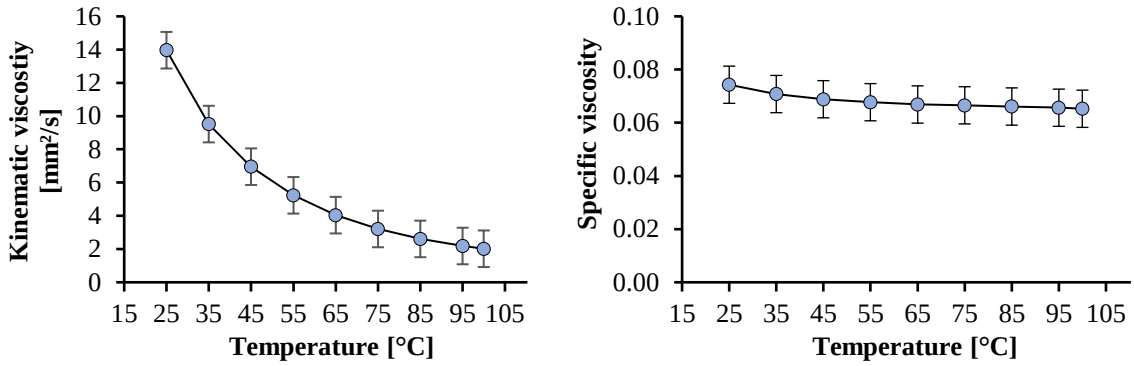

Figure 201: Kinematic (left) and specific (right) viscosity for generation 4 in Nynas NS8 at 20 mM.

8.2.6.2 Measurement in Nexbase 3020

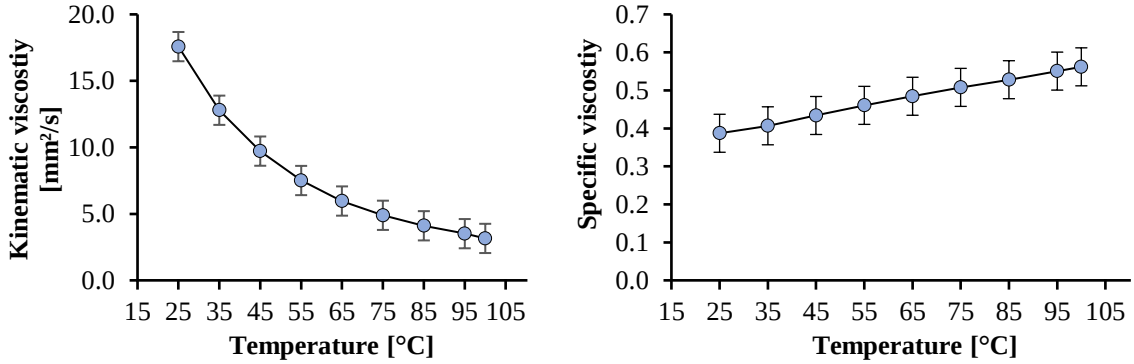

Figure 202: Kinematic (left) and specific (right) viscosity for generation 4 in Nexbase 3020 at 60 mM.

8.3 DLS Measurements

8.3.1 DLS Measurement of the Third Generation in 60 mM DMSO

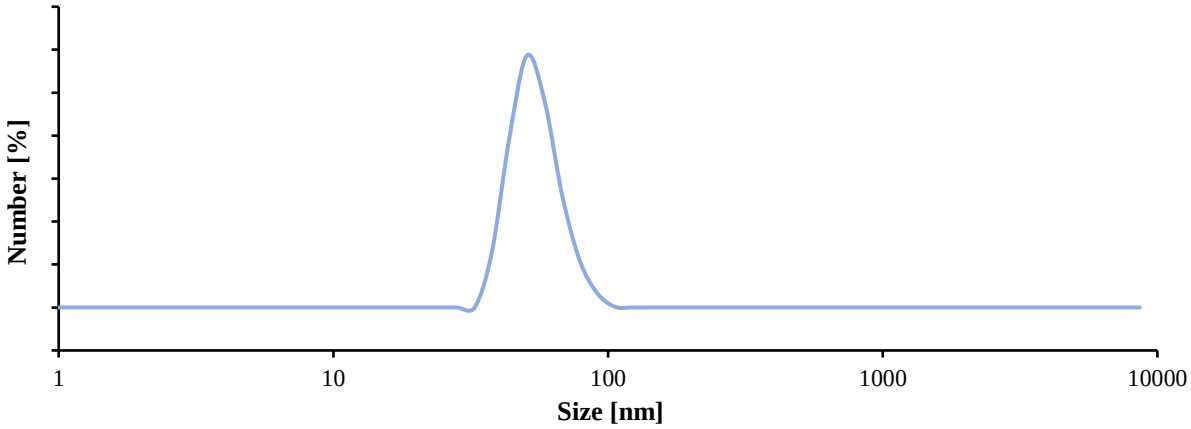

Figure 203: DLS measurement of the third generation in 60 mM DMSO at 25 °C. Signal number peak: 100%.

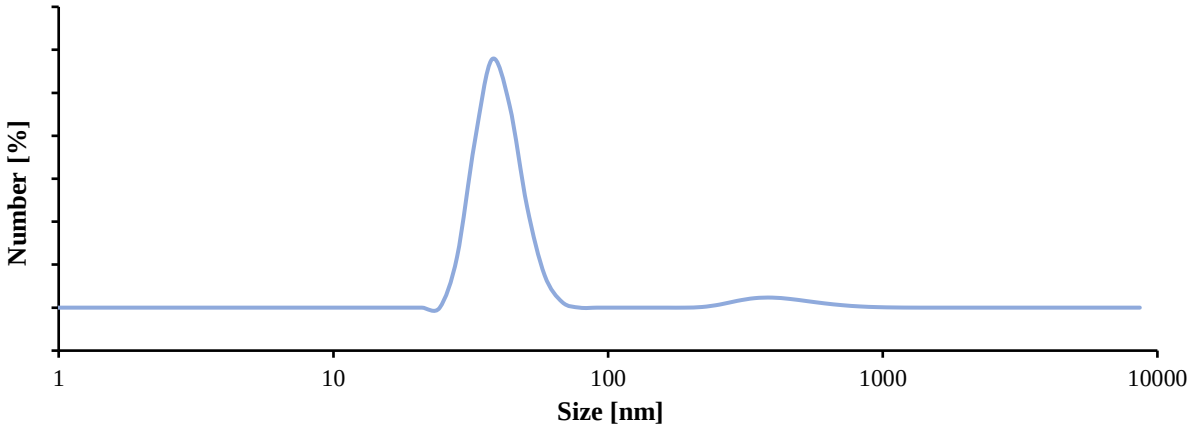

Figure 204: DLS measurement of the third generation in 60 mM DMSO at 60 °C. Signal number peak left: 93.7% peak right 6.3%.

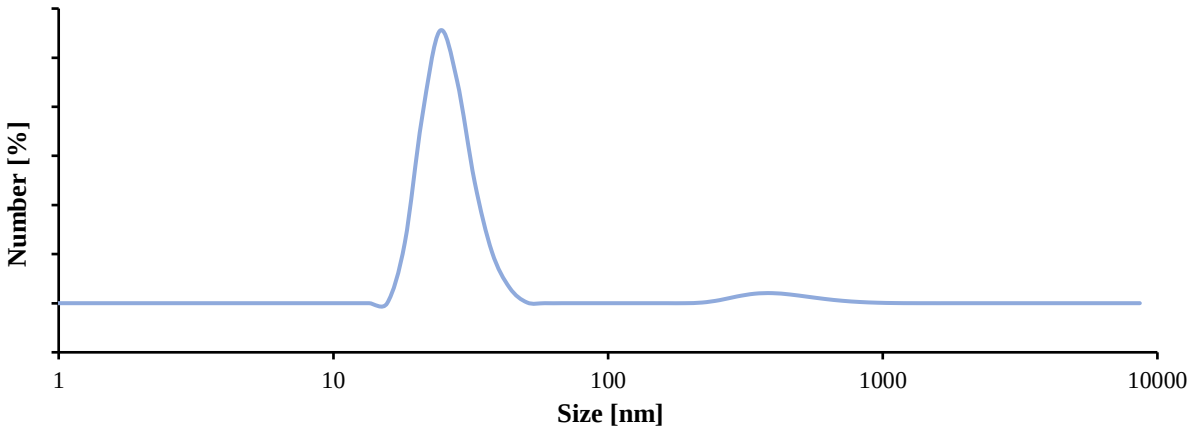

Figure 205: DLS measurement of the third generation in 60 mM DMSO at 100 °C. Signal number peak left: 94.5% peak right 5.5%.

8.3.2 DLS Measurement of the Fourth Generation in 60 mM DMSO

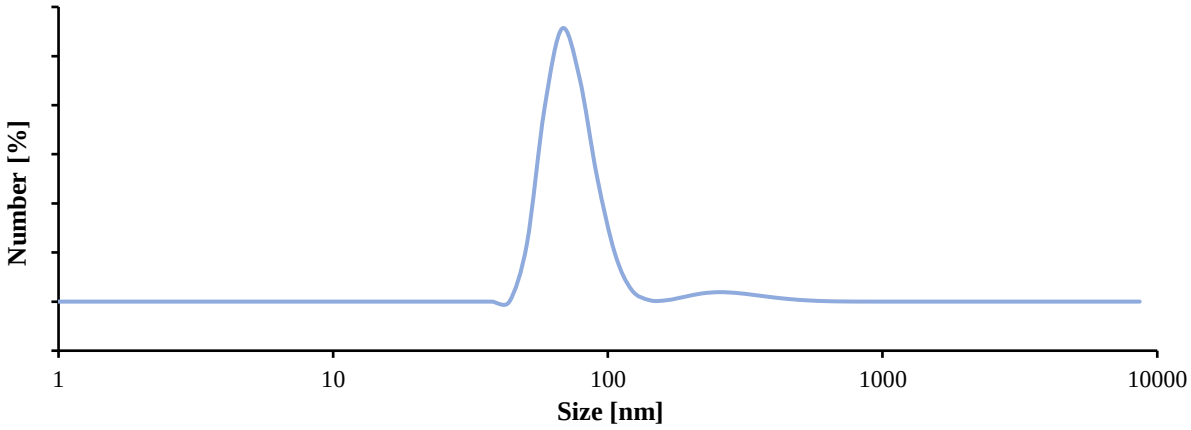

Figure 206: DLS measurement of the fourth generation in 60 mM DMSO at 25 °C. Signal number peak left: 95.1% peak right 4.9%.

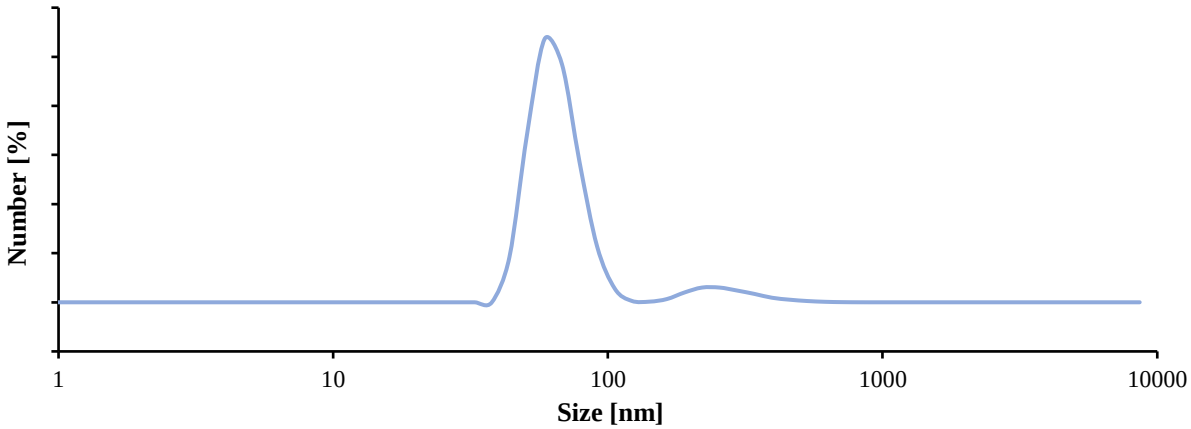

Figure 207: DLS measurement of the fourth generation in 60 mM DMSO at 60 °C. Signal number peak left: 94.1% peak right 4.9%.

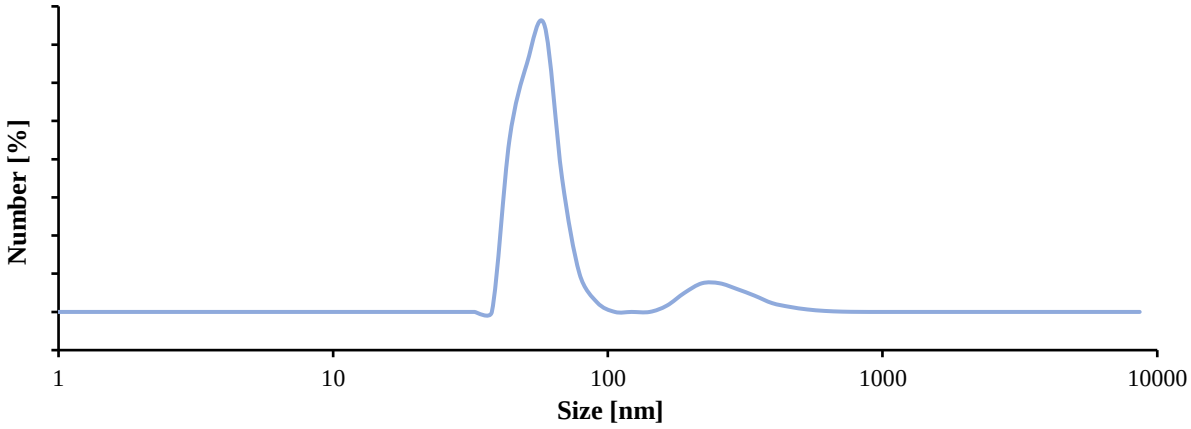

Figure 208: DLS measurement of the fourth generation in 60 mM DMSO at 100 °C. Signal number peak left: 86.4% peak right 13.6%.

8.3.3 DLS Measurement of the Fourth Generation in 60 mM Chloroform

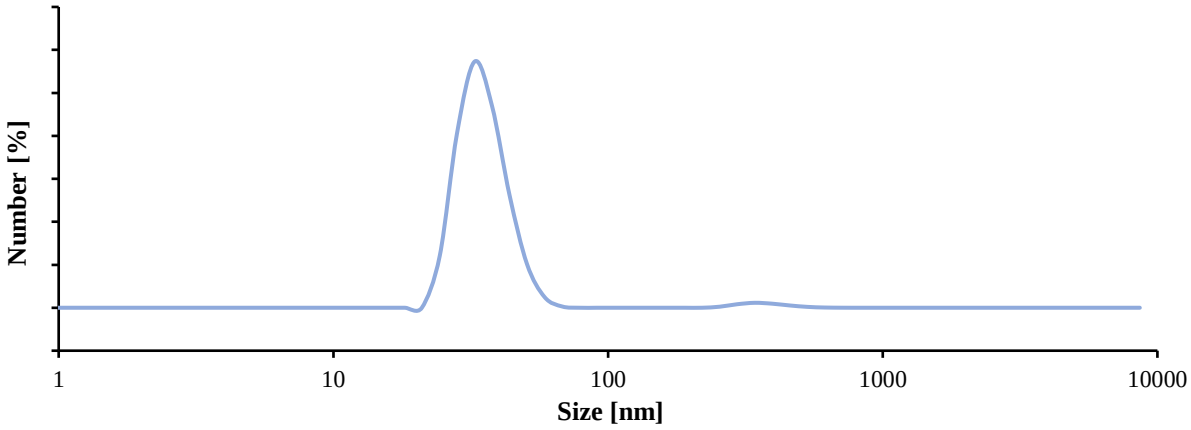

Figure 209: DLS measurement of the fourth generation in 60 mM chloroform at 25 °C. Signal number peak left: 98.0% peak right 2.0%.

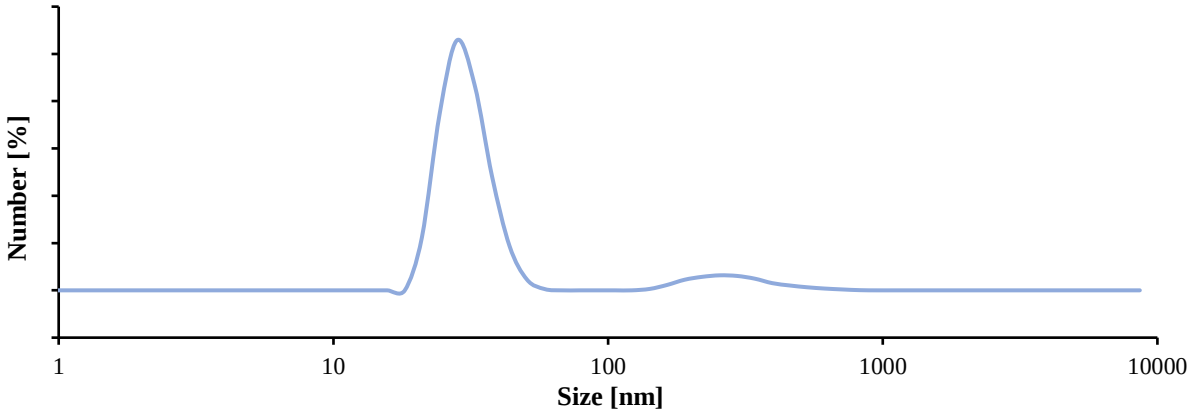

Figure 210: DLS measurement of the fourth generation in 60 mM chloroform at 37 °C. Signal number peak left: 90.5% peak right 9.5%.

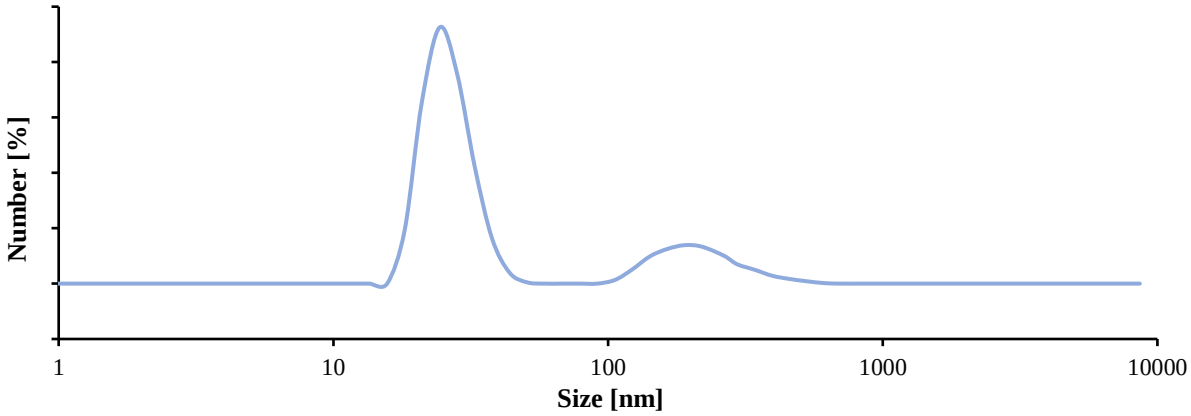

Figure 211: DLS measurement of the fourth generation in 60 mM chloroform at 50 °C. Signal number peak left: 79.2% peak right 20.8%.

8.3.4 DLS Measurement of the Fourth Generation in Toluene

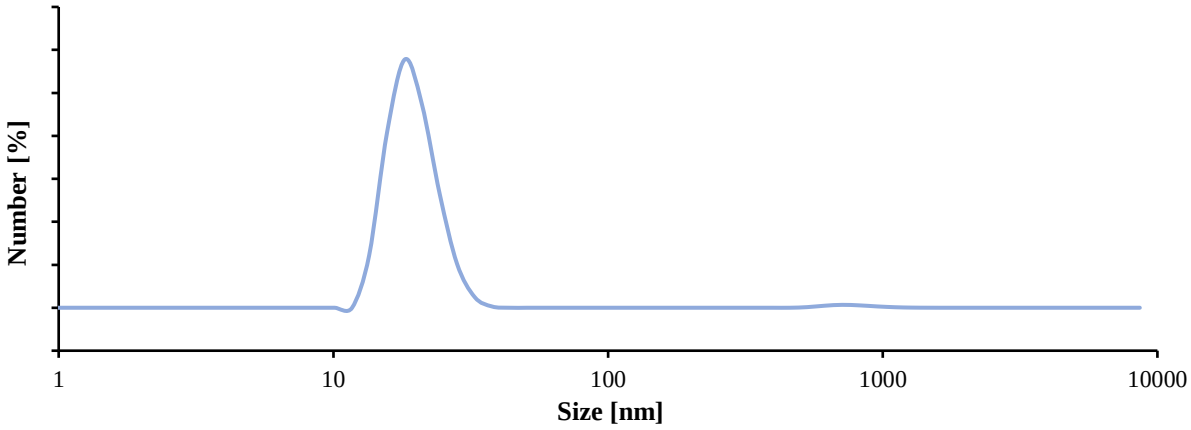

Figure 212: DLS measurement of the fourth generation in 60 mM toluene at 25 °C. Signal number peak left: 98.9% peak right 1.1%.

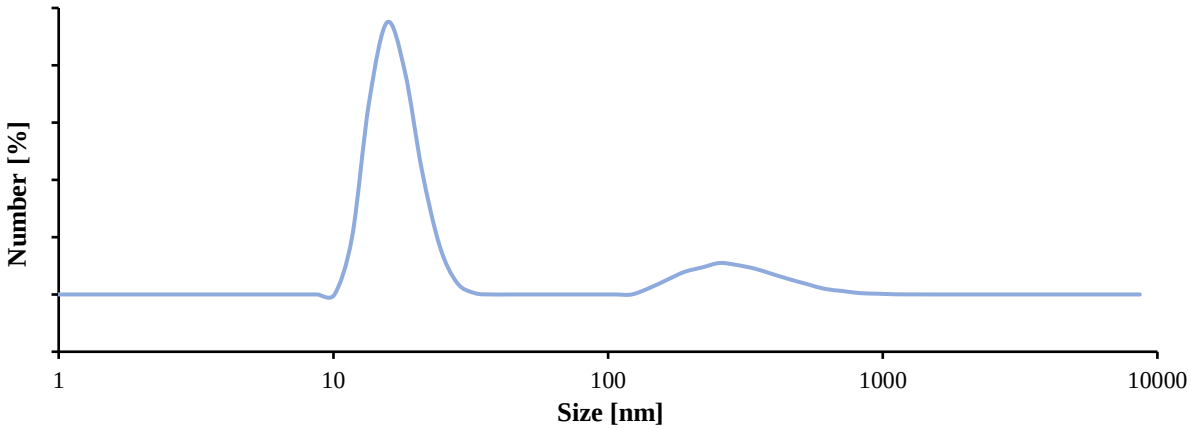

Figure 213: DLS measurement of the fourth generation in 60 mM toluene at 60 °C. Signal number peak left: 81.3% peak right 18.7%.

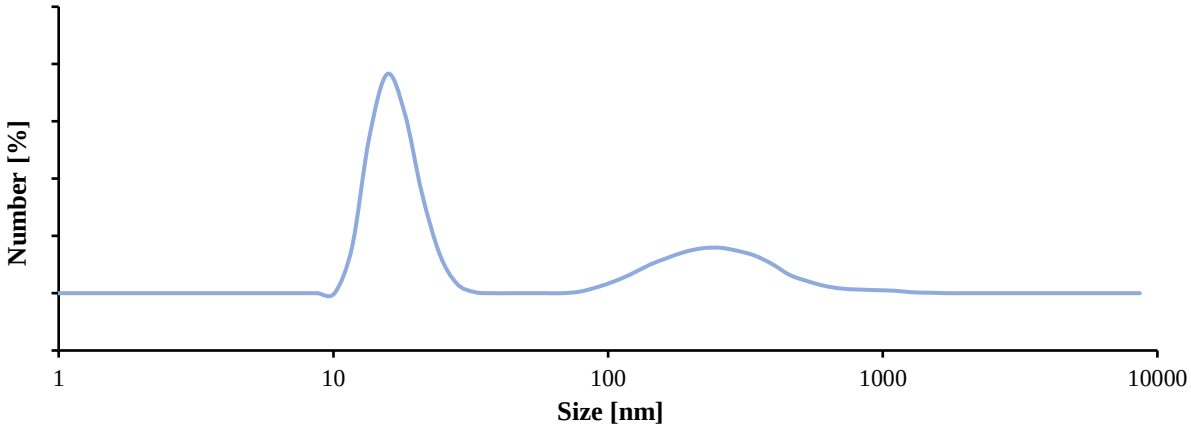

Figure 214: DLS measurement of the fourth generation in 60 mM toluene at 100 °C. Signal number peak left: 65.4% peak right 34.6%.

8.4 NMR-Spectra

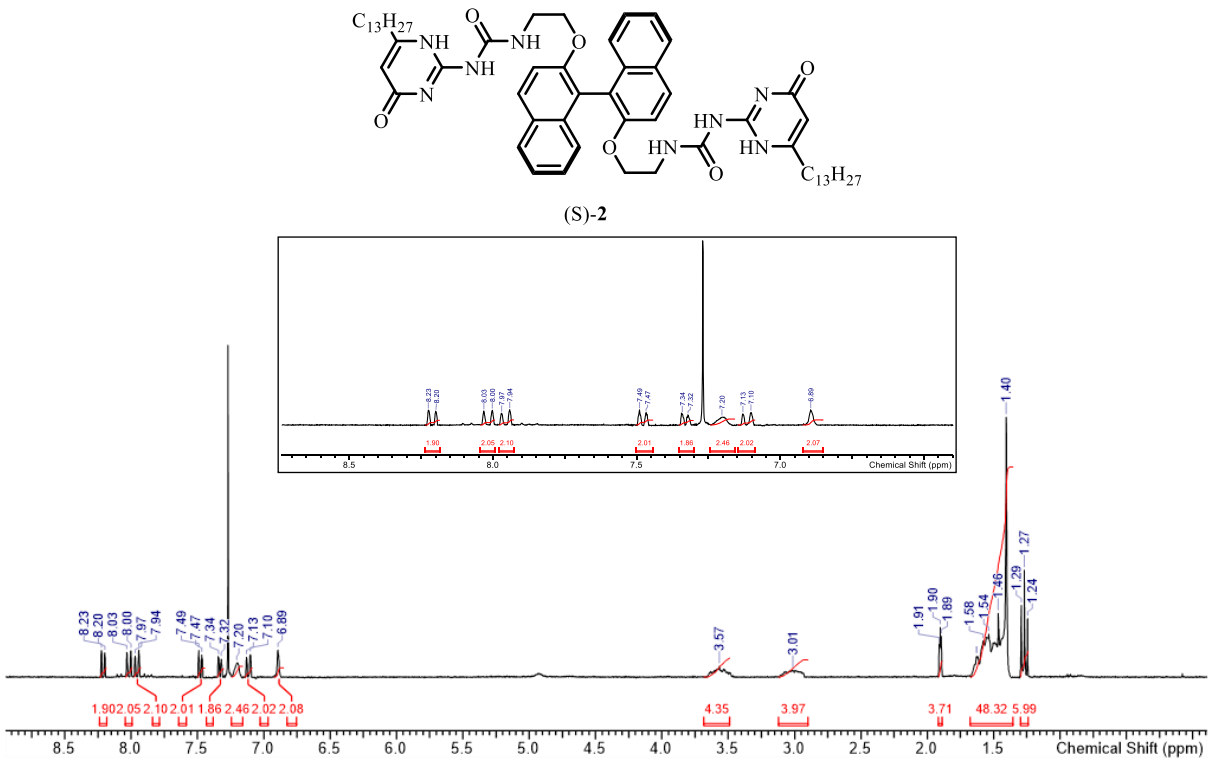

Figure 215: ^{1}H-NMR of *(S)*-2. 300 MHz, Solvent: $CDCl_3$, 27 °C.

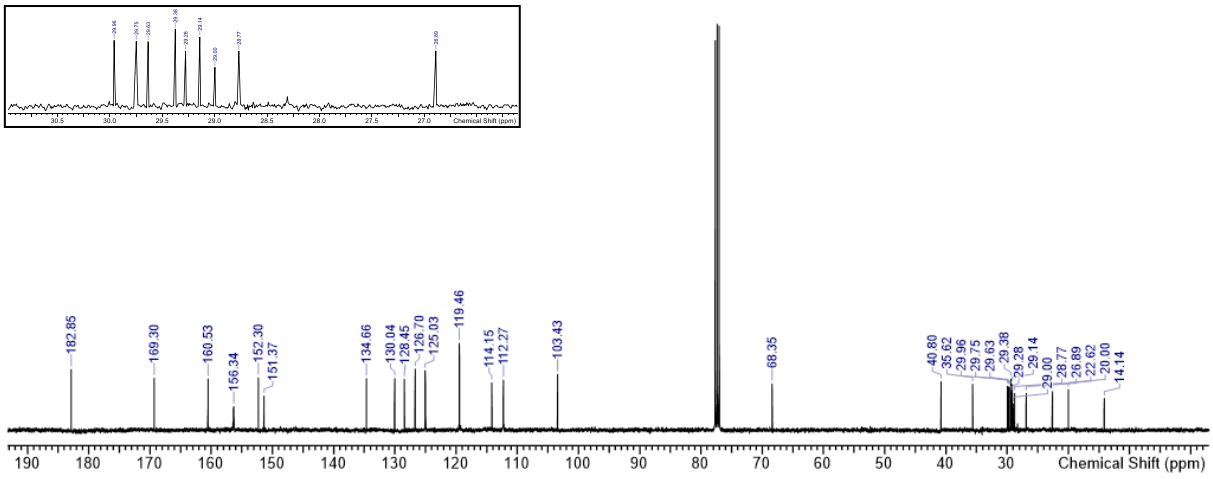

Figure 216: ^{13}C-NMR of *(S)*-2. 151 MHz, Solvent: $CDCl_3$, 25 °C.

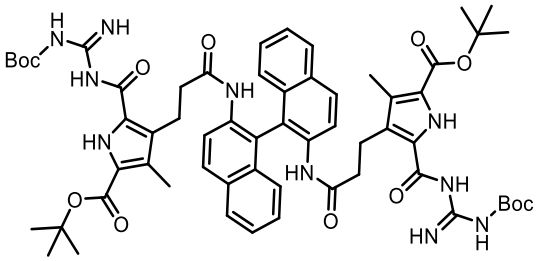

46

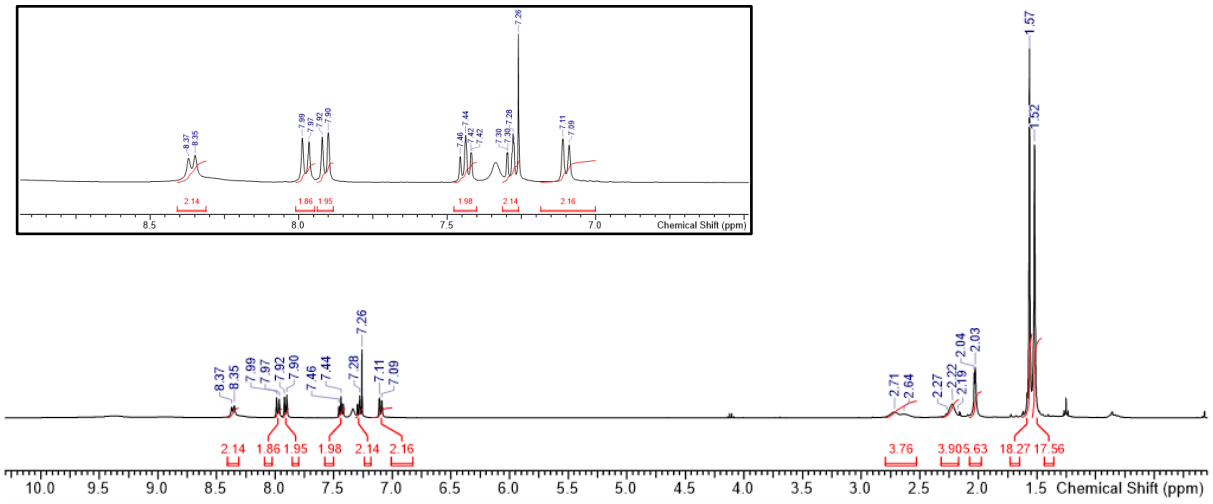

Figure 217: ^{1}H-NMR of 46. 400 MHz, Solvent: $CDCl_3$, 27 °C.

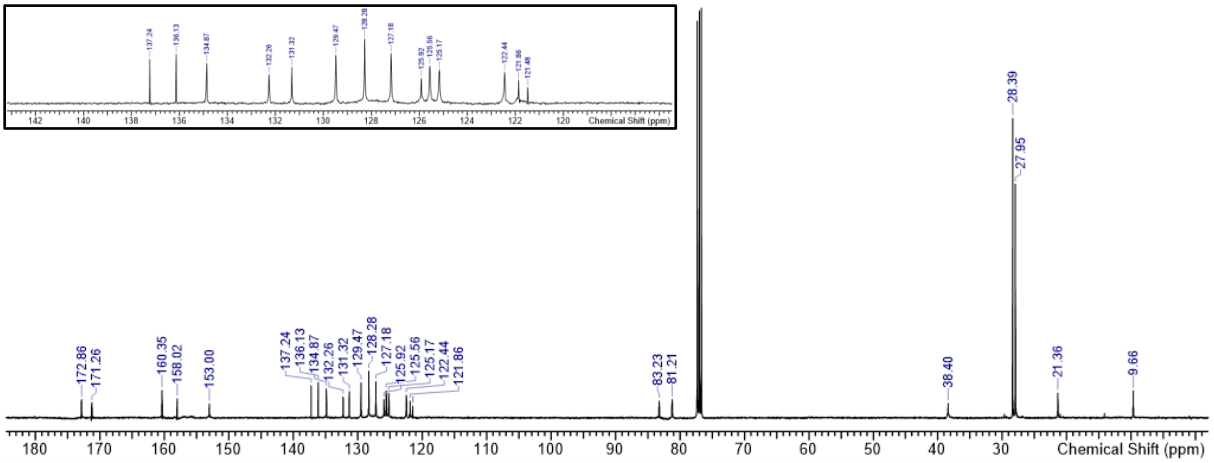

Figure 218: ^{13}C-NMR of 46. 151 MHz, Solvent: $CDCl_3$, 27 °C.

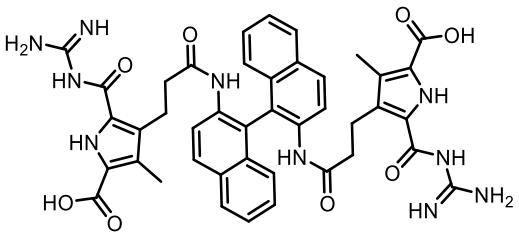

3

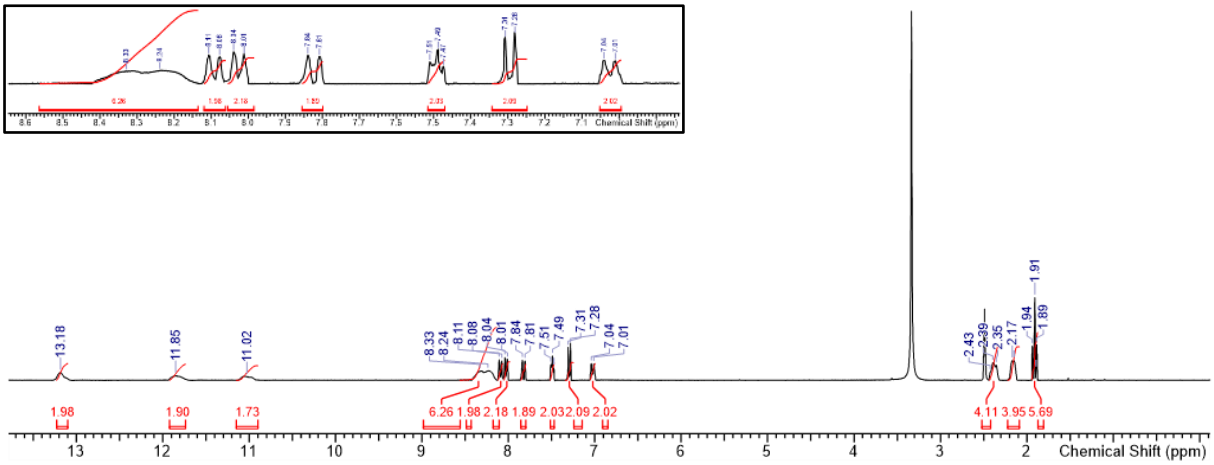

Figure 219: ^{1}H-NMR of 3. 300 MHz, Solvent: DMSO-d$_6$, 27 °C.

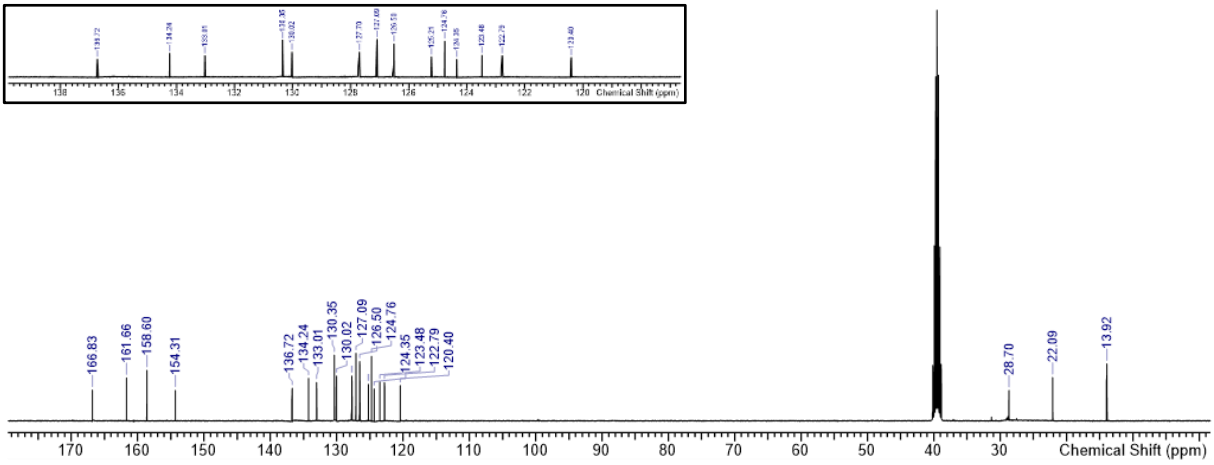

Figure 220: ^{13}C-NMR of 3. 151 MHz, Solvent: DMSO-d$_6$, 27 °C.

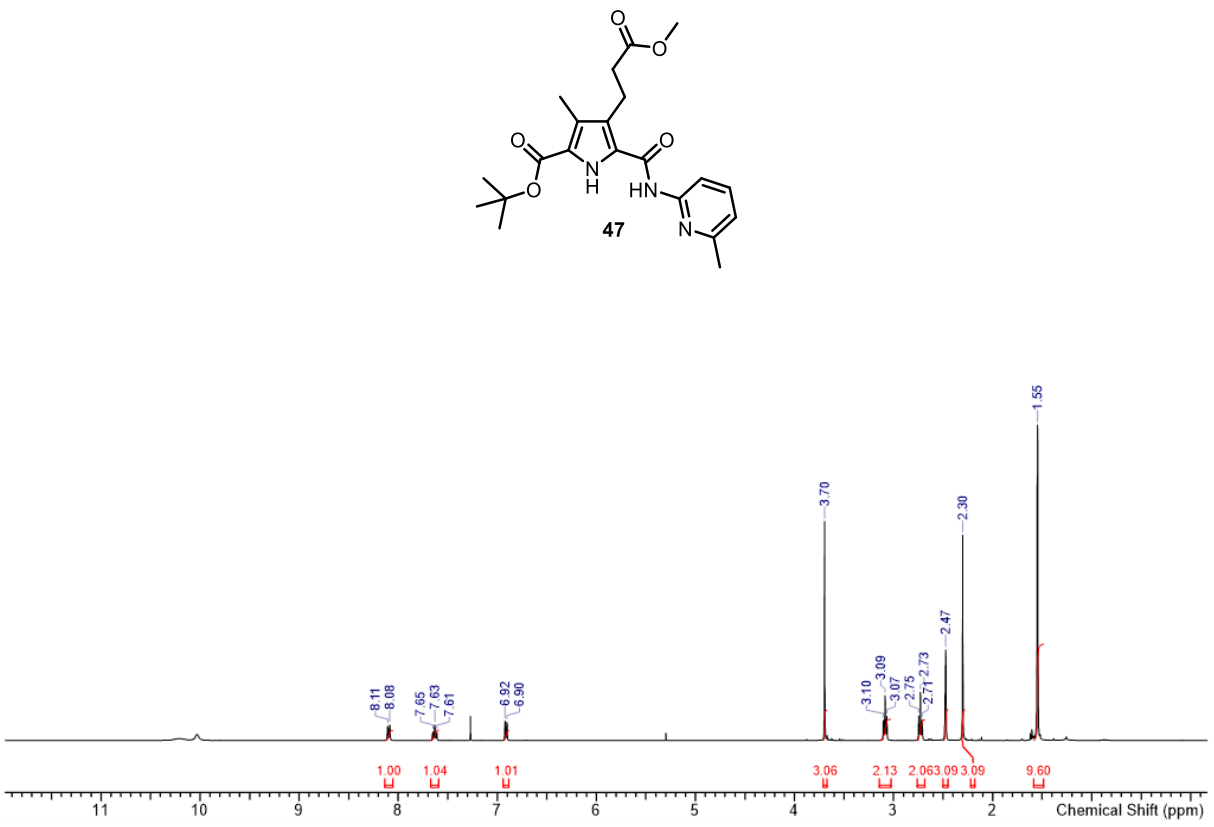

Figure 221: ^{1}H-NMR of 47. 400 MHz, Solvent: $CDCl_3$, 27 °C.

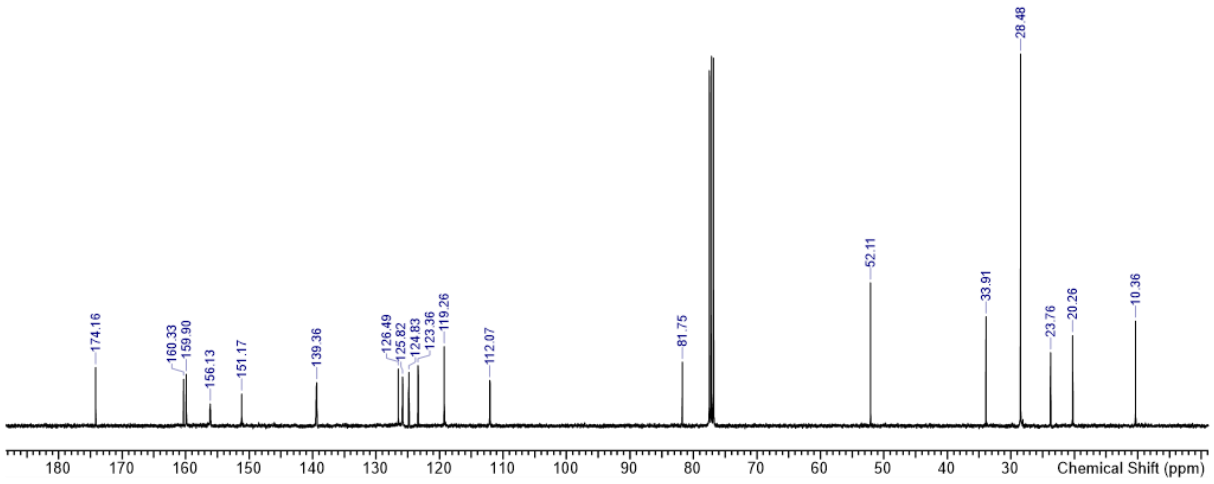

Figure 222: ^{13}C-NMR of 47. 151 MHz, Solvent: $CDCl_3$, 27 °C.

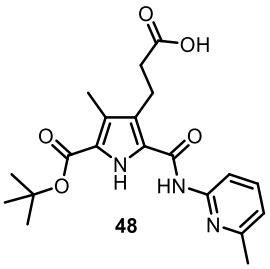

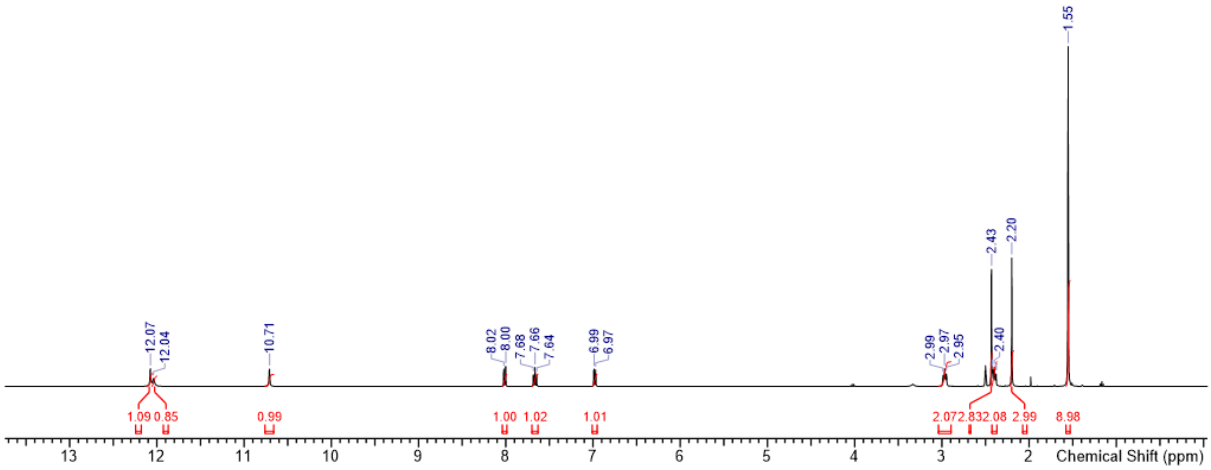

Figure 223: ^{1}H-NMR of 48. 400 MHz, Solvent: DMSO-d$_6$, 27 °C.

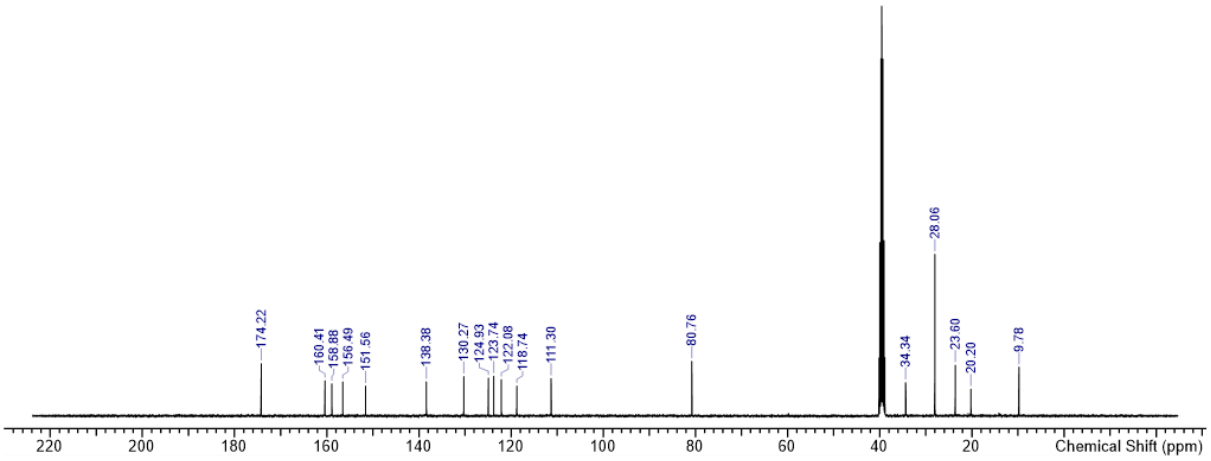

Figure 224: ^{13}C-NMR of 48. 151 MHz, Solvent: DMSOd$_6$, 27 °C.

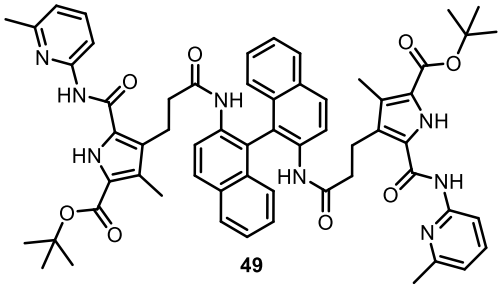

49

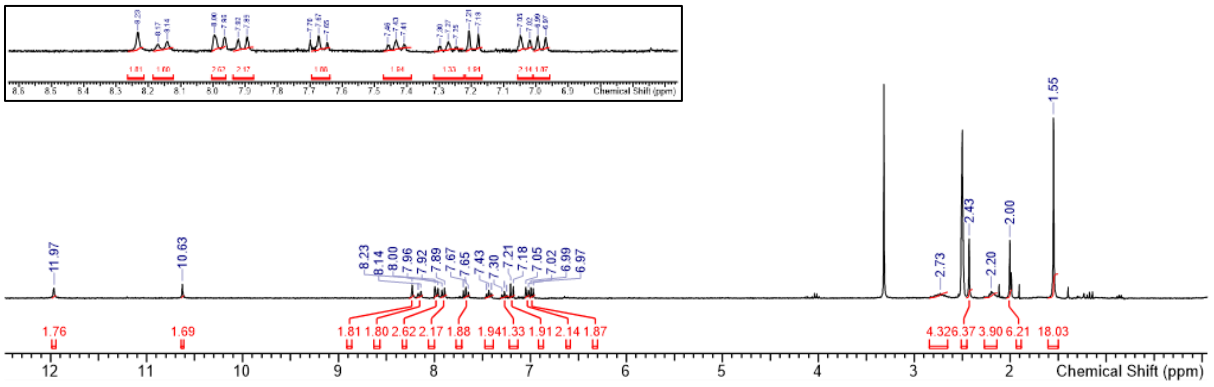

Figure 225: ^{1}H-NMR of 49. 300 MHz, Solvent: DMSO-d$_6$, 27 °C.

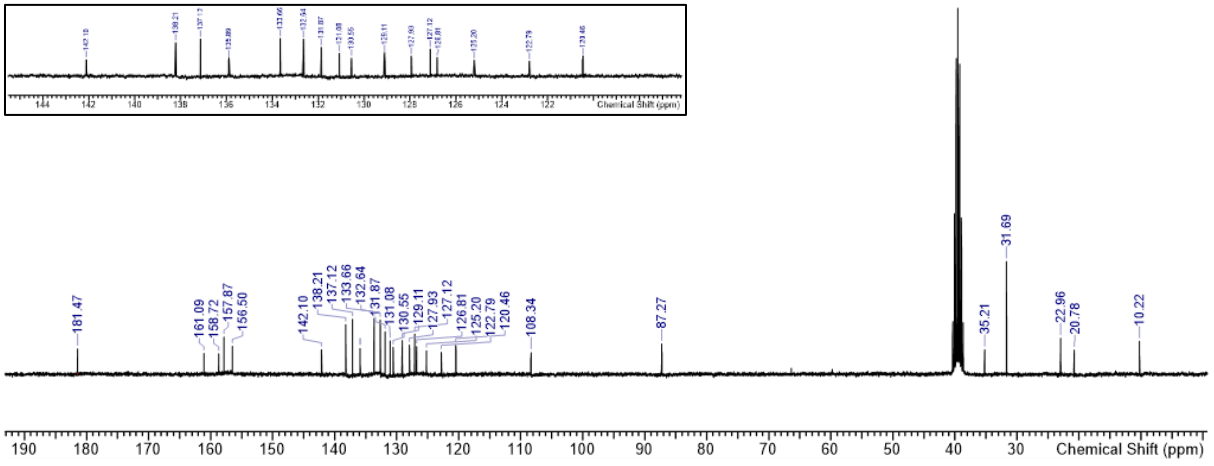

Figure 226: ^{13}C-NMR of 49. 75 MHz, Solvent: DMSO-d$_6$, 27 °C.

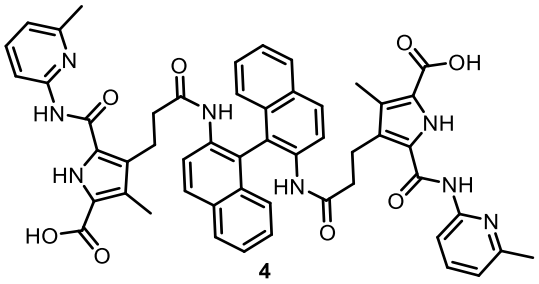

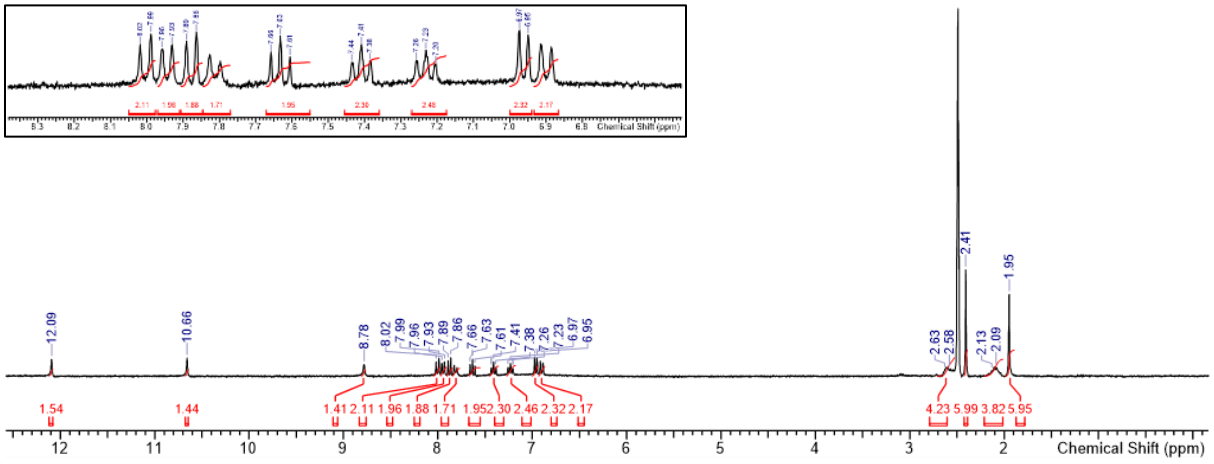

Figure 227: ^{1}H-NMR of 4. 300 MHz, Solvent: DMSO-d$_6$, 27 °C.

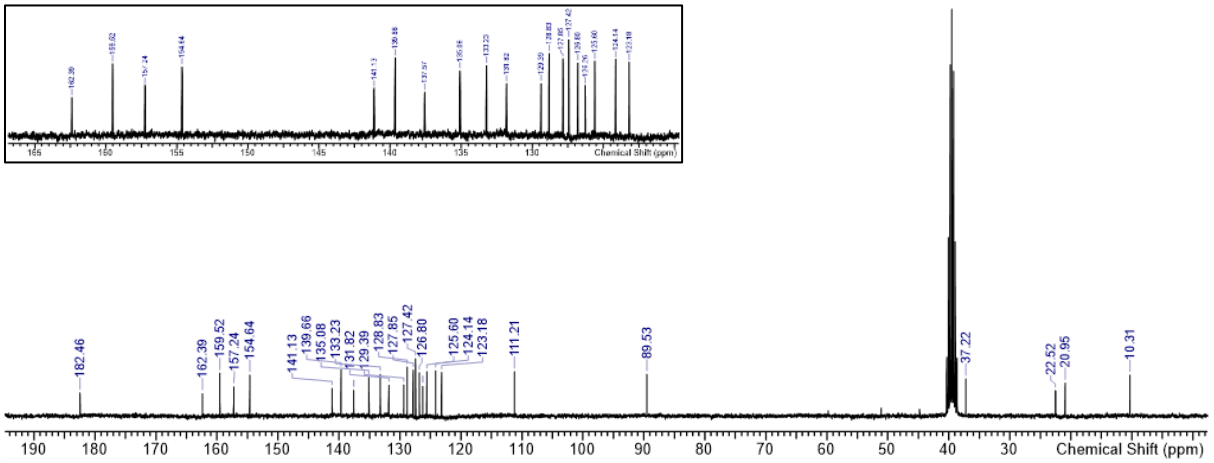

Figure 228: ^{13}C-NMR of 4. 75 MHz, Solvent: DMSO-d$_6$, 27 °C.

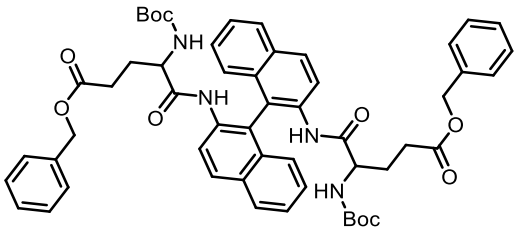

51

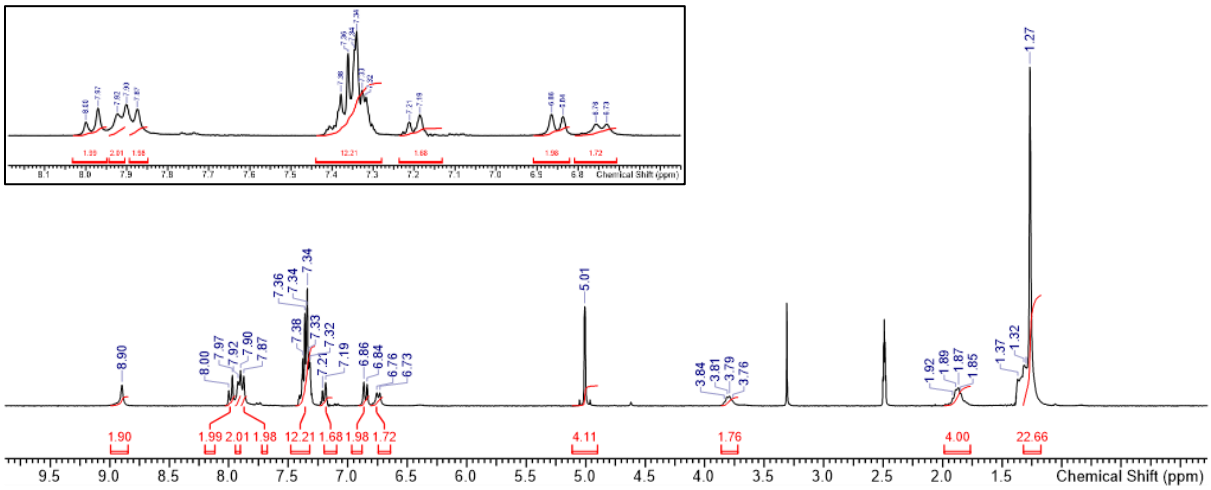

Figure 229: ^{1}H-NMR of 51. 300 MHz, Solvent: DMSO-d$_6$, 27 °C.

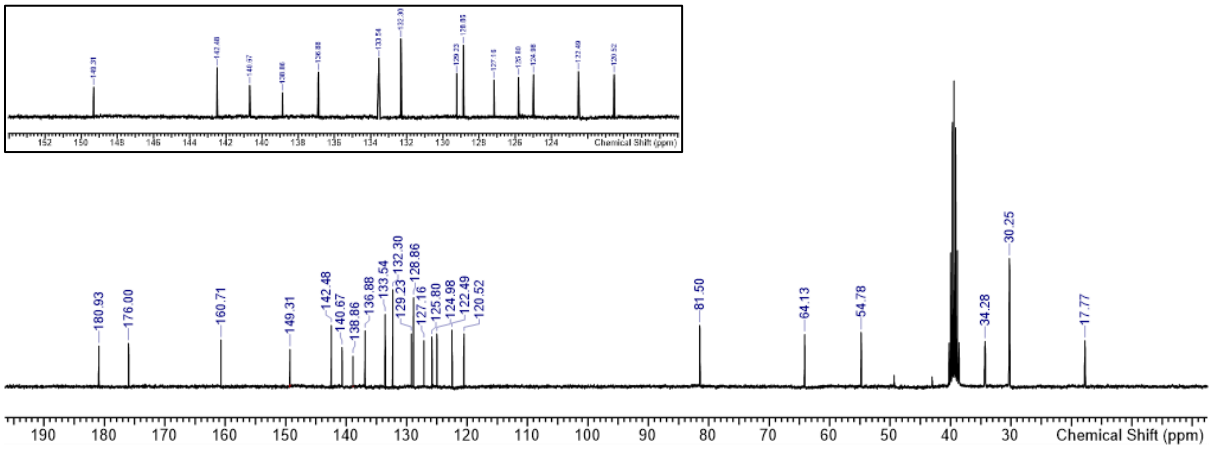

Figure 230: ^{13}C-NMR of 51. 75 MHz, Solvent: DMSO-d$_6$, 27 °C.

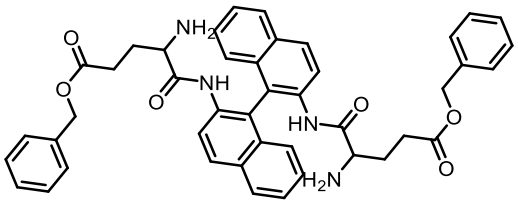

52

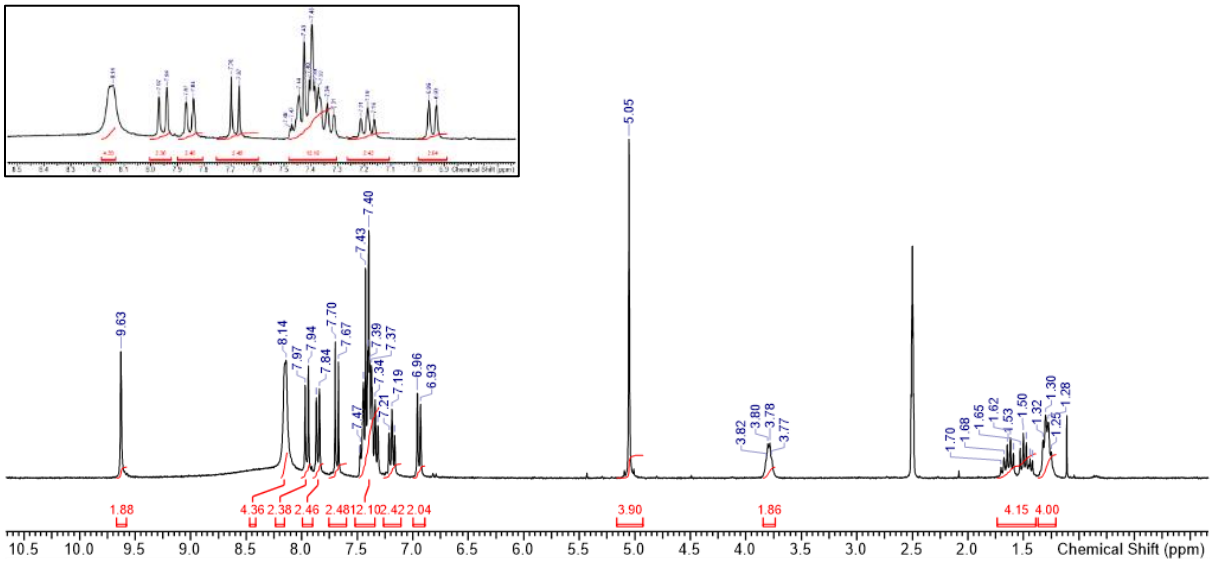

Figure 231: ^{1}H-NMR of 52. 300 MHz, Solvent: DMSO-d$_6$, 27 °C.

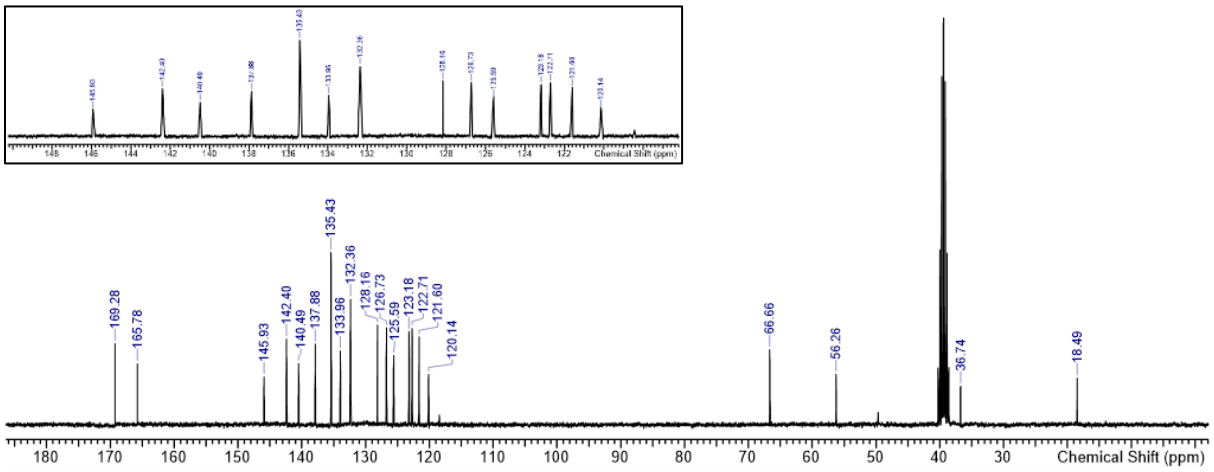

Figure 232: ^{13}C-NMR of 52. 75 MHz, Solvent: DMSO-d$_6$, 27 °C.

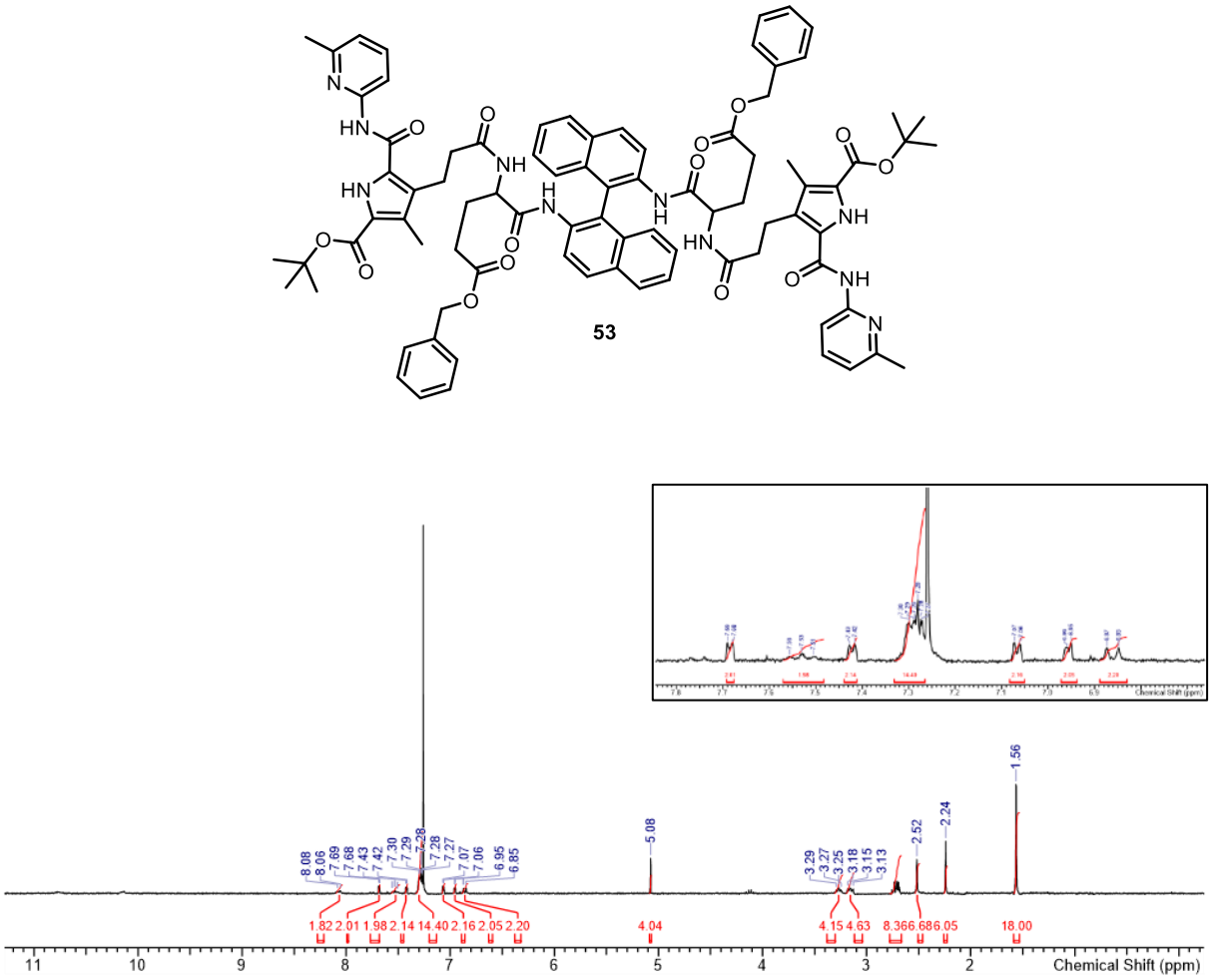

Figure 233: ^{1}H-NMR of 53. 300 MHz, Solvent: $CDCl_3$, 27 °C.

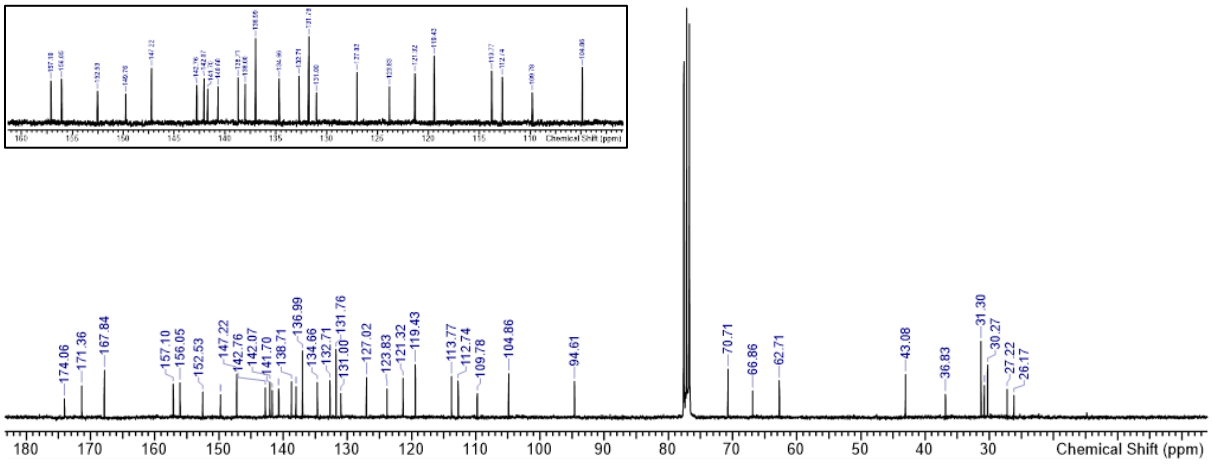

Figure 234: ^{13}C-NMR of 53. 75 MHz, Solvent: $CDCl_3$, 27 °C.

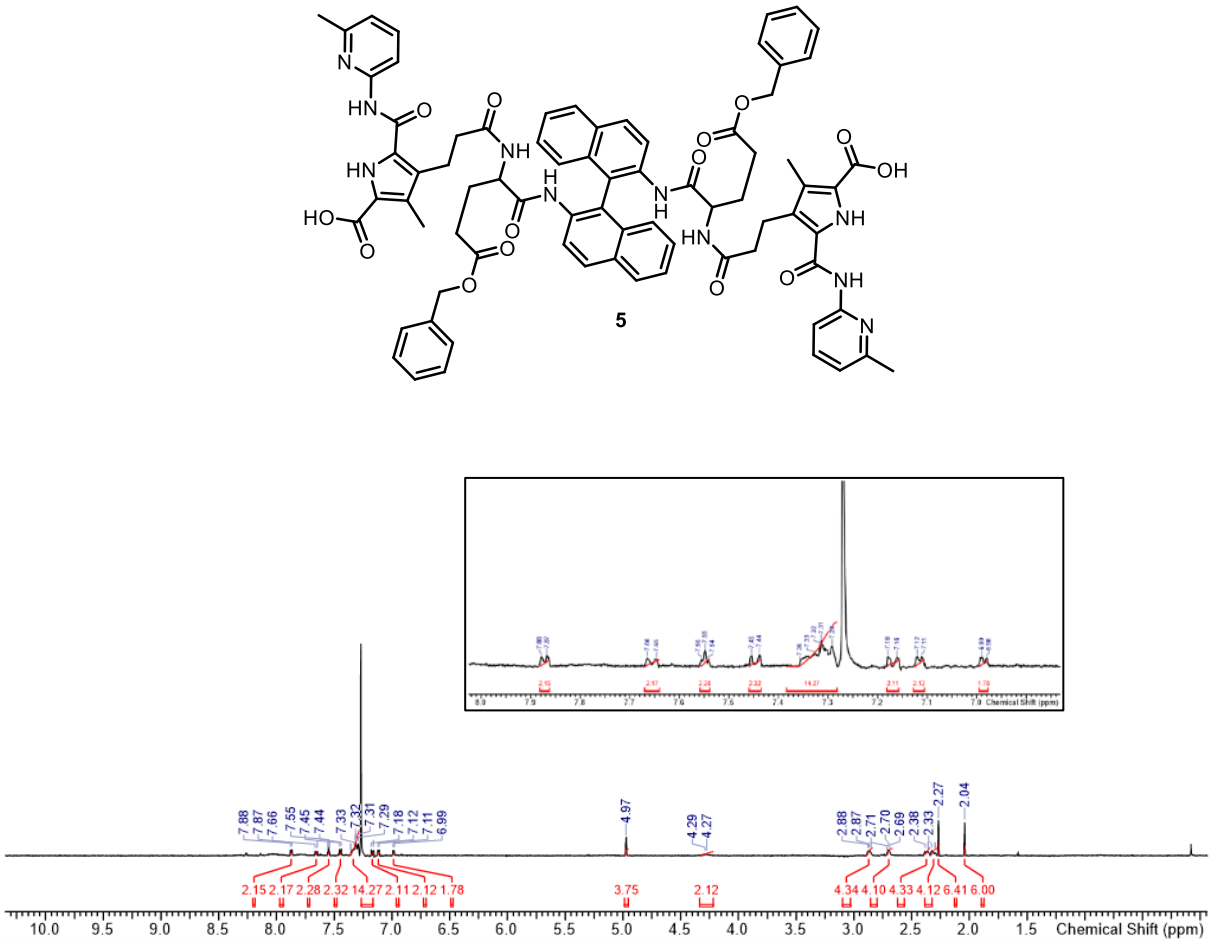

Figure 235: ^{1}H-NMR of 5. 300 MHz, Solvent: $CDCl_3$, 27 °C.

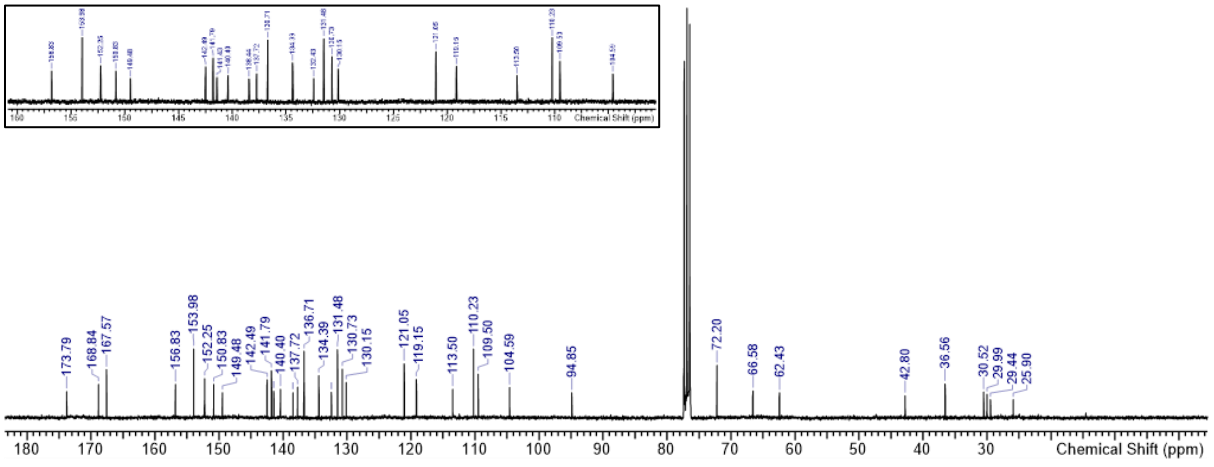

Figure 236: ^{13}C-NMR of 5. 75 MHz, Solvent: $CDCl_3$, 27 °C.

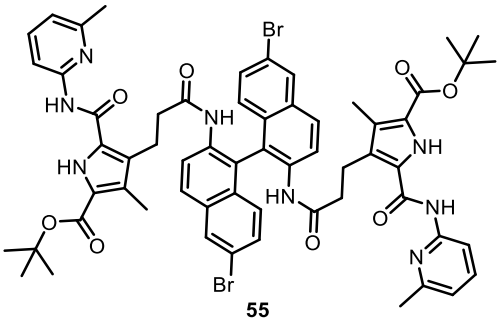

55

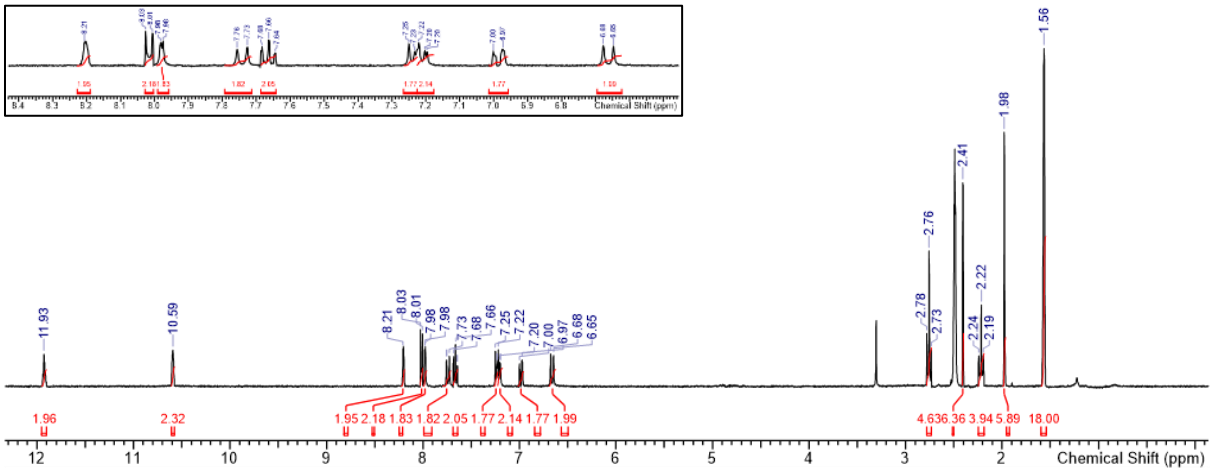

Figure 237: ^{1}H-NMR of 55. 400 MHz, Solvent: DMSO-d$_6$, 27 °C.

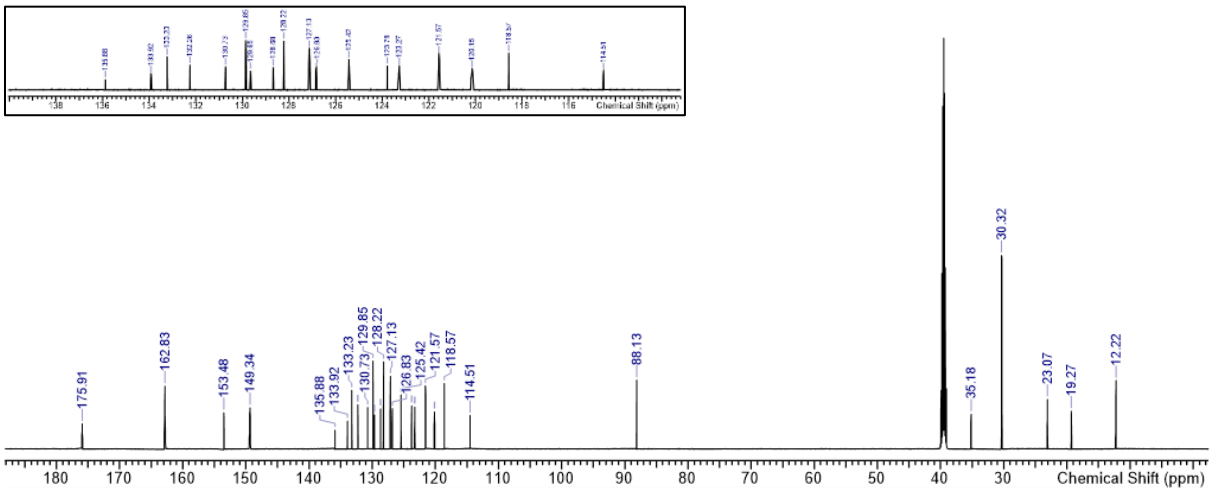

Figure 238: ^{13}C-NMR of 55. 151 MHz, Solvent: DMSO-d$_6$, 27 °C.

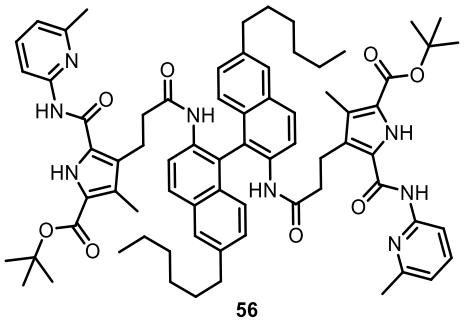

56

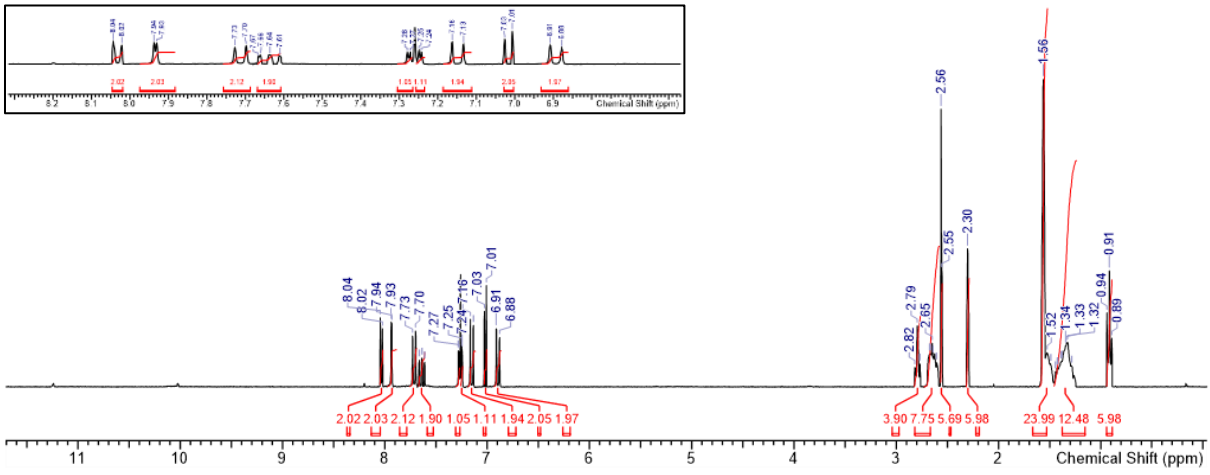

Figure 239: ^{1}H-NMR of 56. 400 MHz, Solvent: $CDCl_3$, 27 °C.

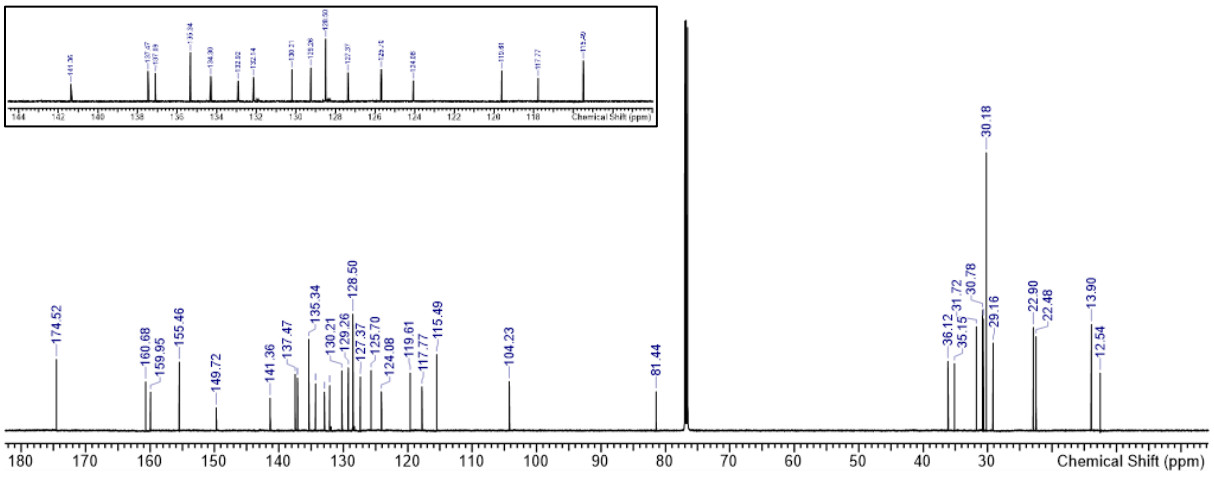

Figure 240: ^{13}C-NMR of 56. 151 MHz, Solvent: $CDCl_3$, 27 °C.

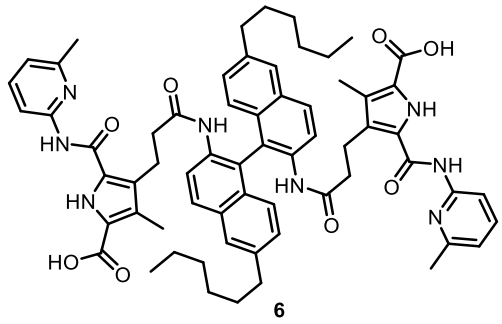

6

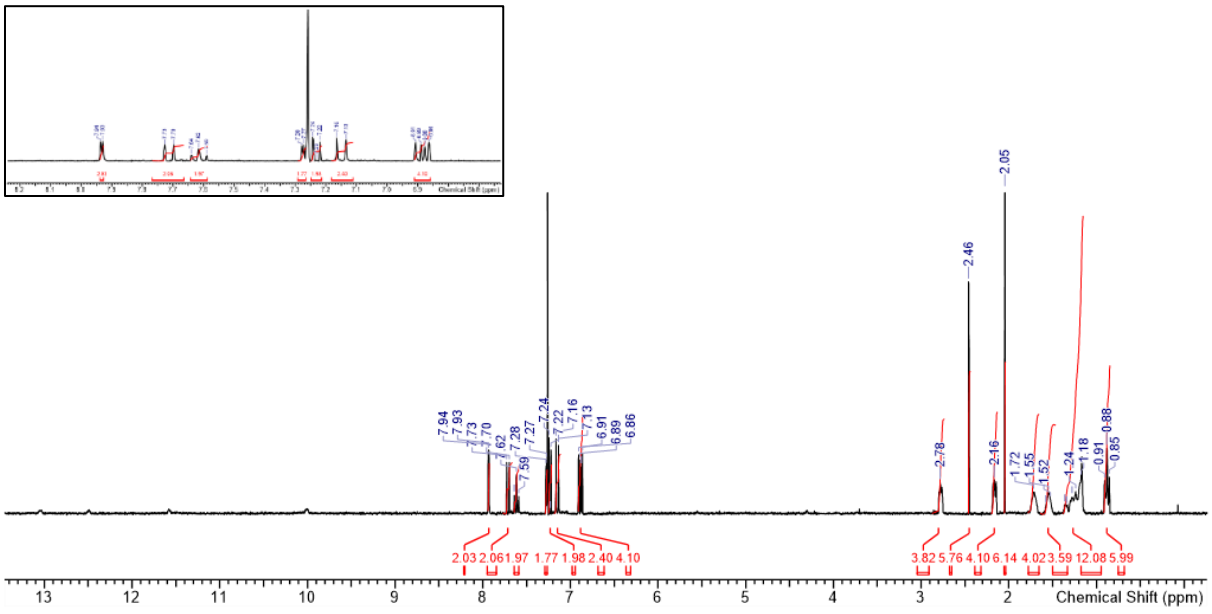

Figure 241: ^{1}H-NMR of 6. 400 MHz, Solvent: $CDCl_3$, 27 °C.

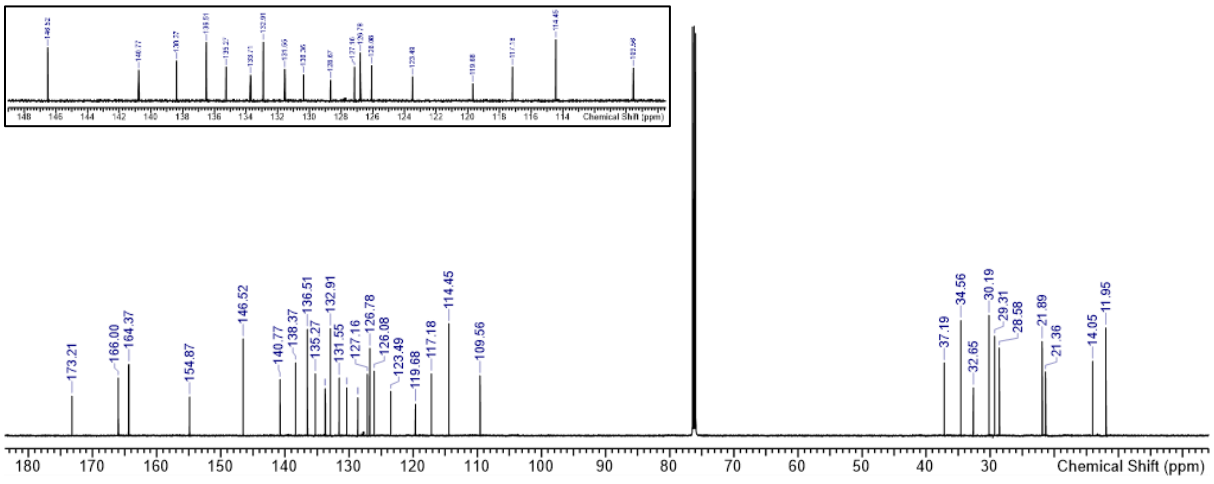

Figure 242: ^{13}C-NMR of 6. 151 MHz, Solvent: $CDCl_3$, 27 °C.

8.6 Curriculum Vitae

Der Lebenslauf ist in der Online-Version aus Gründen des Datenschutzes nicht enthalten.

8.7 Publications

"Dual pH-Induced Reversible Self-Assembly of Gold Nanoparticles by Surface Functionalization with Zwitterionic Ligands."

Huibin He, Jan-Erik Ostwaldt, Christoph Hirschhäuser, Carsten Schmuck, Jochen Niemeyer.

Small **2020**, DOI: 10.1002/smll.202001044.

"A stimuli responsive two component supramolecular hydrogelator with aggregation-induced emission properties."

Dennis Aschmann, Steffen Riebe, Thorben Neumann, Dennis Killa, Jan-Erik Ostwaldt, Christoph Wölper, Prof. Dr. Carsten Schmuck.

Soft Matter **2019**, *15*, 7117 – 7121, DOI: 10.1039/C9SM01513B.

"Formation of Twisted β-Sheet Tapes from a Self-Complementary Peptide Based on Novel Pillararene-GCP Host-Guest Interaction with Gene Transfection Properties."

Dr. Xiao-Yu Hu, Dr. Martin Ehlers, Tingting Wang, Elio Zellermann, Stefanie Mosel, Dr. Hao Jiang, Jan-Erik Ostwaldt, Prof. Dr. Shirley K. Knauer, Prof. Dr. Leyong Wang, Prof. Dr. Carsten Schmuck.

Chem. Eur. J. **2018**, *24*, 9754 – 9759, DOI: 10.1002/chem.201801315.